Supramolecular and entangled polymer materials: rheological models

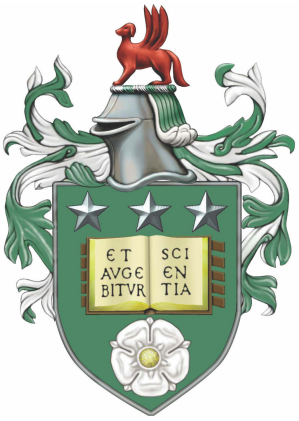

Victor Ange Henri Boudara

School of Mathematics

University of Leeds

Submitted in accordance with the requirements for the degree of

Doctor of Philosophy

August, 2017

This page is intentionally left blank

The candidate confirms that the work submitted is his own, except where work which has formed part of jointly authored publications has been included. The contribution of the candidate and the other authors to this work has been explicitly indicated below. The candidate confirms that appropriate credit has been given within the thesis where reference has been made to the work of others.

Details of contributions to jointly authored publications:

Boudara, V.A.H., and D.J. Read, "Stochastic and preaveraged nonlinear rheology models for entangled telechelic star polymers," *J. Rheol.* **61**, 339–362 (2017).

I contributed to the development of the theoretical expressions for the stochastic and preaveraged models, and I also implemented the computational algorithms. D.J. Read provided supervision and feedback on the paper. This work forms the basis for Chapters 4 and 5 of this thesis.

Acknowledgements

First and foremost, I wish to express my sincere gratitude to my supervisor, Daniel Read, for his efforts to help, for the constant support and motivation he gave me during the course of my PhD, and most importantly, for sharing with me his invaluable knowledge and passion for polymer dynamics and rheology.

This journey has been a formidable adventure which was made possible thanks to the financial support of the European Union through the Marie Skłodowska-Curie ITN SUPOLEN (g.a. no. 607937), and I wish to thank all the SUPOLEN members for the excellent organisation, the quality of the training events and project meetings, and for the memorable time we had during these meetings over past 3.5 years, in Crete, Capri, Copenhagen, Leeds, Montpellier, and Paris. These meetings were a fantastic, but also intimidating, place to present my work and harvest the precious feedback and criticisms from the audience, in particular from Ole Hassager, Giovanni Ianniruberto, Evelyne van Ruymbeke, and Dimitris Vlassopoulos who held a constant attention to details. I am also grateful to all the SUPOLEN PhD students and post-docs – in particular Guanghui Cui, Laurence Hawke, Aamir Shabbir, Ashwinikumar Sharma, and Flanco Zhuge – for the passionate discussions we had on various topics.

I thank Dimitris Vlassopoulos for inviting me to FORTH, and Salvatore Costanzo for his guidance in the lab. I thank Luna Imperiali for introducing me to the material research centre of DSM Netherlands.

I also wish to thank my parents, and all my family and friends, for their encouragement and for the positive time we spent together, in Leeds or away.

Finally, for the love and joy you two bring me every day, Joanna and Hugo, thank you.

This page is intentionally left blank

Abstract

This thesis is concerned with the dynamics and rheology of polymers, and in particular on the influence of entanglements and supramolecular "sticky" groups. The text is organised as follows:

In Part I, we consider these effects in isolation. We begin with an introductory chapter detailing established theory for unentangled polymers, unentangled sticky polymers, and entangled polymers. In Chapter 2, we develop a stochastic model for linear rheology of un-entangled polymers with stickers along the backbone that we then compare with experimental data and the "classic" sticky Rouse model. In Chapter 3, we explore the nonlinear rheology of a mixture of entangled polymeric chains of various lengths (polydisperse) based on coupled equations of similar form the to Rolie-Poly model [Likhtman and Graham, *J. Nonnewton. Fluid Mech.* **114**, 1–12 (2003)].

Part II of this thesis describes the development and testing of a "toy" nonlinear rheology model for entangled supramolecular polymeric materials. We describe three stages in development and testing of this model [Boudara and Read, *J. Rheol.* **61**, 339–362 (2017)]: Chapter 4, presents a simplified stochastic model for the rheology of entangled telechelic star polymers. In both linear and nonlinear regimes, we produce maps of the whole parameter space, indicating the parameter values for which qualitative changes in response to the applied flow are predicted. Preaveraging the stochastic equations described above, we obtain a set of non-stochastic coupled equations that produce very similar predictions. This is detailed in Chapter 5. Finally, in Chapter 6, we use the preaveraged model to explore complex flow behaviour. In Chapters 4 and 5, we observed that for some parameter values, the steady state stress versus shear rate curve is non-

monotonic, which is a signature of shear banding [Fielding, *J. Rheol.* **60**, 821–834 (2016)]. Our simulations confirm shear banding. Surprisingly, for some parameter values, the system never reaches a steady state but instead it oscillates in time between homogeneous state and recoil (coexistence of positive and negative shear rates). We investigate the mechanism behind this oscillatory behaviour.

Contents

List of Figures

Notations

k_B	Boltzmann's constant
k_BT	Thermal energy
a_0	Average distance between entanglements
b	Kuhn (or statistical) length
(β, δ)	Rolie-Poly parameters [Likhtman & Graham (2003)]
Z	Entanglement number
ζ	Monomeric friction coefficient
M_e	Entanglement molar mass (Graessley/Fetters definition [Fetters *et al.* (1994); Graessley (1980)])
M_n	Number-average molar mass
M_w	Weight-average molar mass
η^+, η_E^+	Stress growth coefficient (viscosity) in shear and elongation
$\dot{\varepsilon}$	Hencky strain rate
$\dot{\gamma}$	Shear rate
τ_d	Reptation time
τ_s	Stretch relaxation time
τ_as	Typical time a sticker says attached
ϕ_as	Fraction of attached stickers at equilibrium
λ	Stretch ratio
λ_max	Maximum stretch ratio in extension
$\mathrm{f_E}$	Finite extensibility function
$\equiv$	Provides a definition
$\approx$	Approximative equality (e.g. $k \equiv 3k_\mathrm{B}T/Nb^2 \approx k_\mathrm{B}T/Nb^2$)
$\propto$	Proportionality (e.g. $k \propto N^{-1}$)
ln	Natural logarithm
log	Logarithm base 10

This page is intentionally left blank

Part I

Polymers, stickers and entanglements

This page is intentionally left blank

Chapter 1

Introduction: Polymers and their rheology

1.1 Overview

1.1.1 A brief history of polymeric materials

Ink in ancient Egypt (3000 B.C.) was made by mixing carbon black with Arabic gum; Amazonian Indians collected sap from the hevea tree to make their gummy boots [de Gennes & Badoz (1994; 1996)]. A little more recently, Charles Goodyear (1800-60) boiled a mixture of sap from hevea tree and sulphur: rubber for automobile tyres was invented. However, he did not know that the sap was in fact latex, nor what latex was. It was in 1920 that the macromolecular nature of polymeric materials was suggested by Hermann Staudinger [Staudinger (1920)]. He hypothesised that polymers were composed of long molecules made from the repetition of chemical groups linked by covalent bonds.

The architecture and sequence of polymers are crucial to understanding their properties. Some biological polymers like DNA or RNA contain a huge amount

of information. They are linear molecules, i.e. no branching; information is contained in the very sequence of the monomers. Some natural polymers and most synthetic polymers are linear and with the same repeating unit (homopolymers). Three of the most used polymers are shown in Figure 1.1. All information is contained in the architecture of the polymer, i.e. branching and linear portions. Intermediate between the above are copolymers. Their sequence contains a few different type of monomers.

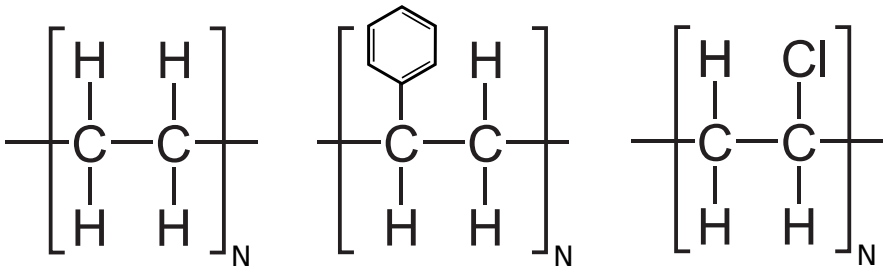

Figure 1.1: Common polymers. Left to right: polyethylene (PE), polystyrene (PS), and polyvinylchloride (PVC). The degree of polymerisation, N, typically ranges from 10^2 to 10^6.

Polymers are essential and ubiquitous in everyday life and, even though they have been known for less than a century, worldwide production outpaced that of metal. Some factors can explain why. First, plastics can be formed easily. Due to their relatively low melting point and high malleability compared to other materials, they can be shaped in any complex geometry. Additionally, unlike metals, they can be painted or tainted prior to fabrication, which suppresses the need for a post-treatment. And finally, we can mention the chemical resistance of plastics (no oxidation or rusting), light weight compared to metals, and, on equal weight basis, they can be up to 10 times stronger than stainless steel, e.g. Kevlar®[1], Dyneema®[2], or M5®[3] high-performance fibres. The common feature of

[1]DuPont Product information brochure: dupont.com
[2]DSM Product information brochure: dsm.com
[3]see Ref. [Northolt *et al.* (2002)]

these fibres is that they all are made of polymer chains which are highly oriented and stretched. This feature was remarkably well anticipated by Ref. [Carothers & Hill (1932)], decades before their actual fabrication. Understanding, from a theoretical standpoint, the orientation and stretching of polymer chains is key to predicting their material properties.

Other than orienting and stretching the polymeric chains, recent developments explored the possibility to build supramolecular polymers [de Greef & Meijer (2008); Rubinstein & Dobrynin (1999); Rubinstein & Semenov (1998)]. While classical polymers, as those mentioned above, are long chains of repeating units connected by covalent (chemical) bonds, supramolecular polymers add a "layer" of complexity by allowing polymer chains to be held together by reversible, i.e. non-covalent (physical), and highly directional interactions, e.g. hydrogen bonds or metal-ligands. Reversible networks can be self-healing [Bergman & Wudl (2008); Binder (2013); Cordier *et al.* (2008); Williams *et al.* (2008)]. Restoration of the initial material properties after an external stimulus is achieved thanks to the presence of a dynamical structure. This new type of polymer architecture is the focus of Chapter 2 and Part II of this thesis.

1.1.2 Polydispersity

It is practically impossible for chemists to make large polymer molecules which are identical in their mass and branching; there will always be a distribution of these quantities in real polymeric materials. Polydispersity is the degree of dispersion of the mass distribution of the molecules synthesised. Most of the time, chemists wish for a polydispersity as low as possible, but sometimes a larger polydispersity is desirable for easy polymer processing.

Calling M_0 the molar mass of the monomer unit, and N the degree of polymerisation of the chain, then $M = NM_0$ is the molar mass of that polymer chain.

Due to synthesis methods, the polymers chains obtained have different degrees of polymerisation N, and therefore different molar masses M. Calling p_i the probability that, if one chooses a *molecule* at random, it will be a polymer of size N_i, then the number-average degree of polymerisation is

$$N_n \equiv \sum_i N_i \, p_i, \tag{1.1}$$

where $\sum_i$ is a shorthand notation for a sum over all possible values of N. The weight-average degree of polymerisation is defined as

$$N_w \equiv \frac{\sum_i N_i^2 \, p_i}{\sum_i N_i \, p_i}. \tag{1.2}$$

We also define, w_i, the probability that, if one chooses a *monomer* at random, it will belong to a polymer of size N_i

$$w_i \equiv \frac{N_i \, p_i}{N_n}, \tag{1.3}$$

and Equation (1.2) can be written as

$$N_w = \sum_i N_i w_i, \tag{1.4}$$

which defines the weight-average degree of polymerisation. Finally, we define the number-average and weight-average molar mass as

$$M_n \equiv \sum_i M_i \, p_i, \quad \text{and} \quad M_w \equiv \sum_i M_i \, w_i, \tag{1.5}$$

respectively, being Equations (1.1), and (1.4) multiplied by M_0. The ratio between these two quantities defines the polydispersity index (PDI) of the sample,

it is written Đ:

$$Đ \equiv \frac{M_w}{M_n} = \frac{N_w}{N_n}. \tag{1.6}$$

A perfectly monodisperse sample has $Đ = 1$ and, the greater $Đ$, the more polydisperse the sample is.

1.1.3 Rheology

Stress and deformation

Rheology is the study of mechanical and flow properties of materials. It aims at understanding the stress within a material and how this relates to its history of deformation. We may imagine (virtually) dividing a material into two parts, with a surface $\mathcal{S}$ in between (see Figure 1.2 left). The top part of the material applies a force F on the lower half, through the surface $\mathcal{S}$, while the bottom part applies an opposite force $-F$ on the upper half. We define $\sigma(t) = F/\mathcal{S}$ to be the force acting between the layers of material, per unit surface, measured in Pascal (Pa).

The schematic representations described above, and in Figure 1.2, are an oversimplification of the reality. Indeed, σ is a local quantity which can vary through the material if the deformation is not uniform – which means that $\mathcal{S}$ is infinitesimal. Additionally, the surface $\mathcal{S}$ can be chosen in the three different directions (perpendicular to each of the axes), and given the three possible components of the force F, we need to define stress to be a tensorial quantity with, in principle, nine components. The strain (deformation) of the material, γ, is also a tensorial quantity where each component relates to the amplitude of deformation between two points (relative displacement) per unit distance between them. When the displacement is perpendicular to the line joining these points, it is called shear deformation; when it is parallel, it is called elongational deformation, though in generality deformations can be of mixed character between shear and elongation.

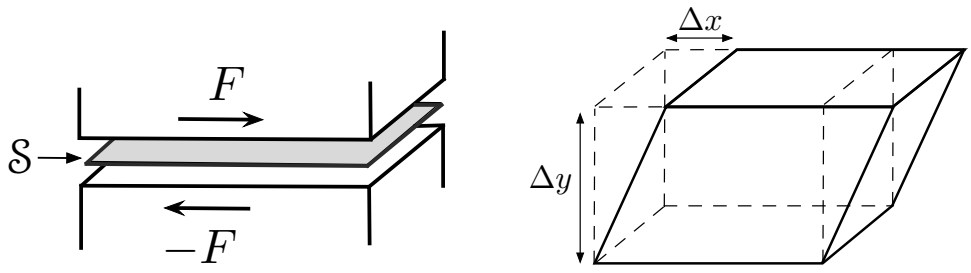

Figure 1.2: Left: Shear stress is the force F divided by the surface $\mathcal{S}$. Right: Shear deformation, relative displacement Δx of two points separated by a distance Δy, $\gamma = \Delta x/\Delta y$.

The local rate of deformation is found from gradients of the velocity field, $\boldsymbol{v}(\boldsymbol{r}, t)$, and is called the velocity gradient tensor, or deformation rate tensor

$$\underline{\underline{\boldsymbol{\kappa}}}(\boldsymbol{r}, t) \equiv (\boldsymbol{\nabla}\boldsymbol{v})^T. \tag{1.7}$$

The symmetric part of equation Equation (1.7) represents deformation: the strain rate tensor

$$\underline{\underline{\boldsymbol{D}}} \equiv \frac{1}{2}(\underline{\underline{\boldsymbol{\kappa}}} + \underline{\underline{\boldsymbol{\kappa}}}^T). \tag{1.8}$$

The antisymmetric part of equation Equation (1.7) represents rotation: the vorticity tensor

$$\underline{\underline{\boldsymbol{\Omega}}} \equiv \frac{1}{2}(\underline{\underline{\boldsymbol{\kappa}}} - \underline{\underline{\boldsymbol{\kappa}}}^T). \tag{1.9}$$

From these definitions, we see that $\underline{\underline{\boldsymbol{\kappa}}} = \underline{\underline{\boldsymbol{D}}} + \underline{\underline{\boldsymbol{\Omega}}}$.

Linear viscoelasticity

In a purely viscous fluid, also called Newtonian fluid, the stress is proportional to the derivative of strain with respect to time, known as the *strain rate*. For a

pure shear deformation, the (Newtonian) shear stress is

$$\underline{\underline{\boldsymbol{\sigma}}}^{\mathrm{N}} = 2\eta \underline{\underline{\boldsymbol{D}}}, \tag{1.10}$$

where η is the fluid viscosity. Likewise, for small strains, a purely elastic material (rubber) is characterised by a proportionality constant, G, called the elastic modulus, that relates stress and strain. For a pure shear deformation, the (rubbery) shear stress is given as:

$$\underline{\underline{\boldsymbol{\sigma}}}^{\mathrm{R}} = G \underline{\underline{\boldsymbol{B}}}, \tag{1.11}$$

where $\underline{\underline{\boldsymbol{B}}} \equiv \underline{\underline{\boldsymbol{F}}} \cdot \underline{\underline{\boldsymbol{F}}}^{T}$ is the *Finger tensor*, and $\underline{\underline{\boldsymbol{F}}}$ is the deformation gradient tensor that defines the relationship between a vector $\boldsymbol{r}_0$ connecting any two material points P and Q before, and vector $\boldsymbol{r}$ linking the same material points after the deformation as $\boldsymbol{r} = \underline{\underline{\boldsymbol{F}}} \cdot \boldsymbol{r}_0$ (cf. Chapter 1.4 of Ref. [Macosko (1994)]).
Under a simple shear deformation the xy-component of Equations (1.10) and (1.11) reduce to

$$\sigma^{\mathrm{N}}(t) = \eta \frac{\mathrm{d}\gamma}{\mathrm{d}t}, \qquad \text{and} \qquad \sigma^{\mathrm{R}}(t) = G\gamma(t), \tag{1.12}$$

with γ the strain.

In reality, for an elastic material under strong deformation, the proportionality "constant" varies with the deformation. Similarly, non-Newtonian viscous fluids often have a viscosity which is dependant on the rate of deformation. Most real materials are intermediate between viscous liquids and elastic solids. To characterise a material, we can consider a small constant shear deformation applied at $t = 0$, such that $\gamma(t) = \gamma_0$ for $t \geq 0$. In general, the stress response will depend on the time following the initial deformation. Defining the scalar shear

stress response to be $\sigma(t)$, we define the relaxation modulus $G(t)$ as

$$G(t) \equiv \frac{\sigma(t)}{\gamma_0}. \tag{1.13}$$

For a more general and non-constant shear strain which depends on time, but in which the stress response remains linear in the applied strain (i.e. small deformations), the Boltzmann superposition principle may be formulated as follows: *the action on a material (stress or strain) can be decomposed in many sub-actions; the total response of the material is the sum of its responses to the sub-actions.* Consequently, the integral form of the stress response to a strain is in general

$$\underline{\underline{\boldsymbol{\sigma}}}(t) = \int_{-\infty}^{t} G(t-t') 2\underline{\underline{\boldsymbol{D}}}(t')\,\mathrm{d}t', \tag{1.14}$$

and in one dimension (simple shear)

$$\sigma(t) = \int_{-\infty}^{t} G(t-t') \frac{\mathrm{d}\gamma(t')}{\mathrm{d}t'}\,\mathrm{d}t'. \tag{1.15}$$

In the particular case leading to Equation (1.13), the deformation, $\gamma(t')$, is a Heaviside function, giving a Dirac function of weight γ_0 as its derivative. However, the more general Equation (1.14) allows us to compute the stress related to any history of deformation, once we know the relaxation modulus $G(t)$.

Oscillatory rheology

Small strain oscillatory shear is an important and common experiment. The sample is deformed sinusoidally at a frequency ω, and within a few cycles of start-up and often much less, the stress will also oscillate sinusoidally at the same frequency but in general will be shifted by a phase angle, δ, with respect to the

strain wave. This is expressed as follows: the strain takes the form

$$\gamma(t) = \gamma_0 \sin \omega t, \tag{1.16}$$

and the stress

$$\sigma(t) = \sigma_0 \sin(\omega t + \delta). \tag{1.17}$$

Such data are analysed by decomposing the stress wave into two waves of the same frequency, one in phase with the strain wave and one 90° out of phase with this wave. Hence, we write

$$\begin{aligned} \sigma &= \sigma' + \sigma'' \\ &= \sigma'_0 \sin \omega t + \sigma''_0 \cos \omega t, \quad \text{with} \quad \tan \delta \equiv \sigma''_0/\sigma'_0, \end{aligned} \tag{1.18}$$

which suggests, using Equation (1.13), two dynamic moduli

$$G' \equiv \sigma'_0/\gamma_0, \quad \text{and} \quad G'' \equiv \sigma''_0/\gamma_0, \quad \text{with} \quad \tan \delta = G''/G'. \tag{1.19}$$

G' is the in-phase component, called *elastic modulus* or *storage modulus*, while G'' is the out-of-phase component, called *viscous modulus* or *loss modulus*.

Using Equations (1.15), (1.16) and (1.19) and trigonometric formulae, one obtains

$$G'(\omega) = \omega \int_0^\infty G(t') \sin \omega t' \, \mathrm{d}t', \quad \text{and} \quad G''(\omega) = \omega \int_0^\infty G(t') \cos \omega t' \, \mathrm{d}t'. \tag{1.20}$$

Typically, the experiment is done at a range of different frequency, ω, and is hence called a *frequency sweep* experiment.

Now, suppose that $G(t)$ is an exponential decay with characteristic time τ,

i.e.

$$G(t) = G_0 \exp(-t/\tau), \tag{1.21}$$

which is the so-called *Maxwell model*. Then, Equation (1.20) yields the storage and loss modulus as

$$G'(\omega) = G_0 \frac{\omega^2\tau^2}{1+\omega^2\tau^2}, \quad \text{and} \quad G''(\omega) = G_0 \frac{\omega\tau}{1+\omega^2\tau^2}. \tag{1.22}$$

A logical improvement on this model in treating real materials is to try several relaxation times, τ_i. The relaxation modulus can be written as a series of exponential decays multiplied by weighting constants g_i as

$$G(t) = \sum_i g_i \exp(-t/\tau_i), \tag{1.23}$$

where the sum runs over all the modes. When substituted in Equation (1.20), this gives the *general viscoelastic model*

$$G'(\omega) = \sum_i g_i \frac{\omega^2\tau_i^2}{1+\omega^2\tau_i^2}, \quad \text{and} \quad G''(\omega) = \sum_i g_i \frac{\omega\tau_i}{1+\omega^2\tau_i^2}. \tag{1.24}$$

Note that most real materials can be modelled as a sum of a set of Maxwell modes in their small strain response, however the non-uniqueness of $\{\tau_i, g_i\}$ required to describe a given material can be an issue [Baumgaertel & Winter (1992); Friedrich *et al.* (1996); Honerkamp (1989)].

1.2 Modelling polymeric materials

1.2.1 Universality

The chain conformation, i.e. the structure of the polymer chain in space, is obviously dependent on the chemical properties of the chain elements, but also on the interaction with the surrounding media (other chains, solvent) and with itself.

At small scale, the structure of the polymer is more or less simple and regularly organised. Nevertheless, consecutive segments of the chain have some degree of freedom, which depends on the chemical nature of the chain. On larger scale, the effect is universal, and flexible polymeric chains all adopt a similar distribution of shapes. This large scale conformation distribution is the static effect of the large number of monomers, each having some degrees of freedom. Despite the fact that the local structure differs from one polymer to another, the typical set of conformations adopted by all flexible polymers is the same, as Flory showed [Flory (1969)]. Static properties common to all polymers and the theoretical link between the physics of polymers and critical phenomena are the support for the scaling law approach adopted by de Gennes[1].

1.2.2 Gaussian chain

Properties

Polymer molecules are long chains composed from repeat units linked together. As a consequence of the rotational flexibility of these links, the orientation correlation between neighbouring units in flexible polymers decays over a small number of monomeric units. This decay length is called the *persistence length*. For instance, it is equal to roughly four carbon-carbon bonds in polyethylene. On length

[1] see chapter X of Ref. [de Gennes (1979)]

scales larger than the persistence length, the polymer chain may be modelled as a freely-jointed chain.

Considering a polymeric chain made of N freely-jointed segments of effective bond length b, the spatial configuration of the chain can be modelled by a random walk in which each neighbouring segment has uncorrelated orientation. Therefore, the average end-to-end vector, $\boldsymbol{R}$, of a freely-jointed polymer chain is

$$\langle \boldsymbol{R} \rangle = \boldsymbol{0}, \tag{1.25}$$

where $\langle \cdot \rangle$ is the average over the chain configurations. The mean square end-to-end distance of a freely-jointed polymer chain is

$$\left\langle \boldsymbol{R}^2 \right\rangle = Nb^2. \tag{1.26}$$

The probability distribution of the end-to-end vector, $\boldsymbol{R}$, of an ideal random walk of N steps of length b is

$$p(N, \boldsymbol{R}) = \left(\frac{3}{2\pi N b^2} \right)^{3/2} \exp\left(-\frac{3\boldsymbol{R}^2}{2Nb^2} \right), \quad |\boldsymbol{R}| \ll Nb. \tag{1.27}$$

Note that the Gaussian probability is non-zero for end-to-end vectors larger than the maximum length, Nb, of the chain, which is unphysical, so Equation (1.27) only applies for $|\boldsymbol{R}| \ll Nb$.

Entropic force

One can derive the free energy, $\mathcal{F}$, of the polymer chain from the Gaussian probability density function [McLeish (2002)]

$$\mathcal{F}(\boldsymbol{R}) = U - TS, \tag{1.28}$$

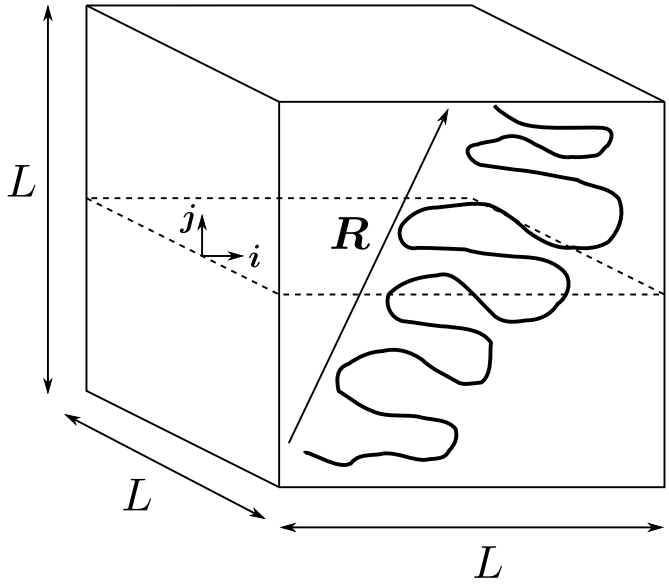

Figure 1.3: Contribution of a single chain segment to the stress tensor. The polymer carries a tension across the surface of normal $\boldsymbol{j}$. Adapted from Ref. [McLeish (2002)].

where U is the internal energy ($U = 0$ here as there is no source of internal energy), T is the temperature, and $S = \text{const.} + k_\text{B} \ln p(N, \boldsymbol{R})$ is the entropy of the system, with p given by Equation (1.27). The thermodynamic force, $\boldsymbol{f}$, (Brownian tension) on the chain end-to-end vector is given by

$$\begin{aligned} \boldsymbol{f}(\boldsymbol{R}) &= -\boldsymbol{\nabla}\mathcal{F}(\boldsymbol{R}) \\ &= -\frac{3k_\text{B}T}{Nb^2}\boldsymbol{R} \\ &= -k\boldsymbol{R}. \end{aligned} \tag{1.29}$$

We recognize a linear elastic spring law: a random walk is a Hookean spring with spring constant $k = 3k_\text{B}T/Nb^2$. The change in entropy in a polymer chain causes it to exert a force when deformed.

Polymeric stress

In Figure 1.3, a polymer chain with end-to-end vector $\boldsymbol{R}$, is in an elementary volume L^3, and the chain carries a tension, $\boldsymbol{f}(\boldsymbol{R})$, described by Equation (1.29). Given that:

(i) according to Equation (1.29), the i^{th} component of the force transmitted by this chain across the plane is $f_i = 3k_{\text{B}}TR_i/Nb^2$;

(ii) a chain will cross a plane with normal in the j-direction with probability R_j/L;

(iii) a box of size L^3 contains n_M/N polymer chains, where n_M is the number of monomers per unit volume[1] (i.e. there are $n_M L^3/N$ polymer chains in L^3);

the total stress tensor reads

$$\begin{aligned} \sigma_{ij} &= \frac{n_M}{N}\left\langle f_i R_j \right\rangle \\ &= \frac{3k_{\text{B}}T}{N^2b^2} n_M \left\langle R_i R_j \right\rangle , \end{aligned} \tag{1.30}$$

where $\langle \cdot \rangle$ denotes the configurational average. Note that equilibration below the largest length scale of the chain should be achieved for the above expression to hold, i.e. all modes apart from end-to-end vector are equilibrated.

1.2.3 The dumbbell model

The dumbbell model is one of the simplest models used to describe the nonlinear rheology of a dilute solution of polymer chains. We will illustrate, at the end of this Section, how we can use it to predict nonlinear rheology in simple flow (uniaxial extension and shear), and use a multi-mode version of that model in

[1] Notation "n_M" according to Ref. [Larson *et al.* (2003)]

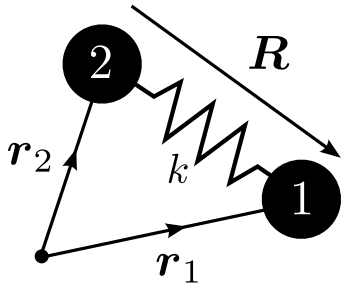

Figure 1.4: Dumbbell model. Two beads in position $\boldsymbol{r_1}$ and $\boldsymbol{r_2}$ are linked with a spring of stiffness k, and $\boldsymbol{R} \equiv \boldsymbol{r_1} - \boldsymbol{r_2}$.

Section 2.6 to predict, from the linear rheology data, the elongational viscosity of a supramolecular polymeric material.

Derivation of the model

The dumbbell model considers a real polymer of N monomers of length b, and that all drag forces are acting at the ends of the polymer chain. As presented in Figure 1.4, the polymer is then modelled as two beads linked with a spring of stiffness $k = 3k_{\mathrm{B}}T/Nb^2$, see Equation (1.29). Considering that the fluid surrounding the polymer moves with a velocity $\boldsymbol{u}(\boldsymbol{r_i})$ at the point $\boldsymbol{r_i}$, each bead experiences a drag force proportional to the difference between its velocity $\boldsymbol{v_i} = \frac{\mathrm{d}\boldsymbol{r_i}}{\mathrm{d}t}$ and $\boldsymbol{u}(\boldsymbol{r_i})$, with constant of proportionality given by the friction coefficient, ζ. We also consider the thermal force on each bead, $\boldsymbol{f_{\mathrm{th}}}$, which arises from the random collision of the (small) beads with the molecules of the solvent. This thermal force is considered as a Gaussian white noise. We apply the fundamental principle of dynamics to find the coupled equations of motion of the two beads, and neglect inertia effects, to find

$$\zeta\left(\frac{\mathrm{d}\boldsymbol{r_1}}{\mathrm{d}t} - \boldsymbol{u}(\boldsymbol{r_1})\right) = k\left(\boldsymbol{r_2} - \boldsymbol{r_1}\right) + \boldsymbol{f_{\mathrm{th,1}}}, \tag{1.31}$$

$$\zeta\left(\frac{\mathrm{d}\boldsymbol{r_2}}{\mathrm{d}t} - \boldsymbol{u}(\boldsymbol{r_2})\right) = k\left(\boldsymbol{r_1} - \boldsymbol{r_2}\right) + \boldsymbol{f_{\mathrm{th,2}}}. \tag{1.32}$$

We define the end-to-end vector $\boldsymbol{R} \equiv \boldsymbol{r_1} - \boldsymbol{r_2}$, see Figure 1.4.

Using the dimensionless tensor $\underline{\underline{\boldsymbol{A}}} \equiv 3\langle \boldsymbol{RR} \rangle / Nb^2$, the dumbbell model reduces to

$$\frac{\mathrm{D}\underline{\underline{\boldsymbol{A}}}}{\mathrm{D}t} = \underline{\underline{\boldsymbol{\kappa}}} \cdot \underline{\underline{\boldsymbol{A}}} + \underline{\underline{\boldsymbol{A}}} \cdot \underline{\underline{\boldsymbol{\kappa}}}^T - \frac{1}{\tau}(\underline{\underline{\boldsymbol{A}}} - \underline{\underline{\boldsymbol{I}}}). \tag{1.33}$$

The tensor $\underline{\underline{\boldsymbol{A}}}$ is modified by the flow $\underline{\underline{\boldsymbol{\kappa}}}$ and relaxes with a characteristic time $\tau = \zeta/4k$. The derivative $\mathrm{D}/\mathrm{D}t$ is the Lagrangian derivative, or convective derivative, $\partial/\partial t + (\boldsymbol{u} \cdot \boldsymbol{\nabla})$.

The polymeric stress, $\underline{\underline{\boldsymbol{\sigma}}}$, is related to the dimensionless conformation tensor, $\underline{\underline{\boldsymbol{A}}}$, through Equation (1.30), as

$$\begin{aligned} \underline{\underline{\boldsymbol{\sigma}}} &= \frac{3k_\mathrm{B}T}{N^2b^2} n_M \langle \boldsymbol{RR} \rangle \\ &= \frac{k_\mathrm{B}T}{N} n_M \underline{\underline{\boldsymbol{A}}} \\ &= G\underline{\underline{\boldsymbol{A}}}, \end{aligned} \tag{1.34}$$

where $G \equiv n_M k_\mathrm{B} T/N$.

If we assume multiple relaxation modes, τ_i, then there is an equation of form Equation (1.34) for each mode, with relaxation time τ_i, and then the stress is a weighted sum of the $\underline{\underline{\boldsymbol{A}}}$ tensors for each mode multiplied by the modulus, i.e.

$$\underline{\underline{\boldsymbol{\sigma}}} = \sum_i g_i \underline{\underline{\boldsymbol{A_i}}}. \tag{1.35}$$

In the linear rheology regime, this reduces to Equation (1.23).

The above Equation (1.34) together with Equation (1.33) is known as the *upper convected Maxwell model*. Equation (1.33) is solvable analytically for some particular flows. We will derive the solutions for uniaxial elongation flow and simple shear flow in the following sections, and use a multi-mode version of that model in Section 2.6 to predict, from the linear rheology data, the elongational

viscosity of a supramolecular polymeric material.

Uniaxial elongation

We consider a uniaxial elongational flow in the x-direction, with a constant stretch rate $\dot{\varepsilon}$. The velocity gradient tensor is written

$$\underline{\underline{\boldsymbol{\kappa}}} = \begin{pmatrix} \dot{\varepsilon} & 0 & 0 \\ 0 & -\dot{\varepsilon}/2 & 0 \\ 0 & 0 & -\dot{\varepsilon}/2 \end{pmatrix}. \tag{1.36}$$

We solve the differential equations Equation (1.33) with the initial condition $\underline{\underline{\boldsymbol{A}}}(t=0) = \underline{\underline{\boldsymbol{I}}}$, to find

$$\underline{\underline{\boldsymbol{A}}}(t) = \begin{pmatrix} A_{xx}(t) & 0 & 0 \\ 0 & A_{yy}(t) & 0 \\ 0 & 0 & A_{zz}(t) \end{pmatrix}, \tag{1.37}$$

with

$$A_{xx}(t) = \frac{1 - 2\dot{\varepsilon}\tau \exp\left(-\left(1 - 2\dot{\varepsilon}\tau\right) t/\tau\right)}{1 - 2\dot{\varepsilon}\tau}, \tag{1.38}$$

$$A_{yy}(t) = A_{zz}(t) = \frac{1 + \dot{\varepsilon}\tau \exp\left(-\left(1 + \dot{\varepsilon}\tau\right) t/\tau\right)}{1 + \dot{\varepsilon}\tau}. \tag{1.39}$$

The two components A_{yy} and A_{zz} always converge to $(1 + \dot{\varepsilon}\tau)^{-1}$. However, the convergence of A_{xx} depends on how $2\dot{\varepsilon}\tau$ compares to 1. We study the linear/slow-stretch-rate regime, i.e. $\dot{\varepsilon}\tau \ll 1$, in the following paragraph.

Linear regime: If we place the system in a linear regime, i.e. we consider the limit $\dot{\varepsilon}\tau \ll 1$, then the above expressions of $A_{xx},\ A_{yy},\ A_{zz}$ can be approximated

to the first order in $\dot{\varepsilon}\tau$ as

$$A_{xx}(t) \approx \frac{1-2\dot{\varepsilon}\tau\exp\left(-t/\tau\right)}{1-2\dot{\varepsilon}\tau}, \quad \dot{\varepsilon}\tau \ll 1, \tag{1.40}$$

$$A_{yy}(t) = A_{zz}(t) \approx \frac{1+\dot{\varepsilon}\tau\exp\left(-t/\tau\right)}{1+\dot{\varepsilon}\tau}, \quad \dot{\varepsilon}\tau \ll 1. \tag{1.41}$$

We can compute the first normal stress difference N_1, defined as $N_1 \equiv \sigma_{xx} - \sigma_{yy}$, to the first order in $\dot{\varepsilon}\tau$

$$\begin{aligned} N_1(t) &= G\big(A_{xx}(t) - A_{yy}(t)\big) \\ &\approx G\left[\frac{1-2\dot{\varepsilon}\tau\exp\left(-t/\tau\right)}{1-2\dot{\varepsilon}\tau} - \frac{1+\dot{\varepsilon}\tau\exp\left(-t/\tau\right)}{1+\dot{\varepsilon}\tau}\right], \quad \dot{\varepsilon}\tau \ll 1 \\ &\approx 3G\dot{\varepsilon}\tau\big(1-\exp\left(-t/\tau\right)\big), \quad \dot{\varepsilon}\tau \ll 1. \end{aligned} \tag{1.42}$$

Hence, the expression of the tensile stress growth coefficient, η_{E}^{+}, (also known as transient extensional viscosity) in the linear regime

$$\begin{aligned} \eta_{\mathrm{E}}^{+}(t) &\equiv N_1(t)/\dot{\varepsilon} \\ &\approx 3G\tau\big(1-\exp\left(-t/\tau\right)\big), \quad \dot{\varepsilon}\tau \ll 1. \end{aligned} \tag{1.43}$$

The viscosity does not depend on the elongation rate $\dot{\varepsilon}$ as long as the condition $\dot{\varepsilon}\tau \ll 1$ is verified. It depends only on the modulus G and relaxation time τ. Equation (1.43) is known as the linear viscoelastic envelope (LVE) – for this dumbbell model – as it describes the evolution of the transient extensional viscosity in the linear regime.

Simple shear

We place our dumbbell model into a simple shear flow. For a simple shear flow with velocity in the x-direction and shear gradient in the y-direction, the velocity

gradient tensor is

$$\underline{\underline{\boldsymbol{\kappa}}} = \begin{pmatrix} 0 & \dot{\gamma} & 0 \\ 0 & 0 & 0 \\ 0 & 0 & 0 \end{pmatrix}, \tag{1.44}$$

where $\dot{\gamma} \equiv \mathrm{d}\gamma/\mathrm{d}t$ is the constant applied shear rate. We find the analytic solution of Equation (1.33) by solving the differential equations with the initial condition $\underline{\underline{\boldsymbol{A}}}\,(t=0) = \underline{\underline{\boldsymbol{I}}}$. We obtain

$$\underline{\underline{\boldsymbol{A}}}(t) = \begin{pmatrix} A_{xx}(t) & A_{xy}(t) & 0 \\ A_{xy}(t) & 1 & 0 \\ 0 & 0 & 1 \end{pmatrix}, \tag{1.45}$$

with

$$A_{xx}(t) = 1 + 2\dot{\gamma}^2\tau^2\big(1 - \exp\left(-t/\tau\right)\big) - 2\dot{\gamma}^2\tau t \exp\left(-t/\tau\right), \tag{1.46}$$

$$A_{xy}(t) = \dot{\gamma}\tau\big(1 - \exp\left(-t/\tau\right)\big). \tag{1.47}$$

Note that here the two components A_{xx} and A_{xy} are convergent, independently of the value of the shear rate $\dot{\gamma}$. The model predicts a first normal stress difference

$$N_1(t) = 2G\dot{\gamma}^2\tau^2\big(1 - \exp\left(-t/\tau\right)\big) - 2G\dot{\gamma}^2\tau t \exp\left(-t/\tau\right), \tag{1.48}$$

and a shear stress growth coefficient, η^+, (also known as transient shear viscosity)

$$\eta^+(t) \equiv \frac{\sigma_{xy}(t)}{\dot{\gamma}} = G\tau\big(1 - \exp\left(-t/\tau\right)\big). \tag{1.49}$$

We note that similarly to the elongation case, the transient shear viscosity only depends on the modulus G and the characteristic relaxation time τ. We also note that η^+ is three times smaller than η_E^+, cf. Equation (1.43). Hence, the Trouton ratio [Trouton (1906)], defined as the ratio of extensional viscosity to shear viscosity, is 3 in the linear regime.

1.2.4 The Rouse model

Description of the Rouse model

The Rouse model first appeared in a 1953 paper by P. E. Rouse [Rouse (1953)], and it describes the conformational dynamics of an ideal chain. In this model, the single chain diffusion is represented by Brownian motion of beads connected by harmonic springs, i.e. "multiple dumbbells". There are no excluded volume interactions between the beads and each bead is subjected to a random thermal force and a drag force as in Langevin dynamics [Langevin (1908)]. We can summarize the model's ideas as follows [de Gennes (1971)]:

(i) ideal chain: bead-springs obeying Gaussian statistics;

(ii) phantom chain: the chain *can* "cross itself";

(iii) locality: each bead experiences forces from its two neighbours.

Figure 1.5 is a schematic view of the Rouse model with N beads, and springs connecting them. The average distance between them is b (see Section 1.2.2). In the following, we present scaling arguments to derive the expression of the dynamic modulus, $G(t)$. One should refer to, e.g., [Doi & Edwards (1988)], for an exact solution that we briefly outline at the end of this Section.

Scaling in the Rouse model

To move a distance R, the red bead, see Figure 1.5, has to drag with it all other connected beads in the "sphere" of size R. Since the beads undergo a random walk of step length b, it follows that the number, n, of beads correlated with the movement of the red one over a distance R is

$$n = \frac{R^2}{b^2}. \tag{1.50}$$

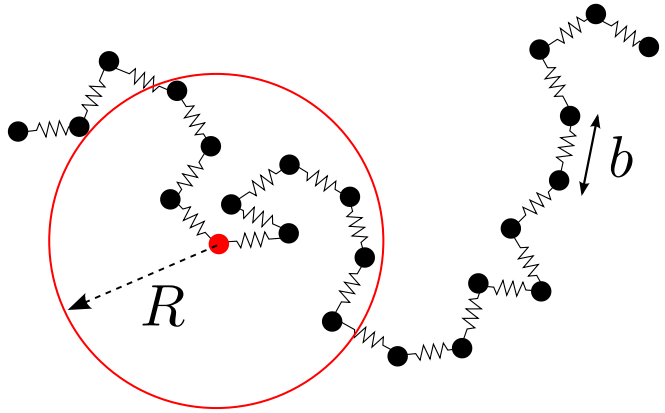

Figure 1.5: Schematic view of the Rouse model with N beads and springs connecting them. The average distance between them is b.

The total total friction involved is $\zeta' = n\zeta$, where ζ is the friction experienced by one monomer. The diffusion coefficient of one bead is given by the Einstein relation $D = k_{\mathrm{B}}T/\zeta$. Now, the effective diffusion coefficient of the red bead when moving a distance R is

$$D' = \frac{k_{\mathrm{B}}T}{\zeta'} = \frac{k_{\mathrm{B}}T}{n\zeta}. \tag{1.51}$$

Calling t the time needed by the red bead to move a distance R, we have the

relation $R^2 = D't$, which, using Equation (1.51), gives

$$\begin{aligned} R^2 &= \frac{k_B T b^2}{R^2 \zeta} t \\ R^4 &= b^4 \frac{t}{\tau_{bead}}, \end{aligned} \tag{1.52}$$

where $\tau_{bead} \equiv b^2\zeta/k_B T$. Given that $R^2 = nb^2$, it follows that the number of beads correlated with the motion of the red bead over time, t, is

$$n(t) = \left(\frac{t}{\tau_{bead}}\right)^{1/2}. \tag{1.53}$$

Using the definition of $G(t)$ [Doi & Edwards (1988)]:

$$G(t) \approx \frac{n_M}{N} k_B T \times (\text{number of stress carrying objects in chain}), \tag{1.54}$$

we obtain, using Equation (1.53),

$$\begin{aligned} G(t) &\approx \frac{n_M}{N} k_B T \frac{N}{n(t)} \\ &\propto t^{-1/2}. \end{aligned} \tag{1.55}$$

Figure 1.6 sketches the characteristic shape of the dynamic modulus as a function of time in a log-log scale. The prediction is that the dynamic modulus decays over time with a slope of $-1/2$. After a time τ_R, defined in the next paragraph, the entire chain relaxes, hence the final decay of $G(t)$.

Exact solution of the Rouse model

Having outlined the scaling argument above, we present succinctly the exact solution of the Rouse model [Doi & Edwards (1988)]. It gives a set of "modes"

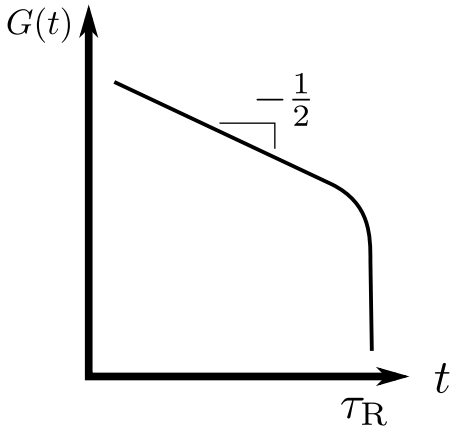

Figure 1.6: Dynamic modulus function of time in log-log scale from the Rouse scaling argument Section 1.2.4.

of relaxation, with timescales $\tau_p = \tau_{\mathrm{R}}/p^2$, with

$$\tau_{\mathrm{R}} = \frac{\zeta N^2 b^2}{3\pi^2 k_{\mathrm{B}} T}, \tag{1.56}$$

the longest relaxation time, also called Rouse time. It is the time for relaxation of the overall shape of the molecule. The Rouse time has a special significance. On timescales shorter than τ_{R}, the chain exhibits viscoelastic modes (see Equation (1.57)). However, on timescales longer than τ_{R}, the stress response of the chains to flow is simply viscous.

In nonlinear flow, each Rouse mode acts like a "dumbbell", so that the stress is a sum over dumbbell modes (of form Equation (1.33)) with different relaxation times but equal modulus. For polymer melts, at long times, the Rouse chains can be regarded as being composed of N flexible segments, referred to as Rouse segments, and the Rouse relaxation modulus can be written as [Barlow *et al.* (1964); Ferry (1980)]

$$G(t) = \frac{\rho RT}{M} \sum_{p=1}^{N} \exp\left(-p^2 t/\tau_{\mathrm{R}}\right), \tag{1.57}$$

with RT the thermal energy per mole of material, ρ the polymer density, M the chain molecular mass. Note that this equation gives exactly the form of $G(t)$ sketched in Figure 1.6.

The Rouse model gives a first insight on the spectrum of relaxation times that arises due to the connectivity of polymer chains. It is regarded as an appropriate model for short, unentangled, chains in a polymer melt (no solvent), but not for dilute solutions because it neglects hydrodynamic interactions, unlike the Zimm model[1] – not discussed here.

1.2.5 Entanglements

So far we have not considered the chain-chain interactions that arise at high chain concentration, i.e. topological constraints or entanglement effects. As thread-like objects, polymer chains are subject to entanglements. However, due to their small size, thermal agitation plays a crucial role on polymer chains. Hence, the properties of entangled polymers are more complex than those of macroscopic objects where thermal fluctuations are negligible.

The models presented in the previous Sections 1.2.3 and 1.2.4 are valid for a single chain in solution. When one increases the number of such dumbbells or Rouse chains, interactions will occur due to the very nature of the polymer: they *cannot* cross each other. This topological constraint is known as the *entanglement effect*. For linear polymers and simple branched polymers (as compared to rings), this does not affect the static properties since all configurations are accessible [Gay (1997)]. On the other hand, the dynamical properties will be highly perturbed as entanglements provide constraints on the motion of polymers. While a precise definition of an entanglement has not been generally agreed upon, we consider that an entanglement is a topological interaction between one polymer molecule

[1] see section 4.2 of Ref. [Doi & Edwards (1988)]

and its neighbours that greatly impedes its motion and thus its ability to relax after a deformation is imposed [Dealy & Larson (2006)].

Reptation

To account for entanglement effects, the most successful theoretical approach is the "tube model" of de Gennes and Doi & Edwards [de Gennes (1971); Doi & Edwards (1988)]. The main idea of the tube theory is that polymers cannot move perpendicular to their own contour as this motion would involve the motion of several other of their neighbours at the same time (to avoid chain crossing). However, the motion of a polymer along its own contour is much easier and does not require crossing other chains. This gives rise to the idea that each polymer is confined within a tube-like region where the major mode of motion is reptation [de Gennes (1971)], i.e. random thermal motion along the tube.

The tube follows the coarse-grained conformation of the polymer chain, the *primitive path*. In molecular dynamics simulations of polymers, the primitive path is (virtually) obtained by taking the average over configurations of chains over short times [Bisbee *et al.* (2011); Kremer & Grest (1990); Likhtman (2014)], or via chain-shrinking methods [Everaers *et al.* (2004); Kröger (2005); Tzoumanekas & Theodorou (2006); Zhou & Larson (2005)] – see chapter 6 of Ref. [Dealy & Larson (2006), second edition], or Ref. [Masubuchi *et al.* (2008)] for more details. Therefore, the tube has a random walk (or random flight) configuration but the *tube diameter*, a_0, is much larger than the diameter of the polymer molecule, and also larger than the effective segment length, b, of the polymer chain. For a flexible polymer molecule, the diameter of the tube, a_0, is taken to be equal to the random walk step length of the tube, and a single random walk step of the tube is called a *tube segment*. It can be shown that the tube diameter, a_0, is

related to the average distance between entanglements (at equilibrium) as

$$a_0^2 = N_e b^2, \tag{1.58}$$

where $N_e \equiv M_e/M_0$ is the average number of chain segments of length b between two entanglements, M_e is the entanglement molar mass, i.e. average molar mass between two entanglements, and M_0 is the molar mass of a chain segment of length b. Note that the details of the chain structure and dynamics at length scales smaller than a_0 are described by the Rouse model, Section 1.2.4, since entanglement effects are then irrelevant.

The motion of a chain, composed of N segments, inside its tube is analogous to a unidimensional diffusion. The friction constant, ζ_{tube}, is proportional to the chain length: $\zeta_{tube} = N\zeta$, where ζ is the monomer friction coefficient. Hence, the diffusion coefficient is inversely proportional to N: $D_{tube} = k_B T/\zeta_{tube} \propto 1/N$. The characteristic time needed for the chain to renew its primitive path (new tube), i.e. the time needed for the chain to move a distance equal to its length, is called *reptation time*, or *disengagement time*, τ_d. Since the tube length is $L_{tube} = Za_0$, with $Z \equiv N/N_e$ the entanglement number, we have

$$\begin{aligned} \tau_d \approx \frac{L_{tube}^2}{D_{tube}} &= \frac{(Za_0)^2}{k_B T/N\zeta} \\ &= \frac{N^3 b^2 \zeta}{k_B T N_e} \propto N^3. \end{aligned} \tag{1.59}$$

This simple argument shows that entangled polymers can have huge characteristic relaxation times. We can compare this expression of the reptation time with the

Rouse time, Equation (1.56). The ratio is

$$\begin{aligned} \frac{\tau_{\mathrm{d}}}{\tau_{\mathrm{R}}} &\approx \frac{N^3 b^2 \zeta}{k_{\mathrm{B}} T N_{\mathrm{e}}} \frac{3\pi^2 k_{\mathrm{B}} T}{\zeta N^2 b^2} \\ &\approx N/N_{\mathrm{e}} = Z. \end{aligned} \tag{1.60}$$

The reptation time becomes much larger than the Rouse time for large degree of polymerisation N.

Doi and Edwards [Doi & Edwards (1988)] derived the exact expression for τ_{d}. In reptation the molecule escapes from its tube by sliding back and forth in it, gradually protruding more and more of its mass outside of the tube. Every time a portion of the tube is vacated by the chain, that portion of the tube is "forgotten". The survival fraction, $P(t)$, is the fraction of the tube that remains occupied by the molecule at time t, assuming that the whole chain is in the tube at time zero. An analysis of the reptation process leads to [Doi & Edwards (1988)]

$$P(t) = \frac{8}{\pi^2} \sum_{i_{\mathrm{odd}}} i^{-2} \exp\left(-i^2 t/\tau_{\mathrm{d}}\right), \tag{1.61}$$

with

$$\tau_{\mathrm{d}} = \frac{\zeta N^3 b^4}{\pi^2 k_{\mathrm{B}} T a_0^2}, \tag{1.62}$$

where ζ is the monomeric friction coefficient. The exact form of the ratio Equation (1.60) is thus

$$\frac{\tau_{\mathrm{d}}}{\tau_{\mathrm{R}}} = 3Z. \tag{1.63}$$

Limitations and other relaxation mechanisms

Despite the success of the initial tube theory of de Gennes and Doi & Edwards [de Gennes (1971); Doi & Edwards (1988)] in capturing several aspects of the rheological properties of monodisperse melt of linear chains, some predic-

tions are not in agreement with experimental data. For instance

(i) Experimentally, the zero shear viscosity scales as the molecular weight, M_w, of the chain to the power 3.4, while an exponent 3 is predicted by the model;

(ii) The dependence of the reptation time, τ_d, with the degree of polymerisation, N, of the chain is more complex than Equation (1.59);

To address these issues, the tube theory has been refined to predict quantitatively the linear rheology [Likhtman & McLeish (2002); Milner & McLeish (1998)] and the nonlinear rheology [Graham *et al.* (2003); Marrucci (1996); Mead *et al.* (1998); Read *et al.* (2008)] of a *monodisperse* melt of linear entangled polymers with considerations such as constraint release (CR), contour length fluctuations (CLF) – plus chain stretch and convective constraint release (CCR) in the nonlinear regime. "Toy models" for nonlinear rheology that include these effects have been developed recently. Examples are the Rolie-Poly model [Likhtman & Graham (2003)] (that we use extensively in this thesis), the Mead-Larson-Doi model [Mead *et al.* (1998)], or models by Ianniruberto & Marrucci [Ianniruberto & Marrucci (2002a)]. Finally, we must mention the slip-link based models that, with the progress of computing power, have become a formidable predicting tool, especially in the linear regime [Doi & Takimoto (2003); Likhtman (2005); Schieber *et al.* (2007)].

Industrial polymers embody a broad range of molar masses (chain lengths). Recently, a detailed tube theory for *bidisperse* melt of entangled polymers (long chains blended with short chains) has been developed by Read and co-workers [Read *et al.* (2012)], which successfully describes experiments on bidisperse blends. Building on this work, in Chapter 3, we propose a simplified tube model, based on the Rolie-Poly model [Likhtman & Graham (2003)], for a polydisperse melt of entangled polymers that aims at predicting nonlinear rheology, whilst being

consistent with the "double reptation" theory [des Cloizeaux (1988)] in linear rheology.

1.2.6 Supramolecular polymers

Definition

Amongst the first scientific articles in the field of supramolecular chemistry, we can mention Donald Cram [Cram (1988)], Charles Pedersen [Pedersen (1967)] or Jean-Marie Lehn [Lehn (1995)] who introduced the term "supramolecular chemistry" defined as *the chemistry of molecular assemblies and of the intermolecular bonds*. In the Nobel prize lecture Lehn gave in 1987 he declared [Lehn (1988)]: "*Supramolecular chemistry may be defined as 'chemistry beyond the molecule', bearing on the organized entities of higher complexity that result from the association of two or more chemical species held together by intermolecular forces*". In that definition, he distinguishes the "classic" chemistry (i.e. chemistry of covalent bonds) from the more complex supramolecular chemistry which concerns the organisation of molecules.

Supramolecular chemistry allows for the design of novel materials. Compared to classic polymeric materials (of large molecular mass), supramolecular polymers can be composed of low molar mass polymers that bind together through directional and *non-covalent* interactions, which are reversible and tunable via external stimuli (e.g. temperature, pH, counter-ion).

"Stickers"

There are several different inter- and intramolecular interactions covering binding energies ranging from 1 to 120 kJ/mol with van der Waals forces at the weak-end and coordinate bonds at the strong-end of the scale [Friese & Kurth (2009)],

Table 1.1: Strength of different types of intra- and intermolecular binding energies, adapted from [Friese & Kurth (2009)].

Type of "force"	Strength (kJ/mol)
RT at room temperature	2.5
Van der Waals	1–5
Π-donnor-acceptor	7–20
Hydrogen bonding	10–20
Hydrophobic/hydrophilic	12–15
Ion pairing	12–20
Coordinate bond	40–120
Covalent bond	150–1000

see Table 1.1. We can compare the magnitude of these binding energies to the thermal energy (per mole) $RT = k_{\mathrm{B}}TN_{\mathrm{A}}$, with N_{A} the Avogadro constant.

Hydrogen bonds are the most commonly used supramolecular link [Sijbesma & Meijer (1999)] due to their ubiquitous presence in both synthetic and biological systems (e.g. DNA double helix structure or molecular recognition [Brienne *et al.* (1989); Johnson & Lam (2010)]). Also, hydrogen bonding is directional, temperature controlled (RT is of comparable strength at "high" temperature), and relatively strong compared to other type of non-covalent bonds presented Table 1.1 [Brunsveld *et al.* (2001); Grzybowski *et al.* (2009)].

Since non-covalent bonding can be integrated in any place of the polymer chain, the architecture of supramolecular polymers is versatile. For example, linear polymers can incorporate non-covalent bonding at the chain extremities or as side groups [Feldman *et al.* (2009)].

Rheological models describing some supramolecular systems have been established. The key parameters of these models are (i) the reversible-bond lifetime, (ii) their density or concentration and (iii) structure, i.e. placement of the supramolecular groups, length, and architecture of the polymer chains. We now

summarise a few relevant models in the literature:

Sticky-Rouse model: The dynamics of unentangled reversible networks formed by (usually linear) polymers with many associating groups per chain are described by a modified Rouse model, called the "sticky-Rouse model". Chains move via multiple breaking and reforming of reversible bonds connecting them to each other. These bonds act as effective friction centres of the sticky-Rouse model [Chen *et al.* (2013); Colby *et al.* (1998); Green & Tobolsky (1946); Leibler *et al.* (1991)]. We discuss this model in more detail in Chapter 2, and extend it by proposing a "stochastic" sticky-Rouse model that incorporates (i) the random placement of the stickers along the backbone, (ii) the intrinsic distribution of the number of stickers along the chain, and (iii) a finite size "hop" of the sticker when it detaches and changes partner.

Nonlinear models for unentangled telechelic polymers: Tripathi and coworkers [Tripathi *et al.* (2006)] derived a nonlinear constitutive model for unentangled linear telechelic chains. It is a two-species network model which incorporates mechanisms for the creation and destruction of elastically active chains and account for the contributions of both the bridging chains (those between micelles) and the dangling chains (chains not connected at both ends) to the final stress tensor. The model also quantitatively captures both the shear thickening and subsequent shear thinning observed in the rheology at high deformation rates and predicts transient extensional stress growth curves in close agreement with those measured using a filament stretching rheometer on telechelic polymers.

Similar nonlinear models for unentangled telechelic polymers have been proposed by Tanaka and Edwards [Tanaka & Edwards (1992a;b;c;d)], Vaccaro and Marrucci [Vaccaro & Marrucci (2000)] (inspired partially by the simulation results of van den Brule and Hoogerbrugge [van den Brule & Hoogerbrugge (1995)]),

and more recently, molecular dynamics/Monte Carlo simulations were proposed by Amin and co-workers [Amin *et al.* (2016)].

Sticky reptation model: Leibler and co-workers developed a theory of "sticky reptation" to model the linear rheology and dynamics of entangled solutions of associating entangled polymers with many stickers per chain [Leibler *et al.* (1991)]. At times shorter than the lifetime of a cross-link, such networks behave as elastic rubbers (gels). On longer time scales, the successive breaking of only a few cross-links allows the chain to diffuse along its confining tube. Rubinstein & Semenov [Rubinstein & Semenov (2001)] argued that at high degree of association, there are very few unassociated stickers. It is therefore very difficult for a sticker to find a new partner to associate with after breaking the bond with an old one. In the sticky reptation model, the search for a new partner is restricted to a part of the tube confining the entangled chain.

Entangled telechelic stars: van Ruymbeke and co-workers developed a tube model for the linear rheology of entangled telechelic stars and linear telechelic chains [van Ruymbeke *et al.* (2010)] based on the time-marching algorithm [van Ruymbeke *et al.* (2005)], where they incorporate the association status of the chains via the sticker interactions at each time step. There is good agreement of the predictions with the experimental data which they report, using two adjustable parameters: the average times when two stickers remain associated or free.

To this author's knowledge, nonlinear rheology models for entangled telechelic star polymers are nonexistent in the literature. In Part II, we develop such a model. In Chapter 4, we propose a stochastic model where the evolution of thousands of chains is monitored and the attachment/detachment is a stochastic process, and entanglements are handled using the Rolie-Poly model [Likhtman

& Graham (2003)]. In Chapter 5, we propose a preaveraged version of that model, i.e. we get rid of the stochastic character of the model, based on two tensors (attached and detached chains) and a scalar (instantaneous fraction of attached chains). The predictions of the resulting model closely resembles those of the stochastic one, but it is less demanding computationally and therefore suitable for flow computation. Finally, in Chapter 6, we explore the shear banding properties of the preaveraged constitutive model, demonstrating that it is suitable for nonlinear flow computations.

1.3 Structure of this thesis

In summary, the structure of this thesis is as follows: In Part I we consider two separate rheology models, one (the sticky-Rouse model, in Chapter 2) which is dominated by the sticker dynamics in unentangled chains, and another (polydisperse entangled linear polymers, in Chapter 3) where entanglements govern rheology. In Part II, we develop a nonlinear model which combines the effects of entanglements and stickers, through a stochastic model (Chapter 4), a preaveraged model (Chapter 5), and finally nonlinear flow computation in a shear banding study (Chapter 6). We conclude, in Part III, with a summary of the main achievements of this thesis.

This page is intentionally left blank

Chapter 2

Stochastic sticky-Rouse model

2.1 Introduction

In this Chapter, we present a model aiming at predicting the linear rheology of a melt of unentangled linear polymer chains with stickers along the backbone. Figure 2.1 presents the cartoon of the system we are considering.

This work was initially constructed to model the data obtained by G. Cui on a novel linear polymer composed of a Poly-N-hydroxyethylacrylamide (PEHA) backbone where 2-ureido-4[1H]-pyrimidinone (UPy) monomers were randomly grafted along the backbone as side groups. The UPy groups act as reversible

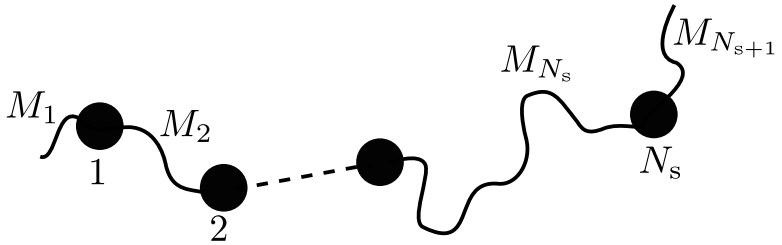

Figure 2.1: Cartoon of the system. N_s stickers are randomly placed along the backbone, separated by chains strands of molar masses M_i, $i = \{1, \ldots, N_s + 1\}$. M_1 and M_{N_s+1} are the molar masses of the two chain-ends.

crosslinks (stickers): they associate pair-wise through hydrogen bonds [Brunsveld *et al.* (2001); de Greef & Meijer (2008); Feldman *et al.* (2009)]. The resulting polymeric system exhibits complex dielectric and viscoelastic properties. In this Chapter, we propose a rheological model that is able to match, at a quantitative level, the experimental linear rheology data (frequency sweep). The entanglement effect is negligible for this system as the chains are "short" ($M_n < M_e$). The model we propose is based on the established sticky-Rouse model, presented in Section 2.2.1, that we modify to account for specific details of the chain structure and its anticipated motion, as discussed in Section 2.2.2.

2.2 Sticky-Rouse model

2.2.1 Presentation of the existing model

The idea of the sticky-Rouse model is to take into account the effect of the breaking and reformation of the reversible crosslinks (stickers) on the viscoelastic response of the system. At time scales longer than the sticker timescale, τ_{as}, the system behaves in a Rouse-like way [Baxandall (1989); Rouse (1953)]. However, it is clear that the stickers delay the terminal response of the stress relaxation when compared to their non-functionalised counterpart, i.e. short linear chain without the "sticky" side groups. The stickers can be seen as an additional drag (or friction) at times shorter that τ_{as}, and therefore can delay the terminal relaxation time [Green & Tobolsky (1946); Leibler *et al.* (1991)].

At this point, we should mention that the relevant sticker lifetime (from a rheological standpoint), called τ_{as} in the rest of the chapter, is the "effective" lifetime of the bond, and not the bare breaking and reformation time of the bond. This "effective" bond lifetime has been described theoretically by Rubinstein & Semenov, see Ref. [Rubinstein & Semenov (1998; 2001)]. The argument for using

an effective lifetime and not the bare chemical bond lifetime (i.e. the average time during which a sticker stays attached) is the following: a sticker that breaks and reforms a bond with the *same partner* will not relax any stress (or very little) because the chain configuration is essentially unchanged. Thus, if the system has a high degree of association, as is the case in "sticky systems", i.e. most of the stickers have a partner, a sticker will not find a new partner easily. In fact, the stickers are more likely to attach and detach to the same "old" partner many times before finding a new partner. Hence, only after a time much longer than the bare lifetime of the sticky bond it will find a new partner to attach to and, only then, stress relaxation occurs. In the rest of this Chapter, τ_{as} refers to the "effective" bond lifetime.

In the sticky-Rouse model, the stress relaxation is split-up into two contributions: from the transient network arising from the stickers, and the Rouse motion of the chain strands between stickers. The relaxation modulus is written as [Baxandall (1989); Chen *et al.* (2013); Leibler *et al.* (1991)]

$$G_s(t) = \sum_i \frac{\rho w_i RT}{M_i} \left[\sum_{p=1}^{N_{\text{s},i}} \exp\left(-tp^2/\tau_{\text{as}} N_{\text{s},i}^2\right) + \sum_{p=N_{\text{s},i}+1}^{N_i} \exp\left(-tp^2/\tau_0 N_i^2\right) \right], \tag{2.1}$$

where the first sum sets the polydispersity of the sample, w_i is the weight fraction of the chain of mass M_i in the i^{th} fraction; the first sum in brackets accounts for the sticky modes where $N_{\text{s},i} = M_i/M_{\text{strand}}$ is the number of strands between sticky groups on the i^{th} chain with M_{strand} the average chain mass between stickers; finally, the last sum accounts for the Rouse modes, see Section 1.2.4, where $N_i = M_i/M_0$ is the number of Rouse monomers per chain, with M_0 the molar mass of a Rouse monomer, and τ_0 is the characteristic relaxation time of a Rouse monomer.

2.2.2 Limitations of the sticky-Rouse model

A limitation of the sticky-Rouse model resides in the fact that it considers all chains to have the same number of stickers, and the stickers to be placed uniformly along the chain backbone. Additionally, it treats the sticky groups as having increased friction, rather than considering finite sized hops of the chain. In real polymers, like the ones synthesised by G. Cui, we expect that:

(i) the number of stickers per chain follows a certain probability distribution characterised by an average number, N_s, of stickers, i.e. some chains have more stickers or less stickers than N_s;

(ii) the stickers are placed randomly along the backbone;

(iii) a sticker finding a new partner will undergo a finite size hop in space.

In the following Sections, we develop a stochastic model based on the existing sticky-Rouse model, whose aim is to address the above mentioned limitations. Firstly, we explain how we generate a population of chains with the features (i) and (ii). Then, we propose a "hop" mechanism to address (iii). Subsequently, we propose a way to compute the stress relaxation function, and thus the elastic and loss moduli, of a system composed by a polydisperse mixture of such chains, and finally we compare our model with frequency-sweep experimental data of PEHA-UPy polymer melts with various sticker concentrations, i.e. samples with different N_s.

2.3 Initialisation of the chains

2.3.1 Placement of stickers on a chain

As a starting point, we consider a linear polymer chain of molar mass M. From rheology and NMR, we can estimate the average number, N_s, of stickers in each chain. The chemical synthesis process suggests that we need to place stickers at random positions along each chain.

From any chosen point on a chain, the molar mass, M_i, to the next sticker follows an exponential distribution (this also gives the distribution of molar mass stickers). The expected value of the molar mass between stickers is given by $M_\mathrm{strand} = M/N_\mathrm{s}$. The probability distribution function of M_i is[1]

$$p(M_i) = \frac{1}{M_\mathrm{strand}} \exp\left(-\frac{M_i}{M_\mathrm{strand}}\right). \tag{2.2}$$

Therefore, from uniformly distributed (pseudo) random numbers, $0 < \theta_i < 1$, we generate the molar masses M_i of the strands of chain between stickers and of the dangling chain-ends, that follow the above probability distribution, by using

$$M_i = -M_\mathrm{strand} \ln(\theta_i). \tag{2.3}$$

Hence, the first sticker is placed after after a chain length M_1, then another sticker is placed after a chain length M_2, etc., until we exceed the given molecular weight of the considered chain, i.e. we stop when $\sum_i M_i > M$, see Figure 2.1.

We generate N_c chains according to this process. Each chain, k, has $N_{\mathrm{s},k}$ stickers distributed along the chain according to the set of strand molar masses connecting them: $\{M_{k,i}\}$, $i = \{1, 2, \ldots, N_{\mathrm{s},k}\}$, see Figure 2.2. It is anticipated that the number of stickers per chain will follow a Poisson distribution with

[1] see Chapter VIII of Ref. [Flory (1953)]

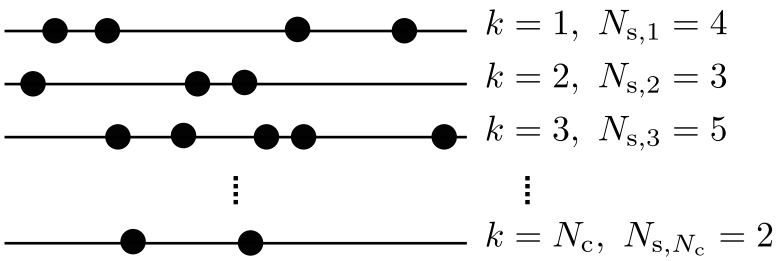

Figure 2.2: Illustrations of a set of N_{c} chains. On each chain k the stickers (black circles) are placed via Equation (2.3).

mean N_{s}.

In the following Section 2.3.2, we present the method used to initialise the spatial configuration of each of the N_{c} chains, now that we have fixed the stickers (randomly) on the chains.

2.3.2 Spatial configuration

This Section is only relevant for the computation of the "sticky" relaxation function, G_{sticky}, which is presented in Section 2.4.2. We do not need to define a spatial configuration to compute the "fast" stress relaxation function, G_{sticky}, in Section 2.4.1.

Each of the N_{c} chains is initialized to have a Gaussian configuration (cf. Section 1.2.2). We start by positioning the first sticker at an arbitrary position, $\boldsymbol{R_0}$, (e.g. $\boldsymbol{R_0} = \boldsymbol{0}$) and define the position of the following sticker, i, (relative to the previous sticker) by subsequently generating a random vector, $\Delta\boldsymbol{R_i}$, sampled from the Gaussian probability distribution (adapted from Equation (1.27))

$$p(\Delta\boldsymbol{R_i}) = \left(\frac{3}{2\pi b^2 N_i}\right)^{3/2} \exp\left(-\frac{3(\Delta\boldsymbol{R_i})^2}{2b^2 N_i}\right), \tag{2.4}$$

where $N_i \equiv M_i/M_0$ is the number of Rouse monomers on the strand connecting the stickers $(i-1, i)$, and M_0 the molar mass of a Rouse monomer. Then, we

place the sticker i at the position $\boldsymbol{R_i}$ such that

$$\boldsymbol{R_i} = \boldsymbol{R_{i-1}} + \Delta\boldsymbol{R_i}. \tag{2.5}$$

2.4 Stress relaxation

We assume that the stickers stay attached, on average, for a time, τ_{as}, much longer than the longest Rouse mode that the chain between stickers would have if relaxing subject to monomer friction alone, i.e. $(N/N_{\text{s}})^2\tau_0 \ll \tau_{\text{as}}$. Consequently, we assume that during the Rouse relaxation process, all stickers stay attached. This allows us to decouple the relaxation due to the internal Rouse motion of the chain segments (delimited by the stickers) from the relaxation due to the motion of the stickers. The total stress relaxation function, $G(t)$, is then split into two contributions

$$G(t) = G_{\text{fast}}(t) + G_{\text{sticky}}(t). \tag{2.6}$$

The first term, G_{fast}, is the contribution of the portions of chain "trapped" between stickers, and that of the dangling ends. It closely resembles the "fast" modes of the sticky-Rouse model of Equation (2.1). We slightly modify it to account for the non-uniform distribution of the stickers, and the dangling ends. We detail the model for G_{fast} in Section 2.4.1. The second term, G_{sticky}, is the contribution of the sticker "motion". The 'hop" model we propose is different from the treatment of the "sticky" modes of Equation (2.1). We detail our model for G_{sticky} in Section 2.4.2.

2.4.1 "Fast" Rouse modes – G_{fast}

Let us consider that the number of chains per unit volume is n_M/N, where N is the degree of polymerisation of the chain, and $n_M = \rho N_{\text{A}}/M_0$ is the number of

Rouse monomers per unit volume, with ρ the polymer density, N_A the Avogadro constant and M_0 the Rouse monomer molar mass. Thus, the "unit of modulus" per chain is

$$\begin{aligned} G^0_\mathrm{chain} &= \frac{n_M k_\mathrm{B} T}{N} \\ &= \frac{\rho RT}{M}, \end{aligned} \tag{2.7}$$

where we used the relation between the gas constant R and the Boltzmann constant k_B, $R = N_\mathrm{A} k_\mathrm{B}$, T is the temperature, and $M = NM_0$ is the chain molar mass.

We have to consider the Rouse relaxation process of the segments "trapped" between two stickers, and that of the "dangling ends" (chain extremities). For each chain k, of molar mass M, we write the relaxation modulus of the "fast" Rouse modes as

$$G_{\mathrm{fast},k}(t) = \frac{\rho RT}{M}\big(G_{\mathrm{trapped},k}(t) + G_{\mathrm{ends},k}(t)\big), \tag{2.8}$$

which then yields the relaxation modulus of the "fast" Rouse modes, averaged over the N_c chains

$$\begin{aligned} G_\mathrm{fast}(t) &= \frac{1}{N_\mathrm{c}} \sum_{k=1}^{N_\mathrm{c}} G_{\mathrm{fast},k}(t) \\ &= \frac{\rho RT}{N_\mathrm{c} M} \sum_{k=1}^{N_\mathrm{c}} \big(G_{\mathrm{trapped},k}(t) + G_{\mathrm{ends},k}(t)\big). \end{aligned} \tag{2.9}$$

Polydispersity

The above Equation (2.9) assumes a perfectly monodisperse system, i.e. all chains have the same molar mass M: the relaxation functions $G_{\mathrm{trapped},k}$ and $G_{\mathrm{ends},k}$ in

Equation (2.9) are specifically defined for a chain of molar mass M.

We can generalise to the polydisperse case. If we assume that the molecular mass distribution is discretised into a set of q modes, $\{(w_\ell, M_\ell)\}$, $\ell = \{1, \dots, q\}$, and that, for the mode ℓ, $N_{\mathrm{c},\ell}$ chains are generated as described in Section 2.3.1, then relaxation modulus of the "fast" Rouse modes is written

$$G_{\mathrm{fast}}(t) = \sum_{\ell=1}^{q} \frac{\rho w_\ell RT}{M_\ell} \frac{1}{N_{\mathrm{c},\ell}} \sum_{k=1}^{N_{\mathrm{c},\ell}} G_{\mathrm{fast},k,\ell}(t). \tag{2.10}$$

In the following paragraphs, we omit, for simplicity, the subscript ℓ.

Trapped chain segments: For each chain k of molar mass M, the strand of chain of molar mass $M_{k,i}$, "trapped" between two stickers, $(i-1)$ and i, behaves as a Rouse chain with both ends fixed, and so relaxes via Rouse modes with relaxation times $\tau_{k,i} = N_{k,i}^2 \tau_0 / p^2$, with $p = \{1, 2, 3, \dots\}$, and $N_{k,i} \equiv M_{k,i}/M_0$ the number of Rouse monomers in the i^{th} strand (of molar mass $M_{k,i}$) of the k^{th} chain. Hence,

$$G_{\mathrm{trapped},k}(t) = \sum_{i=2}^{N_{\mathrm{s},k}} \sum_{p=1}^{N_{k,i}} \exp\left(-\frac{tp^2}{N_{k,i}^2 \tau_0}\right). \tag{2.11}$$

Note that the first sum excludes the chain ends. The second-sum cut-off, $N_{k,i}$, is chosen such that the fastest Rouse mode corresponds to the relaxation time of a Rouse monomer, τ_0.

Chain ends: For each chain k of molar mass M, the two chain-ends of molar masses $M_{k,1}$ and $M_{k,(N_{\mathrm{s},k}+1)}$, cf. Figure 2.1, behave as a Rouse chain with one end free and one end fixed, and so relax with the same Rouse spectrum corresponding to the "odd" modes of a chain twice as long. Thus, the Rouse relaxation times are $\tau_{k,i} = (2N_{k,i})^2 \tau_0 / p^2$, with $p = \{1, 3, 5, \dots\}$. The corresponding relaxation

function is

$$G_{\text{ends},k}(t) = \sum_{i=\{1,N_{\text{s},k}+1\}} \sum_{p=1,\ p_{\text{odd}}}^{N_{k,i}} \exp\left(-\frac{tp^2}{4N_{k,i}^2\tau_0}\right). \tag{2.12}$$

Storage and loss moduli: The expressions for the (dimensionless) storage and loss moduli, for each chain k of molar mass M, are obtained by transforming the sum of Equations (2.11) and (2.12), using Equation (1.20). This gives

$$\begin{aligned} G'_{\text{fast},k}(\omega) &= \sum_{i=2}^{N_{\text{s},k}} \sum_{p=1}^{N_{k,i}} \frac{(\omega N_{k,i}^2\tau_0 p^{-2})^2}{1+(\omega N_{k,i}^2\tau_0 p^{-2})^2} \\ &\quad + \sum_{i=\{1,N_{\text{s},k}+1\}} \sum_{p_{\text{odd}}}^{N_{k,i}} \frac{(4\omega N_{k,i}^2\tau_0 p^{-2})^2}{1+(4\omega N_{k,i}^2\tau_0 p^{-2})^2}, \end{aligned} \tag{2.13}$$

$$\begin{aligned} G''_{\text{fast},k}(\omega) &= \sum_{i=2}^{N_{\text{s},k}} \sum_{p=1}^{N_{k,i}} \frac{\omega N_{k,i}^2\tau_0 p^{-2}}{1+(\omega N_{k,i}^2\tau_0 p^{-2})^2} \\ &\quad + \sum_{i=\{1,N_{\text{s},k}+1\}} \sum_{p_{\text{odd}}}^{N_{k,i}} \frac{4\omega N_{k,i}^2\tau_0 p^{-2}}{1+(4\omega N_{k,i}^2\tau_0 p^{-2})^2}. \end{aligned} \tag{2.14}$$

The expressions of the total elastic and loss moduli from the contribution of the "fast Rouse" motion is obtained by summing over the N_{c} chains of identical molar mass M

$$G'_{\text{fast}}(\omega) = \frac{\rho RT}{M}\frac{1}{N_{\text{c}}}\sum_{k=1}^{N_{\text{c}}} G'_{\text{fast},k}(\omega), \tag{2.15}$$

$$G''_{\text{fast}}(\omega) = \frac{\rho RT}{M}\frac{1}{N_{\text{c}}}\sum_{k=1}^{N_{\text{c}}} G''_{\text{fast},k}(\omega). \tag{2.16}$$

Finally, in the polydisperse case we have, according to Equation (2.10),

$$G'_{\text{fast}}(\omega) = \sum_{\ell=1}^{q} \frac{\rho w_\ell RT}{M_\ell} \frac{1}{N_{\text{c},\ell}} \sum_{k=1}^{N_{\text{c},\ell}} G'_{\text{fast},k,\ell}(\omega), \tag{2.17}$$

$$G''_{\text{fast}}(\omega) = \sum_{\ell=1}^{q} \frac{\rho w_\ell RT}{M_\ell} \frac{1}{N_{\text{c},\ell}} \sum_{k=1}^{N_{\text{c},\ell}} G''_{\text{fast},k,\ell}(\omega). \tag{2.18}$$

2.4.2 "Sticky" modes – G_{sticky}

We now describe a stochastic algorithm, which we use to model the motion of chains on long times scales, and which we can use to obtain the relaxation spectrum for the slow chain modes.

Sticker "hop"

We made the assumption that the average time during which the stickers stay attached is much longer than any of the internal Rouse relaxation times of the segments of chain delimited by the stickers. We consider that once a sticker, i, detaches, it takes a "hop" to a new position which is a vector $\Delta\boldsymbol{R}$ from a mean position $\bar{\boldsymbol{R}}_i$, where it re-attaches, see Figure 2.3. As described in the introduction of this Chapter, this "hop" motion is the result of the change of partner that a sticker undergoes, on average, every τ_{as}. Here we assume that between detachment and reattachment, the sticker is able to explore the full configurational space available to it, given that it is constrained by the chain and its neighbouring stickers do not move, see Figure 2.3. The mean position $\bar{\boldsymbol{R}}_i$, around which the sticker re-attaches, is defined by the molecular weight of the strands (M_i, M_{i+1}) that are connected to the sticker and by the position of the neighbouring stickers $(\boldsymbol{R}_{i-1}, \boldsymbol{R}_{i+1})$ as the weighted average position,

$$\bar{\boldsymbol{R}}_i = \frac{M_{i+1}\boldsymbol{R}_{i-1} + M_i\boldsymbol{R}_{i+1}}{M_i + M_{i+1}}. \tag{2.19}$$

Additionally, we obtain the probability distribution function of the "hop standard deviation", $\Delta \boldsymbol{R}_i$, (i.e. how far from the average position, $\bar{\boldsymbol{R}}_i$, the sticker will attach) as

$$p(\Delta \boldsymbol{R}_i) = \left(\frac{1}{2\pi\sigma_i^2}\right)^{3/2} \exp\left(-\frac{(\Delta \boldsymbol{R}_i)^2}{2\sigma_i^2}\right), \tag{2.20}$$

where $\sigma_i^2 = k_\mathrm{B}T/k_{\mathrm{eff},i}$, with $k_{\mathrm{eff},i}$ the effective spring constant associated to the sticker i, which depends on the neighbouring chain segments

$$k_{\mathrm{eff},i} = \frac{3k_\mathrm{B}T}{b^2 N_i} + \frac{3k_\mathrm{B}T}{b^2 N_{i+1}}, \tag{2.21}$$

with b the length of a Rouse monomer, and N_i the number of Rouse monomers segments in a chain of molar mass M_i.

Assuming isotropy of the "hop", each coordinate $(\Delta x_i, \Delta y_i, \Delta z_i)$ of $\Delta \boldsymbol{R}_i$ follows the same probability distribution

$$p(\Delta x_i) = \left(\frac{1}{2\pi\sigma_i^2}\right)^{1/2} \exp\left(-\frac{(\Delta x_i)^2}{2\sigma_i^2}\right). \tag{2.22}$$

Therefore, when a sticker detaches and reattaches, its new position, $\boldsymbol{R}_i^{\mathrm{new}}$ is given by

$$\boldsymbol{R}_i^{\mathrm{new}} = \bar{\boldsymbol{R}}_i + \Delta \boldsymbol{R}_i. \tag{2.23}$$

For the stickers first sticker ($i = 1$) and last sticker ($i = N_\mathrm{s}$), we use

$$\bar{\boldsymbol{R}}_1 = \boldsymbol{R}_2, \quad \text{and} \quad \bar{\boldsymbol{R}}_{N_\mathrm{s}} = \boldsymbol{R}_{N_\mathrm{s}-1}, \tag{2.24}$$

and for the effective spring constants Equation (2.21), we use

$$k_{\mathrm{eff},1} = \frac{3k_\mathrm{B}T}{b^2 N_2}, \quad \text{and} \quad k_{\mathrm{eff},N_\mathrm{s}} = \frac{3k_\mathrm{B}T}{b^2 N_{N_\mathrm{s}}}, \tag{2.25}$$

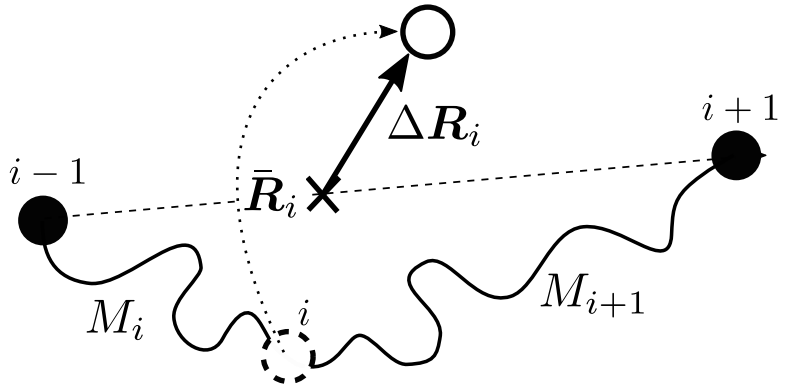

Figure 2.3: Sticker i detaches (dashed circle), takes a local "hop", and reattaches to a new position: $\boldsymbol{R}_i^{\text{new}} = \bar{\boldsymbol{R}}_i + \Delta \boldsymbol{R}_i$, (circle).

where $N_2 = M_2/M_0$ and $N_{N_\text{s}} = M_{N_\text{s}}/M_0$, see Figure 2.1.

The above rules ensure that the chains continue to obey the correct equilibrium Gaussian chain distribution upon hopping. We assume the time between detachment and reattachment is negligible.

Sticker detachment dynamics

For a given molar mass M, we have N_c chains having a certain amount of stickers on them – which were generated according to Equation (2.2). The total amount of stickers over the N_c chains is $N_{\text{s,tot}} = \sum_{k=1}^{N_\text{c}} N_{\text{s},k}$.

For a given sticker, the cumulative distribution function for the detachment time t_d of that sticker (time after which an associated sticker detaches) is

$$p(t_\text{d} \leq t) = 1 - \exp\left(-\frac{t}{\tau_\text{as}}\right). \tag{2.26}$$

Therefore, the probability that a sticker did not detach after a time t is $p(t \leq t_\text{d}) = \exp(-t/\tau_\text{as})$. Hence, the probability that none of the $N_{\text{s,tot}}$ stickers have

detached after a time t is

$$\left[p(t \leq t_{\mathrm{d}})\right]^{N_{\mathrm{s,tot}}} = \exp\left(-\frac{N_{\mathrm{s,tot}}\, t}{\tau_{\mathrm{as}}}\right). \tag{2.27}$$

We conclude that the probability density function of the detachment time of the first sticker to detach amongst the $N_{\mathrm{s,tot}}$ stickers is

$$p(t_{\mathrm{d,first}}) = \frac{N_{\mathrm{s,tot}}}{\tau_{\mathrm{as}}} \exp\left(-\frac{N_{\mathrm{s,tot}}\, t_{\mathrm{d,first}}}{\tau_{\mathrm{as}}}\right). \tag{2.28}$$

Given a uniformly distributed (pseudo) random number $0 < \theta < 1$, we generate from Equation (2.28) a time, $t_{\mathrm{d,first}}$, after which a first sticker detaches:

$$t_{\mathrm{d,first}} = -\tau_{\mathrm{as}} \ln(\theta)/N_{\mathrm{s,tot}}. \tag{2.29}$$

Then, we choose a sticker randomly amongst the $N_{\mathrm{s,tot}}$ stickers and allow it to make a "hop" as described by Equation (2.23). We then repeat this process many times to find the next detachment time amongst the stickers, selecting a random sticker to move each time.

Stress tensor from the N_{c} chains

A microscopic expression for the stress tensor is [Doi & Edwards (1988)]

$$\sigma_{\alpha\beta} = \frac{1}{V} \sum_{\mathrm{springs},m} F_{m\alpha} R_{m\beta}, \tag{2.30}$$

where the summation is made over all the springs in the system, the Greek letters are the Cartesian coordinates, $\boldsymbol{F_m} = 3k_{\mathrm{B}}T\boldsymbol{R_m}/N_m b^2$ is the entropic spring force acting in the m^{th} strand, $\boldsymbol{R_m}$ is the vector connecting the two beads neighbouring the strand m, and $V = N_{\mathrm{c}}N/n_M$ is the volume occupied by the N_{c} chains.

Equation (2.30) can be written in terms of a sum over the N_{c} chains and, for

each chain, a sum over the number of chain strands between stickers

$$\begin{aligned}\sigma_{\alpha\beta} &= \frac{1}{V}\sum_{k=1}^{N_c}\sum_{i=2}^{N_{s,k}}\frac{3k_BT}{N_ib^2}R_{i,\alpha}R_{i,\beta} \\ &= \frac{\rho RT}{MN_c}\sum_{k=1}^{N_c}\sum_{i=2}^{N_{s,k}}\frac{3}{N_ib^2}R_{i,\alpha}R_{i,\beta},\end{aligned} \tag{2.31}$$

where M is the molar mass of the chain. Note that the two end segments (polymers ends) are excluded from this stress expression as we consider that they are relaxed and their contributions were already accounted for in G_{fast}, cf. Section 2.4.1.

Stress autocorrelation function

In computer simulations, the most convenient way of evaluating the stress autocorrelation function, $G_{\text{sticky}}(t)$, is by using the fluctuation-dissipation theorem [Likhtman (2012); Ramirez *et al.* (2010)]. It is written

$$\begin{aligned}G_{\text{sticky}}(t) &= \frac{V}{k_BT}\frac{1}{t_{\text{sim}}-t}\int_0^{t_{\text{sim}}-t}\sigma_{xy}(t+\tau)\sigma_{xy}(\tau)\,\mathrm{d}\tau \\ &= \frac{V}{k_BT}\big\langle\sigma_{xy}(t+\tau)\sigma_{xy}(\tau)\big\rangle \\ &= \frac{MN_c}{\rho RT}\big\langle\sigma_{xy}(t+\tau)\sigma_{xy}(\tau)\big\rangle\end{aligned} \tag{2.32}$$

where xy is any two orthogonal directions, and t_{sim} the total simulation time.

Since our system is isotropic, one can average over different directions defining the pair of perpendicular axis (xy). In isotropic systems there are two arbitrary angles to select the direction of x axis and one more angle to select the direction of y-axes perpendicular to it. Averaging over these three angles gives the following

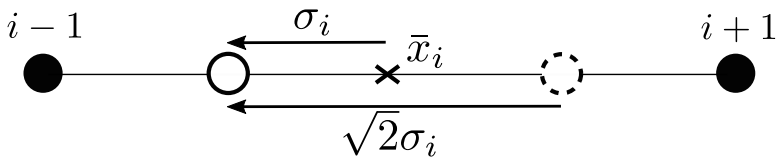

Figure 2.4: Sticker "hop" projected on the x-axis. Upon detachment its new position (circle) is defined, on average, as $x^{\text{new}} = \bar{x}_i + \sigma_i$, which is, on average, $\sqrt{2}\sigma_i$ away from its current position (dashed circle).

result [Likhtman (2012); Ramirez *et al.* (2010)]

$$G_{\text{sticky}}(t) = \frac{MN_{\text{c}}}{5\rho RT}\Big(\big\langle\sigma_{xy}(t)\sigma_{xy}(\tau)\big\rangle + \big\langle\sigma_{yz}(t)\sigma_{yz}(\tau)\big\rangle + \big\langle\sigma_{zx}(t)\sigma_{zx}(\tau)\big\rangle\Big) + \frac{MN_{\text{c}}}{30\rho RT}\Big(\big\langle N_{xy}(t)N_{xy}(\tau)\big\rangle + \big\langle N_{xz}(t)N_{xz}(\tau)\big\rangle + \big\langle N_{yz}(t)N_{yz}(\tau)\big\rangle\Big), \tag{2.33}$$

where $N_{\alpha\beta} = \sigma_{\alpha\alpha} - \sigma_{\beta\beta}$. Using the latter expression instead of Equation (2.32) improves the statistical accuracy of the results.

In order to evaluate correlation functions in simulations, we use a multiple-tau correlator algorithm proposed by Ramirez *et al.* [Ramirez *et al.* (2010)].

Polydispersity

If we assume that the molecular mass distribution is discretised into a set of q modes, $\{(w_\ell, M_\ell)\}$, $\ell = \{1, \ldots, q\}$, then we compute G_{sticky} as

$$G_{\text{sticky}} = \sum_{\ell=1}^{q} w_\ell G_{\text{sticky},M_\ell}, \tag{2.34}$$

where G_{sticky,M_ℓ} is computed using Equation (2.33) for a chain of molar mass M_ℓ.

Comparison of the sticker times

In what follows, we will show that, to compare the values of the sticker time τ_{as} in the "classic" sticky-Rouse model defined by Equation (2.1) with the stochastic

sticky-Rouse model developed in this Chapter in a fair way, we need to multiply the former by a factor π^2.

We take the special case where the stickers are equally spaced along the chain. Therefore, the number of Rouse monomers between stickers is fixed to $N_\mathrm{m} = N/N_\mathrm{s}$, and so Equation (2.21) reduces to

$$k_\mathrm{eff} = \frac{3k_\mathrm{B}T}{b^2 N_\mathrm{m}} + \frac{3k_\mathrm{B}T}{b^2 N_\mathrm{m}} = \frac{6k_\mathrm{B}T}{b^2 N_\mathrm{m}}. \tag{2.35}$$

In Equation (2.22), σ_i represents the standard deviation around the mean position defined by $\bar{\boldsymbol{R}}$. Figure 2.4 illustrates this process, projected on the x-axis. Upon detachment, a sticker "hops" to its new position defined, on average, as

$$x^\mathrm{new} = \bar{x}_i + \sigma_i. \tag{2.36}$$

This new position is, on average, at a distance $\sqrt{2}\sigma_i$ away from its current position (because σ_i is measured from the centre position $\bar{x}_i$, and we add the variance). Therefore, the actual mean square displacement of the sticker $\langle x^2 \rangle$, is

$$\begin{aligned} \langle x^2 \rangle &= 2\sigma_i^2 \\ &= 2k_\mathrm{B}T/k_\mathrm{eff} \\ &= \frac{b^2 N_\mathrm{m}}{3}. \end{aligned} \tag{2.37}$$

In one dimension, the effective diffusion coefficient, D, is of form

$$\langle x^2 \rangle = 2Dt, \tag{2.38}$$

where here $t \equiv \tau_{\text{as}}$. Hence, we have

$$D = \frac{b^2 N_{\text{m}}}{6\tau_{\text{as}}}, \tag{2.39}$$

and we can define the effective sticker friction coefficient as

$$\begin{aligned} \zeta_{\text{sticker}} &\equiv k_{\text{B}}T/D \\ &= \frac{6\tau_{\text{as}} k_{\text{B}} T}{b^2 N_{\text{m}}}. \end{aligned} \tag{2.40}$$

Now, we can use the definition of the Rouse time, Equation (1.56), to find the Rouse time of a chain composed of N_{s} "springs" of effective length $(N_{\text{m}}b^2)^{1/2}$. We therefore make the following substitutions in Equation (1.56):

$$N \to N_{\text{s}}, \quad b^2 \to N_{\text{m}}b^2, \quad \zeta \to \zeta_{\text{sticker}},$$

to obtain the Rouse relaxation time of a Rouse chain composed of N_{s} springs

$$\begin{aligned} \tau_{\text{R}} &= \frac{\zeta_{\text{sticker}} N_{\text{s}}^2 N_{\text{m}} b^2}{3\pi^2 k_{\text{B}} T} \\ &= \frac{2N_{\text{s}}^2 \tau_{\text{as}}}{\pi^2}. \end{aligned} \tag{2.41}$$

Finally, the relaxation modulus for such chain is

$$G(t) = \frac{\rho RT}{M} \sum_p \exp\left(\frac{-2p^2 t}{\tau_{\text{R}}}\right). \tag{2.42}$$

The reason for the factor of two appearing in the exponential is that there is a factor of two difference between the relaxation time for the stress contribution of the p^{th} mode and the relaxation time of molecular orientation from the p^{th} mode

(τ_R) [Dealy & Larson (2006)]. Using Equation (2.41), we obtain

$$G(t) = \frac{\rho RT}{M} \sum_p \exp\left(\frac{-\pi^2 p^2 t}{N_s^2 \tau_{as}}\right). \tag{2.43}$$

Comparing the latter expression for the relaxation modulus with Equation (2.1), we see that there is a factor π^2 difference. This factor π^2 is included in the values of the sticker time for the "classic" sticky-Rouse model (Equation (2.1)) reported in Table 2.1, i.e. we used Equation (2.1), but reported $\pi^2 \times \tau_{as}$ in Table 2.1.

2.5 Comparison with experimental data

Four samples of PEHA-UPy polymers with various UPy-content aiming for (2%, 6%, 9%, and 14% UPy weight fraction) were synthesised by G. Cui, and analysed by gel permeation chromatography (GPC) to determine their respective molecular weight distributions. One should be cautious about the absolute meaning of the GPC results. Indeed, such devices are calibrated with precisely known polymer chains (e.g. polystyrene standards in THF solvent) but the topology (and stickyness) of the PEHA-UPy might alter and bias the results. Hence, the molecular weight distribution inferred from a GPC run should be taken into account with this caveat in mind. Nevertheless, in our model, we use a molecular weight distribution that closely resemble the GPC curves.

Our model contains three parameters, similarly to the "classic" sticky-Rouse model: the effective sticker lifetime, τ_{as}, the Rouse monomer relaxation time τ_0, and the average molar mass between stickers, M_{strand}. We summarise, in Table 2.1, the *best-fit* parameters that we used in our stochastic sticky-Rouse model to fit the data. To account for the polydispersity of the systems, we extract the PDI and weight-average molecular weight (M_w) from the GPC measurements and

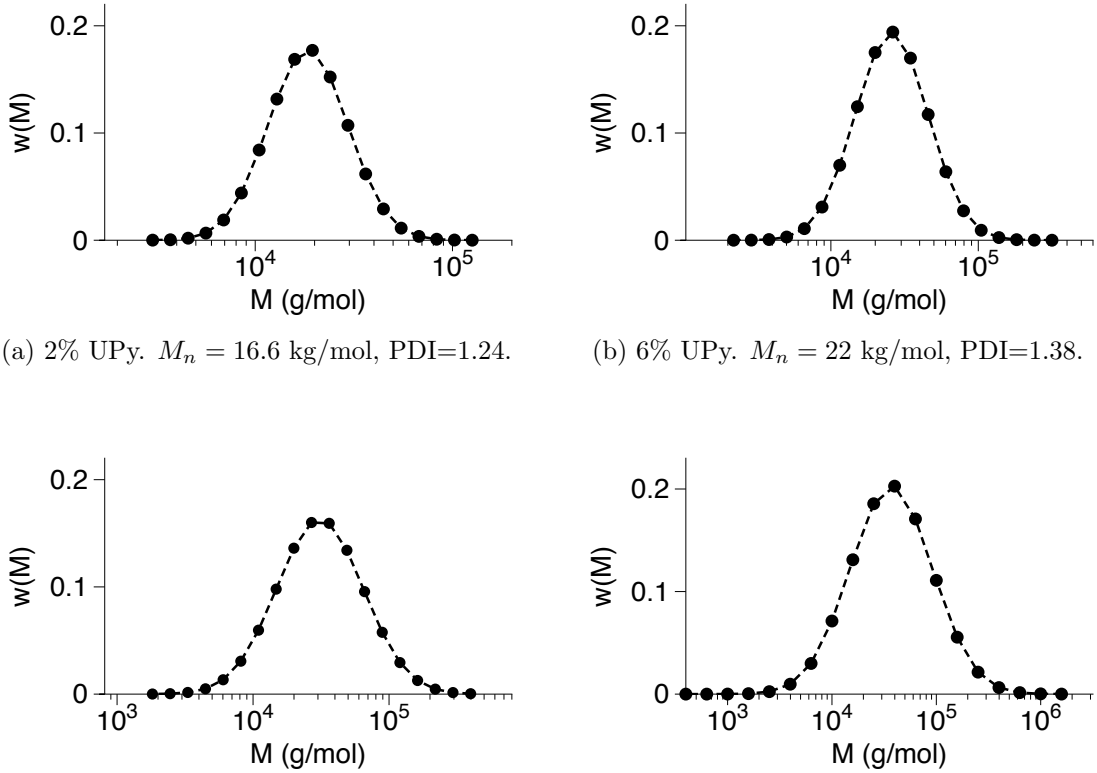

(a) 2% UPy. $M_n = 16.6$ kg/mol, PDI=1.24.

(b) 6% UPy. $M_n = 22$ kg/mol, PDI=1.38.

(c) 9% UPy. $M_n = 23.7$ kg/mol, PDI=1.71.

(d) 14% UPy. $M_n = 24.6$ kg/mol, PDI=2.26.

Figure 2.5: Weight-average molar mass distribution used to produce the model predictions Figure 2.8.

we assume that the molecular weight distribution follows a log-normal distribution [Weßlau (1956)].

2.5.1 Log-normal distribution

In the log-normal distribution, the number biased distribution of molecular weight, n, is

$$n(\ln M) = \frac{1}{(2\pi S^2)^{1/2}} \exp\left(-\frac{(\ln M - \ln \overline{M})^2}{2S^2}\right), \tag{2.44}$$

where $\overline{M}$ is the median value, and S the standard deviation. Hence, the number-average molar mass is

$$\begin{aligned} M_n &\equiv \int M \times n(\ln M)\, \mathrm{d}(\ln M) \\ &= \exp\left(\ln \overline{M} + S^2/2\right), \end{aligned} \tag{2.45}$$

and similarly, the weight-average molecular weight is obtained as

$$\begin{aligned} M_w &\equiv \frac{1}{M_n} \int M^2 \times n(\ln M)\, \mathrm{d}(\ln M) \\ &= \exp\left(\ln \overline{M} + 3S^2/2\right). \end{aligned} \tag{2.46}$$

Thus, using Equations (2.45) and (2.46), the two parameters, $\overline{M}$ and S, that characterise the log-normal distribution can be related to the number-average molar mass (M_n) and weight-average molar mass (M_w) through

$$S^2 = \ln(M_w M_n^{-1}), \tag{2.47}$$

$$\overline{M} = \ln(M_n^{3/2} M_w^{-1/2}). \tag{2.48}$$

Finally, the weight biased distribution of molecular weight, w, is obtained as

$$w(\ln M) = \frac{1}{(2\pi S^2)^{1/2}} \exp\left(-\frac{\left(\ln M - (\ln \overline{M} + S^2)\right)^2}{2S^2}\right). \tag{2.49}$$

We use 19 molar masses, equally spaced in the log-space, to accurately describe the molar mass distribution. We generate the corresponding weight-average molecular weights (w_i) using Equation (2.49) in order to span the width of the molecular mass distribution. The resulting molecular weight distributions corresponding to the 2%, 6%, 9%, and 14% UPy are presented in Figures 2.5a–2.5d, respectively.

Table 2.1: Characteristics of the PEHA-UPy samples.

%UPy	PDI	M_n (kg/mol)	N_s		τ_{as} (μs)		τ_0 (ns)
			NMR	Models	Stocha	Classic†	
2%	1.24	16.6	1	0.2	5	25	0.70
6%	1.38	22.0	7	3	29	65	1.0
9%	1.71	23.7	13	8	56	100	2.5
14%	2.38	24.6	17	21	83	200	500

†Includes the factor π^2

2.5.2 Data fit

The parameter M_{strand}, which describes the average "chain-length" between stickers, fixes the value of the plateau modulus of G'_{sticky}. Best agreements with rheology data are found for M_{strand} values that are reported in Table 2.1, which are of the same order of magnitude as the values suggested by nuclear magnetic resonance (NMR) experiments.

We present the experimental elastic and loss moduli together with our stochastic sticky-Rouse model fits and "classic" sticky-Rouse model (Equation (2.1)) for the 2%, 6%, 9%, and 14% UPy sample in Figure 2.8.

The slopes at low frequency are very well captured by the stochastic model and the sticky-Rouse model, which indicates that the "hop" picture, described above in Section 2.4.2, for the large scale chain motion is meaningful, and that the polydispersity of the system is well captured in both models. However, the value of the relevant fitting parameter, the sticker time τ_{as}, is substantially different for the two models. The reason for this discrepancy is that the stochastic model considers finite distance hops of the discrete sticker groups, which are randomly placed along the chain, whereas the sticky-Rouse model, Equation (2.1), considers continuous motion of a chain with distributed friction. We consider that the stochastic model is closer to the physical reality.

The stochastic model improves intermediate frequency predictions as a consequence of the use of polydisperse strands between stickers and because dangling ends relaxation is treated separately. This can be seen in Figure 2.6 where we detailed, for the 6% UPy sample, the contributions to the elastic and loss moduli of the trapped chain strands, the dangling chain ends, and of the chains without stickers. At low frequency, the dangling chain ends contribution dominates G_{fast}.

In Figure 2.7, we justify the importance of the use of molar mass polydispersity. It can be seen that the data for the polydisperse sample does not match the predictions for any of the monodisperse samples, but rather appears to be an average over the responses of the various monodisperse samples. We also note that, as the molecular mass increases from 10 kg/mol to 100 kg/mol, a clear power law emerges corresponding to the sticky Rouse motion of the chains before the terminal relaxation is reached. We also note that polydispersity does not change significantly the G_{fast} predictions, therefore we restricted Figure 2.7 to the low frequencies only, and did not represent G_{fast}.

It is evident that some discrepancies still remain in the intermediate frequency regime, especially in G''. Possible additions to the model will be discussed in the concluding remarks, Section 2.7.

On the "effective" sticker lifetime

One feature of the fitted value of the sticker time, τ_{as}, true for both models, is that it increases with increasing concentration of stickers, see Figure 2.9. It has been pointed out by Rubinstein and Semenov [Rubinstein & Semenov (1998)] that the effective sticker time in the model is not the bare sticker lifetime, since a dissociated sticker will many times return to the same partner, before finally finding another free partner with which to associate. Since returns to the same partner do not result in a chain rearrangement, they do not relax the stress.

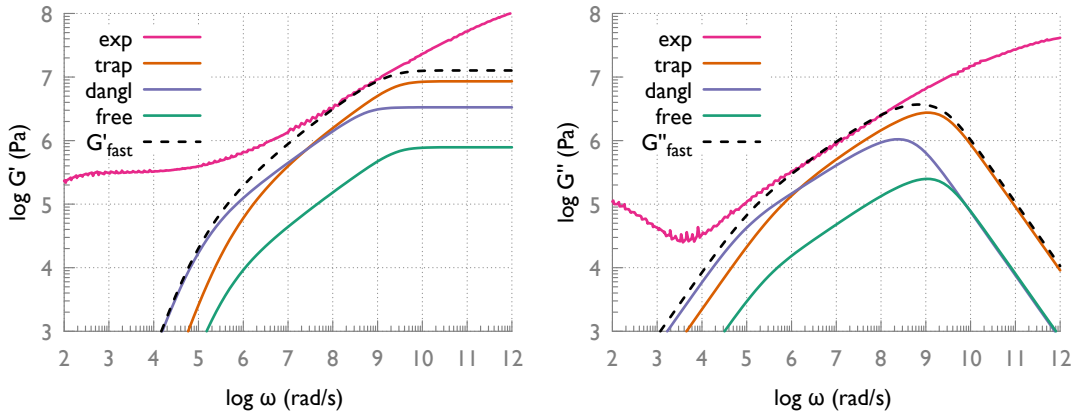

(a) (b)

Figure 2.6: Detailed contribution of the trapped chain strands, dangling chain ends, and chains without stickers (free) to G_{fast} for the 6% UPy sample. The black dashed lines are the sum of the three contributions. The pink lines are the experimental G' and G''. We present separately the elastic modulus (a) and loss modulus (b) for clarity.

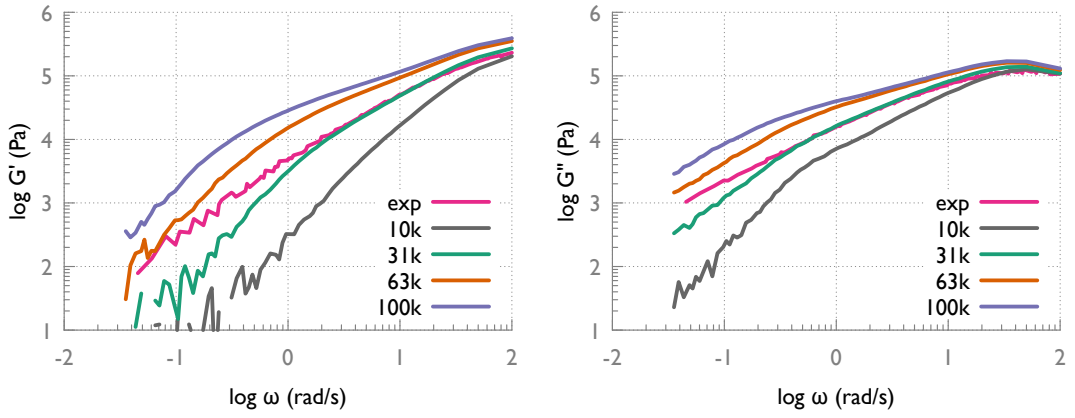

(a) (b)

Figure 2.7: Comparison of the G'_{sticky} predictions for various monodisperse molecular masses in 10, 31, 63, 100 kg/mol. The pink lines represent the experimental data. We present separately the elastic modulus (a) and loss modulus (b) for clarity.

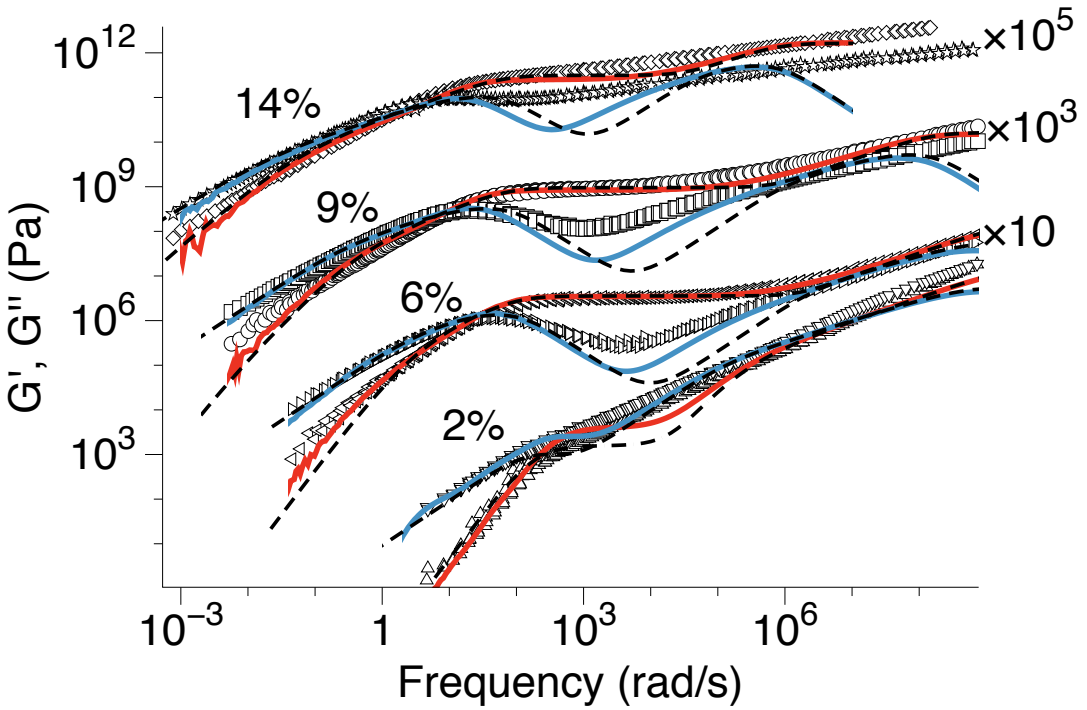

Figure 2.8: Experimental data for the four samples of various UPy content (symbols) together with the models retro-fitting for the stochastic sticky-Rouse (lines) and "classic" sticky-Rouse model, Equation (2.1), (dashed lines). Some curves are shifted vertically for clarity.

Consequently, the sticker time, τ_{as}, should be interpreted as the time to find a new partner.

While it may be that the fundamental sticker dissociation time changes with UPy content, it is appealing to suggest that the differences in sticker time, τ_{as}, might be attributed to the relative difficulty of finding a new partner as UPy content is increased, i.e. stickers return more often to the same "old" partner before swapping for a new partner. This suggestion can be supported with a scaling argument showing that an increase of the number of UPy group per chain implies a decrease of the number of stickers present in a "search" volume of detached sticker.

Calling the volume of a sticker or monomer b^3, and the average number of monomers between stickers $N_{\mathrm{m}} \equiv N/N_{\mathrm{s}}$, then the number of stickers per unit volume, n_{s}, is defined as

$$n_{\mathrm{s}} = \frac{\text{number of stickers per chain}}{\text{volume occupied by a chain}} \approx \frac{N_{\mathrm{s}}}{N_{\mathrm{s}} N_{\mathrm{m}} b^3} = (N_{\mathrm{m}} b^3)^{-1}. \tag{2.50}$$

When a sticker is free, it explores its neighbourhood in a volume limited by the typical dimensions of the chain between stickers which obeys random walk statistics. Hence the explored volume, V_{search}, is of order

$$V_{\mathrm{search}} \approx (N_{\mathrm{m}}^{1/2} b)^3. \tag{2.51}$$

Therefore, the number of stickers, N_{partner}, in the exploration volume, V_{search}, defined by Equation (2.51) scales as

$$\begin{aligned} N_{\mathrm{partner}} &\approx n_{\mathrm{s}} V_{\mathrm{search}} \\ &\approx N_{\mathrm{m}}^{1/2} \\ &\propto N_{\mathrm{s}}^{-1/2}. \end{aligned} \tag{2.52}$$

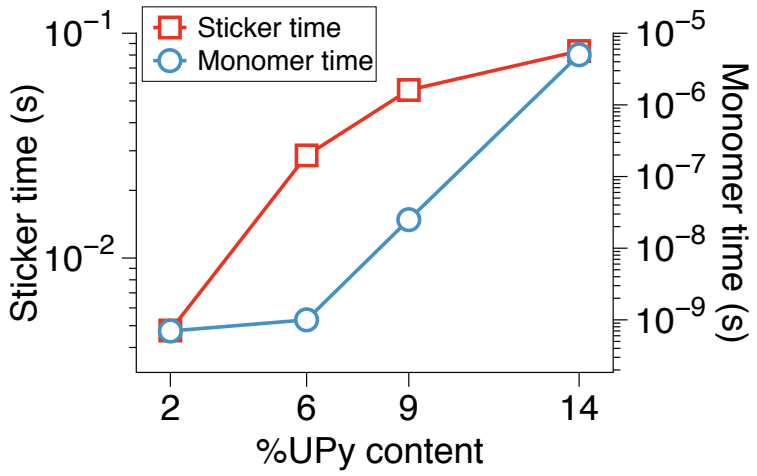

Figure 2.9: Sticker time, τ_{as}, and Rouse monomer relaxation time, τ_0, used to model the experimental data, as a function of the UPy content.

$N_{partner}$ represents the number of potential partners available to a sticker, and it decreases as the number of stickers per chain, N_s, increases. Consequently, we expect the effective sticker time, τ_{as}, to increase with increasing number of stickers per chain.

2.6 Nonlinear rheology

It is important to emphasise that in this section we are *not* using "sticky" physics, which is in contrast with the main body of this chapter. Indeed, independently of the sticky-Rouse and stochastic sticky-Rouse models presented before, we use the "simple" upper-convected Maxwell (UCM) model, Equations (1.34) and (1.33), to predict the extensional rheology of the 6% UPy sample. Note that the UCM model does not contain any description of the stickers.

The set of weights and relaxation times $\{(g_i, \tau_{d,i})\}$ are taken from a multi-mode UCM fit of the linear rheology data, Equation (1.24): we allow two relaxation modes per decade and use a least-square method to find the "best" values. This

procedure used on the linear rheology data of the 6% UPy sample leads to a set of 32 relaxation modes $\{(g_i, \tau_i)\}$. Figure 2.10a presents the linear rheology data, together with the multi-mode Maxwell fit. Note that both the linear and nonlinear experiments were performed at 70°C.

The experimental data and the prediction for the nonlinear rheology, in extension, are shown Figure 2.10b. The excellent description of the data, capturing the extension hardening up to the point of sample fracture or termination of the experiment, is a demonstration that the chain motion is governed by Rouse-like chain motion, because the Rouse model is predicted to obey a multi-mode UCM model in nonlinear flow. However, we note that the multi-mode UCM model only predicts successfully the initial start-up of the nonlinear rheology in extension, but it does not predict the point of fracture or transition towards steady state (this physics is not contained in the UCM model). Similarly, although we do not have experimental data to compare with, we anticipate that the nonlinear shear predictions of the UCM model would be successful in predicting the initial start-up behaviour of the shear stress. Nevertheless, it is very likely that the behaviour at larger shear strains, and the transition to steady state under shear, would not be well captured by the UCM model. One feature of the UCM model is that the steady state shear viscosity is the same at any flow rate; we suspect that real systems, such as the UPy systems considered in this Chapter, exhibit more complex shear rheological behaviour. It may also be that finite extensibility of the chains give rise to shear hardening, in a similar manner to our predictions for a different model in Chapters 4 and 5. Therefore, more work needs to be done to model the nonlinear rheology of this class of sticky materials.

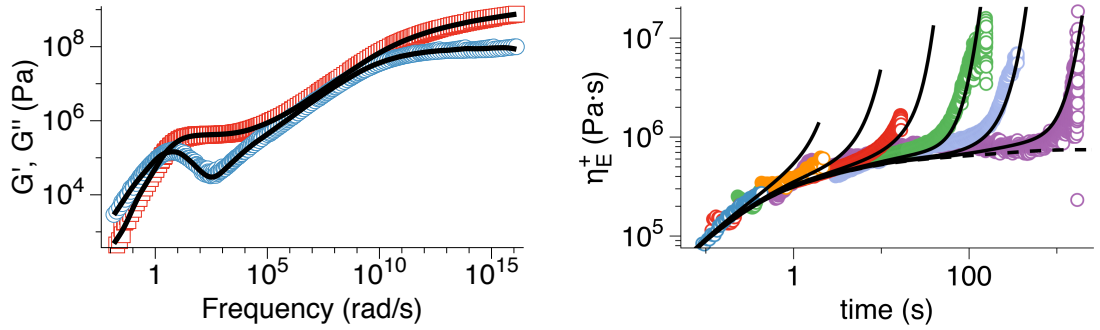

(a) (b)

Figure 2.10: Left: Experimental linear rheology data of the 6% UPy sample at 70°C (symbols) together with a multi-mode Maxwell fit (black lines). Right: Tensile stress growth coefficient for $\dot{\varepsilon}$ ={0.003, 0.01, 0.03, 0.1, 0.3, 1}. Experimental data (symbols) together with predictions (lines) of the multi-mode upper-convected Maxwell model, Equation (1.33), obtained from the set of relaxation modes $\{(g_i, \tau_i)\}$ extracted from the linear rheology data. The dashed line is the LVE prediction.

2.7 Concluding remarks

We proposed a new model for the linear rheology of linear polymeric chains with functionalized groups (stickers) along the backbone. Our stochastic sticky-Rouse model is based on a similar assumption to the sticky-Rouse model [Baxandall (1989); Chen *et al.* (2013); Leibler *et al.* (1991)] that the sticker timescale and the characteristic relaxation time of Rouse monomer are well separated, allowing us to write the stress relaxation function, $G(t)$, as the sum of a stress relaxation related to the motion of the Rouse monomers at fixed sticker position and a stress relaxation function related to the sticker motion.

We noted however that the original sticky-Rouse model does not account for the distribution of the number of stickers along polymer chains, and random spacing of the stickers along the chain, nor does it account for the finite sized hops when a sticker detaches and reattaches. To address these issues we developed a

computational model, the stochastic sticky-Rouse model, which produces many chains of a precise molar mass with stickers randomly distributed along the chain according to a probability distribution. The resulting number of stickers per chain effectively follows a Poisson distribution, and the distance between stickers follows an exponential distribution. Then, we defined the relaxation modes undergone by the dangling ends (of various length) and strands of chain (of various length) trapped between stickers as well as a "hopping" mechanism for the sticker motion leading to delayed relaxation.

The "effective" lifetime of the stickers, τ_{as}, appears to increase with increasing UPy content, i.e. it seems that the search for a new partner is more difficult when the density of stickers grafted on the chain increases. We supported this statement with a scaling argument.

Finally, we exemplified the use of the multi-mode upper-convected Maxwell model, Equation (1.24), by predicting the extensional rheology data of the 6% UPy sample, from the linear rheology data.

Our stochastic sticky-Rouse model is fully defined by physical parameters. Some are fixed a priori by the chemistry: the average number of stickers per chain M_{strand}, the molecular weight distribution M_n and the polydispersity index $Đ$. Other physical parameters: the "effective" lifetime of a sticker, τ_{as}, and the characteristic relaxation time of a Rouse segment, τ_0, are left as best fit parameters.

Both models were applied to experimental data provided by G. Cui. The resulting best fits to the linear rheology data of various UPy content samples are shown in Figure 2.8, where it is clear that our stochastic model improves the intermediate frequency predictions as compared to the "standard" sticky-Rouse model (Equation (2.1)) while matching it at low frequencies. However improved, the stochastic model still fails at accurately predicting the intermediate frequency

regime. Some ideas that could be considered to further develop the stochastic model include:

(i) The associated state may be quite complex. There could be a distribution of association lifetimes leading to a broadening of the low frequency relaxation peak;

(ii) The "hopping distance" Figure 2.3 could be set to depend upon the time the sticker stays free before reattaching which would be drawn from a distribution, akin to Equation (2.26). There would then be narrower moves associated with short free time.

(iii) We could replace the log-normal distribution of the molecular weight (Equation (2.44)) by a more complex one, such as a bi-modal distribution.

One should keep in mind that the above propositions all result in additional model parameters, resulting in an improved fit at the expense of our purpose to keep the model simple. We therefore did not feel that such modification would result in greater insight.

This page is intentionally left blank

Chapter 3

Toy model for blends of linear polymers

Industrial polymers are typically polydisperse, i.e. they contain a broad range of molecular weight. A detailed tube theory for *bidisperse* melt of entangled polymers has been developed by Read and co-workers [Read *et al.* (2012)] that successfully describes nonlinear rheology experiments on bidisperse blends. In this Chapter, we propose a simplified tube model, based on the Rolie-Poly model [Likhtman & Graham (2003)], for polydisperse melts of entangled polymers that aims at predicting nonlinear rheology, whilst being consistent with the "double reptation" theory [des Cloizeaux (1988)] in linear rheology. We first briefly present the double reptation theory, then detail the simplified model in case of a bidisperse blend, before generalising to the polydisperse case.

3.1 Double reptation

For polydisperse melts, discrepancies exist between the theoretical prediction of the Doi-Edwards theory [Doi & Edwards (1988)] ("simple reptation") and

experimental data for the stress relaxation function, $G(t)$. One cause of this is constraint release (CR), specifically the fact that reptation of short chains relaxes some of the entanglements on the long chains, hence relaxing stress. The process of constraint release is in general very complex, and a completely general, rigorous, theory has not yet been developed. Nevertheless, there is a simple description of constraint release called *double reptation* that is reasonably accurate for many cases of practical importance [Dealy & Larson (2006)]. Building on (and to an extent simplifying) Rubinstein & Colby's idea [Rubinstein & Colby (1988)], the double reptation approximation of des Cloizeaux [des Cloizeaux (1988)] shows that the predictions of reptation theory for polydisperse melts can be greatly improved, without introducing additional parameters.

Double reptation is based on a "binary" picture of entanglements, in which each entanglement is an interaction between two chains. If reptation of a chain causes the release of an entanglement, then the entanglement is lost to both the chain which reptates, and the chain with which it is entangled. If the unrelaxed stress at time t is assumed to be proportional to the fraction of surviving entanglement points at that time, and if the two chains participating in the entanglement reptate independently, then it follows that the relaxation modulus should be proportional to the square of the tube survival probability, $F(t)$, for a single chain. The relaxation modulus is then written as [Dealy & Larson (2006); des Cloizeaux (1988)]

$$G(t) = G_N^0 \big(F(t)\big)^2. \tag{3.1}$$

Calling τ_d the longest stress relaxation time of chain in a monodisperse melt, with constraint release effects included via double reptation (i.e. τ_d is half the reptation time), then we may approximate the stress relaxation as a single exponential decay:

$$G(t) = G_N^0 \exp(-t/\tau_\mathrm{d}). \tag{3.2}$$

Combining the latter equation with Equation (3.1), we have that the survival probability takes the form

$$F(t) = \exp(-t/2\tau_{\mathrm{d}}). \tag{3.3}$$

For binary blends comprising a volume fraction ϕ_{S} of chains of mass M_{S} and volume fraction $\phi_{\mathrm{L}} = 1 - \phi_{\mathrm{S}}$ of chains of mass M_{L}, the tube survival probability for the whole melt is the weighted average over the two types of chain

$$F(t) = \phi_{\mathrm{S}} \exp(-t/2\tau_{\mathrm{d,S}}) + \phi_{\mathrm{L}} \exp(-t/2\tau_{\mathrm{d,L}}), \tag{3.4}$$

where $\tau_{\mathrm{d,S}}$ and $\tau_{\mathrm{d,L}}$ are the longest relaxation times of the short and long chains, respectively. The stress relaxation modulus is then, according to Equation (3.1),

$$\begin{aligned} G(t) \;=\; G_N^0 \Big[& \phi_{\mathrm{S}}^2 \exp\left(-t/\tau_{\mathrm{d,S}}\right) + \phi_{\mathrm{L}}^2 \exp\left(-t/\tau_{\mathrm{d,L}}\right) \\ & + 2\phi_{\mathrm{S}}\phi_{\mathrm{L}} \exp\left(-t(1/2\tau_{\mathrm{d,S}} + 1/2\tau_{\mathrm{d,L}})\right)\Big]. \end{aligned} \tag{3.5}$$

The linear rheology of Equation (3.5) is sketched in Figure 3.1, in the limit $\tau_{\mathrm{d,S}} \ll \tau_{\mathrm{d,L}}$. A fraction $\phi_{\mathrm{S}}^2 + 2\phi_{\mathrm{S}}\phi_{\mathrm{L}}$ of the stress relaxes at $\omega \approx \tau_{\mathrm{d,S}}^{-1}$ and a fraction ϕ_{L}^2 relaxes at $\omega \approx \tau_{\mathrm{d,L}}^{-1}$.

For binary blends double reptation often breaks down in the sense that dilution with short chains speeds up the long chain relaxation rate. However, for polydisperse systems many of the detailed dynamics are hidden by the broad distribution of relaxation times, and double reptation is often successful [Dealy & Larson (2006)].

3.2 Nonlinear rheology of bidisperse blends

We are now going to develop a nonlinear constitutive model for polydisperse linear entangled polymers designed to be consistent, in linear rheology, with double reptation, Section 3.1. We begin by outlining the model for a binary blend before generalising to many components in Section 3.3. Note that a model of this form has been proposed before, cf. microscale polymer processing[1] (μPP, μPP[2]) and Reptate software[2], but not published. We will implement a correction which speeds up the long chain relaxation time with dilution, by including the effects of contour length fluctuations in the diluted tube [Likhtman & McLeish (2002); Read *et al.* (2012)].

3.2.1 Description of the model

To understand the effect of polydispersity on entangled linear polymer chains, we consider a blend of two monodisperse entangled linear polymers. As a simple model describing the entanglement effects, we use the Rolie-Poly model [Likhtman & Graham (2003)] that we decorate with finite extensibility.

In the following, we denote the quantities related to the shorter chains with a subscript "S", and the longer chains the subscript "L". We consider that our blend contains a volume fraction ϕ_S of short chains, and a fraction ϕ_L of long chains. We write the total stress tensor as

$$\underline{\underline{\boldsymbol{\sigma}}} = G_N^0 \left(\phi_\mathrm{S}\, \mathrm{f_E}(\lambda_\mathrm{S}) \underline{\underline{\boldsymbol{A}}}_\mathrm{S} + \phi_\mathrm{L}\, \mathrm{f_E}(\lambda_\mathrm{L}) \underline{\underline{\boldsymbol{A}}}_\mathrm{L} \right), \tag{3.6}$$

where G_N^0 is the (experimental) plateau modulus, $\underline{\underline{\boldsymbol{A}}}_\mathrm{S}$ and $\underline{\underline{\boldsymbol{A}}}_\mathrm{L}$ are the average conformation tensors for an entanglement segment of short and long chains re-

[1] http://www1.irc.leeds.ac.uk/mupp/, http://www1.irc.leeds.ac.uk/mupp2/
[2] http://reptate.com

spectively,

$$\lambda_{\mathrm{S}} = \left(\frac{1}{3}\,\mathrm{tr}\,\underline{\underline{\boldsymbol{A}}}_{\mathrm{S}}\right)^{1/2}, \quad \text{and} \quad \lambda_{\mathrm{L}} = \left(\frac{1}{3}\,\mathrm{tr}\,\underline{\underline{\boldsymbol{A}}}_{\mathrm{L}}\right)^{1/2}, \tag{3.7}$$

are the stretch ratios of the S-chains and L-chains, respectively, and the finite extensibility function is the Warner approximation [Warner (1972)] of the inverse Langevin function

$$\mathrm{f_E}(\lambda) = \frac{1-\lambda_{\max}^{-2}}{1-\lambda^2\lambda_{\max}^{-2}}, \tag{3.8}$$

with $\lambda_{\max}$ the maximum stretch ratio in extension. For the rest of this Chapter, we take $\lambda_{\max} = 5$, unless stated otherwise.

The short chains and long chains entangle with other short and long chains, releasing their entanglements on different timescales. Therefore, we break down the conformation tensors $\underline{\underline{\boldsymbol{A}}}_{\mathrm{S}}$ and $\underline{\underline{\boldsymbol{A}}}_{\mathrm{L}}$ as

$$\underline{\underline{\boldsymbol{A}}}_{\mathrm{S}} = \phi_{\mathrm{S}}\underline{\underline{\boldsymbol{A}}}_{\mathrm{SS}} + \phi_{\mathrm{L}}\underline{\underline{\boldsymbol{A}}}_{\mathrm{SL}} \tag{3.9}$$

$$\underline{\underline{\boldsymbol{A}}}_{\mathrm{L}} = \phi_{\mathrm{L}}\underline{\underline{\boldsymbol{A}}}_{\mathrm{LL}} + \phi_{\mathrm{S}}\underline{\underline{\boldsymbol{A}}}_{\mathrm{LS}}, \tag{3.10}$$

where $\underline{\underline{\boldsymbol{A}}}_{IJ}$ accounts for the effect of entanglements from chains of type J on the average configuration of chains of type I (where I and J could be short (S) or long (L)). $\underline{\underline{\boldsymbol{A}}}_{\mathrm{SS}}$ and $\underline{\underline{\boldsymbol{A}}}_{\mathrm{LL}}$ follow the "classic" Rolie-Poly equation [Likhtman & Graham (2003)], where we add finite extensibility effects via $\mathrm{f_E}$ Equation (3.8),

$$\overset{\nabla}{\underline{\underline{\boldsymbol{A}}}}_{\mathrm{SS}} = -\frac{1}{\tau_{\mathrm{d,S}}}\left(\underline{\underline{\boldsymbol{A}}}_{\mathrm{SS}} - \underline{\underline{\boldsymbol{I}}}\right) - \frac{2(1-\lambda_{\mathrm{S}}^{-1})}{\tau_{\mathrm{s,S}}}\,\mathrm{f_E}(\lambda_{\mathrm{S}}) \times \left[\underline{\underline{\boldsymbol{A}}}_{\mathrm{SS}} + \beta_{\mathrm{CCR}}\lambda_{\mathrm{S}}^{2\delta}\left(\underline{\underline{\boldsymbol{A}}}_{\mathrm{SS}} - \underline{\underline{\boldsymbol{I}}}\right)\right], \tag{3.11}$$

$$\overset{\nabla}{\underline{\underline{\boldsymbol{A}}}}_{\mathrm{LL}} = -\frac{1}{\tau_{\mathrm{d,L}}}\left(\underline{\underline{\boldsymbol{A}}}_{\mathrm{LL}} - \underline{\underline{\boldsymbol{I}}}\right) - \frac{2(1-\lambda_{\mathrm{L}}^{-1})}{\tau_{\mathrm{s,L}}}\,\mathrm{f_E}(\lambda_{\mathrm{L}}) \times \left[\underline{\underline{\boldsymbol{A}}}_{\mathrm{LL}} + \beta_{\mathrm{CCR}}\lambda_{\mathrm{L}}^{2\delta}\left(\underline{\underline{\boldsymbol{A}}}_{\mathrm{LL}} - \underline{\underline{\boldsymbol{I}}}\right)\right]. \tag{3.12}$$

The timescales τ_{d}, and τ_{s} are respectively the disengagement time (comprising

reptation and constraint release, see Section 3.2.4) and stretch relaxation times, the coefficients $(\beta_{\rm CCR}, \delta)$ are the CCR coefficients taken equal to $(1, -1/2)$, and we define the upper-convected time derivative as

$$\overset{\nabla}{\underline{\underline{\boldsymbol{A}}}} \equiv \mathrm{D}_t \underline{\underline{\boldsymbol{A}}} - \left(\underline{\underline{\boldsymbol{\kappa}}} \cdot \underline{\underline{\boldsymbol{A}}} + \underline{\underline{\boldsymbol{A}}} \cdot \underline{\underline{\boldsymbol{\kappa}}}^T \right), \tag{3.13}$$

with $\mathrm{D}_t \equiv \dfrac{\partial}{\partial t} + \boldsymbol{u} \cdot \nabla$ the convective (or material) derivative, and $\boldsymbol{u}$ the flow velocity.

Now we define the evolution equation of the "stress" (conformation tensor) on the S-chains from their entanglements with the L-chains

$$\begin{aligned} \overset{\nabla}{\underline{\underline{\boldsymbol{A}}}}_{\rm SL} \;=\; & -\frac{1}{2\tau_{\rm d,S}} \left(\underline{\underline{\boldsymbol{A}}}_{\rm SL} - \underline{\underline{\boldsymbol{I}}} \right) - \frac{2(1-\lambda_{\rm S}^{-1})}{\tau_{\rm s,S}} \, \mathrm{f_E}(\lambda_{\rm S}) \underline{\underline{\boldsymbol{A}}}_{\rm SL} \\ & - \left(\underline{\underline{\boldsymbol{A}}}_{\rm SL} - \underline{\underline{\boldsymbol{I}}} \right) \left(\underbrace{\frac{\beta_{\rm th}}{2\tau_{\rm d,L}}}_{\text{thermal CR}} + \underbrace{2\beta_{\rm CCR} \frac{(1-\lambda_{\rm L}^{-1})}{\tau_{\rm s,L}} \, \mathrm{f_E}(\lambda_{\rm L}) \lambda_{\rm S}^{2\delta}}_{\text{CCR}} \right), \end{aligned} \tag{3.14}$$

where $\beta_{\rm th}$ is the thermal constraint release coefficient, taken equal to 1. It accounts for the reptation of the L-chains. The factor 2, in front of the orientation relaxation times, makes the set of equations consistent, in the linear regime, with the double reptation model [des Cloizeaux (1988)], as demonstrated below in Section 3.2.2. The term $(1 - \lambda_{\rm L}^{-1})$ gives the rate of entanglement release from the long chains, and the factor $\lambda_{\rm S}^{2\delta}$ arose in the original Rolie-Poly equation from considering the effect of the constraint release on the stretched chains. This is why the subscripts are as they are in the CCR expression.

Similarly, we define the evolution equation of the "stress" on the L-chains

from their entanglements with the S-chains

$$\overset{\nabla}{\underline{\underline{\boldsymbol{A}}}}_{\mathrm{LS}} = -\frac{1}{2\tau_{\mathrm{d,L}}}\left(\underline{\underline{\boldsymbol{A}}}_{\mathrm{LS}} - \underline{\underline{\boldsymbol{I}}}\right) - \frac{2(1-\lambda_{\mathrm{L}}^{-1})}{\tau_{\mathrm{s,L}}}\,\mathrm{f_E}(\lambda_{\mathrm{L}})\underline{\underline{\boldsymbol{A}}}_{\mathrm{LS}} - \left(\underline{\underline{\boldsymbol{A}}}_{\mathrm{LS}} - \underline{\underline{\boldsymbol{I}}}\right)\left(\underbrace{\frac{\beta_{\mathrm{th}}}{2\tau_{\mathrm{d,S}}}}_{\text{thermal CR}} + \underbrace{2\beta_{\mathrm{CCR}}\frac{(1-\lambda_{\mathrm{S}}^{-1})}{\tau_{\mathrm{s,S}}}\,\mathrm{f_E}(\lambda_{\mathrm{S}})\lambda_{\mathrm{L}}^{2\delta}}_{\text{CCR}}\right). \tag{3.15}$$

3.2.2 Linear rheology

Equation (3.6) contains 4 different Maxwell times in the linear rheology. In the limit where we consider that the short chain have a disengagement time smaller than the long chains, $\tau_{\mathrm{d,S}} \ll \tau_{\mathrm{d,L}}$, we have

$\underline{\underline{\boldsymbol{A}}}_{\mathrm{SS}}$ relaxes at time $(\frac{1}{2\tau_{\mathrm{d,S}}} + \frac{\beta_{\mathrm{th}}}{2\tau_{\mathrm{d,S}}})^{-1} \approx \tau_{\mathrm{d,S}}^{-1}$ and contributes a weight ϕ_{S}^2 to the stress,

$\underline{\underline{\boldsymbol{A}}}_{\mathrm{SL}}$ relaxes at time $(\frac{1}{2\tau_{\mathrm{d,S}}} + \frac{\beta_{\mathrm{th}}}{2\tau_{\mathrm{d,L}}})^{-1} \approx (2\tau_{\mathrm{d,S}})^{-1}$ and contributes a weight $\phi_{\mathrm{S}}\phi_{\mathrm{L}}$ to the stress,

$\underline{\underline{\boldsymbol{A}}}_{\mathrm{LL}}$ relaxes at time $(\frac{1}{2\tau_{\mathrm{d,L}}} + \frac{\beta_{\mathrm{th}}}{2\tau_{\mathrm{d,L}}})^{-1} \approx \tau_{\mathrm{d,L}}^{-1}$ and contributes a weight ϕ_{L}^2 to the stress,

$\underline{\underline{\boldsymbol{A}}}_{\mathrm{LS}}$ relaxes at time $(\frac{1}{2\tau_{\mathrm{d,L}}} + \frac{\beta_{\mathrm{th}}}{2\tau_{\mathrm{d,S}}})^{-1} \approx (2\tau_{\mathrm{d,S}})^{-1}$ and contributes a weight $\phi_{\mathrm{S}}\phi_{\mathrm{L}}$ to the stress.

These results are consistent with the double reptation, Equation (3.5). Figure 3.1 sketches the predictions in the linear regime, for a frequency sweep experiment. A fraction $\phi_{\mathrm{S}}^2 + 2\phi_{\mathrm{S}}\phi_{\mathrm{L}}$ of the stress relaxes at $\omega \approx \tau_{\mathrm{d,S}}^{-1}$ and a fraction ϕ_{L}^2 relaxes at $\omega \approx \tau_{\mathrm{d,L}}^{-1}$.

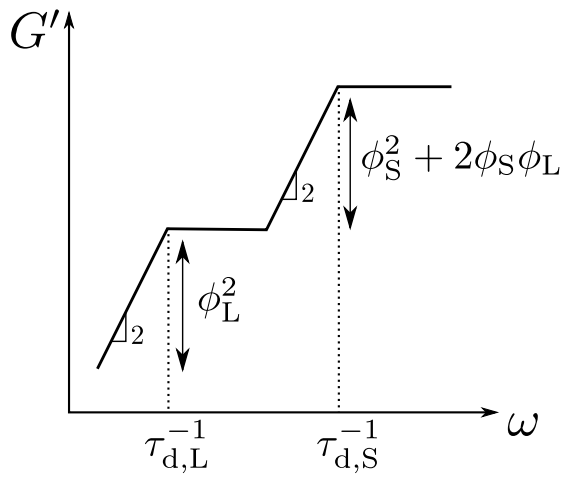

Figure 3.1: Sketch of the linear regime predictions for Equation (3.5) and Equation (3.6) for a frequency sweep experiment.

3.2.3 Enhanced stretch relaxation time

The onset of chain stretch and emergent extension hardening in the nonlinear rheological response of molten binary blends (of long and short polymer chains) is set by an effective stretch relaxation time of the long chains. It has been found experimentally [Auhl *et al.* (2009)] that this effective stretch relaxation time of the long chains initially increases proportionally to the inverse volume fraction of long chains $\phi_L^{-\alpha}$, where α is the dilution exponent for entanglements (we assume $\alpha = 1$ here). In elongation experiments, if the flow rate exceeds the inverse of the stretch relaxation time of the long molecules, they are stretched by the flow, i.e. their length along the tube contour grows. The macroscopic consequence of chain stretch is *elongation hardening*, i.e. the elongational viscosity, η_E^+, grows above the linear viscoelastic envelope prediction.

A detailed theoretical framework for bidisperse blend of entangled polymers has been established by Read *et al.* [Read *et al.* (2012)], where the enhanced relaxation time appears naturally within the theory. Although much simpler, the "blend of Rolie-Poly equations", presented in Section 3.2.1, *do* contain the

enhanced relaxation time. Indeed, if the extension rate, $\dot{\varepsilon}$, is smaller than the reptation time of the short chains, $\dot{\varepsilon}\tau_{\mathrm{d,S}} \ll 1$, then $\underline{\underline{\boldsymbol{A}}}_{\mathrm{LS}} \approx \underline{\underline{\boldsymbol{I}}}$. Hence the stretch λ_{L} of the L-chain, defined Equation (3.7), is

$$\begin{aligned} \lambda_{\mathrm{L}}^2 &= \frac{1}{3}\left(\phi_{\mathrm{S}} \operatorname{tr} \underline{\underline{\boldsymbol{A}}}_{\mathrm{LS}} + \phi_{\mathrm{L}} \operatorname{tr} \underline{\underline{\boldsymbol{A}}}_{\mathrm{LL}}\right) \\ &\approx \phi_{\mathrm{S}} + \frac{1}{3}\phi_{\mathrm{L}} \operatorname{tr} \underline{\underline{\boldsymbol{A}}}_{\mathrm{LL}}, \quad \dot{\varepsilon}\tau_{\mathrm{d,S}} \ll 1. \end{aligned} \tag{3.16}$$

Taking the time derivative of Equation (3.16) and reorganizing, we have

$$2\lambda_{\mathrm{L}} \frac{\mathrm{d}\lambda_{\mathrm{L}}}{\mathrm{d}t} = \frac{\phi_{\mathrm{L}}}{3} \frac{\mathrm{d} \operatorname{tr} \underline{\underline{\boldsymbol{A}}}_{\mathrm{LL}}}{\mathrm{d}t}. \tag{3.17}$$

Using Equation (3.12), and keeping only the stretch term, we obtain

$$2\lambda_{\mathrm{L}} \frac{\mathrm{d}\lambda_{\mathrm{L}}}{\mathrm{d}t} \approx \frac{\phi_{\mathrm{L}}}{3}\left(-\frac{2}{\tau_{\mathrm{s,L}}}(1-\lambda_{\mathrm{L}}^{-1}) \operatorname{tr} \underline{\underline{\boldsymbol{A}}}_{\mathrm{LL}}\right). \tag{3.18}$$

We then use Equation (3.16) to arrive at

$$\frac{\mathrm{d}\lambda_{\mathrm{L}}}{\mathrm{d}t} = -\frac{1}{\tau_{\mathrm{s,L}}} \frac{(1-\lambda_{\mathrm{L}}^{-1})(\lambda_{\mathrm{L}}^2 - \phi_{\mathrm{S}})}{\lambda_{\mathrm{L}}}. \tag{3.19}$$

We write the stretch as $\lambda_{\mathrm{L}} = 1 + \ell_{\mathrm{L}}$, where ℓ_{L} is the "extra" stretch. Therefore we have

$$1 - \lambda_{\mathrm{L}}^{-1} = \ell_{\mathrm{L}}/(1+\ell_{\mathrm{L}}), \quad \text{and} \quad \lambda_{\mathrm{L}}^2 - \phi_{\mathrm{S}} = \phi_{\mathrm{L}} + 2\ell_{\mathrm{L}} + \ell_{\mathrm{L}}^2, \tag{3.20}$$

so Equation (3.19) gives the time evolution of the extra stretch

$$\begin{aligned}\frac{\mathrm{d}\ell_{\mathrm{L}}}{\mathrm{d}t} &= -\frac{1}{\tau_{\mathrm{s,L}}}\frac{\ell_{\mathrm{L}}(\phi_{\mathrm{L}}+2\ell_{\mathrm{L}}+\ell_{\mathrm{L}}^2)}{(1+\ell_{\mathrm{L}})^2} \\ &\approx \begin{cases} -\dfrac{\phi_{\mathrm{L}}}{\tau_{\mathrm{s,L}}}\ell_{\mathrm{L}}, & \ell_{\mathrm{L}} \ll 1 \\ -\dfrac{1}{\tau_{\mathrm{s,L}}}\ell_{\mathrm{L}}, & \ell_{\mathrm{L}} \gg 1 \end{cases} .\end{aligned} \tag{3.21}$$

We see that the "effective" stretch relaxation time of the L-chains at small stretch ($\ell_{\mathrm{L}} \ll 1$) is

$$\tau_{\mathrm{s,L}}^{\mathrm{eff}} = \frac{\tau_{\mathrm{s,L}}}{\phi_{\mathrm{L}}}. \tag{3.22}$$

The stretch relaxation time is therefore renormalised by a factor $\phi_{\mathrm{L}}^{-1} > 1$, so, the L-chains (blended with S-chains) will start to stretch at smaller flow rate than if there were no S-chains. At large stretch, $\ell_{\mathrm{L}} \gg 1$, there is no renormalisation of the stretch relaxation time.

We illustrate this phenomenon in Figure 3.2 where the predictions of our "blend" of Rolie-Poly equations in uniaxial extension are shown, virtually without finite extensibility ($\lambda_{\max} \gg 1$). The short chains ($\tau_{\mathrm{d,S}} = 0.05$, $\tau_{\mathrm{s,S}} = 0.01$), are blended with 5% of long chains ($\tau_{\mathrm{d,L}} = 100$, $\tau_{\mathrm{s,L}} = 1$). When the elongation rate, $\dot{\varepsilon}$, is small, the stress growth coefficient (viscosity), η_{E}^{+}, follows the LVE. The onset of elongation hardening is clearly seen for $\dot{\varepsilon} = 0.05$ and above. It is in agreement with Equation (3.21) as $\tau_{\mathrm{s,L}} = 1$ and $\phi_{\mathrm{L}} = 0.05$. Another feature of Figure 3.2 is that the stress grows but then stops for flow rates between 0.05 and 1; but then it continues to grow for larger flow rates. This has to do with nonlinear terms in Equation (3.21), i.e. for large ℓ_{L}, the effective relaxation time is simply $\tau_{\mathrm{s,L}}^{-1}$.

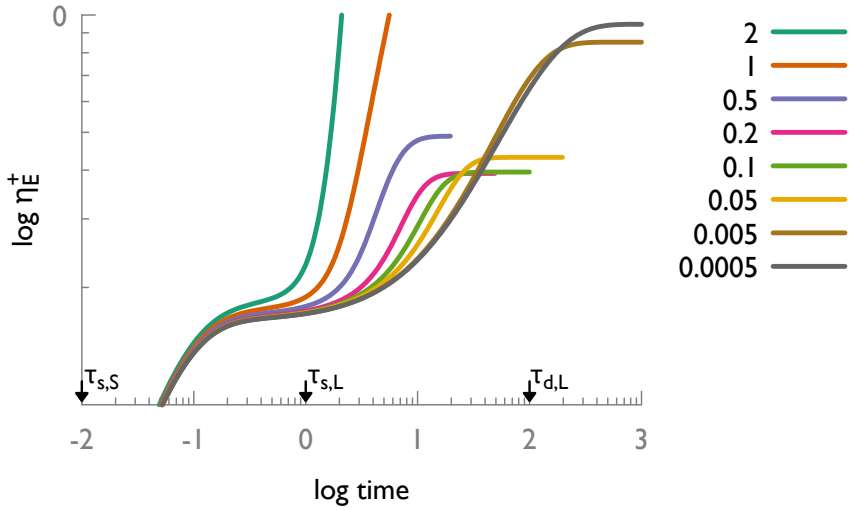

Figure 3.2: Illustration of the enhanced stretch relaxation time. Logarithms of the stress growth coefficient in elongation, η_E^+ as a function of time for different elongation rates for a blend of S-chains ($\tau_{d,S} = 0.05$, $\tau_{s,S} = 0.01$) with, $\phi_L = 0.05$, L-chains ($\tau_{d,L} = 100$, $\tau_{s,L} = 1$). We set $\lambda_{max} \gg 1$. According to Equation (3.22), the enhanced stretch relaxation time is $\tau_{s,L}/\phi_L = 20$.

3.2.4 Comparison with experimental data

In this section, we compare our model predictions with experimental data of four bidisperse melts found in Ref. [Read *et al.* (2012)]. The majority of the parameters of the model are fixed by chemistry, taken from literature values, or calculated from these. Only one parameter is used as a fitting parameter in linear rheology, which then yields a parameter-free prediction of the nonlinear rheology (shear and extension).

Fixed parameters

We use the parameters $\{\tau_e, M_e, M_L, M_S, G_e\}$, provided in Table II of Ref. [Read *et al.* (2012)], for four blends of (long and short) linear monodisperse entangled chains [Auhl *et al.* (2008)]. We reproduce them in Table 3.1.

Table 3.1: Parameters of four binary blends, from Ref. [Read *et al.* (2012)].

	PI226_23_20	PI226_23_40	PI483_34_40	PS blend 2
T (°C)	25	25	25	130
$\phi_{\rm L}$	0.2	0.4	0.4	0.1437
$G_{\rm e}$ (kPa)	595.5	595.5	595.5	276
$M_{\rm L}$ (kg/mol)	226	226	483.1	390
$M_{\rm S}$ (kg/mol)	23.4	23.4	33.6	51.7
$M_{\rm e}$ (kg/mol)	4.816	4.816	4.816	18.1
$\tau_{\rm e}$ (s)	1.314×10^{-5}	1.314×10^{-5}	1.314×10^{-5}	0.91

Calculated parameters

Stretch relaxation times: The stretch relaxation times of the short (S) and long (L) chains are computed from the fixed parameters, Table 3.1, as follows

$$\tau_{\rm s,S} = Z_{\rm S}^2\tau_{\rm e}, \quad \text{and} \quad \tau_{\rm s,L} = Z_{\rm L}^2\tau_{\rm e}, \tag{3.23}$$

with $Z = M/M_{\rm e}$ the entanglement number, M is the molecular mass of the S- or L-chains, $M_{\rm e}$ is the entanglement molecular mass, and $\tau_{\rm e}$ is the Rouse time of an entanglement segment.

Reptation times: The relaxation times $\tau_{\rm d,S}$ and $\tau_{\rm d,L}$ have to be understood as Maxwell relaxation times. They contain all the relaxation mechanisms of the stress related to the tubes. For monodisperse chains, the many chain relaxation function of the stress accumulated in the tubes was written as [Likhtman & McLeish (2002)]

$$G(t) = \frac{4}{5}G_{\rm e}R(t)\mu(t) \approx \frac{4}{5}G_{\rm e}\mu^2(t), \tag{3.24}$$

where $R \approx \mu^\alpha$ is the relaxation via CR (α is the dilution exponent that we take equal to 1) and μ the relaxation via reptation and CLF that occurs in a

characteristic time $\tau_{\rm d}^{\mu}$. It is defined as [Doi (1983); Likhtman & McLeish (2002)]

$$\tau_{\rm d}^{\mu} = 3Z^3\tau_{\rm e}\, f_{\mu}(Z), \quad \text{with} \quad f_{\mu}(Z) = 1 - \frac{2C_1}{Z^{1/2}} + \frac{C_2}{Z} + \frac{C_3}{Z^{3/2}}, \tag{3.25}$$

where the function $f_{\mu}(Z)$ accounts for contour length fluctuation effects. The coefficient are $C_1 = 1.69$, $C_2 = 4.17$, and $C_3 = -1.55$ [Likhtman & McLeish (2002)]. Taking a similar approach, for our binary blend, we assume:

$$\tau_{\rm d,S}^{\mu} = 3Z_{\rm S}^3\tau_{\rm e}\, f_{\mu}(Z_{\rm S}), \quad \text{and} \quad \tau_{\rm d,L}^{\mu} = 3Z_{\rm L}^3\tau_{\rm e}\, f_{\mu}(\tilde{Z}_{\rm L}), \tag{3.26}$$

where $\tilde{Z}_{\rm L} = \phi_{\rm L} Z_{\rm L}$ is the number of long chain entanglements per long chain, assuming a dilution exponent of 1 [Viovy *et al.* (1991)]. The reason for using $\tilde{Z}_{\rm L}$ instead of $Z_{\rm L}$ is that we assume contour length fluctuations occur in the fat tube, as explained in Ref. [Read *et al.* (2012)]. Assuming that the relaxation modulus, Equation (3.24), is relaxing on a Maxwell time $\tau_{\rm d}$ (which contains all the relaxation mechanisms related to the tube), then

$$\begin{aligned} G(t) \approx \exp(-t/\tau_{\rm d}) &\approx \mu(t)^2 \\ &= \exp(-2t/\tau_{\rm d}^{\mu}). \end{aligned} \tag{3.27}$$

Therefore, in Equations (3.11) to (3.15), the relaxation times, $\tau_{\rm d}$, are taken as half that of Equation (3.26)

$$\tau_{\rm d,S} = \frac{1}{2}\tau_{\rm d,S}^{\mu}, \quad \text{and} \quad \tau_{\rm d,L} = \frac{1}{2}\tau_{\rm d,L}^{\mu}. \tag{3.28}$$

Plateau modulus: Doi-Edwards theory predicts the plateau modulus to be 4/5 of the rubber modulus, $G_{\rm e} = \rho RT/M_{\rm e}$, because entanglements do allow longitudinal motion along the tube and therefore are different from cross-links.

The value of the (experimentally observed) plateau modulus, G_N^0, that we use in Equation (3.6) is taken as ("Graessley–Fetters" definition [Fetters *et al.* (1999); Graessley (1980)])

$$G_N^0 = \frac{4}{5}\frac{\rho RT}{M_e} = \frac{4}{5}G_e, \tag{3.29}$$

where G_e is the value reported in Table 3.1.

In Table 3.2, we summarize the calculated parameters used to produce the predictions in Figures 3.3–3.6.

Fitting parameter $\tilde{\phi}_L$

The volume fraction of long chains, ϕ_L, reported in Table 3.1, is given by the chemistry. In the model, we need to adjust that parameter to account for the partial relaxation of long chains on the timescale of the relaxation of the short chains. Indeed, during the time needed by the fraction $\phi_S = 1-\phi_L$ of short chains to relax, a portion of the ϕ_L long chains have relaxed too, leaving only a volume fraction $\tilde{\phi}_L \leq \phi_L$ of long chain unrelaxed.

$\tilde{\phi}_L$ is obtain from "best fit" between the model and the data in the linear rheology, cf. Figures 3.3a–3.6a. A similar fitting parameter was used in [Read *et al.* (2012)]. Note that with only two relaxation times, we are able to obtain a reasonably good match between the linear rheology predictions and the data. Then, the nonlinear rheology predictions are produced *without* extra fitting parameters.

Results

Non linear data and model predictions are shown in Figures 3.4b–3.6b. The model quantitatively matches the experimental data in elongation at all elongation rates. This means that we are capturing the enhanced stretch relaxation time correctly. However, in shear, the model fails at predicting the moderate to high shear rates, which the more detailed model of Ref. [Read *et al.* (2012)] achieved. The failure at

Table 3.2: Computed parameters using Equation (3.23) and Equation (3.26). ϕ_L is adjusted to $\tilde{\phi}_L$ for best fit in the linear rheology.

	PI226_23_20	PI226_23_40	PI483_34_40	PS blend 2
G_N^0 (kPa)	476	476	476	221
$\tau_{d,L}$ (s)	0.48	0.75	10.2	1930
$\tau_{s,L}$ (s)	2.89×10^{-2}	2.89×10^{-2}	0.13	422
$\tau_{d,S}$ (s)	4.07×10^{-4}	4.07×10^{-4}	1.16×10^{-3}	8.84
$\tau_{s,S}$ (s)	3.10×10^{-4}	3.10×10^{-4}	6.40×10^{-4}	7.42
$\tilde{\phi}_L$	0.15	0.3	0.3	0.1437

high rates indicates that a simple 2-mode model is not enough, and probably the coupling between different chain sections of the long-chains, produced by stretch relaxation, in the "full chain" Read model [Read *et al.* (2012)] is needed.

3.3 Blend of n species

3.3.1 Generalisation of the model to n species

We can generalize Equation (3.6) to a blend of n monodisperse entangled linear polymers. The total stress is then the sum of the stresses coming from each species i, weighted by their volume fraction, ϕ_i, and finite extensibility function related to their stretch λ_i

$$\underline{\underline{\boldsymbol{\sigma}}} = G_N^0 \sum_{i=1}^{n} \phi_i \, f_E(\lambda_i) \underline{\underline{\boldsymbol{A}}}_i, \quad \text{with} \quad \lambda_i = (\text{tr}\, \underline{\underline{\boldsymbol{A}}}_i/3)^{1/2}. \tag{3.30}$$

The conformation tensor $\underline{\underline{\boldsymbol{A}}}_i$ accounts for the stresses that come from the interaction of the species i with itself and the other $(n-1)$ species. Hence, we write

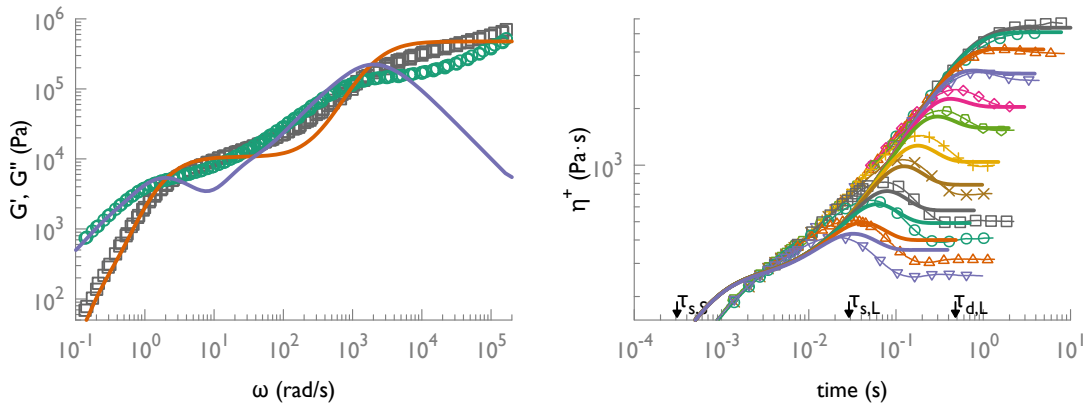

(a) LVE. (b) Nonlinear rheology.

Figure 3.3: PI226_23_20. Experimental data (symbols) and model predictions using $\tilde{\phi}_{\mathrm{L}}$ (lines). (a) LVE. (b) Nonlinear rheology, shear stress growth coefficients ($\dot{\gamma} = \{0.03493, 0.4416, 1.164, 2.22, 4.416, 6.661, 13.25, 22.2, 44.16, 66.61, 132.5, 222\}$).

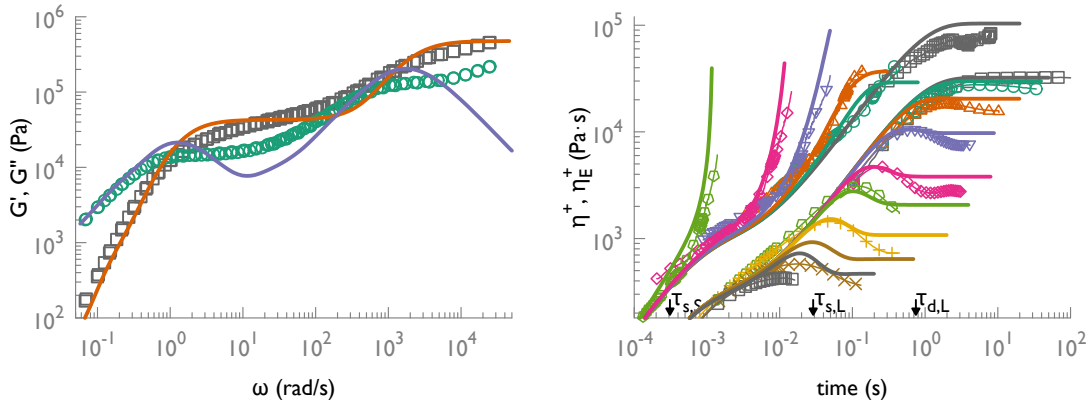

(a) LVE. (b) Nonlinear rheology.

Figure 3.4: PI226_23_40. Experimental data (symbols) and model predictions using $\tilde{\phi}_{\mathrm{L}}$ (lines). (a) LVE. (b) Nonlinear rheology, stress growth coefficients. Elongation ($\dot{\varepsilon} = \{0.2321, 6.796, 22.65, 67.64, 225.5\}$); shear ($\dot{\gamma} = \{0.02903, 0.2903, 0.9676, 2.903, 9.676, 22.65, 67.96, 226.5, 679.6\}$), top and bottom curves respectively.

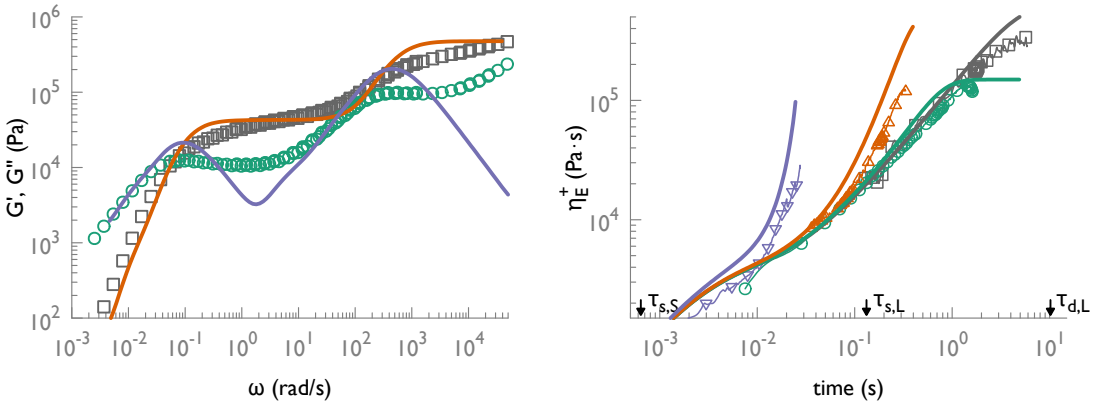

(a) LVE. (b) Nonlinear rheology.

Figure 3.5: PI483_34_40. Experimental data (symbols) and model predictions using $\tilde{\phi}_{\mathrm{L}}$ (lines). (a) LVE. (b) Nonlinear rheology, stress growth coefficients in elongation ($\dot{\varepsilon} = \{0.12, 1.2, 10.4, 100.4\}$).

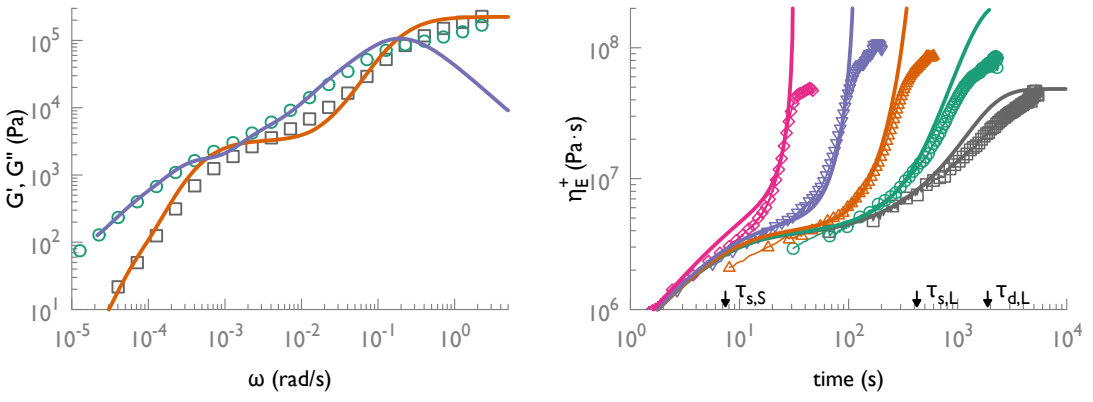

(a) LVE. (b) Nonlinear rheology.

Figure 3.6: PS 2. Experimental data (symbols) and model predictions using $\tilde{\phi}_{\mathrm{L}}$ (lines). (a) LVE. (b) Nonlinear rheology, stress growth coefficients in elongation ($\dot{\varepsilon} = \{0.001, 0.003, 0.01, 0.03, 0.1\}$).

$$\underline{\underline{\boldsymbol{A}}}_i = \sum_{j=1}^{n} \phi_j \underline{\underline{\boldsymbol{A}}}_{ij}, \tag{3.31}$$

where $\underline{\underline{\boldsymbol{A}}}_{ij}$ is the stress on the i-chains coming from their entanglements with the j-chains. Analogously to Equation (3.14), we have

$$\begin{aligned} \overset{\nabla}{\underline{\underline{\boldsymbol{A}}}}_{ij} \;=\; & -\frac{1}{2\tau_{\mathrm{d},i}}\left(\underline{\underline{\boldsymbol{A}}}_{ij} - \underline{\underline{\boldsymbol{I}}}\right) - \frac{2(1-\lambda_i^{-1})}{\tau_{\mathrm{s},i}}\, \mathrm{f_E}(\lambda_i)\underline{\underline{\boldsymbol{A}}}_{ij} \\ & - \left(\underline{\underline{\boldsymbol{A}}}_{ij} - \underline{\underline{\boldsymbol{I}}}\right)\left(\frac{\beta_{\mathrm{th}}}{2\tau_{\mathrm{d},j}} + 2\beta_{\mathrm{CCR}}\frac{(1-\lambda_j^{-1})}{\tau_{\mathrm{s},j}}\, \mathrm{f_E}(\lambda_j)\lambda_i^{2\delta}\right). \end{aligned} \tag{3.32}$$

3.3.2 Comparison with experimental data

Molar mass distribution

We exemplify the use of Equations (3.30–3.32) with two polystyrene (PS) melts. It has been shown that the elongation hardening, defined as the viscosity going above the linear viscoelastic envelope, very much depends on the molar mass distribution of the melt rather than just its weight-average molar mass, M_w. For instance, by considering two PS melts of different molar mass distribution, Münstedt [Münstedt (1980)] reported that the nonlinear rheology is strongly influenced by the high molar mass components. In the following, we use Equations (3.30–3.32) with two (theoretical) PS samples that reproduce two PS blends used by Münstedt [Münstedt (1980)]. We extract the molar mass distribution presented in Fig.1 of Ref. [Münstedt (1980)] using *WebPlotDigitizer*[1], a web based tool to extract data from plots, images, and maps. The result is shown in Figure 3.8a. We discretise the molar mass distributions of these two PS samples as indicated Figure 3.8b. Note that since the high molar mass components are "diluted"

[1] http://arohatgi.info/WebPlotDigitizer

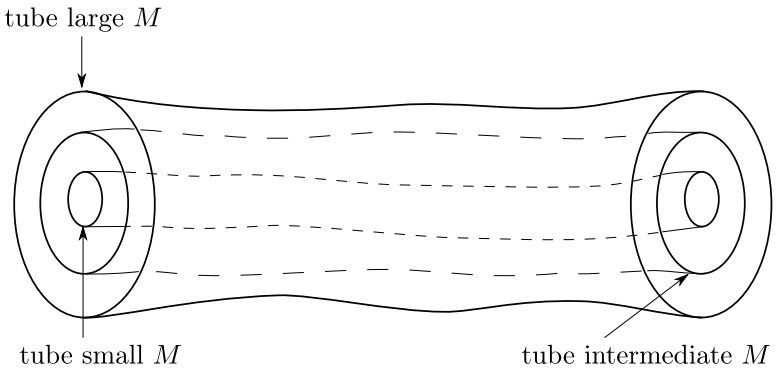

Figure 3.7: Sketch of the different tubes within which the species are confined. The species with the highest molar mass (M) has the fattest tube, made of entanglements with its own species only. The species with the smallest molar mass experiences the thinnest tube, made of entanglements with all other species. Intermediate molar mass species are confined somewhere in between.

into others, their effectiveness does not become as pronounced as in the case of separated peaks of the molecular weight, as seen Section 3.2 for binary blends.

The characteristics of the two PS samples are tabulated in Table 3.3, where

$$\frac{\langle M^k \rangle}{M^k} \equiv \frac{\sum_i w_i M_i^k}{\left(\sum_i w_i M_i\right)^k}, \quad k \geq 2 \tag{3.33}$$

are high-order molar mass averages that emphasize the high molar mass tail of the molar mass distribution, Figure 3.8. We can see from Table 3.3 that while the PS III sample has a higher weight-average molar mass, M_w, than the PS IV sample, it has a smaller polydispersity, M_w/M_n, and a shorter high-molar mass tail.

Relaxation times and dilution

For each molecular mass component, M_i, we approximate the reptation time, $\tau_{\mathrm{d},i}$, and stretch relaxation time $\tau_{\mathrm{s},i}$, from the entanglement relaxation time of

polystyrene at 160°C, $\tau_e = 10^{-2}$ s [Pattamaprom *et al.* (2000)], as

$$\tau_{d,i} = 3Z_i^3 f_\mu(\tilde{Z}_i)\tau_e, \quad \text{and} \quad \tau_{s,i} = Z_i^2 \tau_e, \tag{3.34}$$

with $Z_i = M_i/M_e$ the entanglement number of the i^{th} species, $M_e = 16\,625$ g/mol the entanglement molecular mass of polystyrene, and $f_\mu(Z)$ is the CLF correction as in Equation (3.26) [Likhtman & McLeish (2002)], and $\tilde{Z}_i = \phi_{dil,i} Z_i$ is the effective number of entanglements on the chain i, assuming a dilution exponent of 1 [Viovy *et al.* (1991)].

Equation (3.34) works, broadly, within the "dynamic dilution" picture of tube dynamics, which considers that the effective "tube" constraint felt by a given test chain depends on the timescale of the motion being considered. After relaxation of shorter chains, they release their entanglements on longer chains and so, in some sense, act as "solvent" for the longer chains. Hence, depending on the timescale, a test chain may "feel" different tubes, as illustrated in Figure 3.7, with different tubes representing the dilution as various short chain species relax. However, it is pointed out by Read and co-workers [Read *et al.* (2012)] for the case of binary blends, that the relevant tube depends upon the motion being considered. Reptation motion along the contour of a smoother "diluted" tube requires the chain to move a shorter distance, but it involves a larger friction because each step along the diluted tube requires constraint release from the shorter chains. On the other hand, reptation along the thinnest tube is subject only to the friction from the chain monomers. In most cases, the fastest reptation motion remains the low-friction motion along the thinnest tube, and this is reflected in Equation (3.34) because the undiluted number of entanglements is raised to the third power.

However, as pointed out by Read and co-workers [Read *et al.* (2012)], even if reptation is fastest along the thinner tube, the extra freedom given to the chain by constraint release events can permit deeper contour length fluctuations

commensurate with the diluted tube, which speeds up the terminal relaxation because CLF shortens the distance required to reptate. This is reflected in the factor $f_\mu(\tilde{Z})$ of Equation (3.34), but we need to make a choice as to which diluted tube is appropriate for the CLF of a given test chain. For a given dilution, $\phi_{\rm dil}$, the predicted CLF timescale is, according to Ref. [Read *et al.* (2012)], $\tau_{\rm s}/\phi_{\rm dil}$. For the purposes of the present work, we make the following assumptions: (i) the effective dilution at a given timescale t is $\phi_{\rm dil}(t)$ which is equal to the sum of the volume fractions of all chains with relaxation time greater than t; (ii) CLF makes use of the most diluted tube available at the CLF timescale. Hence, the dilution $\phi_{\rm dil}$ used in the formula for the effective CLF time $\tau_{\rm s}^{\rm eff} = \tau_{\rm s}/\phi_{\rm dil}$ is simply the effective dilution at that timescale, i.e. $\phi_{\rm dil}(\tau_{\rm s}^{\rm eff})$. This gives a self-consistent formula which can be solved to obtain the CLF time, and appropriate dilution factor for CLF, for a given chain species. The value of $\tilde{Z}$ for that species is then $\tilde{Z} = \phi_{\rm dil} Z$. This rule allows a first guess to be made for the relaxation time of each species, and so gives a prediction for the linear rheology. It is likely that, in practice, the detailed chain dynamics are more complicated (e.g. each chain has different relaxation times associated with chain ends and chain centres) so we would not expect this prediction to be perfect, and certainly more detailed work is required on linear rheology prediction.

In practice, to find the value of the dilution factor, $\phi_{{\rm dil},i}$, for the species i, we solve

$$\begin{cases} \tau_{{\rm s},i}^{\rm eff} = \dfrac{Z_i^2 \tau_{\rm e}}{\phi_{{\rm dil},i}}, \\ \phi_{{\rm dil},i} = \sum_{j_{{\rm min},i}}^{n} \phi_j, \end{cases} \tag{3.35}$$

with $j_{{\rm min},i}$ the smallest j such that $\tau_{{\rm s},i}^{\rm eff} < \tau_{{\rm d},j}$, assuming the species are ordered: $\tau_{\rm d,1} < \tau_{\rm d,2} < \cdots < \tau_{{\rm d},n}$, and ϕ_j is the volume fraction of the species j, as in Equation (3.30). In case $\tau_{{\rm s},i}^{\rm eff} > \tau_{{\rm d},n}$, we set $\phi_{{\rm dil},i} = \phi_n$.

We solve Equation (3.35) iteratively, starting with the shortest chains (i.e.

$i = 1$), for which we set $\phi_{\text{dil},1} = 1$ (no dilution), and the reptation times are computed using Equation (3.34), where the unknown dilution factors, ϕ_{dil}, are initially set equal to 1.

Due to the discretization of the molar mass distribution, Equation (3.35) gives the same ϕ_{dil} for all species i such that $\tau_{\text{d},j-1} < \tau_{\text{s},i}^{\text{eff}} < \tau_{\text{d},j}$, and so ϕ_{dil} follows steps as a function of i. In practice, we do a linear interpolation to ensure that the dilution factor is "smoothly" decreasing, i.e. we do

$$\phi_{\text{dil},i} = \phi_{\text{int},i} + \sum_{j_{\text{min},i}}^{n} \phi_j, \quad \text{where} \quad \phi_{\text{int},i} = \frac{\tau_{\text{d},j_{\text{min},i}} - \tau_{\text{s},i}^{\text{eff}}}{\tau_{\text{d},j_{\text{min},i}} - \tau_{\text{d},j_{\text{min},i}-1}} \phi_{j_{\text{min},i}-1}. \tag{3.36}$$

The interpolated value, $\phi_{\text{int},i}$, depends on the "distance" between $\tau_{\text{s},i}^{\text{eff}}$ and the two neighbouring values of τ_{d}.

In case where the dilution factor obtained is such that $Z_i \phi_{\text{dil},i} < 1$, i.e. the species i is effectively unentangled, we set $\tau_{\text{d},i}$ to be a solution of $Z_i \phi_{\text{dil},i}(\tau_{\text{d},i}) = 1$, using Equation (3.36) to do the interpolation of $\phi_{\text{dil},i}$. This gives the time when the species i becomes unentangled, resulting in a constraint-release Rouse motion [Milner *et al.* (1998); Viovy *et al.* (1991)].

Results

Figure 3.9 presents the predicted elongational viscosity, or stress growth coefficient, for the PS III and PS IV samples at various elongation rates. We may note that the linear rheology is not perfectly predicted. The theory slightly over predicts the LVE for the PS IV blend. We note that we have simply taken literature values for M_{e}, G_{e} and τ_{e}, and made predictions using the "recipe" suggested in Equations (3.34) to (3.36), with no free fitting parameters. This indicates that more work is required on the linear rheology prediction. Our focus, however, is on the nonlinear rheology, and we can see that despite the relatively small dif-

Table 3.3: Characteristics of the two (model) PS melts used to produce the predictions Figure 3.9.

	PS III		PS IV	
	Reference	Model	Reference	Model
M_w (kg/mol)	253	253	219	219
M_w/M_n	1.9	1.2	2.3	1.8
$\langle M^2\rangle/M^2$	1.19	1.1	1.69	1.4
$\langle M^3\rangle/M^3$	1.55	1.7	4.2	5.3
$\langle M^4\rangle/M^4$	2.23	2.3	14.55	17.4

ferences between the molar mass distribution of these two samples, cf. Figure 3.8 and Table 3.3, there is a strong difference in their response to nonlinear flow, which is captured by our model, especially the elongation hardening feature, i.e. where the viscosity departs from the LVE.

Experimental data of the PS IV sample showed a clear elongation hardening at the two highest elongation rate, $\dot{\varepsilon} = \{0.07, 0.3\}$, see Figure 3.9, and marginally at $\dot{\varepsilon} = 0.015$. These features were captured by the model which showed elongation hardening occurring at the two highest elongation rates, $\dot{\varepsilon} = \{0.07, 0.3\}$. In contrast, our PS III sample does not present elongation hardening, even at the highest flow rate, $\dot{\gamma} = 0.07$. These results are in qualitative agreement (for the elongation hardening feature) with experimental data of Münstedt [Münstedt (1980)], where the PS III sample do not present elongation hardening at $\dot{\varepsilon} = 0.07$, while the PS IV sample is above the LVE at that flow rate.

3.4 Conclusions

In this Chapter, we proposed a simplified tube model, based on the Rolie-Poly model [Likhtman & Graham (2003)], for a polydisperse melt of entangled poly-

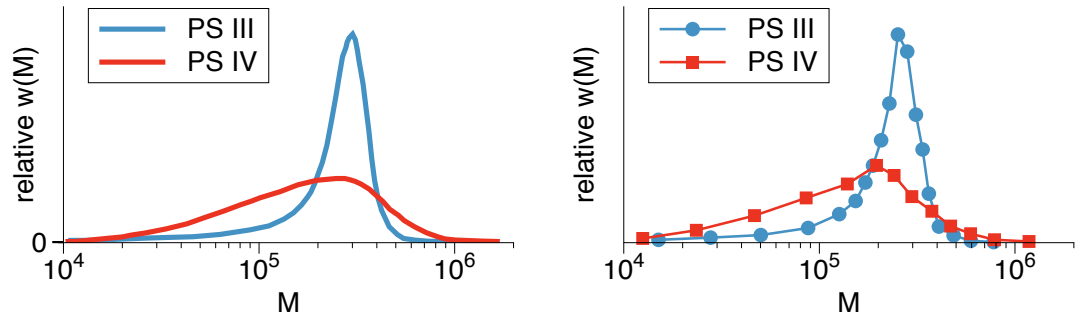

(a) Reference (b) Model

Figure 3.8: Molar mass distribution (in g/mol) of the PS III and PS IV blends of Ref. [Münstedt (1980)] (a), and of the two (theoretical) PS samples used to produce Figure 3.9 (b). Characteristics of these distributions are reported in Table 3.3

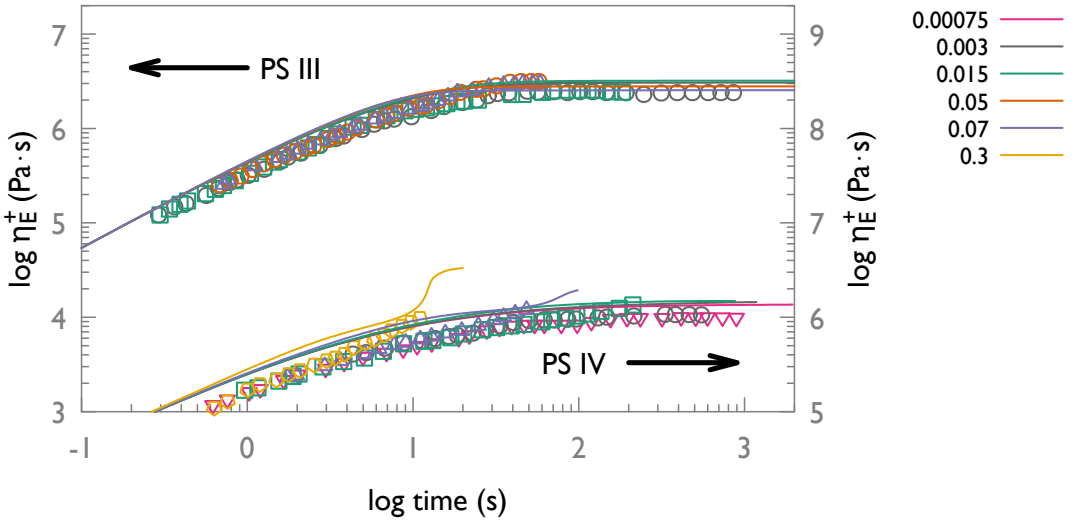

Figure 3.9: Logarithm of the elongational viscosity as a function of time for the two PS blends described in Figure 3.8. Top curves: PS III with $\dot{\varepsilon} = \{0.003,\ 0.015,\ 0.05,\ 0.07\}\ \mathrm{s}^{-1}$. Bottom curves: PS IV with $\dot{\varepsilon} = \{0.00075,\ 0.0031,\ 0.015,\ 0.07,\ 0.3\}\ \mathrm{s}^{-1}$. For comparison, we show the experimental data (symbols) from Ref. [Münstedt (1980)]. Parameters are $\tau_\mathrm{e} = 0.01$ s, $M_\mathrm{e} = 16\,625$ g/mol, $G_N^0 = 2 \times 10^5$ Pa, $\lambda_\mathrm{max} = 10$.

mers that aims at predicting nonlinear rheology, whilst being consistent with the "double reptation" theory [des Cloizeaux (1988)] in linear rheology.

For the case of bidisperse blends (blend of long and short chains), we have compared the predictions of the model with experimental data from Ref. [Read *et al.* (2012)]. The model presented has only one fitting parameter that is adjusted using linear rheology data. Then, there are no extra fitting parameter to produce the prediction of nonlinear rheology (shear and extension). The model quantitatively matches the experimental data in elongation at all elongation rates. This means that we are the capturing enhanced stretch relaxation time, first discussed by Auhl et al. [Auhl *et al.* (2008)], correctly. However, in shear, the model fails at predicting the moderate to high shear rates, which the more detailed model of Read *et al.* achieved. The failure at high rates indicates that a simple 2-mode model is not enough, and probably the coupling between different parts of the long chain, produced by chain retraction, in the "full chain" model of Read et al. [Read *et al.* (2012)] is needed.

Finally, we generalised the model to polydisperse melts and compared our model predictions to experimental data of Münstedt [Münstedt (1980)]. Given that the nonlinear rheology is strongly influenced by the high molar-mass components (i.e. it depends on the molecular weight distribution of the melt rather than just its weight-average molar mass, M_w), we investigated the nonlinear rheological properties of two PS melts having different molar mass distribution. The model slightly over predicted the LVE of the PS IV sample. This, essentially, is a problem with the double reptation formalism we used. Nevertheless, our goal was to develop a simple model for the *nonlinear* rheology of polydisperse melts. The elongation hardening that was seen experimentally in Ref. [Münstedt (1980)] for the sample with high molar mass component could be qualitatively reproduced using our polydisperse model. Experimental data of the PS IV sam-

ple showed elongation hardening, i.e. where the viscosity departs from the LVE, at the two highest elongation rates. These features were captured by the model which showed elongation hardening occurring at the same elongation rates. Note that, due to the finite extensibility term in the model, the viscosity saturates to a steady state after hardening. It is possible that experimental data would show a similar feature if the experiments were run for larger strain (longer time). On the other hand, the experimental data of the PS III sample did not present any sign of shear hardening, and nor did the model prediction. Hence, given a molecular mass distribution, the model can successfully predict when, and at which elongation rate, elongation hardening might occur. It is worth noting that the model does it without any fitting parameter.

Part II

Models for entangled telechelic star polymers

This page is intentionally left blank

Introduction

Telechelic polymers, as introduced by Ref. [Uraneck *et al.* (1960)], are defined as polymer molecules possessing functional terminal end-groups. Because these end-groups, also referred to as "stickers", can create transient networks, they modify the (long time) flow properties of the material. By tuning the strength or the nature of the stickers, one can modify the supramolecular structure of the system. Previous theoretical works and simulations have tried to understand the different interactions leading to the self assembling process of unentangled solutions of linear telechelic polymers [Semenov *et al.* (1995a); Tripathi *et al.* (2006)], or polymers with stickers along the backbone [Rubinstein & Semenov (1998); Semenov & Rubinstein (1998); Semenov *et al.* (1995b)], or linear entangled polymers with stickers along the backbone [Baxandall (1989); Leibler *et al.* (1991); Rubinstein & Semenov (2001)].

Our goal in this second Part of the thesis is to produce a "toy" (i.e. "single mode") constitutive model that captures elements of the nonlinear rheology of entangled telechelic polymers, and to explore the interaction between timescales set by the stickers, timescales set by the entangled polymer, and the flow rate. In creating such a toy model, we have chosen to consider a star polymer architecture and, since this does not immediately seem the most obvious choice, we feel it requires some explanation before proceeding. In particular: why did we choose a star architecture instead of a linear?

An entangled star arm is pinned at one end by its branch point – which is fixed in our simple model (we ignore, for simplicity, branch point withdrawal [Bick & McLeish (1996); Hawke *et al.* (2015); McLeish & Larson (1998); Wagner & Rolon-Garrido (2008)]). Hence, as presented in Figure 4.1, we consider that the star arm has strictly only two possible states: (i) when the sticker is "attached" then no relaxation is possible – except through convective constraint release in nonlinear flows [Marrucci (1996)] – and the arm is trapped in the entanglement network; (ii) when the sticker is "detached" then relaxation becomes possible by contour length fluctuation (CLF).

In contrast, the other "simple" architecture, telechelic linear chains (with stickers at both ends), has a greater number of states to consider: linear chains can stick together to form longer linear chains, somewhat akin to wormlike micelles [Cates (1990)], which can still relax by reptation (i.e. the stickers do not prevent relaxation, but only increase the reptation time), which, in turn, delays the nonlinear effects (stretching of the chains) that we aim at studying here. Moreover, in practice, even stickers designed to be difunctional commonly have additional weaker associations with other stickers, so that they tend to form clusters, suppressing the reptation [Tam *et al.* (1998)] – when this occurs the possible relaxation pathways of the material start to become somewhat complex, which wholly defeats the object of our intended "toy" model study.

In some materials, the stickers are actually designed to form clusters rather than pair-wise associations, e.g. zwitterionic groups that forms "clusters of sticker pairs" [Fetters *et al.* (1988); van Ruymbeke *et al.* (2010); Vlassopoulos *et al.* (1999; 2000)]. Telechelic linear chains have stickers at both ends so that release of either sticker could give rise to relaxation of the entangled chain. However, we could assume that, when one sticker is released, the other normally remains

attached to its cluster. In this case, the attached cluster acts in a similar way to the branch point in a star polymer, suppressing reptation, so that relaxation is via CLF (breathing modes/arm retraction) [Ball & McLeish (1989); McLeish & Milner (1999); Milner & McLeish (1997)]. Only when both stickers are released can reptation occur (a rare event if the stickers are strong). Again, consideration of these effects gives rise to a greater number of states for the linear chains, as compared to the "simpler" star arm.

Linear chains are therefore more complicated than the star architecture for the purposes of the present study since whether we consider pair-wise association, or clusters of stickers, the star arm is a two-state system whilst the linear chain requires consideration of multiple states. Nevertheless, given the above argument that in practice the relaxation of linear chains shares features with star chains, we might hope that our toy model captures the essence of the nonlinear rheology for many linear chain systems. In this sense, we consider our model to be an equivalent of the "pom-pom" model for branched polymers [Hawke *et al.* (2015); McLeish & Larson (1998)] – it is based on a simplified picture of a representative architecture, and designed to capture the essential physics. Star polymers, first reported in Ref. [Morton *et al.* (1962); Schaefgen & Flory (1948)], exhibit unique properties due to their spatially defined and compact three-dimensional structure. Efficient synthetic routes and unique rheological properties make them promising tools for use in drug delivery, biomedical applications, or thermoplastics, amongst other applications [Hadjichristidis *et al.* (2012); Ren *et al.* (2016)]. Entangled telechelic star polymers have been the focus of previous work where they successfully established a linear rheology model [van Ruymbeke *et al.* (2010)]. We now aim at establishing a nonlinear rheology model for entangled telechelic stars, that would, in the limit of the linear regime, be compatible with Ref. [van Ruymbeke *et al.* (2010)].

We propose a simplified stochastic tube model for telechelic star polymers able to account for both the associating dynamics of telechelic groups and the entanglement constraints. For simplicity we consider in our model that the stickers are designed to form clusters to avoid the complications arising from bifunctional (pair-wise) associations where partner exchange and the time to search for a new free partner should be considered [Rubinstein & Semenov (1998)]. In our model, the stickers have a probability to become free (or attached) that does not depend on the surrounding chain states. Nevertheless, we note that more complex sticker dynamics could easily be incorporated into our model.

However simple, our resulting model exhibits interesting constitutive behavior. We find that the nature of the response to flow depends very much on the interaction between timescales set by the entanglements, and timescales set by the stickers. In principle, these timescales vary with temperature (and other factors) in different ways. This leads to (i) thermorheological complexity and (ii) the – perhaps obvious – possibility of using temperature as a control variable to change the processing properties of the material. In order to illustrate these effects, we present "maps" of the parameter space, showing how the response may be expected to change as parameters are varied.

Whilst the stochastic model gives interesting results, it is preferable for flow computations to have a simplified model which exhibits broadly the same behavior. We, therefore, get rid of the stochastic nature of our model by preaveraging our set of equations. The resulting model, quantitatively very close to that of the stochastic model, is computationally far less expensive and allows for future flow simulations. As an example of this, we present studies of the shear-banding properties of our preaveraged model in the final substantive chapter of this part of the thesis.

Part II is therefore organised as follows. In Chapter 4, we develop our stochastic model, compare the predictions in the linear regime with experimental data, and give predictions for nonlinear shear and extension rheology. Then, the preaveraged model is presented in Chapter 5 and compared against the predictions of the stochastic model. Finally, Chapter 6 illustrates flow simulations using the preaveraged model, focussing specifically on shear banding.

This page is intentionally left blank

Chapter 4

Stochastic model for entangled telechelic star polymers

4.1 Presentation of the model

In this Chapter, we develop a simplified model for entangled star polymers with sticky end groups, as a test model to explore linear and nonlinear rheology of entangled supramolecular systems. We explore the effects of interplay between entanglement timescales and sticker lifetimes within a highly simplified nonlinear constitutive model. The entanglement effect gives orientation and stretch relaxation times, $\tau_{\rm d}$ and $\tau_{\rm s}$ respectively, whilst stickers give three (non-independent) parameters: the association lifetime (i.e. the typical time a sticker stays associated before detaching), the free lifetime (i.e. the typical time a sticker stays free before reattaching), and the fraction of associated stickers, $\tau_{\rm as}, \tau_{\rm free},$ and $\phi_{\rm as}$ respectively. Different assumptions about sticker attachment and detachment dynamics have been listed in Ref. [Tripathi *et al.* (2006)]. For our initial model development, we have chosen to use the simplest possible assumption for attachment/detachment dynamics [Green & Tobolsky (1946)], but we note that other assumptions could

straightforwardly be incorporated into the model. We will match our model parameters with those used in the literature and run simulations to understand how the parameters influence the linear and nonlinear rheology. We explore the parameter space and characterize the different behaviour of the system in each region of this space.

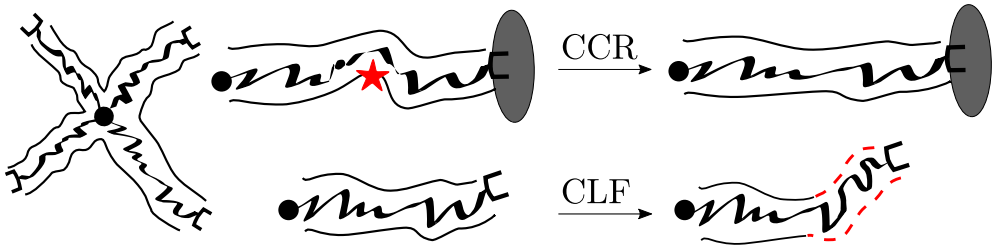

Figure 4.1: Left: representation of an entangled telechelic 4-arms star polymer. Each arm has a sticky group " ⊏ " on one end, and is fixed to the branch point " • " on the other end. Right, top: if the sticker is attached (to the grey area), CCR event (red star) contributes to stress relaxation. Bottom: if the sticker is detached, CLF relaxes stress by renewing the tube (red dashed line), in addition to CCR.

Figure 4.1 illustrates our model of star polymer. Each arm has a sticky group that can associate and dissociate due to thermal fluctuations. For the purposes of initial model development, we assume that each sticker attaches to, and detaches from, a mean field "sticky background". This is an approximation to the situation where stickers associate to micelles, with many stickers per micelle. On the right is the simplified model we are working with where only two states are possible: either the sticker is attached or detached. Our model is a single arm model. The main ingredients of our model are:

(i) probabilities of association and dissociation of the sticky end group;

(ii) entanglement effects – which give rise to tube orientation and stretching of the chain within the tube. Although star polymers have a range of relaxation times [Ball & McLeish (1989); McLeish & Milner (1999); Milner & McLeish

(1997)], we consider in our model a single orientation relaxation time and single stretch relaxation time;

(iii) finite extensibility of polymer chains.

Note that the number of star arms per molecule does not appear directly in our model but it would be a crucial parameter for the branch point withdrawal effect, which is not included in our simple model. Branch point withdrawal is, however, unlikely or rare if the number of arms per star is significant. The force balance for branch point withdrawal would require a situation where one arm is significantly stretched whilst all other arms are not stretched. Such situations may occur from time to time, but will not provide the dominant rheological response.

4.1.1 Entanglements

As a toy model for entanglements we base our single orientation relaxation time model on the Rolie-Poly equation of Likhtman and Graham [Likhtman & Graham (2003)]. Let us present a brief review of the model and its origins.

Graham and co-workers proposed a molecular theory for entangled polymer chains under fast deformation, referred to as GLaMM model [Graham *et al.* (2003)]. The GLaMM model includes the processes of reptation, thermal constraint release, chain stretch, and contour length fluctuation (CLF), but differs in the treatment of convective constraint release (CCR) – as introduced by Marrucci [Marrucci (1996)] – from previous models [Ianniruberto & Marrucci (2002b); Mead *et al.* (1998)]. However successful in predicting the rheology of fast flows, the GLaMM model requires solving partial differential equations which means intensive calculations. From the GLaMM model, Likhtman and Graham derived a simplified constitutive equation, called the Rolie-Poly equation (for Rouse linear entangled polymers) [Likhtman & Graham (2003)]. It is a simple one-mode differ-

ential constitutive equation for the stress tensor that contains reptation, stretch and CCR. In that theory, the time evolution equation of the conformation tensor of the polymer chain, $\underline{\underline{\boldsymbol{\tau}}}$, is given by

$$\frac{\mathrm{d}\underline{\underline{\boldsymbol{\tau}}}}{\mathrm{d}t} = \underline{\underline{\boldsymbol{\kappa}}} \cdot \underline{\underline{\boldsymbol{\tau}}} + \underline{\underline{\boldsymbol{\tau}}} \cdot \underline{\underline{\boldsymbol{\kappa}}} + \underline{\underline{\mathbf{f}}}(\underline{\underline{\boldsymbol{\tau}}}), \tag{4.1}$$

with the function $\underline{\underline{\mathbf{f}}}$ given by

$$\underline{\underline{\mathbf{f}}}(\underline{\underline{\boldsymbol{\tau}}}) = -\frac{1}{\tau_\mathrm{d}}(\underline{\underline{\boldsymbol{\tau}}} - \underline{\underline{\boldsymbol{I}}}) - \frac{2}{\tau_\mathrm{s}}\left(1 - \left(3/\operatorname{tr}\underline{\underline{\boldsymbol{\tau}}}\right)^{1/2}\right)\left(\underline{\underline{\boldsymbol{\tau}}} + \beta\left(\operatorname{tr}\underline{\underline{\boldsymbol{\tau}}}/3\right)^{\delta}(\underline{\underline{\boldsymbol{\tau}}} - \underline{\underline{\boldsymbol{I}}})\right), \tag{4.2}$$

and where $\underline{\underline{\boldsymbol{\kappa}}}$ is the velocity gradient tensor, τ_d the reptation or disengagement time, τ_s is the slowest Rouse time or stretch time, β is the CCR parameter as in Ref. [Marrucci (1996)] and analogous to c_ν in the GLaMM model, δ is a negative power that can be obtained by fitting to the GLaMM model, and $\underline{\underline{\boldsymbol{I}}}$ is the isotropic or equilibrium tensor.

Our stochastic system is composed of N_c chains with their own history of attachment/detachment of their sticker. We shall detail our model for the stochastic dynamics of attachment and detachment below, in Section 4.1.3. At any given time of the simulation, each chain i has either its sticker attached or detached. If the sticker is detached, we set the stretch relaxation time $\tau_{\mathrm{s},i} = \tau_\mathrm{s}$, and the orientation relaxation time $\tau_{\mathrm{d},i} = \tau_\mathrm{d}$. On the other hand, if the sticker is attached, the chain is anchored between the branch point of the star and the sticker. Therefore, stretch relaxation and orientation relaxation are prohibited, so we set $\tau_{\mathrm{s},i} \to \infty, \tau_{\mathrm{d},i} \to \infty$. Hence as each individual chain in our simulation undergoes its history of detachment and attachment, it switches from being able to relax its stress and stretch, or not. However, surrounding chains are still moving and release entanglement constraints: we allow our N_c chains to interact with one another via the CCR mechanism. Additionally, we include the finite

extensibility of the arm to the Rolie-Poly model using the Warner approximation of the inverse Langevin function [Warner (1972)], as introduced Equation (3.8).

Considering the arm i, the evolution equation of its conformation tensor, $\underline{\underline{\boldsymbol{\tau_i}}}$, reads

$$\begin{aligned}\frac{\mathrm{d}\underline{\underline{\boldsymbol{\tau_i}}}}{\mathrm{d}t} &= \underline{\underline{\boldsymbol{\kappa}}}\cdot\underline{\underline{\boldsymbol{\tau_i}}} + \underline{\underline{\boldsymbol{\tau_i}}}\cdot\underline{\underline{\boldsymbol{\kappa}}}^{\mathrm{T}} - \frac{1}{\tau_{\mathrm{d},i}}(\underline{\underline{\boldsymbol{\tau_i}}} - \underline{\underline{\boldsymbol{I}}}) \\ &\quad - \frac{2(1-\lambda_i^{-1})}{\tau_{\mathrm{s},i}}\,\mathrm{f_E}(\lambda_i)\underline{\underline{\boldsymbol{\tau_i}}} + 2\beta\nu\lambda_i^{2\delta}(\underline{\underline{\boldsymbol{\tau_i}}} - \underline{\underline{\boldsymbol{I}}}),\end{aligned} \tag{4.3}$$

where

$$\tau_{\mathrm{d},i} = \begin{cases}\tau_{\mathrm{d}} & \text{if } i \text{ detached}\\ \infty & \text{if } i \text{ attached}\end{cases} \quad \text{and} \quad \tau_{\mathrm{s},i} = \begin{cases}\tau_{\mathrm{s}} & \text{if } i \text{ detached}\\ \infty & \text{if } i \text{ attached}\end{cases}$$

$$\lambda_i = (\mathrm{tr}\,\underline{\underline{\boldsymbol{\tau_i}}}/3)^{1/2} \quad \text{is the stretch of the arm,}$$

$$\mathrm{f_E}(\lambda_i) = \frac{1-\lambda_{\max}^{-2}}{1-\lambda_i^2\lambda_{\max}^{-2}} \quad \text{is a finite extensibility function,}$$

with $\lambda_{\max}$ the maximal stretch, $\underline{\underline{\boldsymbol{\kappa}}}$ the velocity gradient tensor, and ν the CCR rate defined below in Section 4.1.2. For the rest of the study, we take $(\beta, \delta) = (1, -1/2)$, as suggested by Ref. [Likhtman & Graham (2003)]. The stress tensor, $\underline{\underline{\boldsymbol{\sigma}}}$, is obtained by averaging over the N_{c} chains the individual stress contributions, including the contribution from finite extensibility

$$\underline{\underline{\boldsymbol{\sigma}}} = G\frac{1}{N_{\mathrm{c}}}\sum_{i=1}^{N_{\mathrm{c}}}\mathrm{f_E}(\lambda_i)\underline{\underline{\boldsymbol{\tau_i}}}, \tag{4.4}$$

where G is the plateau modulus. In the rest of the document we take $G = 1$ without loss of generality.

4.1.2 CCR rate

We consider that the length of the chains in the tube at equilibrium is L_0, the current length of the chain i is L_i, and we define the stretch ratio $\lambda_i = L_i/L_0$. The relative velocity between the chain-end and the tube when the chain is retracting is $v_{\mathrm{rel},i} = L_0(\lambda_i - 1)\,\mathrm{f_E}(\lambda_i)/\tau_{\mathrm{s},i}$. At this point, we assume that the number of entanglements per arm is fixed, even when the arm stretches [Everaers (2012); Heinrich & Kaliske (1997); Rubinstein & Panyukov (1997)]. It follows that the average distance between entanglements on an arm increases as the chain stretches. We consider the average distance between entanglements to be $a = a_0\lambda_i$, with a_0 the average distance between entanglements at equilibrium. Therefore, the rate at which the chain-end passes the entanglements is

$$\frac{v_{\mathrm{rel},i}}{a} = \frac{L_0(\lambda_i - 1)\,\mathrm{f_E}(\lambda_i)/\tau_{\mathrm{s},i}}{a_0\lambda_i}. \tag{4.5}$$

Thus, the average CCR rate, ν, is obtained by summing over the contribution of the N_c chains, and dividing by the total number of entanglement $N_\mathrm{c}L_0/a_0$. Therefore, we obtain

$$\nu = \frac{\sum_{i=1}^{N_\mathrm{c}} L_0(\lambda_i - 1)\,\mathrm{f_E}(\lambda_i)/a_0\lambda_i\tau_{\mathrm{s},i}}{N_\mathrm{c}L_0/a_0} = \frac{1}{N_\mathrm{c}}\sum_{i=1}^{N_\mathrm{c}} \frac{1-\lambda_i^{-1}}{\tau_{\mathrm{s},i}}\,\mathrm{f_E}(\lambda_i).$$

We see that only the detached chains contribute to the CCR coefficient because $(\tau_{\mathrm{s},j})_{\mathrm{attached}} \to \infty$. Therefore, we obtain

$$\nu = \frac{1}{N_\mathrm{c}}\frac{1}{\tau_\mathrm{s}} \sum_{i,\mathrm{detached}} (1-\lambda_i^{-1})\,\mathrm{f_E}(\lambda_i). \tag{4.6}$$

4.1.3 Sticker dynamics

First, let us consider the association dynamics. In this model, the association dynamics is set to the simplest, yet sensible, expression from a large range of possible assumptions about sticker dynamics [Tripathi *et al.* (2006)]. Hence, to model a specific chemical system it is likely that the exact form of the expressions in this Section would need to be revisited. This can be done without any significant structural change to the model. Our purpose here is to explore a simple set of assumptions and to illustrate the consequences.

The dynamical equations in the previous section must be integrated numerically, i.e. using a discrete time steps Δt. During any given time step, there is a finite probability that a free sticker will become attached, or that an attached sticker will become free. Based on the typical time the stickers spend free, τ_{free}, the survival probability that a free sticker becomes associated in a simulation time step Δt is

$$p_{\text{free}\to\text{as}} = 1 - \exp\left(-\frac{\Delta t}{\tau_{\text{free}}}\right).$$

This leads us to the expression for the rate of association, in the limit where $\Delta t \ll \tau_{\text{free}}$

$$r_{\text{free}\to\text{as}} = \frac{p_{\text{free}\to\text{as}}}{\Delta t} \approx \tau_{\text{free}}^{-1}. \tag{4.7}$$

The higher the value of the parameter τ_{free}, the lower the number of transitions from free to attached per unit time. For the purpose of initial model development, we chose the simplest possible model for the rate of attachment, which is here independent of the flow rate or stretch – in contrast with more detailed models (e.g. Ref. [Tripathi *et al.* (2006)] on unentangled polymers).

The rest of this Section aims at defining a *stretch dependent* rate of detachment. Indeed, we expect the rate of detachment to increase as the chain stretches because the energy barrier that the sticker has to overcome to detach is dimin-

ished as the arm pulls on the bond. We start by defining the rate of detachment, at equilibrium, and when the arm is not stretched, similarly to the attachment rate:

$$r^{\text{eq}}_{\text{as}\to\text{free}} = \tau_{\text{as}}^{-1}, \tag{4.8}$$

where τ_{as} is the typical time an attached sticker stays attached. The bigger τ_{as}, the fewer the number of transitions from the attached state to the detached state per unit time. A steady-state implies that the total number of chains attaching per unit time equals the total number of chains detaching. This condition gives us a relation between the rate of dissociation for a non stretched arm ($\lambda = 1$) at equilibrium, and the fraction, ϕ_{as}, of associated arms at equilibrium:

$$\phi_{\text{as}}\, r^{\text{eq}}_{\text{as}\to\text{free}} = (1 - \phi_{\text{as}})\, r_{\text{free}\to\text{as}}, \tag{4.9}$$

where $r^{\text{eq}}_{\text{as}\to\text{free}} = p^{\text{eq}}_{\text{as}\to\text{free}}/\Delta t$. By substitution of Equations (4.7) & (4.8) into Equation (4.9), we obtain a relation between $\phi_{\text{as}}, \tau_{\text{as}}, \tau_{\text{free}}$:

$$\phi_{\text{as}} = \frac{\tau_{\text{as}}}{\tau_{\text{free}} + \tau_{\text{as}}}. \tag{4.10}$$

van Ruymbeke and co-workers suggested that for their experimental systems the average time spent associated is much longer than the average time spent free, i.e. $\tau_{\text{free}} \ll \tau_{\text{as}}$, this leads to a fraction of associated arms at equilibrium close to unity [van Ruymbeke *et al.* (2010)]. Typical systems called "sticky" or "supramolecular" are usually designed such that most bonds are formed, so ϕ_{as} is close to 1. We note that temperature or chemical modification of the solvent may affect the strength of the stickers, e.g. an increase of temperature deactivates hydrogen bonds; counter-ions inactivates metal-ligands stickers [Brassinne *et al.* (2013)]. These might also affect the rate at which supramolecular bonds are formed and

broken. Hence a system might be classed as "sticky" (ϕ_{as} close to 1) and yet have either a fast or slow rate of bond formation and breaking. Conversely, but perhaps less likely, it could be "not sticky" (small ϕ_{as}) but have a slow transition between attachment and detachment. All these situations are characterised by different values of ϕ_{as} and τ_{as}.

Under "strong" flows, the arms are stretched. The detachment process depends on the stretch of the arm inside the tube. Indeed, we assume that it is more likely for an attached sticker to detach when the arm is stretched because the entropic forces are pulling more strongly on the sticker.

Following previous work [Hernández Cifre *et al.* (2003); Tripathi *et al.* (2006)], we incorporate the effect of the nonlinear spring force on the exit rate (detachment rate) of the sticky group. We write the extra force acting on the sticker as

$$F(L) = \frac{3k_{\text{B}}T}{Nb^2}\frac{1 - L_{\text{eq}}^2 L_{\text{max}}^{-2}}{1 - L^2 L_{\text{max}}^{-2}}L - f_T, \tag{4.11}$$

where $L, L_{\text{eq}}, L_{\text{max}}$ are the current, equilibrium, and maximal length of the arm, respectively; $k_{\text{B}}T$ is the thermal energy, N is the number of Kuhn segments per arm in equivalent freely jointed chain, and b is the Kuhn or statistical segment length. The first term is the force pulling the arm end (i.e. pulling the sticker) inside the tube, the second term, $f_T = 3k_{\text{B}}T/a_0$, with a_0 the distance between entanglements at equilibrium, is the entropic force pulling the arm-end off the tube (Section 6.4 of Ref. [Doi & Edwards (1988)]). Note that, because we included the numerator $(1 - L_{\text{eq}}^2 L_{\text{max}}^{-2})$ in the nonlinear Warner spring factor, the net force is null at equilibrium, $F(L_{\text{eq}}) = 0$.

The detachment is considered as an activated process. Attached stickers are residing within an energy well, so that they must overcome an energy barrier in order to detach. This energy barrier is reduced by the force $F(L)$ acting over a typical length, r, which is the width of the potential energy well i.e. the "sticky

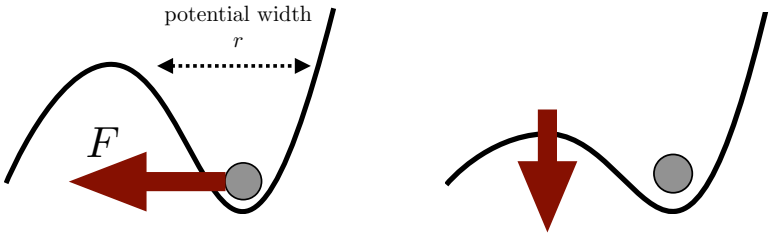

Figure 4.2: Schematic representation of the effect of a force, F, pulling on the sticker. The energy barrier that the sticker has to overcome in order to detach is reduced when a force is pulling.

zone". Figure 4.2 illustrates how pulling on the sticker reduces the energy barrier that the sticker has to overcome to jump from an attached state to a detached state, i.e. a detachment event is more likely to happen as F grows. It is a first passage problem, also known as Kramers problem [Kramers (1940)], for which the survival probability for simple cases such as a Brownian particle in a potential well is known. Since Kramers seminal work [Kramers (1940)], more complex situation have been studied. For instance, Likhtman and co-workers [Cao *et al.* (2015); Likhtman & Marques (2006)] recently developed an exact analytical method for describing the kinetics of end-chain reactions, i.e. the first passage problem of a Rouse chain (cf. Section 1.2.4) arising in the reaction diffusion theory of polymer chains.

In the case pictured in Figure 4.2, the detachment probability takes the form

$$p_{\text{as}\to\text{free}}(L) \propto \exp\left(\frac{1}{k_{\text{B}}T}\int_{L-r}^{L} F(l)dl\right),$$

with r a length characteristic of the sticker. After integration we obtain

$$p_{\text{as}\to\text{free}}(L) \propto \exp\left(-\frac{3r}{a_0}\right)\left(\frac{1-L^2L_{\text{max}}^{-2}}{1-L_{\text{max}}^{-2}\left(L-r\right)^2}\right)^{-\frac{3N}{2}\left(1-L_{\text{eq}}^2L_{\text{max}}^{-2}\right)}. \tag{4.12}$$

When the length of the arm gets close to the maximal value, L_{max}, the probability

of detachment diverges and the arm is forced to detach. This result is very similar to Ref. [Tripathi *et al.* (2006)] except that (i) in Equation (4.11), we considered the entropic force f_T arising from the entanglement effects, (ii) we added the numerator in Equation (4.11) to have $F(L_{\text{eq}}) = 0$, and (iii) we used a scalar quantity, L, to describe the arm length.

We rewrite Equation (4.12) using the dimensionless stretch ratio $\lambda = L/L_{\text{eq}} = L/Za_0$, the entanglement number $Z = Nb^2/a_0^2$, and the maximal stretch ratio $\lambda_{\text{max}} = L_{\text{max}}/L_{\text{eq}} = Nb/Za_0$, to obtain

$$p_{\text{as}\to\text{free}}(\lambda) = p_0 \exp\left(-\frac{3r}{a_0}\right)\left(\frac{1-\lambda^2\lambda_{\text{max}}^{-2}}{1-\lambda_{\text{max}}^{-2}\left(\lambda-\frac{r}{Za_0}\right)^2}\right)^{-\frac{3}{2}Z\lambda_{\text{max}}^2\left(1-\lambda_{\text{max}}^{-2}\right)}. \tag{4.13}$$

We find the proportionality constant, p_0, using Equation (4.9), and Equation (4.13) with $\lambda = 1$. It follows that the expression for the rate of detachment, $r_{\text{as}\to\text{free}}(\lambda) = p_{\text{as}\to\text{free}}(\lambda)/\Delta t$, of an associated sticker as a function of the stretch ratio λ is:

$$r_{\text{as}\to\text{free}}(\lambda) = \tau_{\text{as}}^{-1}\left(\frac{1-\lambda^2\lambda_{\text{max}}^{-2}}{1-\lambda_{\text{max}}^{-2}\left(\lambda-\frac{r}{Za_0}\right)^2}\,\frac{1-\lambda_{\text{max}}^{-2}\left(1-\frac{r}{Za_0}\right)^2}{1-\lambda_{\text{max}}^{-2}}\right)^{-\frac{3}{2}Z\lambda_{\text{max}}^2\left(1-\lambda_{\text{max}}^{-2}\right)}. \tag{4.14}$$

Throughout the present work, we assume "typical" values are $Z = 6$, $r/a_0 = 0.01$, $\lambda_{\text{max}} = 10$. Increasing λ_{max} has a clear impact on the predictions in non-linear shear or extensional flows, at flow rates greater than the inverse effective stretch time or inverse of the association time (timescales defined in Section 4.2), whichever is smaller. In shear flow, at high flow rates, it increases the strain value at which the stress is maximum and also increases the steady state stress value, however, the maximum stress value is nearly unchanged. In extensional flow, at

high extension rates, it increases the maximum and steady state stress value, and the strain at which the maximum stress occurs.

A variation of the ratio r/Za_0 has a small or no impact on the predictions as the ratio has to remain smaller than 1, the reason being that the distance between entanglement at equilibrium, a_0, is bigger than the "sticky length", r, and the entanglement number, Z, cannot be much smaller than 6 for our tube model to hold.

Therefore, some terms of Equation (4.14) are negligible: $\lambda_{\max}^{-2} \ll 1$, and $r/Za_0 \ll 1$. Under these approximations, we obtain a compact form for the rate of detachment

$$r_{\text{as}\to\text{free}}(\lambda) \approx \tau_{\text{as}}^{-1} \left(\frac{1-\lambda^2\lambda_{\max}^{-2}}{1-\lambda_{\max}^{-2}\left(\lambda - \frac{r}{Za_0}\right)^2} \right)^{-\frac{3}{2}Z\lambda_{\max}^2} . \tag{4.15}$$

4.1.4 Numerical implementation

We consider thousands of arms, each arm has its own history of attachment/detachment. When an arm is attached, i.e. the sticker at the arm-end is associated, there is a probability that at the next time step, the sticker will be detached. Similarly, when the arm is free, there is a probability that at the next time step the sticker will be associated. When the sticker is associated, we use

$$r_{\text{as}\to\text{free}}(\lambda_i) = \tau_{\text{as}}^{-1} \left(\frac{1-\lambda_i^2\lambda_{\max}^{-2}}{1-\lambda_{\max}^{-2}\left(\lambda_i - \frac{r}{Za_0}\right)^2} \right)^{-\frac{3}{2}Z\lambda_{\max}^2} , \tag{4.16}$$

$$\frac{\mathrm{d}\underline{\underline{\boldsymbol{\tau_i}}}}{\mathrm{d}t} = \underline{\underline{\boldsymbol{\kappa}}} \cdot \underline{\underline{\boldsymbol{\tau_i}}} + \underline{\underline{\boldsymbol{\tau_i}}} \cdot \underline{\underline{\boldsymbol{\kappa}}}^{\mathrm{T}} - 2\beta\nu\lambda_i^{-1}(\underline{\underline{\boldsymbol{\tau_i}}} - \underline{\underline{\boldsymbol{I}}}). \tag{4.17}$$

When the sticker is detached, we use:

$$r_{\text{free}\to\text{as}} = \tau_{\text{free}}^{-1}, \tag{4.18}$$

$$\frac{\mathrm{d}\underline{\underline{\boldsymbol{\tau_i}}}}{\mathrm{d}t} = \underline{\underline{\boldsymbol{\kappa}}}\cdot\underline{\underline{\boldsymbol{\tau_i}}} + \underline{\underline{\boldsymbol{\tau_i}}}\cdot\underline{\underline{\boldsymbol{\kappa}}}^{\mathrm{T}} - 2\beta\nu\lambda_i^{-1}(\underline{\underline{\boldsymbol{\tau_i}}} - \underline{\underline{\boldsymbol{I}}}) - \frac{1}{\tau_{\mathrm{d}}}(\underline{\underline{\boldsymbol{\tau_i}}} - \underline{\underline{\boldsymbol{I}}}) - \frac{2(1-\lambda_i^{-1})}{\tau_{\mathrm{s}}}\,\mathrm{f_E}(\lambda_i)\underline{\underline{\boldsymbol{\tau_i}}}, \tag{4.19}$$

where ν is the CCR rate defined Equation (4.6), and $\lambda_i = (\mathrm{tr}\,\underline{\underline{\boldsymbol{\tau_i}}}/3)^{1/2}$. Equations (4.16) and (4.18) are the rates of detachment and attachment of the stickers. Equations (4.17) and (4.19) are the evolution equations that the conformation tensor, $\underline{\underline{\boldsymbol{\tau_i}}}$, follows when the sticker is associated or free, respectively. The total stress is then computed according to Equation (3.6).

At each simulation time step, Δt, a uniformly distributed random number, $0 < \theta < 1$, is generated, and we compare it with the probabilities of attachment or detachment.

- If the sticker is attached and $\theta < r_{\text{as}\to\text{free}}(\lambda_i)/\Delta t$, then the sticker detaches;
- If the sticker is detached and $\theta < r_{\text{free}\to\text{as}}/\Delta t$, then the sticker attaches;
- Otherwise, the sticker stays in its previous state.

4.2 Predictions of the model: linear regime

4.2.1 Method

In order to explore the rheological response of the linear regime of our set of equations presented in Section 4.1, we perform a step strain of 1% in shear, i.e. we apply a strain rate $\dot{\gamma}$ during a short period of time, t_{step}, such that $\dot{\gamma}t_{\text{step}} = 0.01$. Then we monitor the decay of the dynamic modulus, $G(t)$, while no flow is

imposed. In many cases, the decay of $G(t)$ is rather slow, when $\phi_{\text{as}} \approx 1$, as the stickers remain attached during a time orders of magnitude greater than the simulation time step. Therefore, no relaxation of the dynamic modulus G occurs for a long period of time when $\phi_{\text{as}} \approx 1$.

Indeed, in practice, if $\tau_{\text{free}} \approx 10^{-4}\,\tau_{\text{as}}$, ($\phi_{\text{as}} \approx 0.9999$), then $\Delta t = \tau_{\text{free}}/100$ would be the biggest possible time step with Euler's method. It means that to see the first detachment event, likely to happen after a time τ_{as}, one should use 10^6 time steps. Given we consider of order 10^3 chains, we expect 10^9 Euler steps to get to the first detachment event. This number may seem acceptable, but, because multiple detachments are required to fully relax the arms, the simulation time becomes enormous.

We present the method we used to avoid unnecessary long simulations. If the chain is associated, the probability that an associated sticker has not detached during a time Δt is

$$p_{\text{as}\to\text{as}}(\Delta t) = \exp\left(-\Delta t/\tau_{\text{as}}\right).$$

We invert the probability distribution in order to obtain, from a uniformly distributed (pseudo) random number $0 < \theta < 1$, a random time, $(\Delta t)_{\text{detachment}}$, during which the sticker stays attached (or time before detachment). This time is defined as

$$(\Delta t)_{\text{detachment}} = \tau_{\text{as}} \ln(1/\theta).$$

Therefore, we can generate time intervals corresponding to times the sticker spends associated. Similarly, the time intervals corresponding to the time the sticker stays free (or time before attachment) are generated using

$$(\Delta t)_{\text{attachment}} = \tau_{\text{free}} \ln(1/\theta).$$

During the times $(\Delta t)_{\text{detachment}}$ where the sticker is attached, the modulus G for

an individual chain stays constant, and relaxation occurs only when the sticker is free. The decay of $G(t)$ for an individual chain during the times, $(\Delta t)_{\text{attachment}}$, when the sticker is free is written as

$$G(t + \Delta t) = G(t) \exp\left(-\Delta t/\tau_{\text{d}}\right). \tag{4.20}$$

This method allows us to obtain the full relaxation of $G(t)$ in a shorter simulation time than with the classic Euler method. For each chain, we simply generate randomly the history of attachment and detachment in terms of the times between these events, using the above equations. For each period of time when the chain is detached, we relax the stress according to Equation (4.20). So, for an individual chain, the stress relaxation becomes a series of plateaus (during the attached state) together with periods of stress relaxation (during the detached state). When averaged over many chains, a smooth relaxation profile $G(t)$ is attained.

From $G(t)$, we use a Schwarzl transformation [Schwarzl (1971)] to reconstruct the elastic and loss moduli G' and G''. In this section the strain applied is small, as a consequence, the system stays in the linear regime and the arms do not stretch ($\lambda = 1$). The stretch relaxation time, τ_{s}, is, therefore, irrelevant here. Note that the method just described only applies to the linear rheology predictions. This is due to the simplicity of Equations (4.17) and (4.19) when $\lambda = 1$ and no flow is imposed ($\underline{\underline{\boldsymbol{\kappa}}} = \underline{\underline{\mathbf{0}}}$): the RHS of (4.17) is zero, and the RHS of (4.19) only contains the orientation relaxation term. In the nonlinear rheology regime (see Section 4.3), there is no such simplification and we integrate Equations (4.17) and (4.19) for each stochastic arm using Euler's scheme, as described in Section 4.3.1.

4.2.2 Predictions: map of the linear regime

We are left with three parameters to explore: the orientation relaxation time, the average time a sticky group stays free, and the average time a sticky group stays attached; τ_d, τ_{free}, and τ_{as} respectively. We have found it useful to "map" out our results on a graph with the typical "free" time (τ_{free}) on the horizontal axis, and typical "associated" time (τ_{as}) on the vertical axis. Note that, on a log-log scale, lines of constant fraction of associated chains, ϕ_{as}, are parallel lines at 45 degrees to the horizontal and vertical axes. Values of ϕ_{as} close to 1 (i.e. sticky systems) are found towards the upper left of the diagram, whilst values of ϕ_{as} close to zero (i.e. non-sticky systems) are found towards the bottom right of the diagram. For linear rheology, the values of τ_{free} and τ_{as} should be compared to the orientation relaxation time, τ_d, (whilst in our equivalent maps for the nonlinear rheology, Section 4.3, we compare them against the stretch relaxation time τ_s).

Figure 4.3 reports the characteristic trends of the loss modulus, $G''(\omega)$, for different values of the parameters. Depending on how τ_{as} and τ_{free} compare with τ_d, different relaxation profiles are seen.

The dashed lines in Figure 4.3 separate the parameter map into three regions where the loss modulus as a function of the frequency has a clearly different trend. Between the regions B and C sits the horizontal line that is defined by $\tau_{as} = \tau_d$. Above that line, in the region C, the loss modulus presents two relaxation modes, at frequencies τ_d^{-1} and τ_{as}^{-1}. It is explained as follows: initially, a fraction $(1-\phi_{as})$ of polymer arms is detached, and, because $\tau_d \ll \tau_{free}$, the stickers stay free long enough so that fraction $(1-\phi_{as})$ of arms can fully relax before the sticky groups reattach. On the other hand, the fraction ϕ_{as} of polymers that was initially attached stays attached, on average, during a time τ_{as}. Once they have detached, they can fully relax in a relatively short time τ_d. Thus, the second relaxation mode is located at $\omega = (\tau_{as} + \tau_d)^{-1} \approx \tau_{as}^{-1}$, because $\tau_{as} \gg \tau_d$ in region C. Below

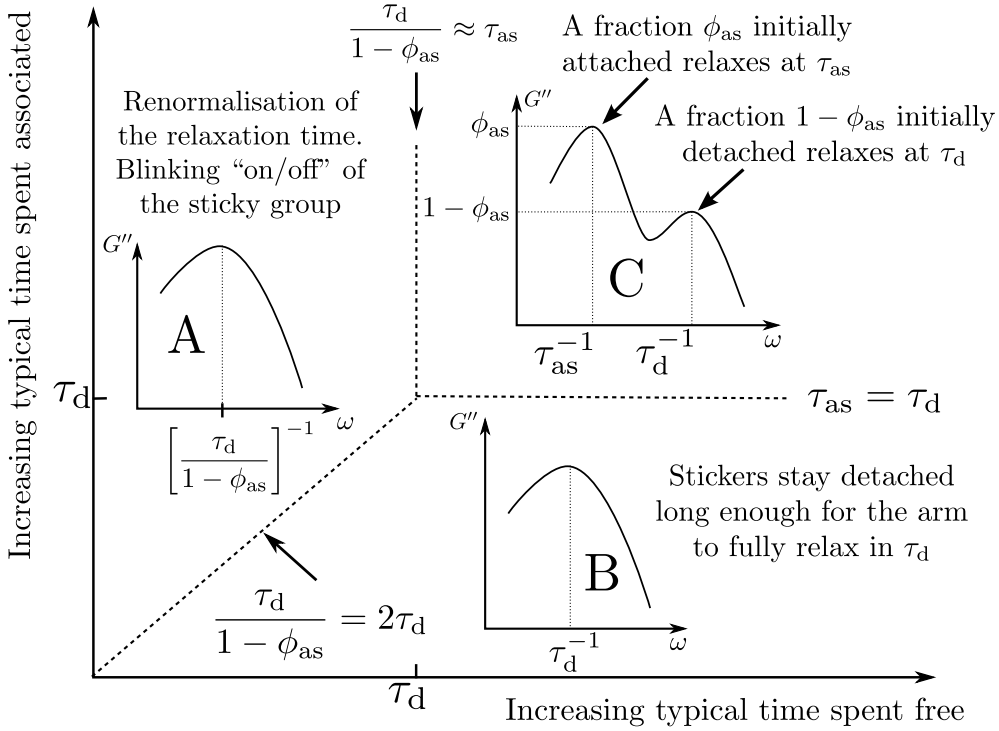

Figure 4.3: Sketches of the predictions of our model for frequency sweep, the subplots represent the loss modulus as a function of the frequency in log-log scale. Three distinct relaxation behaviors are observed in the region A, B, and C. The discontinuous lines indicate where we expect to see a change in the qualitative shape of G''.

that horizontal line, in the region B, $\tau_{as} \ll \tau_d$, and $\tau_{as} \ll \tau_{free}$. The latter relation means that the sticky groups are mostly detached ($\phi_{as} \ll 1$), and the arms can relax their orientation in a time τ_d before the sticky group can possibly attach because $\tau_d \ll \tau_{free}$ in that region. Therefore, we expect the peak in loss modulus to be located at $\omega = \tau_d^{-1}$ similarly to systems with no sticky groups – in fact, in this regime the effect of sticky groups is negligible.

The vertical line is defined by $\tau_d/(1-\phi_{as}) \approx \tau_{as}$, which occurs, according to Equation (4.10) and given that $\phi_{as} \approx 1$, when $\tau_{free} = \tau_d$. It separates the region C from the region A. In region A, $\tau_{free} \ll \tau_d$ and $\tau_d \ll \tau_{as}$ and the loss modulus relaxation peak is located at $\omega = (\tau_d/(1-\phi_{as}))^{-1}$. The factor $(1-\phi_{as})$ comes

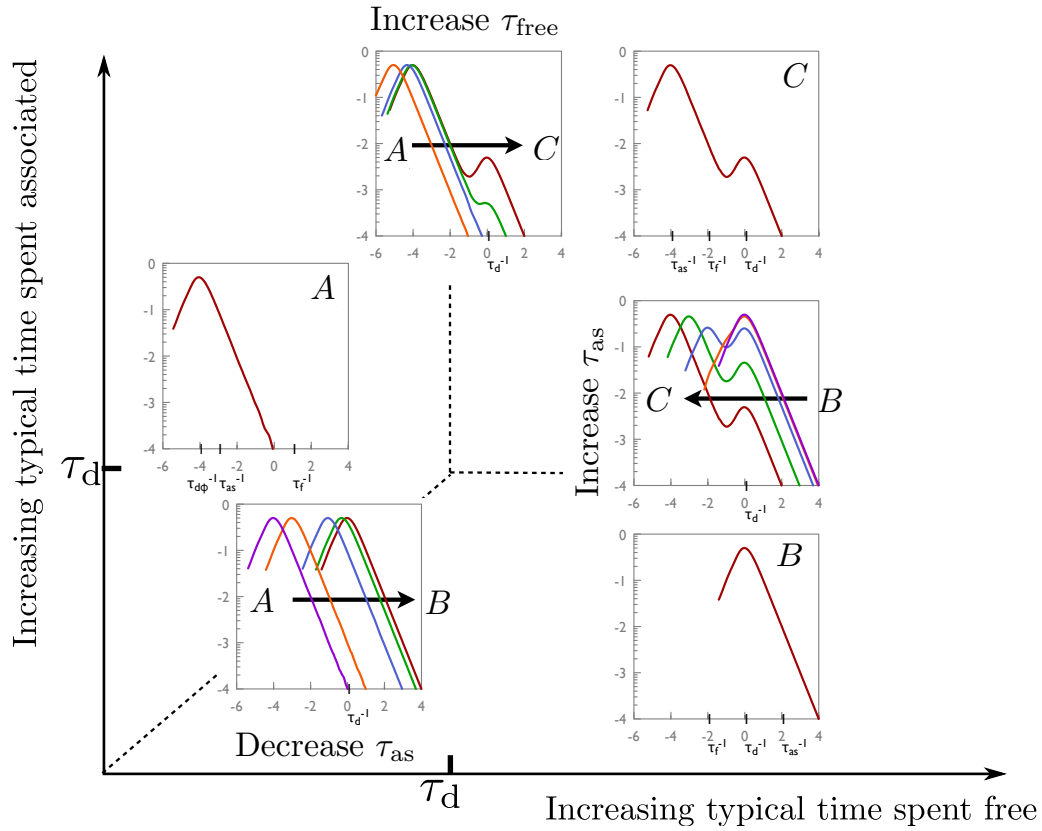

Figure 4.4: Predictions in the linear regime. Characteristic behavior of the loss modulus as a function of frequency (log-log scale) for each region of Figure 4.3, and details on what happens when we cross the lines separating the regions A, B, and C.

from the fact that the sticky group is blinking between the attached and detached states, at a rate which is much faster than the tube orientation relaxation time. The chain is only able to relax stress while detached, which is, on average, a fraction $(1 - \phi_{\text{as}})$ of the time. Hence the effective relaxation time is increased by the factor $(1 - \phi_{\text{as}})$ – this can be considered as an increased "drag" due to the stickers, although the physics of attachment and detachment ensures that the increase in friction is proportional to the bare chain friction. In other words, during the time after an arm detaches and before it is re-attached, it has time to relax only a small amount of orientation. It then needs to wait for another

detachment event before it can relax more orientation.

The diagonal line separates the region A from the region B. It is defined by $\tau_{\text{free}} = \tau_{\text{as}}$, which, according to Equation (4.10), is equivalent to $\phi_{\text{as}} = 1/2$. Thus, on that line we have $\tau_{\text{d}}/(1 - \phi_{\text{as}}) = 2\tau_{\text{d}}$.

Typical simulation results are presented Figure 4.4, for each of the three regions. We also illustrate the transitions between the regions to show how the loss modulus is affected. From region A to region B, the relaxation peak is moved to lower frequencies as we decrease τ_{as} at constant τ_{free}, i.e. $(1 - \phi_{\text{as}})$ is increasing. From the region A to the region C, the second relaxation time becomes evident as we increase τ_{free} at constant τ_{as}. Finally, from region B to region C, the second relaxation peak emerges as we increase τ_{as} at fixed τ_{free}.

4.2.3 Comparison with literature

We compare our results with experimental data of van Ruymbeke and co-workers [van Ruymbeke *et al.* (2010)], where they performed linear rheology measurements on entangled telechelic star polymers. We focus on the 12-arms star polyisoprene functionalized with zwitterionic groups. Figure 4.5 presents the data for 12PZw-PI-10. Ref. [van Ruymbeke *et al.* (2010)] have evidence that some of the arms were not "sticky". One cause could be the synthesis process i.e. some arms do not carry a zwitterionic group (sticker). We expect the fraction of unfunctionalized arms to relax at τ_{d}^{-1}. We observe a bump at intermediate frequencies that we identify with the relaxation of the unfunctionalized arms. At this point, we want to emphasize that our simplified model contains only one orientation relaxation mode, whereas it is known that stars have a broad spectrum of orientation relaxation times [Ball & McLeish (1989); McLeish & Milner (1999); Milner & McLeish (1997)]. Thus, graphically, we can extract a range of values for the orientation relaxation time corresponding to our model: $10^2 < \tau_{\text{d}} < 10^4$ seconds.

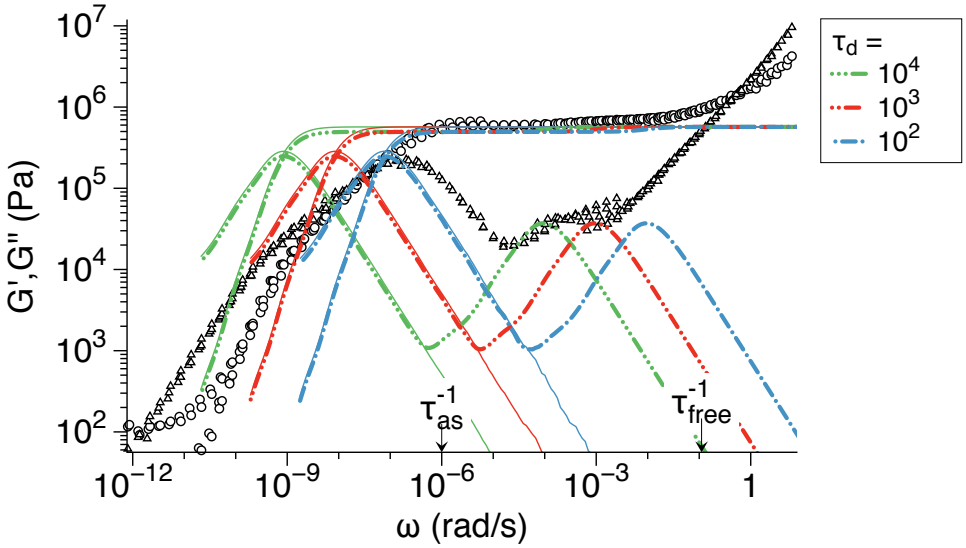

Figure 4.5: Linear rheology of 12PZw-PI-10 from Ref. [van Ruymbeke *et al.* (2010)] (symbols) together with the predictions of our model for different values of the orientation relaxation time in the range $10^2 < \tau_d < 10^4$ s (thin colored lines). We also present the predictions of our model with 13% of non-functionalized arms (dot-dashed thick lines). Parameters are $\tau_{as} = 10^6$ s, $\tau_{free} = 9$ s, plateau modulus $G_N^0 = 0.57$ MPa.

On the other hand, for the population of stars with functionalized arms, the sticky groups have been characterized. For the 12PZw-PI-10, according to Ref. [van Ruymbeke *et al.* (2010)], the typical time spent associated is $\tau_{as} = 10^6$ s, the typical time spent free is $\tau_{free} = 9$ s, hence, the fraction of free arms at equilibrium is $1 - \phi_{as} \approx 10^{-5}$ according to our Equation (4.10). From these values we know that this system is located in the part A of Figure 4.3 because $\tau_{free} \ll \tau_d \ll \tau_{as}$.

Therefore, the relaxation peak for the population of stars with stickers is expected to occur in the range $10^{-9} < (\tau_d/(1-\phi_{as}))^{-1} < 10^{-7}$ rad/s.

We present in Figure 4.5 the predictions of our model for three different orientation relaxation times $\tau_d = 10^2$, 10^3, and 10^4 s, and the above mentioned values for τ_{as} and τ_{free}. Each of the three τ_d values exhibit a single peak of relaxation,

therefore, we see in Figure 4.5 three "single" peaks of relaxation centered at $((1-\phi_{\rm as})/\tau_{\rm d})$ rad/s, corresponding to the thin colored lines. We can also include a fraction (13% as reported by Ref. [van Ruymbeke *et al.* (2010)]) of "non-active arm" to our model, i.e. non-functionalized arms, corresponding to the sticker being "always free" in our model: the thick dot-dashed lines Figure 4.5. The loss modulus has now an additional peak corresponding to the relaxation of the "non-active arms".

It is evident that our simple model captures with success the height of the different loss modulus peaks, and the characteristic relaxation events. For each considered $\tau_{\rm d}$, we obtain two narrow peaks. As we vary $\tau_{\rm d}$ across the considered range (10^2 to 10^4 s), the left peak spans the observed range of relaxation frequencies for the attached arms, whilst the right-hand peak spans the observed range of relaxation frequencies for the non-sticky arms. Hence, in the linear regime, our model with a single orientation relaxation can be considered a simplified version of the more elaborate linear rheology model of van Ruymbeke and co-workers [van Ruymbeke *et al.* (2010)]. One effect captured by their more refined model is the shape of the relaxation peaks due to dynamic dilution as the different part of the star arms relax. It is impossible to capture such details in our single mode model! Note that our model does not predict the high-frequency regime where the Rouse modes within the tube are dominant i.e. $G', G'' \propto \omega^{1/2}$.

4.3 Predictions of the model: nonlinear regime

4.3.1 Numerical method

We integrate Equations (4.17) and (4.19) using Euler's scheme, where we set the numerical time step, Δt, of the simulation to be at least 100 times smaller than the minimum amongst: (i) the sticker timescales, $\tau_{\rm as}, \tau_{\rm free}$ (to not miss attachment or

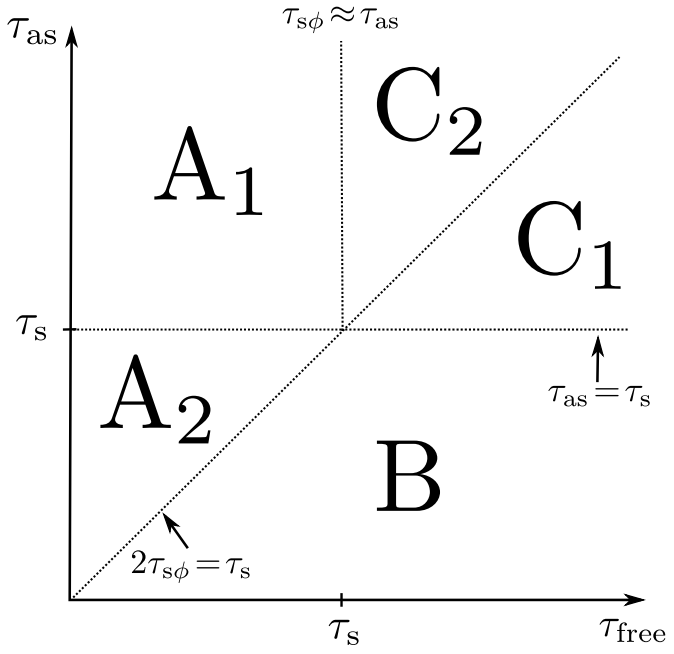

Figure 4.6: Parameter map showing the different regions delimited by the lines where the critical timescales, τ_{as}, τ_s, and $\tau_{s\phi}$ meet.

detachment events), or (ii) the orientation or stretch relaxation timescales, τ_d, τ_s, or (iii) the inverse flow rate. We checked that reducing the numerical time step, Δt, does not modify the results.

The number of chains that we consider in the simulation is initially set to 1 000 chains. However, in some cases, it is necessary to increase the number of chains to avoid noisy data. For instance, when $\phi_{as} = 0.0001$, as it is the case in region B, Figure 4.8, using 1 000 chains implies that, on average, only one chain is attached (and stretch at high flow rate). This gives rise to noisy data. Note that even though we used 10^6 to 10^8 chains in region B, f remains noisy in Figure 4.8.

4.3.2 Presentation of the parameter space

In order to explore the rheological response of the nonlinear regime of the set of equations presented in Section 4.1, we explore the shear and elongation predictions of start-up flows.

In contrast to the broad spectrum of star-arm orientation relaxation times, the nonlinear regime is characterized by a single stretch relaxation time, τ_s. With the same approach as in Section 4.2, we have selected three parameters of our model to explore. We present our predictions for the stress growth coefficient (viscosity), the average stretch of the attached and detached populations, as well as the fraction of the attached stickers, (respectively λ_A, λ_D, and f) as a function of time for different sets of the parameters τ_{as}, τ_{free}, and τ_s, in shear and elongation flows.

In Figure 4.6, boundaries between different regions correspond to places in parameter space where critical rates are equal. Qualitative changes in nonlinear response are observed when the critical flow rates are exceeded. There are also critical flow rates corresponding to orientation relaxation, however, we are exploring flow rates, κ, such that $\kappa\tau_d \gg 1$ – where $\kappa \equiv \dot{\gamma}$ or $\dot{\varepsilon}$, in shear or elongation respectively. We consider that the tubes are all oriented as we perform the simulations in the regime of high Weissenberg number related to the tube orientation relaxation time. Hence, all flow rates considered are above critical orientation rates. At lowest flow rates we get thinning behavior in both shear and extension, i.e. the response follows the linear envelope up to strain of order 1, followed by a plateau in extension, or a weak overshoot and steady state in shear (similar to linear polymers in the regime $\tau_d^{-1} < \dot{\gamma} < \tau_s^{-1}$). At low flow rates, no stretching is seen ($\lambda \approx \lambda_D \approx 1$) and the fraction of attached stickers stays at its initial value ($f(t) \approx \phi_{as}$).

At higher flow rates, stronger nonlinear behaviors are apparent, and in dif-

ferent regions of parameter space, the critical rates are encountered in different orders. In particular, three timescales seem important: τ_{as}, τ_s, and $\tau_{s\phi} = \tau_s/(1-\phi_{as})$. The timescale, τ_{free}, seems less important. Then we can divide space up into different regions A_1, A_2, B, C_1, and C_2 as shown in Figure 4.6.

The timescale $\tau_{s\phi} = \tau_s/(1-\phi_{as})$ is the renormalized stretch relaxation time that arises from the repeated attachment and detachment of the sticker when $\tau_{free} \ll \tau_{as} \ll \tau_s$. In that regime, most of the stickers are initially attached. When the arm is stretched and that the sticker is forced to detach, it stays free, on average, for a time τ_{free} (much shorter than τ_s), which means that the arms are not able to relax all stretch in one detachment event. Stretch relaxation occurs only when the sticker is free, and this is the case for a fraction $(1-\phi_{as})$ of the time. Hence, similarly to renormalization of the orientation relaxation time, τ_d, in the linear regime seen in Section 4.2, this leads to a renormalized *stretch* relaxation time $\tau_{s\phi} = \tau_s/(1-\phi_{as})$, as defined below. This renormalized stretch relaxation time plays a role in the regions A_1 and A_2 Figure 4.6, similarly to the linear regime described in Section 4.2. Note that in regions B and C_1, $\tau_{s\phi} \approx \tau_s$ because $\phi_{as} \ll 1$.

The region A_1 is where $\tau_s \ll \tau_{as} \ll \tau_{s\phi}$, which corresponds to $\tau_{free} \ll \tau_s$ and $\tau_s \ll \tau_{as}$. The transition from A_1 to C is when $\tau_{s\phi} \approx \tau_{as}$ or, equivalently, $\tau_{free} \approx \tau_{as}$. In this region, stickers like to stay associated and free stickers have a short lifetime compared to the stretch relaxation time.

Region A_2 is when $\tau_{as} \ll \tau_s \ll \tau_{s\phi}$ i.e. $\tau_{free} \ll \tau_{as}$ and $\tau_{as} \ll \tau_s$. It is a region where the stickers attach and detach rapidly with respect to the stretch relaxation time, but are initially mostly attached $(1-\phi_{as} \ll 1)$. The transition from A_1 to A_2 is when $\tau_{as} = \tau_s$. The only change between region A_1 and A_2 is the second critical rate encountered on increasing flow rate.

Region B is where $\tau_{as} \ll \tau_{s\phi} \approx \tau_s$, which corresponds to $\tau_s \ll \tau_{free}$ and $\tau_{as} \ll \tau_s$.

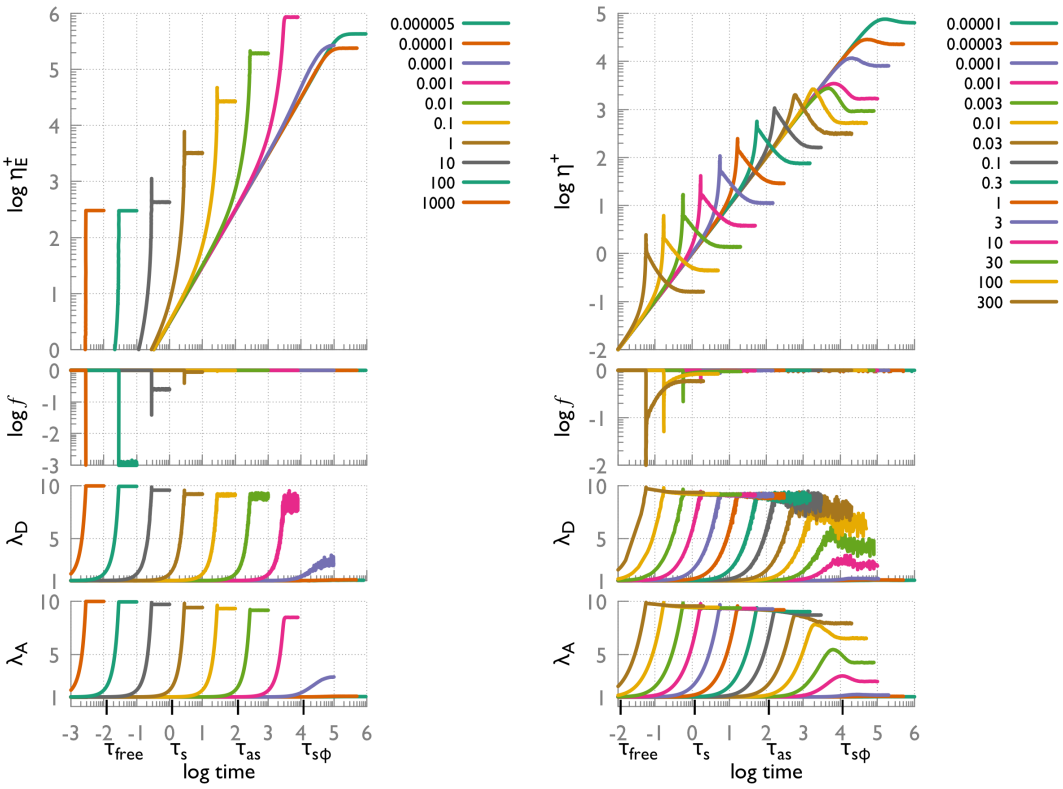

(a) Elongation

(b) Shear

Figure 4.7: Stochastic model predictions for region A_1 in the nonlinear regime. We present the values, as a function of time, of the fraction of attached chains, f, the stretch of the attached chains λ_A and stretch of the detached chains λ_D, and stress growth coefficients, η_E^+ and η^+, for uniaxial extension (left), and step rate (right) respectively. Parameters are $\tau_{free} = 10^{-2}$, $\tau_{as} = 10^2$, $\tau_s = 1$, $\tau_d = 10^6$, $\lambda_{max} = 10$.

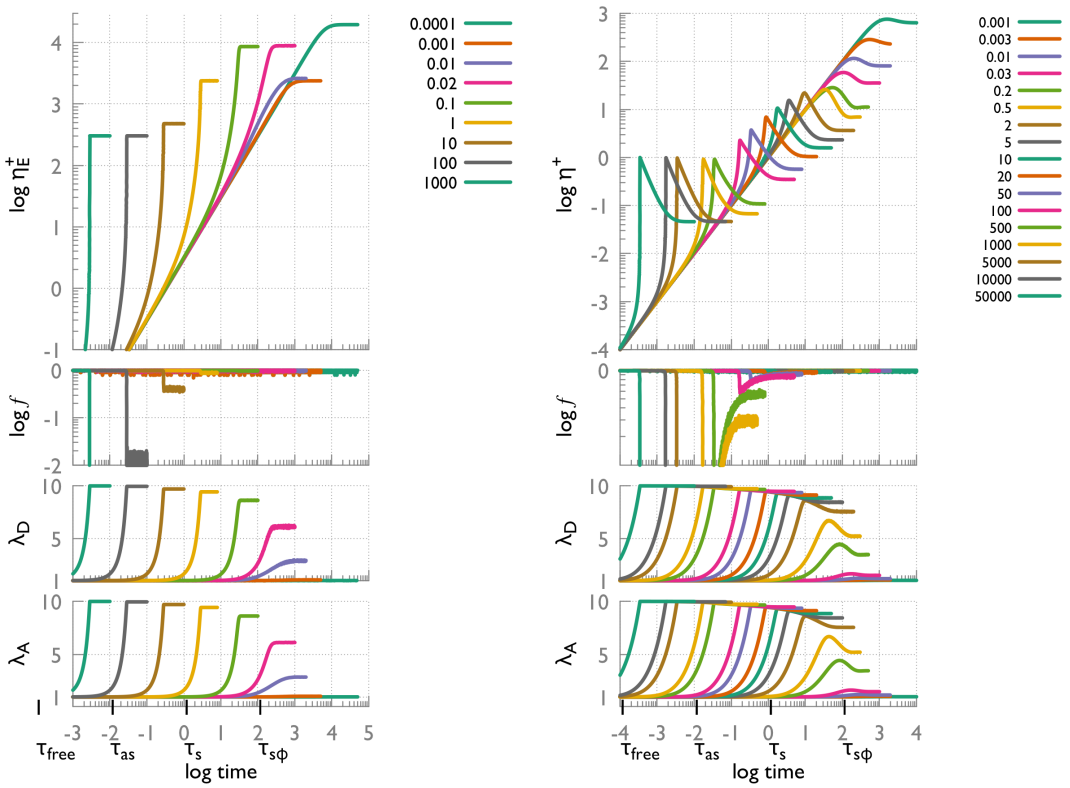

(a) Elongation

(b) Shear

Figure 4.8: Stochastic model predictions for region A_2 in the nonlinear regime. We present the values, as a function of time, of the fraction of attached chains, f, the stretch of the attached chains λ_A and stretch of the detached chains λ_D, and stress growth coefficients, η_E^+ and η^+, for uniaxial extension (left), and step rate (right) respectively. Parameters are $\tau_{free} = 10^{-4}$, $\tau_{as} = 10^{-2}$, $\tau_s = 1$, $\tau_d = 10^6$, $\lambda_{max} = 10$.

The transition from A_2 to B is where $\phi_{as} \approx 1/2$. It is a region where the stickers are initially mostly free and they do not like to stay associated. It is a "non-sticky" region. Indeed, our predictions of the shear stress growth coefficient, η^+, in this regime are consistent with shear experiments on *non-telechelic* entangled star polymers [Snijkers *et al.* (2013)].

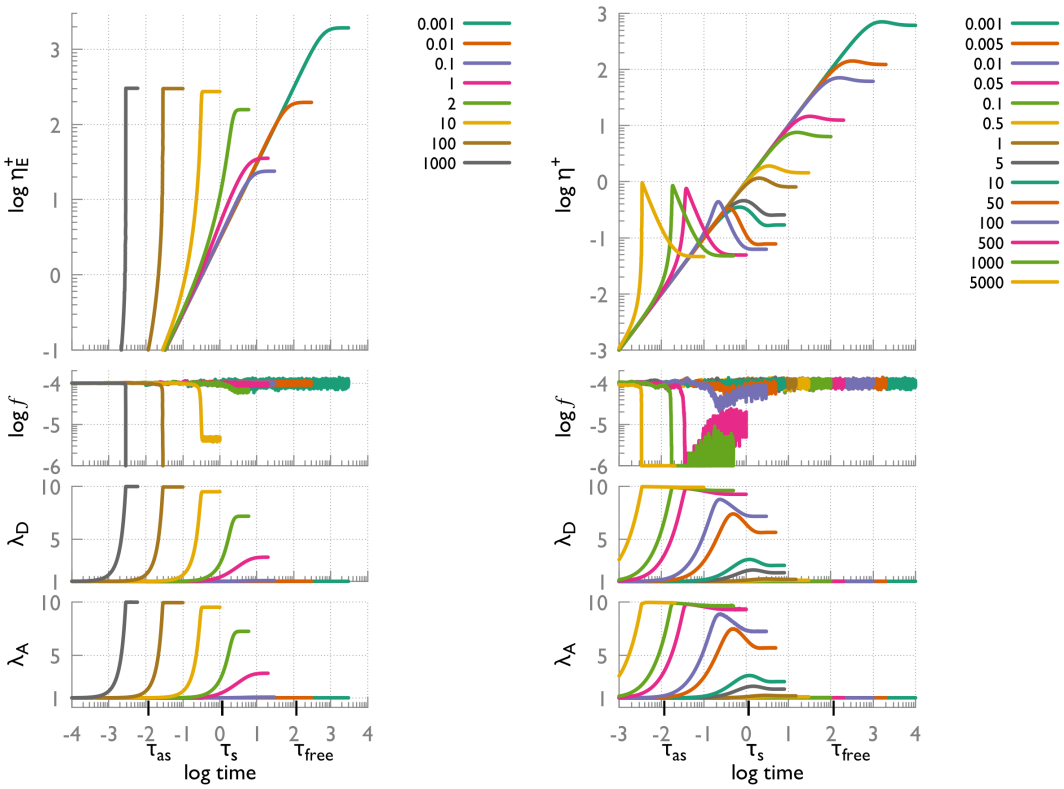

(a) Elongation (b) Shear

Figure 4.9: Stochastic model predictions for region B in the nonlinear regime. We present the values, as a function of time, of the fraction of attached chains, f, the stretch of the attached chains λ_A and stretch of the detached chains λ_D, and stress growth coefficients, η_E^+ and η^+, for uniaxial extension (left), and step rate (right) respectively. Parameters are $\tau_{free} = 10^2$, $\tau_{as} = 10^{-2}$, $\tau_s = 1$, $\tau_d = 10^6$, $\lambda_{max} = 10$.

Region C_1 is where $\tau_s \approx \tau_{s\phi} \ll \tau_{as}$, which corresponds to $\tau_s \ll \tau_{as} \ll \tau_{free}$.

When attached, the stickers stay attached a long time compared to the stretch relaxation time, but most of the stickers are initially detached because ϕ_{as} is close to zero. The transition from B to C_1 is when $\tau_{as} \approx \tau_s$.

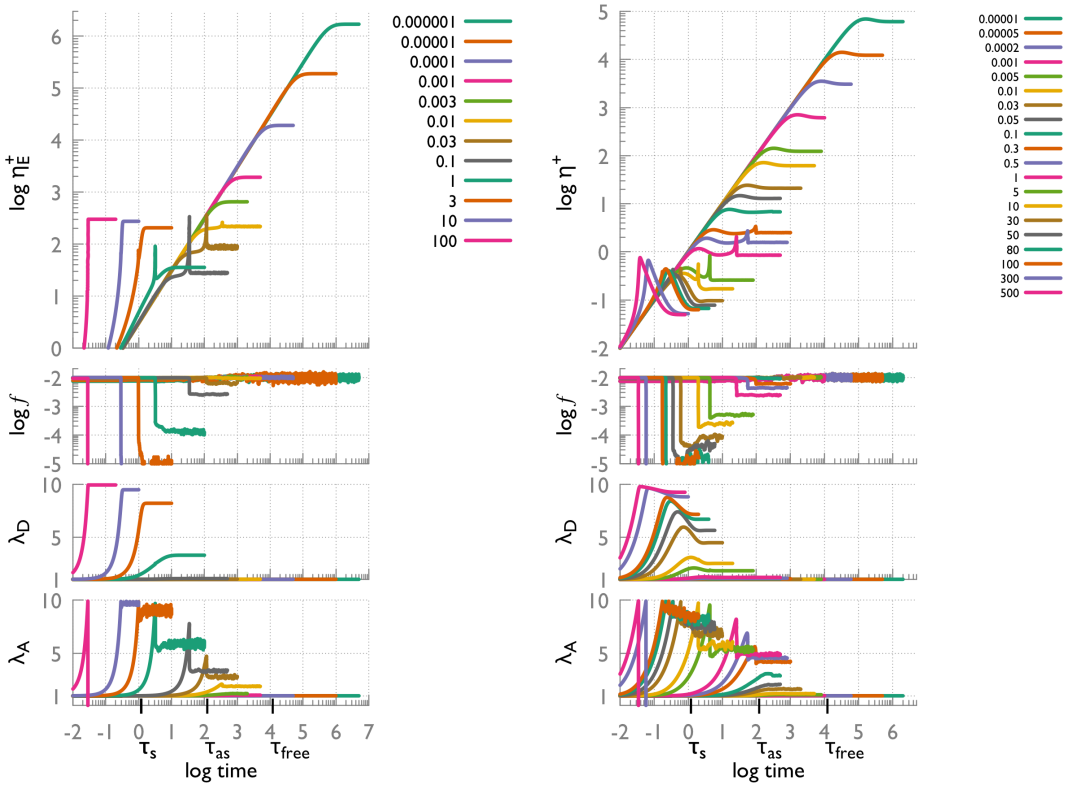

(a) Elongation (b) Shear

Figure 4.10: Stochastic model predictions for region C_1 in the nonlinear regime. We present the values, as a function of time, of the fraction of attached chains, f, the stretch of the attached chains λ_A and stretch of the detached chains λ_D, and stress growth coefficients, η_E^+ and η^+, for uniaxial extension (left), and step rate (right) respectively. Parameters are $\tau_{free} = 10^4$, $\tau_{as} = 10^2$, $\tau_s = 1$, $\tau_d = 10^6$, $\lambda_{max} = 10$.

Finally, region C_2 is where $\tau_s \ll \tau_{s\phi} \ll \tau_{as}$, which corresponds to $\tau_s \ll \tau_{free} \ll \tau_{as}$. When attached, the stickers stay attached a long time compared to the stretch relaxation time, but most of the stickers are initially attached because ϕ_{as} is close to one. The transition from C_1 to C_2 is when $\tau_{as} = \tau_{free}$, or equivalently

$\phi_{as} = 1/2$.

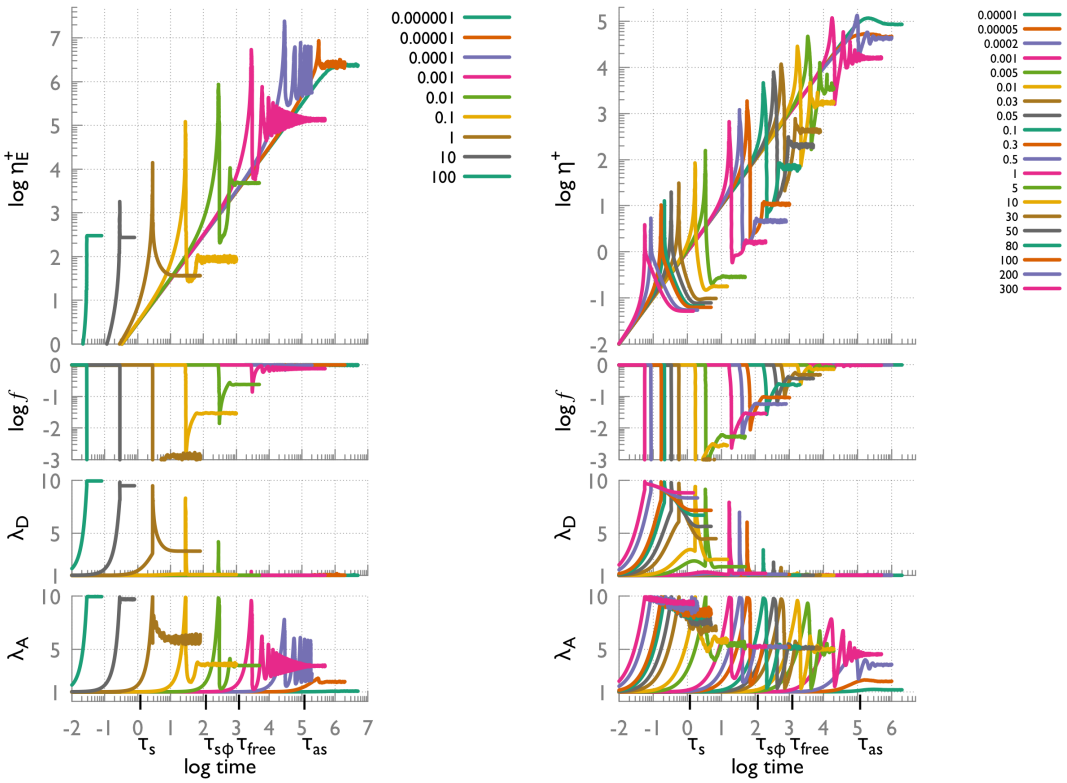

(a) Elongation (b) Shear

Figure 4.11: Stochastic model predictions for region C_2 in the nonlinear regime. We present the values, as a function of time, of the fraction of attached chains, f, the stretch of the attached chains λ_A and stretch of the detached chains λ_D, and stress growth coefficients, η_E^+ and η^+, for uniaxial extension (left), and step rate (right) respectively. Parameters are $\tau_{free} = 10^3$, $\tau_{as} = 10^5$, $\tau_s = 1$, $\tau_d = 10^6$, $\lambda_{max} = 10$.

In regions A_1, A_2, and B, $\tau_{as} \ll \tau_{s\phi}$. This condition ensures that interchange between the attached and detached population keeps the stretch of the attached and detached population approximately equal: $\lambda_A \approx \lambda_D$. On the other hand, the regions C_1 and C_2 have $\tau_{s\phi} \ll \tau_{as}$, which implies a separation between populations of attached and detached chains. Indeed, when the flow rate exceeds the inverse

of $\tau_{s\phi}$ in regions A_1, A_2, and C_2 or τ_s in regions B and C_1, we expect to see an onset of stretch of the attached *and* detached chains. Additionally, if the flow rate exceeds the inverse of τ_{as} before $\tau_{s\phi}$, as is it the case in regions C_1, and C_2 where $\tau_{s\phi} \ll \tau_{as}$, we expect *only* the attached chains to stretch, but not the detached chains. However, because the attached chain will eventually detach due to Equation (4.15), it will consequently increase the average stretch of the detached chains. The bottom graphs of Figures 4.7–4.11, in shear and elongation, where we plotted the average values of the stretch for the attached chains and detached chains as a function of time, support that statement.

To explore the map Figure 4.6, we will, in the following Sections 4.3.3 and 4.3.4, choose "extreme" parameters to separate out timescales by orders of magnitude and clearly delineate different typical responses of the material.

4.3.3 Elongation

On the left parts of the Figures 4.7–4.11, we present the predictions of our model in the regions A_1, A_2, B, C_1, and C_2, respectively, for the logarithms of the tensile stress growth coefficient (sometimes known as extensional viscosity), $\eta_E^+(t, \dot{\varepsilon})$, the instantaneous fraction of attached chains f, and the stretch of the attached and detached chains, λ_A and λ_D, as a function of time. In all five regions, the tensile stress growth coefficient follows the linear viscoelastic envelope up to strain of order 1, i.e. $\dot{\varepsilon}t \approx 1$, where $\dot{\varepsilon}$ is the Hencky strain rate (elongation rate), the chains are not stretched ($\lambda_A \approx \lambda_D \approx 1$) and the fraction of attached chains is not modified, $f(t) \approx \phi_{as}$. For $\dot{\varepsilon}t > 1$, the behavior depends on how $\dot{\varepsilon}$ compares with the different timescales.

In regions A_1 and A_2 Figure 4.6, the stretch relaxation time is rescaled similarly to the linear regime, Section 4.2. The stretch is able to relax mainly when the stickers are free and this is the case for a fraction $1 - \phi_{as}$ of arms. Over

a time t, the arm is effectively detached for a time $t/(1-\phi_{\rm as})$. Thus, the effective stretch relaxation time is longer than $\tau_{\rm s}$ by a factor $1-\phi_{\rm as}$. The stickers are blinking between attached and detached states in regions $\rm A_1$ and $\rm A_2$. When $\dot{\varepsilon} < \tau_{\rm s\phi}^{-1} = [\tau_{\rm s}/(1-\phi_{\rm as})]^{-1}$, the viscosity reaches a steady state plateau, $\lambda_{\rm A} \approx \lambda_{\rm D} \approx 1$, and $f(t) \approx \phi_{\rm as}$. If $\dot{\varepsilon} > \tau_{\rm s\phi}$, we observe elongation hardening due to chain stretching, followed by a steady state plateau.

In region $\rm A_1$, Figure 4.7 left, at intermediate elongation rates when $\tau_{\rm as}^{-1} < \dot{\varepsilon} < \tau_{\rm s}^{-1}$, small overshoots appear: the chains are stretched and reach the maximum extensibility because the flow rate is faster than the average time needed for a sticker to detach: $\tau_{\rm as}^{-1} < \dot{\varepsilon}$. That triggers the detachment of stickers, as confirmed by the undershoot of f, and therefore immediate relaxation of the stretch of the arm because the stretch relaxation time is faster than the flow: $\dot{\varepsilon} < \tau_{\rm s}^{-1}$. However, the time the sticker will spend free is small compared to the stretch relaxation time, hence, only a fraction of stress can be relaxed – in contrast with findings in region $\rm C_2$.

As expected, these small overshoots in $\eta_{\rm E}^{+}$ and undershoots in f, are not seen in the region $\rm A_2$, Figure 4.8 left, as $\tau_{\rm as} \ll \tau_{\rm s}$ implies that increasing elongation rates will exceed $\tau_{\rm s}^{-1}$ before $\tau_{\rm as}^{-1}$. Therefore, when $\tau_{\rm as}^{-1} < \dot{\varepsilon}$, the maximum extensibility is reached and chains are forced to detach but they cannot fully relax the stretch as the flow rate is faster than the stretch relaxation time.

In region B Figure 4.6, we are in a non-sticky regime because most of the stickers are free and the lifetime of an associated sticker is short. As before, in Figure 4.9 left, the viscosity follows the LVE up to strain of order 1. If $\dot{\varepsilon} < \tau_{\rm s}^{-1}$, $\eta_{\rm E}^{+}$ reaches a steady state plateau. If $\dot{\varepsilon} > \tau_{\rm s}^{-1}$ we see elongation hardening due to chain stretching, followed by a steady state plateau.

In regions $\rm C_1$ and $\rm C_2$ Figure 4.6, there is no rescaling of the stretch relaxation time because the dynamic of association/disassociation of the stickers is slow

compared to the stretch relaxation, i.e. there is no renormalization due to the blinking phenomena seen in regions A_1 and A_2. Thus, $\tau_{s\phi}$ is irrelevant in regions C_1 and C_2.

In region C_2, Figure 4.11 left, we observe elongation hardening as soon as the flow rate exceeds the inverse association time, $\dot{\varepsilon} > \tau_{as}^{-1}$. Indeed, ϕ_{as} being close to unity, almost all chains are initially attached and they will stay attached long enough to be stretched by the flow until the chains reach their maximal extensibility where they are forced to detach. On the other hand, the detached chains are not stretched at this point. The dramatic drop in viscosity is due to the fast relaxation of the arms' stretch immediately following the detachment of the stickers. At moderately high flow rates, when $\tau_{as}^{-1} < \dot{\varepsilon} < \tau_{s}^{-1}$, the chains can "fully" relax their stretch before the stickers re-attach and stretch the arm again. This cycle of attachment-stretch/detachment-relaxation is responsible for the undershoot and oscillation in viscosity seen at intermediate elongation rate. At high elongation rates, when $\dot{\varepsilon} > \tau_{s}^{-1}$, the chains that are forced to detach are only able to partially relax their stretch before the stickers re-attach, which produces a smooth transition towards the steady state with no undershoot or oscillation. Indeed, when $\dot{\varepsilon} > \tau_{s}^{-1}$, the detached chains also start to stretch.

In region C_1, Figure 4.10 left, we observe something intermediate between the regions B and C_2. At small elongation rate, $\dot{\varepsilon} < \tau_{s}^{-1}$, η_{E}^{+} follows the LVE and reaches a steady state plateau that is below the LVE, similar to region B. Additionally, at intermediate elongation rates, $\tau_{as}^{-1} < \dot{\varepsilon} < \tau_{s}^{-1}$, sharp spikes of the tensile stress growth coefficient are visible, similar to region C_2. These small spikes are the result of the few initially attached chains (recall that ϕ_{as} is close to zero in region C_1) that stretch until they detach, and because the flow is "slower" than the stretch relaxation time, they can fully relax their stretch. Indeed, at these elongation rates, the detached chains are not stretched. At high flow rates,

$\tau_s^{-1} < \dot{\varepsilon}$, the chains that are forced to detach are only able to partially relax their stretch as they are being dragged by the flow: the detached chains are stretching too. On increasing ϕ_{as}, the spikes are more pronounced. The transition from C_1 to C_2 is when $\phi_{as} \approx 1/2$.

4.3.4 Shear

On the right parts of the Figures 4.7–4.11, we present the predictions of our model in the regions A_1, A_2, B, C_1, and C_2, respectively, for the logarithms of the shear stress growth coefficient (sometimes known as shear viscosity), $\eta^+(t, \dot{\gamma})$, the fraction of attached chains f, and the stretch of the attached and detached chains, λ_A and λ_D, as a function of time.

As in elongation, up to a strain of order 1, the viscosity follows the LVE, the chains are not stretched ($\lambda_A \approx \lambda_D \approx 1$) and the fraction of attached chains is not modified, $f \approx \phi_{as}$. The subsequent behavior strongly depends on the different parameters and the applied shear rate. We detail below the predictions in the different regions.

Regions A_1, A_2, B

(i) When the shear rate is smaller than the inverse of the effective stretch relaxation time, $\tau_{s\phi} = \tau_s/(1-\phi_{as})$, for regions A_1 and A_2, or smaller than the stretch relaxation time τ_s for region B, the viscosity shows a mild overshoot before reaching the steady state. This mild overshoot under the LVE has been observed experimentally for *non-telechelic* entangled stars [Snijkers *et al.* (2013)]. Indeed, at low shear rates, the system is not aware of the stickers.

(ii) As the shear rate exceeds the inverse of τ_s or $\tau_{s\phi}$, the stress overshoot be-

comes more pronounced and its height increases. This is typical for entangled linear chains in the chain stretching regime. The response remains below the LVE, so still in the shear thinning regime. We also start to see the onset of stretch of the attached and detached chains.

(iii) We observe in Figures 4.7–4.9 right, that, above a second critical shear rate, shear hardening occurs, i.e. η^+ goes above the LVE. In regions A_1, A_2, and B, we have found empirically that this critical shear rate above which hardening is seen, $\dot{\gamma}_c^{\text{hard}}$, depends on the maximal stretch $\lambda_{\max}$, on the stretch relaxation time τ_s, and the fraction of associated arms at equilibrium, ϕ_{as}, as

$$\dot{\gamma}_c^{\text{hard}} = \left[\frac{\tau_s}{6\lambda_{\max}(1-\phi_{as})}\right]^{-1}. \tag{4.21}$$

We note that this hardening is a feature of the Rolie-Poly model with finite extensibility, i.e. if ϕ_{as} is set to zero, there remains a critical rate in Equation (4.21) above which shear hardening is seen.

(iv) We observe in region A_1 that, at intermediate to high shear rates, sharp peaks in viscosity appear. Similarly to the elongation case, at moderately high shear rates, $\tau_{as}^{-1} < \dot{\gamma}$, the chains are stretched and reach the maximum extensibility, which triggers the detachment of stickers and therefore immediate relaxation of the stretch of the arm because $\lambda_D < \lambda_A$. On the other hand, in region A_2, $\lambda_A \approx \lambda_D$ so the stress does not relax as fast. Hence, we do not see the sharp decrease in viscosity at high shear rates.

Regions C_1 and C_2

In region C_2, Figure 4.11 right, the critical shear rate at which shear hardening occurs is $\dot{\gamma}_c^{\text{hard}} = \tau_{as}^{-1}$. Note that in region C_2, the regime (ii) (observed in regions A_1, A_2, and B above) is not seen due to the high value of τ_{as}. In addition,

when the shear rate exceeds τ_{as}^{-1}, the associated arms are strongly stretched – this corresponds to the onset of shear hardening – until they reach the maximal stretch ratio. Then the strongly stretched arms are forced to detach and will stay detached during τ_{free} in average. Because $\tau_s \ll \tau_{free}$, the detached arms can fully relax before getting reattached ($\lambda_D < \lambda_A$). This fast relaxation is responsible for the undershoots visible at intermediate shear rates. At higher shear rates, $\dot{\gamma} > \tau_s^{-1}$, the detached arms can only partially relax as they are dragged by the flow, which produces a smooth transition towards the steady state with no undershoot or oscillation ($\lambda_D \approx \lambda_A$).

In region C_1, Figure 4.10 right, we observe a behavior intermediate between the regions B and C_2. Changes in the shape of the stress growth coefficient are seen when the flow rate exceeds either τ_s^{-1} or $\dot{\gamma}_c^{hard}$, similarly to (i), (ii), and (iii) above. Additionally, small spikes appear at intermediate flow rates, when $\tau_{as}^{-1} < \dot{\gamma} < \tau_s^{-1}$, due to the same mechanism described above for the region C_2. However, these spikes are of small amplitude because the initial fraction of attached chain is close to zero ($\phi_{as} \approx 0$). On increasing ϕ_{as}, these spikes are more pronounced.

4.4 Conclusions

The stochastic model presented in this Chapter is in good qualitative agreement with experimental linear rheology data; the reasons listed at the end of Section 4.2.3 explain the discrepancies in the low frequency region (due to dilution effects) and in the plateau region for G'' (the spectrum of orientation relaxation times is not accounted for in our simple model). To our knowledge, no nonlinear rheology data on entangled telechelic star polymers have been published.

The stochastic model predicts a wide range of interesting nonlinear behavior

as parameters are varied e.g. shear hardening, sharp stress peaks and a non-monotonic constitutive curve (see Figure 5.4) which we anticipate may be exhibited in real materials. Given this, there is potential interest in using the constitutive model in computations for more complex flows. Such computations could, for example, allow qualitative investigation of the relationship between the predicted nonlinear viscoelasticity and flow phenomena such as transient or steady state shear banding. Our toy model might also be applicable at the same level as the multimode pom-pom model for branched polymers [McLeish & Larson (1998)], in which the model parameters are usually adjusted freely so as to match available linear and nonlinear rheology, which can then serve to make reasonably accurate predictions in non-viscometric flows.

We may also note that much of the interesting nonlinear behaviour we predict arises from interaction of the flow and sticker timescales with the stretch relaxation time τ_s of the stars. Our toy model is not designed to capture the full spectrum of orientation relaxation times for a "real" star arm, applicable to linear rheology. However, star polymers are expected to possess a single dominant stretch relaxation time: in this respect our model is quite close to reality and we may anticipate that in this sense our nonlinear predictions might be more accurate than the linear ones, especially at high flow rates in the strongly nonlinear regime.

The model we have presented so far is not very efficient for numerical computation in complex flows such as shear banding calculations because of the cost of solving stochastic equations for many arms. Given this, we develop, in the following Chapter 5, a preaveraged version of the stochastic model, which is far less computationally costly and retains most of the features of the stochastic model.

Chapter 5

Preaveraged model for entangled telechelic stars

5.1 Motivations

The stochastic model presented in Chapter 4 is not very efficient for numerical computation in complex flows such as shear banding calculations because of the cost of solving stochastic equations for many arms. Given this, we develop in this Chapter a preaveraged version of the stochastic model, which is far less computationally costly and retains most of the features of the stochastic model.

We get rid of the stochastic nature of the model by preaveraging the contributions to the stress of the attached and detached populations. The outcome is a scalar differential equation for the time-dependent fraction of attached chains, $f(t)$, and two tensorial equations for the conformational average of the associated and dissociated chains, $\underline{\underline{\boldsymbol{Q}}}_{\mathrm{A}}(t)$ and $\underline{\underline{\boldsymbol{Q}}}_{\mathrm{D}}(t)$, similar to Refs. [Tripathi *et al.* (2006); Vaccaro & Marrucci (2000)].

5.2 Assumptions of the model

The evolution equation of the fraction of attached chains, f, is constrained by the balance equation

$$\frac{\mathrm{d}f}{\mathrm{d}t} = \frac{1}{N_\mathrm{c}}\frac{\mathrm{d}n_\mathrm{A}}{\mathrm{d}t} = \big(1 - f(t)\big)r_{\mathrm{free}\to\mathrm{as}} - f(t)r_{\mathrm{as}\to\mathrm{free}}(\lambda_\mathrm{A}), \tag{5.1}$$

where n_A is the instantaneous number of associated chain, N_c is the total number of chains, the rate of dissociation and association $r_{\mathrm{free}\to\mathrm{as}}$, and $r_{\mathrm{as}\to\mathrm{free}}(\lambda_\mathrm{A})$ are defined by Equations (4.7) and (4.15) respectively, and the stretch ratio of the attached population, λ_A, is defined below in Equation (5.6).

The conformation tensor, $\underline{\underline{\boldsymbol{\tau}}}$ defined Section 4.1.1, can be split up into two contributions from the associated and dissociated populations, $\underline{\underline{\boldsymbol{\tau}}}_\mathrm{A}$ and $\underline{\underline{\boldsymbol{\tau}}}_\mathrm{D}$, respectively. The time evolution of the conformation tensor representing the associated chains, $\underline{\underline{\boldsymbol{\tau}}}_\mathrm{A}$, is given by Equation (4.17). The time evolution of the conformation tensor representing the detached chains, $\underline{\underline{\boldsymbol{\tau}}}_\mathrm{D}$, is given by Equation (4.19).

The stress tensor, $\underline{\underline{\boldsymbol{\sigma}}}$, of the full system is then defined as the sum of the contributions of the attached and detached chains, weighted by the fraction of such chains, $f(t)$ and $1 - f(t)$ respectively. Including the finite extensibility function, we obtain, in units of G,

$$\underline{\underline{\boldsymbol{\sigma}}} = f\,\mathrm{f_E}(\lambda_\mathrm{A})\underline{\underline{\boldsymbol{\tau}}}_\mathrm{A} + (1-f)\,\mathrm{f_E}(\lambda_\mathrm{D})\underline{\underline{\boldsymbol{\tau}}}_\mathrm{D}, \tag{5.2}$$

where λ_A and λ_D are the stretch ratio of the attached and detached populations, as defined below. The rest of this Chapter aims at defining the time evolution of Equation (5.2) and concludes by comparing with the predictions of the stochastic model of the previous section. In deriving the preaveraged model, one constraint upon which we insist is that attachment and detachment events, on their own,

should not result in a change in stress – rather stress relaxation occurs when detached chains relax.

5.3 Derivation of the evolution equations

5.3.1 Tensor preaveraging

We consider the two tensors, related to the stress of the attached and detached chains, defined by

$$\underline{\underline{\boldsymbol{Q}}}_{\mathrm{A}} = \mathrm{f_E}\left(\lambda_{\mathrm{A}}\right)\underline{\underline{\boldsymbol{\tau}}}_{\mathrm{A}}, \tag{5.3}$$

$$\underline{\underline{\boldsymbol{Q}}}_{\mathrm{D}} = \mathrm{f_E}\left(\lambda_{\mathrm{D}}\right)\underline{\underline{\boldsymbol{\tau}}}_{\mathrm{D}}, \tag{5.4}$$

where $\lambda_{\mathrm{A}}^2 = \mathrm{tr}\,\underline{\underline{\boldsymbol{\tau}}}_{\mathrm{A}}/3$, and $\lambda_{\mathrm{D}}^2 = \mathrm{tr}\,\underline{\underline{\boldsymbol{\tau}}}_{\mathrm{D}}/3$ are the (squared) preaveraged stretch ratio of, respectively, the attached and detached populations. The total stress tensor, Equation (5.2), can be written

$$\underline{\underline{\boldsymbol{\sigma}}} = f\underline{\underline{\boldsymbol{Q}}}_{\mathrm{A}} + (1-f)\underline{\underline{\boldsymbol{Q}}}_{\mathrm{D}}. \tag{5.5}$$

We can express the two stretch ratios as a function of the traces of the tensors $\underline{\underline{\boldsymbol{Q}}}_{\mathrm{A}}$ and $\underline{\underline{\boldsymbol{Q}}}_{\mathrm{D}}$. The trace of Equation (5.3) gives

$$\begin{aligned}
\mathrm{tr}\left(\underline{\underline{\boldsymbol{Q}}}_{\mathrm{A}}\right) &= \frac{1-\lambda_{\max}^{-2}}{1-\lambda_{\mathrm{A}}^2\lambda_{\max}^{-2}}\,\mathrm{tr}\left(\underline{\underline{\boldsymbol{\tau}}}_{\mathrm{A}}\right) \\
\left(1-\lambda_{\mathrm{A}}^2\lambda_{\max}^{-2}\right)\mathrm{tr}\left(\underline{\underline{\boldsymbol{Q}}}_{\mathrm{A}}\right) &= \left(1-\lambda_{\max}^{-2}\right)3\lambda_{\mathrm{A}}^2 \\
\lambda_{\mathrm{A}}^2 &= \frac{\lambda_{\max}^2\,\mathrm{tr}\left(\underline{\underline{\boldsymbol{Q}}}_{\mathrm{A}}\right)}{3\lambda_{\max}^2 - 3 + \mathrm{tr}\left(\underline{\underline{\boldsymbol{Q}}}_{\mathrm{A}}\right)}.
\end{aligned} \tag{5.6}$$

Similarly, Equation (5.4) gives

$$\lambda_{\mathrm{D}}^2 = \frac{\lambda_{\max}^2 \operatorname{tr}\left(\underline{\underline{\boldsymbol{Q}}}_{\mathrm{D}}\right)}{3\lambda_{\max}^2 - 3 + \operatorname{tr}\left(\underline{\underline{\boldsymbol{Q}}}_{\mathrm{D}}\right)}. \tag{5.7}$$

We deduce the expression of the finite extensibility function, $\mathrm{f_E}$, depending on the tensor $\underline{\underline{\boldsymbol{Q}}}_i$, $i \equiv$ A or D,

$$\mathrm{f_E}(\lambda_i) = \frac{3\lambda_{\max}^2 - 3 + \operatorname{tr}\left(\underline{\underline{\boldsymbol{Q}}}_i\right)}{3\lambda_{\max}^2}. \tag{5.8}$$

We will now express the time evolution the two tensors $\underline{\underline{\boldsymbol{Q}}}_{\mathrm{A}}$ and $\underline{\underline{\boldsymbol{Q}}}_{\mathrm{D}}$. This is a two-fold process. First, we will define the exchange terms that arise from the switch between attached and detached states. Then, we define the flow contribution.

Exchange terms

The exchange term is present to ensure that the total stress remains constant when a fraction of chains detaches or attaches. The exchange term is given by writing the time increment of the quantity $f\underline{\underline{\boldsymbol{Q}}}_{\mathrm{A}}$ between the times t and $t + \Delta t$, in absence of flow or relaxation. At a time $t + \Delta t$, a fraction $f\Delta t\, r_{\mathrm{as}\to\mathrm{free}}(\lambda_{\mathrm{A}})$ of chains have detached, while a fraction $(1-f)\Delta t\, r_{\mathrm{free}\to\mathrm{as}}$ have attached. We write

$$\begin{aligned} f(t+\Delta t)\underline{\underline{\boldsymbol{Q}}}_{\mathrm{A}}(t+\Delta t) \;=\; & f(t)\underline{\underline{\boldsymbol{Q}}}_{\mathrm{A}}(t) + \Delta t \Big(\big(1-f(t)\big) r_{\mathrm{free}\to\mathrm{as}} \underline{\underline{\boldsymbol{Q}}}_{\mathrm{D}}(t) \\ & - f(t) r_{\mathrm{as}\to\mathrm{free}}(\lambda_{\mathrm{A}}) \underline{\underline{\boldsymbol{Q}}}_{\mathrm{A}}(t) \Big). \end{aligned} \tag{5.9}$$

By rearranging the terms we obtain, in a first approximation, the exchange

terms

$$\left.\frac{\mathrm{d}\underline{\underline{\boldsymbol{Q}}}_{\mathrm{A}}}{\mathrm{d}t}\right|_{\text{exchange}} = r_{\text{free}\to\text{as}}\frac{1-f}{f}\left(\underline{\underline{\boldsymbol{Q}}}_{\mathrm{D}} - \underline{\underline{\boldsymbol{Q}}}_{\mathrm{A}}\right), \tag{5.10}$$

and similarly

$$\left.\frac{\mathrm{d}\underline{\underline{\boldsymbol{Q}}}_{\mathrm{D}}}{\mathrm{d}t}\right|_{\text{exchange}} = r_{\text{as}\to\text{free}}(\lambda_{\mathrm{A}})\frac{f}{1-f}\left(\underline{\underline{\boldsymbol{Q}}}_{\mathrm{A}} - \underline{\underline{\boldsymbol{Q}}}_{\mathrm{D}}\right). \tag{5.11}$$

One can easily verify that in the absence of flow and ignoring the orientation or stretch relaxation processes, $\mathrm{d}\underline{\underline{\boldsymbol{\sigma}}}/\mathrm{d}t \equiv \mathrm{d}\left(f\underline{\underline{\boldsymbol{Q}}}_{\mathrm{A}} + (1-f)\underline{\underline{\boldsymbol{Q}}}_{\mathrm{D}}\right)/\mathrm{d}t = \underline{\underline{\mathbf{0}}}$. Therefore, we ensure in this way that the stress stays constant when a chain attaches or detaches. This, in fact, is the reason for writing the dynamics in terms of $\underline{\underline{\boldsymbol{Q}}}_{\mathrm{A}}$ and $\underline{\underline{\boldsymbol{Q}}}_{\mathrm{D}}$, rather than $\underline{\underline{\boldsymbol{\tau}}}_{\mathrm{A}}$ and $\underline{\underline{\boldsymbol{\tau}}}_{\mathrm{D}}$.

Flow terms

We now derive the flow terms using Equations (4.17) and (4.19). Using the chain rule, we take the derivative with respect to time of Equation (5.3), and considering Equation (5.8) we obtain,

$$\begin{aligned}\left.\frac{\mathrm{d}\underline{\underline{\boldsymbol{Q}}}_{\mathrm{A}}}{\mathrm{d}t}\right|_{\text{flow}} &= \underline{\underline{\boldsymbol{\tau}}}_{\mathrm{A}}\frac{\mathrm{d}}{\mathrm{d}t}\left(\frac{3\lambda_{\max}^2 - 3 + \operatorname{tr}\underline{\underline{\boldsymbol{Q}}}_{\mathrm{A}}}{3\lambda_{\max}^2}\right) + \frac{3\lambda_{\max}^2 - 3 + \operatorname{tr}\underline{\underline{\boldsymbol{Q}}}_{\mathrm{A}}}{3\lambda_{\max}^2}\frac{\mathrm{d}\underline{\underline{\boldsymbol{\tau}}}_{\mathrm{A}}}{\mathrm{d}t} \\ &= \underline{\underline{\boldsymbol{\tau}}}_{\mathrm{A}}\frac{1}{3\lambda_{\max}^2}\frac{\mathrm{d}\operatorname{tr}\underline{\underline{\boldsymbol{Q}}}_{\mathrm{A}}}{\mathrm{d}t} + \frac{3\lambda_{\max}^2 - 3 + \operatorname{tr}\underline{\underline{\boldsymbol{Q}}}_{\mathrm{A}}}{3\lambda_{\max}^2}\frac{\mathrm{d}\underline{\underline{\boldsymbol{\tau}}}_{\mathrm{A}}}{\mathrm{d}t}\end{aligned} \tag{5.12}$$

By taking the trace of Equation (5.12) and re-arranging the terms, we get

$$\frac{\mathrm{d}\operatorname{tr}\underline{\underline{\boldsymbol{Q}}}_{\mathrm{A}}}{\mathrm{d}t} = \frac{3\lambda_{\max}^2 - 3 + \operatorname{tr}\underline{\underline{\boldsymbol{Q}}}_{\mathrm{A}}}{3\lambda_{\max}^2}\frac{\mathrm{d}\operatorname{tr}\underline{\underline{\boldsymbol{\tau}}}_{\mathrm{A}}}{\mathrm{d}t}\frac{3\lambda_{\max}^2 - 3 + \operatorname{tr}\underline{\underline{\boldsymbol{Q}}}_{\mathrm{A}}}{3\lambda_{\max}^2 - 3}. \tag{5.13}$$

We substitute the latter equation into Equation (5.12) to obtain

$$\left.\frac{\mathrm{d}\underline{\underline{\boldsymbol{Q}}}_{\mathrm{A}}}{\mathrm{d}t}\right|_{\mathrm{flow}} = \frac{1}{3\lambda_{\max}^2-3}\,\mathrm{tr}\left[\underline{\underline{\boldsymbol{g}}}\left(\underline{\underline{\boldsymbol{Q}}}_{\mathrm{A}}\right)\right]\underline{\underline{\boldsymbol{Q}}}_{\mathrm{A}} + \underline{\underline{\boldsymbol{g}}}\left(\underline{\underline{\boldsymbol{Q}}}_{\mathrm{A}}\right), \tag{5.14}$$

were we have defined a tensor function $\underline{\underline{\boldsymbol{g}}}$ as

$$\begin{aligned}\underline{\underline{\boldsymbol{g}}}\left(\underline{\underline{\boldsymbol{Q}}}_{\mathrm{A}}\right) &\equiv \frac{3\lambda_{\max}^2-3+\mathrm{tr}\,\underline{\underline{\boldsymbol{Q}}}_{\mathrm{A}}}{3\lambda_{\max}^2}\frac{\mathrm{d}\underline{\underline{\boldsymbol{\tau}}}_{\mathrm{A}}}{\mathrm{d}t} \\ &= \mathrm{f_E}(\lambda_{\mathrm{A}})\frac{\mathrm{d}\underline{\underline{\boldsymbol{\tau}}}_{\mathrm{A}}}{\mathrm{d}t}.\end{aligned} \tag{5.15}$$

Recall that the evolution of $\underline{\underline{\boldsymbol{\tau}}}_{\mathrm{A}}$ is defined by Equation (4.17), therefore we write

$$\left\{\begin{aligned}\left.\frac{\mathrm{d}\underline{\underline{\boldsymbol{Q}}}_{\mathrm{A}}}{\mathrm{d}t}\right|_{\mathrm{flow}} &= \underline{\underline{\boldsymbol{g}}}\left(\underline{\underline{\boldsymbol{Q}}}_{\mathrm{A}}\right) + \frac{1}{3\lambda_{\max}^2-3}\,\mathrm{tr}\left[\underline{\underline{\boldsymbol{g}}}\left(\underline{\underline{\boldsymbol{Q}}}_{\mathrm{A}}\right)\right]\underline{\underline{\boldsymbol{Q}}}_{\mathrm{A}}, \\ \underline{\underline{\boldsymbol{g}}}\left(\underline{\underline{\boldsymbol{Q}}}_{\mathrm{A}}\right) &\equiv \underline{\underline{\boldsymbol{\kappa}}}\cdot\underline{\underline{\boldsymbol{Q}}}_{\mathrm{A}} + \underline{\underline{\boldsymbol{Q}}}_{\mathrm{A}}\cdot\underline{\underline{\boldsymbol{\kappa}}}^{\mathrm{T}} - 2\beta\tilde{\nu}\lambda_{\mathrm{A}}^{-1}\left(\underline{\underline{\boldsymbol{Q}}}_{\mathrm{A}} - \mathrm{f_E}(\lambda_{\mathrm{A}})\underline{\underline{\boldsymbol{I}}}\right).\end{aligned}\right. \tag{5.16}$$

The same strategy leads to

$$\left\{\begin{aligned}\left.\frac{\mathrm{d}\underline{\underline{\boldsymbol{Q}}}_{\mathrm{D}}}{\mathrm{d}t}\right|_{\mathrm{flow}} &= \underline{\underline{\boldsymbol{h}}}\left(\underline{\underline{\boldsymbol{Q}}}_{\mathrm{D}}\right) + \frac{1}{3\lambda_{\max}^2-3}\,\mathrm{tr}\left[\underline{\underline{\boldsymbol{h}}}\left(\underline{\underline{\boldsymbol{Q}}}_{\mathrm{D}}\right)\right]\underline{\underline{\boldsymbol{Q}}}_{\mathrm{D}}, \\ \underline{\underline{\boldsymbol{h}}}\left(\underline{\underline{\boldsymbol{Q}}}_{\mathrm{D}}\right) &\equiv \underline{\underline{\boldsymbol{\kappa}}}\cdot\underline{\underline{\boldsymbol{Q}}}_{\mathrm{D}} + \underline{\underline{\boldsymbol{Q}}}_{\mathrm{D}}\cdot\underline{\underline{\boldsymbol{\kappa}}}^{\mathrm{T}} - 2\beta\tilde{\nu}\lambda_{\mathrm{D}}^{-1}\left(\underline{\underline{\boldsymbol{Q}}}_{\mathrm{D}} - \mathrm{f_E}(\lambda_{\mathrm{D}})\underline{\underline{\boldsymbol{I}}}\right) \\ &\quad -\frac{1}{\tau_{\mathrm{d}}}\left(\underline{\underline{\boldsymbol{Q}}}_{\mathrm{D}} - \mathrm{f_E}(\lambda_{\mathrm{D}})\underline{\underline{\boldsymbol{I}}}\right) - \frac{2(1-\lambda_{\mathrm{D}}^{-1})}{\tau_{\mathrm{s}}}\,\mathrm{f_E}(\lambda_{\mathrm{D}})\underline{\underline{\boldsymbol{Q}}}_{\mathrm{D}}.\end{aligned}\right. \tag{5.17}$$

where the stretches λ_{A} and λ_{D} are defined as a function of $\underline{\underline{\boldsymbol{Q}}}_{\mathrm{A}}$ and $\underline{\underline{\boldsymbol{Q}}}_{\mathrm{D}}$ respectively in Equations (5.6) and (5.7), and, similarly to Equation (5.15), we have defined the tensor function $\underline{\underline{\boldsymbol{h}}}\left(\underline{\underline{\boldsymbol{Q}}}_{\mathrm{D}}\right) \equiv \mathrm{f_E}(\lambda_{\mathrm{D}})\mathrm{d}\underline{\underline{\boldsymbol{\tau}}}_{\mathrm{D}}/\mathrm{d}t$, where $\mathrm{d}\underline{\underline{\boldsymbol{\tau}}}_{\mathrm{D}}/\mathrm{d}t$ is defined by Equation (4.19).

Note that the CCR rate, $\tilde{\nu}$, in the preaveraged equations needs to be defined. This is the aim of the following Section 5.3.2.

5.3.2 Preaveraged CCR rate

For the preaveraged model, we could define a CCR rate, $\tilde{\nu}$, that is equivalent to CCR rate defined in Equation (4.6), which would be

$$\tilde{\nu} = (1-f)\frac{1-\lambda_{\mathrm{D}}^{-1}}{\tau_{\mathrm{s}}}\,\mathrm{f}_{\mathrm{E}}(\lambda_{\mathrm{D}}). \tag{5.18}$$

The way the preaveraging is done in Section 5.3.1, using the tensors $\underline{\underline{\boldsymbol{Q}}}_{\mathrm{A}}$ and $\underline{\underline{\boldsymbol{Q}}}_{\mathrm{D}}$, ensures that the total stress is conserved during attachment and detachment events. However, due to the nonlinear relation between stress and stretch, the preaveraged stretches are not conserved during attachment and detachment events. In reality, when detachments or attachments occur, both the stress and the stretch are conserved, but in our preaveraged model, only the stress is conserved, and the stretch "jumps" between the preaveraged stretches of the attached and detached chains, λ_{A}, and λ_{D}, respectively. This behaviour is a direct result of the preaveraging in the context of nonlinear elasticity: in the stochastic ensemble of chains in Chapter 4, each chain conserves its stress *and* stretch but in a preaveraged model of the type developed here one cannot conserve both. Thus, when preaveraging, we must choose whether to conserve stress *or* stretch. In summary, keeping the stress constant but not the stretch is not physical, but this is a necessary sacrifice for self-consistency of the model.

Hence, the CCR rate – that depends on the preaveraged stretch λ_{D} – is incorrect if defined as in Equation (5.18). In Figure 5.1 we show the CCR rate (together with the viscosity) for the stochastic model Equation (4.6) and for the preaveraged model with Equation (5.18), for two shear rates in region C_2 of the map Figure 4.6 ($\tau_{\mathrm{s}} = 1, \tau_{\mathrm{free}} = 10^3, \tau_{\mathrm{as}} = 10^5, \tau_{\mathrm{d}} = 10^6, \lambda_{\mathrm{max}} = 10$). The preaveraged CCR rate from Equation (5.18), in the red lines of Figure 5.1, presents the same overshoot as the stochastic one, but then fails to drop causing the viscosity

to stay at a too high level in the preaveraged model as compared to the stochastic model. As a consequence of using Equation (5.18), the predictions of the stress growth coefficient are qualitatively different (higher) as compared to the stochastic model. The CCR rates (and thus the viscosity) differs qualitatively between the two models, especially at intermediate shear rate. Therefore, we introduce a

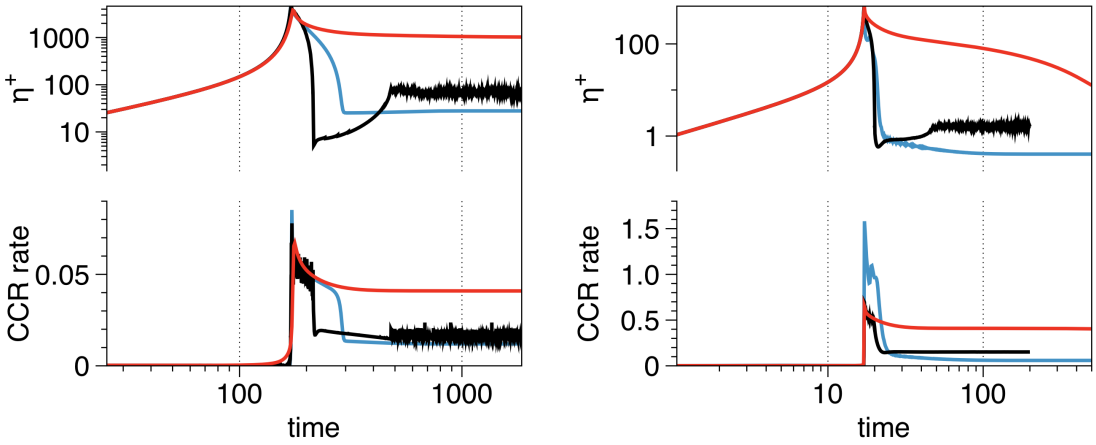

(a) $\dot{\gamma} = 0.1$ (b) $\dot{\gamma} = 1$

Figure 5.1: Region C_2 of Figure 4.6: comparison between the stochastic model (black), and "incorrect" (red) and "correct" (blue) preaveraged model using Equation (5.18) and Equation (5.22), respectively, for $\dot{\gamma} = 0.1$ and $\dot{\gamma} = 1$. Bottom: CCR rates. Top: corresponding viscosity. Parameters are $\tau_s = 1$, $\tau_{free} = 10^3$, $\tau_{as} = 10^5$, $\tau_d = 10^6$, $\lambda_{max} = 10$.

new stretch variable, $\lambda_{D,eq}$, for which the only purpose is to compute the CCR rate. The time evolution of the new preaveraged stretch, $\lambda_{D,eq}$, reads

$$\frac{d\lambda_{D,eq}}{dt} = \left(\underline{\underline{\boldsymbol{\kappa}}} : \underline{\underline{\boldsymbol{S}}}_D\right)\lambda_{D,eq} - \frac{\lambda_{D,eq} - 1}{\tau_s} f_E(\lambda_{D,eq}) + fr_{as\to free}(\lambda_A)(\lambda_A - \lambda_{D,eq}), \quad (5.19)$$

where $\underline{\underline{\boldsymbol{S}}}_D \equiv \underline{\underline{\boldsymbol{Q}}}_D / \operatorname{tr} \underline{\underline{\boldsymbol{Q}}}_D$ is the (unit trace) orientation tensor of the detached population, and λ_A is defined in Equation (5.6). The first term of the RHS is the flow contribution to the stretch, the second term is the stretch relaxation with a characteristic time τ_s and includes finite extensibility, and the last term

is a source term which is proportional to the fraction of attached chains and the rate of detachment. It accounts for the additional stretch that an attached chain brings to the detached population when it detaches.

We then need to split the CCR rate up into two contributions. A first contribution comes from the detached chains similar to Equation (5.18), but using $\lambda_{\mathrm{D,eq}}$

$$\nu_1 = (1-f)\frac{1-\lambda_{\mathrm{D,eq}}^{-1}}{\tau_{\mathrm{s}}}\,\mathrm{f_E}\left(\lambda_{\mathrm{D,eq}}\right). \tag{5.20}$$

A second contribution, ν_2, to the total CCR rate comes from the detachment of (attached) stretched chains as

$$\nu_2 = fr_{\mathrm{as}\to\mathrm{free}}(\lambda_{\mathrm{A}})\frac{\lambda_{\mathrm{A}}-\lambda_{\mathrm{D}}}{(\lambda_{\mathrm{A}}+\lambda_{\mathrm{D}})}. \tag{5.21}$$

We need to include this second contribution because, in the stochastic model, when a chain detaches, it loses stretch (sometimes rapidly) before "joining" the average of the detached population. During this detachment and retraction process, it contributes significantly to CCR, and we capture this through Equation (5.21). The total CCR rate, $\tilde{\nu}$, of the preaveraged model is thus defined using Equations (5.20) and (5.21) as

$$\tilde{\nu} = (1-f)\frac{1-\lambda_{\mathrm{D,eq}}^{-1}}{\tau_{\mathrm{s}}}\,\mathrm{f_E}(\lambda_{\mathrm{D,eq}}) + fr_{\mathrm{as}\to\mathrm{free}}(\lambda_{\mathrm{A}})\frac{\lambda_{\mathrm{A}}-\lambda_{\mathrm{D}}}{(\lambda_{\mathrm{A}}+\lambda_{\mathrm{D}})}. \tag{5.22}$$

By using Equation (5.22) for the CCR rate in the preaveraged model, the predictions match reasonably closely the stochastic model in all regimes of the parameter space. In particular, we show in blue lines Figure 5.1 the CCR rates of the preaveraged model corresponding to Equation (5.22), to be compared with the red lines that correspond to Equation (5.18). It is clear that the CCR rates (and viscosities) of the two models are now in qualitative agreement as we manage

to capture the sharp drop of CCR rate. Figures 5.2 and 5.3 present a similar comparison of the CCR rates for the regions A_1 and A_2 of Figure 4.6, where we see that either Equation (5.18) or Equation (5.22) manage to have the CCR (and viscosity) in good agreement with the stochastic model.

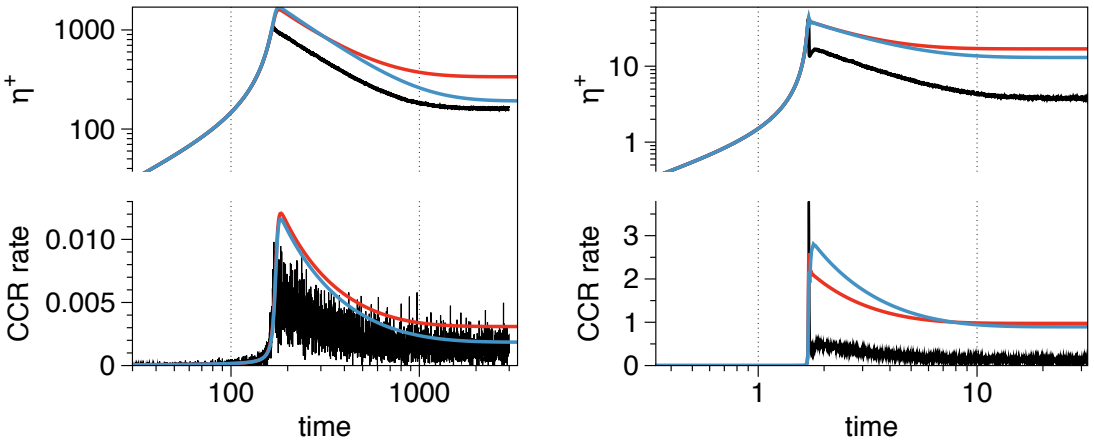

(a) $\dot{\gamma} = 0.1$ (b) $\dot{\gamma} = 10$

Figure 5.2: Region A_1 of Figure 4.6: comparison between the stochastic model (black), and "incorrect" (red) and "correct" (blue) preaveraged model using Equation (5.18) and Equation (5.22), respectively, for $\dot{\gamma} = 0.1$ and $\dot{\gamma} = 10$. Bottom: CCR rates. Top: corresponding viscosity. Parameters are $\tau_s = 1$, $\tau_{free} = 10^{-2}$, $\tau_{as} = 10^2$, $\tau_d = 10^6$, $\lambda_{max} = 10$.

However, in these above examples, the match is not always perfect at a quantitative level, and we anticipate that, when this is the case, the steady state stress in the two model will differ, see Section 5.5.

5.3.3 Summary of the preaveraged set of equations

The time evolution equations of the fraction of attached chains, of the tensors $\underline{\underline{\boldsymbol{Q}}}_A$ and $\underline{\underline{\boldsymbol{Q}}}_D$ – as the sum of the flow terms Equations (5.16) and (5.17), and exchange terms Equations (5.10) and (5.11) – and the relevant variables are summarized in Table 5.1.

Table 5.1: Preaveraged equation set.

Expression for the stress tensor, in units of G:

$$\underline{\underline{\boldsymbol{\sigma}}} = f\underline{\underline{\boldsymbol{Q}}}_{\mathrm{A}} + (1-f)\underline{\underline{\boldsymbol{Q}}}_{\mathrm{D}}.$$

Evolution of the fraction of attached chains:

$$\frac{\mathrm{d}f}{\mathrm{d}t} = r_{\mathrm{free}\to\mathrm{as}}\,(1-f) - r_{\mathrm{as}\to\mathrm{free}}(\lambda_{\mathrm{A}})f.$$

Evolution of the attached chains tensor:

$$\frac{\mathrm{d}\underline{\underline{\boldsymbol{Q}}}_{\mathrm{A}}}{\mathrm{d}t} = \underline{\underline{\boldsymbol{g}}}\left(\underline{\underline{\boldsymbol{Q}}}_{\mathrm{A}}\right) + \frac{1}{3\lambda_{\max}^2-3}\,\mathrm{tr}\left[\underline{\underline{\boldsymbol{g}}}\left(\underline{\underline{\boldsymbol{Q}}}_{\mathrm{A}}\right)\right]\underline{\underline{\boldsymbol{Q}}}_{\mathrm{A}} + r_{\mathrm{free}\to\mathrm{as}}\frac{1-f}{f}\left(\underline{\underline{\boldsymbol{Q}}}_{\mathrm{D}} - \underline{\underline{\boldsymbol{Q}}}_{\mathrm{A}}\right),$$

with

$$\underline{\underline{\boldsymbol{g}}}\left(\underline{\underline{\boldsymbol{Q}}}_{\mathrm{A}}\right) \equiv \underline{\underline{\boldsymbol{\kappa}}}\cdot\underline{\underline{\boldsymbol{Q}}}_{\mathrm{A}} + \underline{\underline{\boldsymbol{Q}}}_{\mathrm{A}}\cdot\underline{\underline{\boldsymbol{\kappa}}}^{\mathrm{T}} - 2\beta\tilde{\nu}\lambda_{\mathrm{A}}^{-1}\left(\underline{\underline{\boldsymbol{Q}}}_{\mathrm{A}} - \mathrm{f_E}(\lambda_{\mathrm{A}})\underline{\underline{\boldsymbol{I}}}\right).$$

Evolution of the detached chains tensor:

$$\frac{\mathrm{d}\underline{\underline{\boldsymbol{Q}}}_{\mathrm{D}}}{\mathrm{d}t} = \underline{\underline{\boldsymbol{h}}}\left(\underline{\underline{\boldsymbol{Q}}}_{\mathrm{D}}\right) + \frac{1}{3\lambda_{\max}^2-3}\,\mathrm{tr}\left[\underline{\underline{\boldsymbol{h}}}\left(\underline{\underline{\boldsymbol{Q}}}_{\mathrm{D}}\right)\right]\underline{\underline{\boldsymbol{Q}}}_{\mathrm{D}} + r_{\mathrm{as}\to\mathrm{free}}(\lambda_{\mathrm{A}})\frac{f}{1-f}\left(\underline{\underline{\boldsymbol{Q}}}_{\mathrm{A}} - \underline{\underline{\boldsymbol{Q}}}_{\mathrm{D}}\right),$$

with

$$\underline{\underline{\boldsymbol{h}}}\left(\underline{\underline{\boldsymbol{Q}}}_{\mathrm{D}}\right) \equiv \underline{\underline{\boldsymbol{\kappa}}}\cdot\underline{\underline{\boldsymbol{Q}}}_{\mathrm{D}} + \underline{\underline{\boldsymbol{Q}}}_{\mathrm{D}}\cdot\underline{\underline{\boldsymbol{\kappa}}}^{\mathrm{T}} - 2\beta\tilde{\nu}\lambda_{\mathrm{D}}^{-1}\left(\underline{\underline{\boldsymbol{Q}}}_{\mathrm{D}} - \mathrm{f_E}(\lambda_{\mathrm{D}})\underline{\underline{\boldsymbol{I}}}\right) - \frac{1}{\tau_{\mathrm{d}}}\left(\underline{\underline{\boldsymbol{Q}}}_{\mathrm{D}} - \mathrm{f_E}(\lambda_{\mathrm{D}})\underline{\underline{\boldsymbol{I}}}\right) - \frac{2(1-\lambda_{\mathrm{D}}^{-1})}{\tau_{\mathrm{s}}}\,\mathrm{f_E}(\lambda_{\mathrm{D}})\underline{\underline{\boldsymbol{Q}}}_{\mathrm{D}}.$$

Preaveraged CCR rate:

$$\tilde{\nu} = (1-f)\frac{1-\lambda_{\mathrm{D,eq}}^{-1}}{\tau_{\mathrm{s}}}\,\mathrm{f_E}(\lambda_{\mathrm{D,eq}}) + f r_{\mathrm{as}\to\mathrm{free}}(\lambda_{\mathrm{A}})\frac{\lambda_{\mathrm{A}}-\lambda_{\mathrm{D}}}{(\lambda_{\mathrm{A}}+\lambda_{\mathrm{D}})}.$$

Evolution of the CCR stretch-variable:

$$\frac{\mathrm{d}\lambda_{\mathrm{D,eq}}}{\mathrm{d}t} = (\underline{\underline{\boldsymbol{\kappa}}} : \underline{\underline{\boldsymbol{Q}}}_{\mathrm{D}}/\,\mathrm{tr}\,\underline{\underline{\boldsymbol{Q}}}_{\mathrm{D}})\lambda_{\mathrm{D,eq}} - \frac{\lambda_{\mathrm{D,eq}}-1}{\tau_{\mathrm{s}}}\,\mathrm{f_E}(\lambda_{\mathrm{D,eq}}) + f r_{\mathrm{as}\to\mathrm{free}}(\lambda_{\mathrm{A}})(\lambda_{\mathrm{A}}-\lambda_{\mathrm{D,eq}}).$$

Rate of attachment and detachment:

$$r_{\mathrm{free}\to\mathrm{as}} = \tau_{\mathrm{as}}^{-1}\frac{\phi_{\mathrm{as}}}{1-\phi_{\mathrm{as}}}, \quad r_{\mathrm{as}\to\mathrm{free}}(\lambda_{\mathrm{A}}) = \tau_{\mathrm{as}}^{-1}\left(\frac{1-\lambda_{\mathrm{A}}^2\lambda_{\max}^{-2}}{1-\lambda_{\max}^{-2}\left(\lambda_{\mathrm{A}}-\frac{r}{Za_0}\right)^2}\right)^{-\frac{3}{2}Z\lambda_{\max}^2}.$$

Stretch of the attached and detached chains:

$$\lambda_{\mathrm{A}} = \left(\frac{\lambda_{\max}^2\,\mathrm{tr}\left(\underline{\underline{\boldsymbol{Q}}}_{\mathrm{A}}\right)}{3\lambda_{\max}^2-3+\mathrm{tr}\left(\underline{\underline{\boldsymbol{Q}}}_{\mathrm{A}}\right)}\right)^{1/2}, \quad \lambda_{\mathrm{D}} = \left(\frac{\lambda_{\max}^2\,\mathrm{tr}\left(\underline{\underline{\boldsymbol{Q}}}_{\mathrm{D}}\right)}{3\lambda_{\max}^2-3+\mathrm{tr}\left(\underline{\underline{\boldsymbol{Q}}}_{\mathrm{D}}\right)}\right)^{1/2}.$$

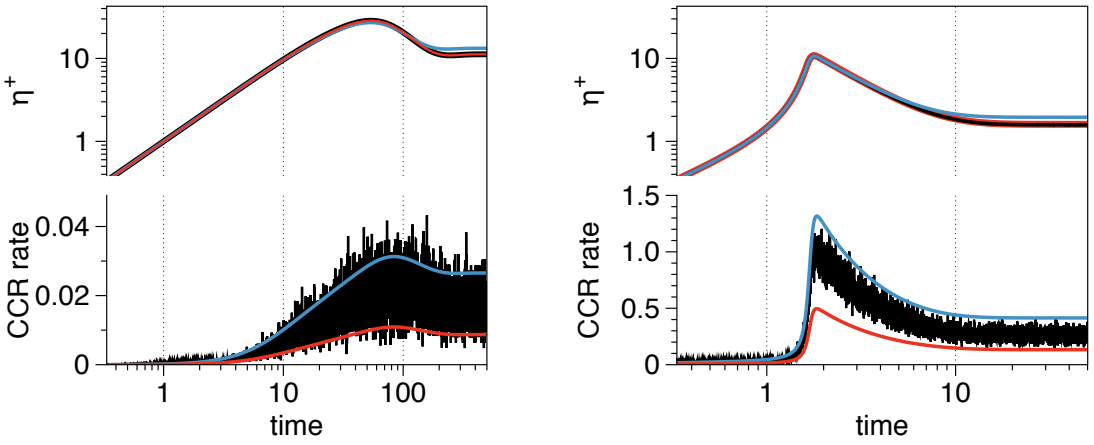

(a) $\dot{\gamma} = 0.2$ (b) $\dot{\gamma} = 10$

Figure 5.3: Region A_2 of Figure 4.6: comparison between the stochastic model (black), and "incorrect" (red) and "correct" (blue) preaveraged model using Equation (5.18) and Equation (5.22), respectively, for $\dot{\gamma} = 0.2$ and $\dot{\gamma} = 10$. Bottom: CCR rates. Top: corresponding viscosity. Parameters are $\tau_s = 1$, $\tau_{free} = 10^{-4}$, $\tau_{as} = 10^{-2}$, $\tau_d = 10^6$, $\lambda_{max} = 10$.

5.4 Predictions of the preaveraged model

We solve the set of differential equations presented in Table 5.1 using the Euler scheme, with a time step $\Delta t < \min(\tau_{as}, \tau_{free}, \tau_s, \kappa^{-1})/100$, where $\kappa = \dot{\gamma}$ or $\dot{\varepsilon}$ is the flow rate.

We present in Figures 5.5–5.9 (at the end of this Chapter) the predictions of the preaveraged model for the regions A_1, A_2, B, C_1, and C_2 respectively. These should be compared against Figures 4.7–4.11 respectively, in Chapter 4. It is evident that the preaveraged model captures most of the features of the stochastic model:

(i) We obtain the same critical shear rate, $\dot{\gamma}_c^{hard}$, at which shear hardening is seen;

(ii) Transients in regions A_1, A_2, and B are in almost perfect quantitative agree-

ment;

(iii) Steady state stress as a function of shear rate curves have the same trend;

(iv) The spikes at intermediate elongation rate in region A_1, Figure 5.5, are well resolved.

Although the preaveraged model successfully captures the onset of the spikes in the regions C_1 and C_2, it suffers from the biggest discrepancies, at intermediate (shear or elongation) rates, with the stochastic predictions:

(v) In the region C_1, Figure 5.8, the preaveraged model produces oscillations in shear that are not present in Figure 4.10 for $\dot{\gamma} = 0.3$ and $\dot{\gamma} = 0.5$;

(vi) In the region C_2, Figure 5.9, the undershoots, both in elongation and shear, are not captured, and the steady state stresses are different at low and intermediate flow rates.

It is, of course, extremely unlikely that a preaveraged model could quantitatively capture every single feature of the stochastic model. We consider the remarkably high level of agreement between the stochastic and preaveraged models to be a significant success of this work. As a result, we have a model which is suitable for flow computation, with physically meaningful parameters, that can be used as a "toy" model for future investigations.

5.5 Constitutive curve comparison

In Figure 5.4, we present the steady state shear and elongation stresses as a function of the flow rate obtained by averaging out the late time values of the stress tensor: σ_{xy} in shear, and $\sigma_{xx} - \sigma_{yy}$ in elongation, for both the stochastic and preaveraged model. We note that

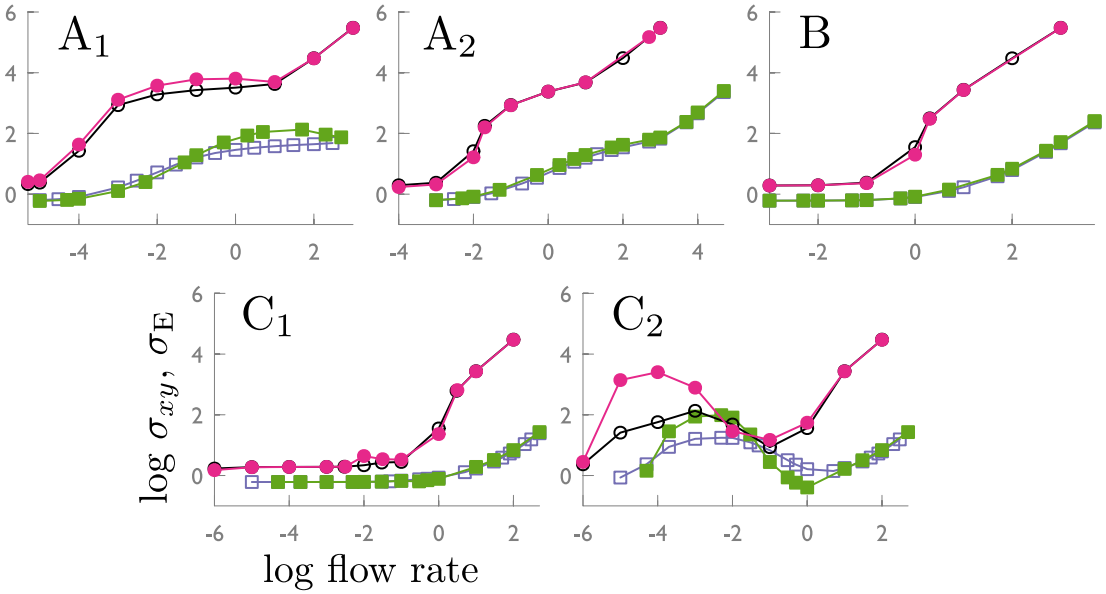

Figure 5.4: Steady state stress as a function of the flow rate (in log-scale) in the different regions of Figure 4.6, in shear (σ_{xy}) and elongation ($\sigma_{\mathrm{E}} = \sigma_{xx} - \sigma_{yy}$), squares and circles respectively. Comparison between the stochastic model (empty symbols) and preaveraged model (filled symbols).

(i) In regions A_2 and B, there is a perfect agreement between the stochastic and preaveraged model in both shear and elongation;

(ii) In region C_2 there is qualitative agreement of the steady state stresses between the stochastic and preaveraged model;

(iii) In region A_1, the preaveraged model predicts slightly negative slope in shear and elongation which are not seen in the stochastic model. This is caused by a too high CCR rate in the preaveraged model which results in a higher stress value;

(iv) Due to the CCR parameter being large enough ($\beta = 1$), the regions A_1, A_2, and B exhibit a monotonic curve. However, the region C_2 shows a clearly non-monotonic relation between steady state stress and shear rate, in both the stochastic and preaveraged model, which, according to recent works,

implies shear banding of the system in the steady state. Also, transient shear banding might occur where shear hardening and rapid stress drop is seen [Adams *et al.* (2011); Cromer *et al.* (2014); Fielding (2016); Moorcroft & Fielding (2013)];

(v) Results presented in this work for the region C_1 are for $\phi_{as} = 0.01$, and do not present a non-monotonic relation for the stochastic model. However, we already see an onset of non-monotonicity in the preaveraged model. As we go towards region C_2 (increasing ϕ_{as}), the non-monotonicity starts to grow. Therefore, we might be able to tune the shear banding properties of the polymeric systems by adjusting the parameter ϕ_{as}.

5.6 Conclusions on the stochastic and preaveraged model

The central goal of Chapters 4 and 5 was to produce a simplified nonlinear constitutive "toy" model which could capture effects of both entanglements and "sticky" telechelic groups in polymeric systems. As argued in the Introduction of Part II, we chose the star polymer as the simplest architecture to consider, since it results in a two-state system in which the single sticker is attached or detached. Our methodology, then, was to create a stochastic model in which each star arm has its own history of attachment and detachment, and then to create a preaveraged model with properties that closely resemble the stochastic system. Both models contain physically meaningful parameters, allowing a "map" of typical behavior in different regions of parameter space to be investigated.

The simplified stochastic tube model for entangled telechelic stars, Chapter 4, exhibits a broad range of behaviors that one is able to tune by adjusting the sticker

parameters, τ_{as}, and τ_{free} with respect to the orientation (in the linear regime) or stretch (in the nonlinear regime) relaxation times. In both the linear and nonlinear regime, we produced a parameter map where we identified different regions defined by how critical timescales compare. In the linear regime, our model is in good agreement with the more detailed work of van Ruymbeke and co-workers [van Ruymbeke *et al.* (2010)].

In the nonlinear regime, we saw dramatic changes in the stress growth coefficient transients as we navigated around the parameter map, i.e. our constitutive model exhibits a rich variety of responses. We observed that particular parameter sets produce shear hardening, extension hardening, sharp stress drops, smoother stress drops, monotonic and non-monotonic curve for the steady state stress as a function of shear rate.

Finally, we developed, in this Chapter, a preaveraged model, that retains the vast majority of the features of the stochastic model. We anticipate that this will serve as a prototypical "toy" model for flow computation. As an example of this, in the following Chapter 6, we shall investigate the shear banding flow instability using this novel constitutive model.

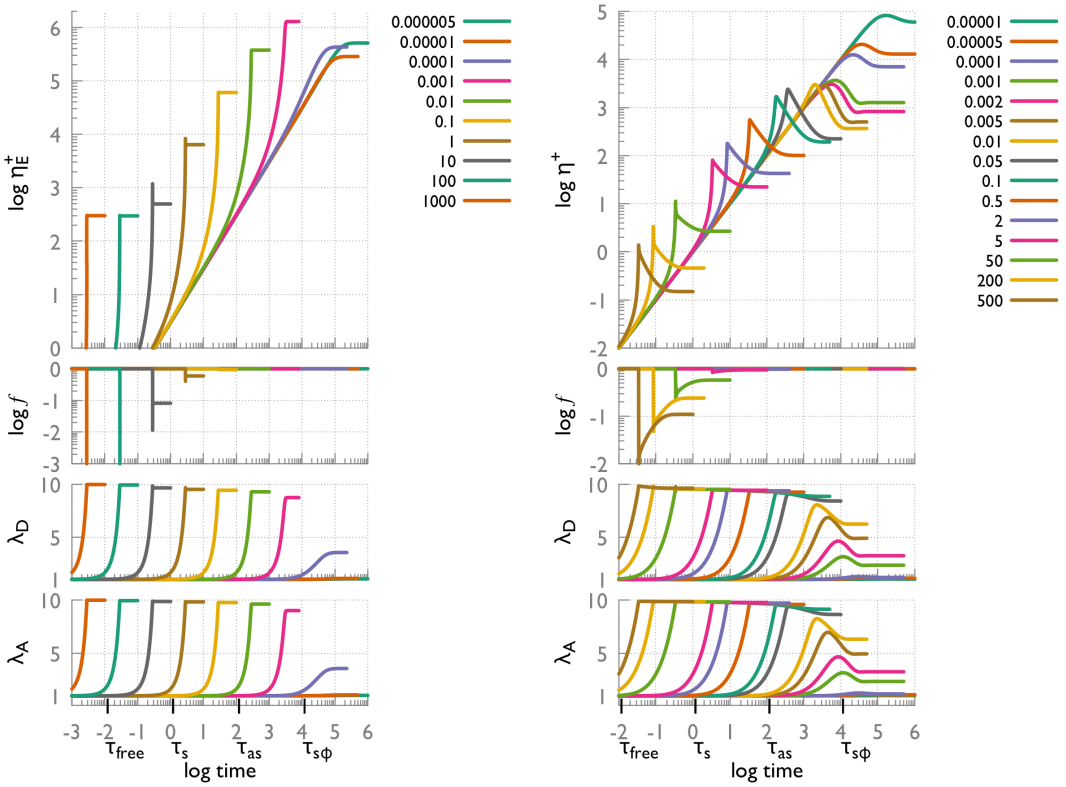

(a) Elongation (b) Shear

Figure 5.5: Preaveraged model predictions for region A_1 in the nonlinear regime, to be compared with Figure 4.7. We present the values, as a function of time, of the fraction of attached chains, f, the stretch of the attached chains λ_A and stretch of the detached chains λ_D, and stress growth coefficients, η_E^+ and η^+, for uniaxial extension (left), and step rate (right) respectively. Parameters are $\tau_{free} = 10^{-2}$, $\tau_{as} = 10^2$, $\tau_s = 1$, $\tau_d = 10^6$, $\lambda_{max} = 10$.

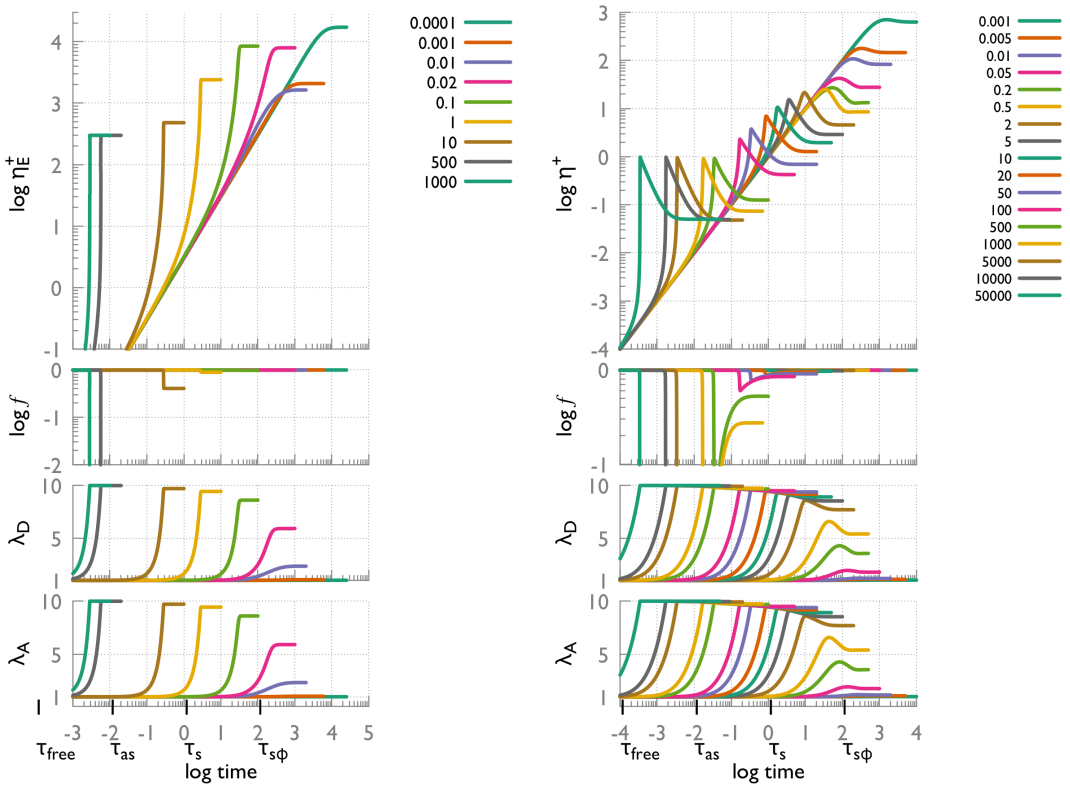

(a) Elongation (b) Shear

Figure 5.6: Preaveraged model predictions for region A_2 in the nonlinear regime, to be compared with Figure 4.8. We present the values, as a function of time, of the fraction of attached chains, f, the stretch of the attached chains λ_A and stretch of the detached chains λ_D, and stress growth coefficients, η_E^+ and η^+, for uniaxial extension (left), and step rate (right) respectively. Parameters are $\tau_{free} = 10^{-4}$, $\tau_{as} = 10^{-2}$, $\tau_s = 1$, $\tau_d = 10^6$, $\lambda_{max} = 10$.

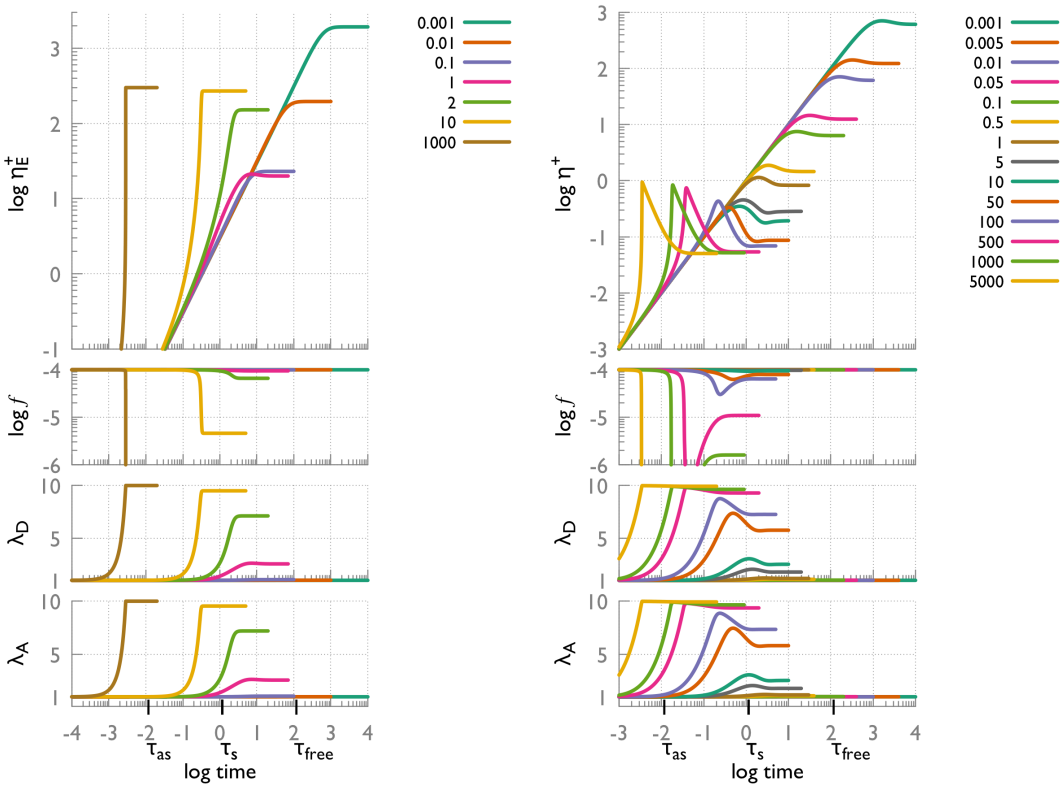

(a) Elongation (b) Shear

Figure 5.7: Preaveraged model predictions for region B in the nonlinear regime, to be compared with Figure 4.9. We present the values, as a function of time, of the fraction of attached chains, f, the stretch of the attached chains λ_A and stretch of the detached chains λ_D, and stress growth coefficients, η_E^+ and η^+, for uniaxial extension (left), and step rate (right) respectively. Parameters are $\tau_{free} = 10^2$, $\tau_{as} = 10^{-2}$, $\tau_s = 1$, $\tau_d = 10^6$, $\lambda_{max} = 10$.

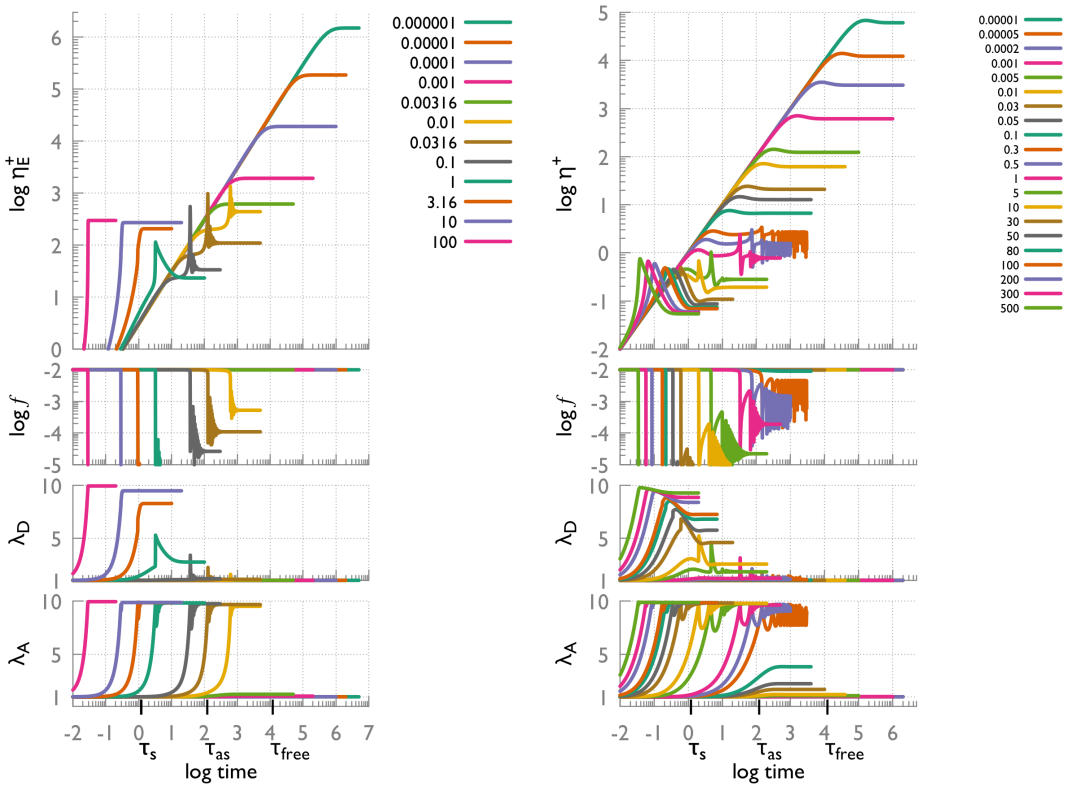

(a) Elongation (b) Shear

Figure 5.8: Preaveraged model predictions for region C_1 in the nonlinear regime, to be compared with Figure 4.10. We present the values, as a function of time, of the fraction of attached chains, f, the stretch of the attached chains λ_A and stretch of the detached chains λ_D, and stress growth coefficients, η_E^+ and η^+, for uniaxial extension (left), and step rate (right) respectively. Parameters are $\tau_{free} = 10^4$, $\tau_{as} = 10^2$, $\tau_s = 1$, $\tau_d = 10^6$, $\lambda_{max} = 10$.

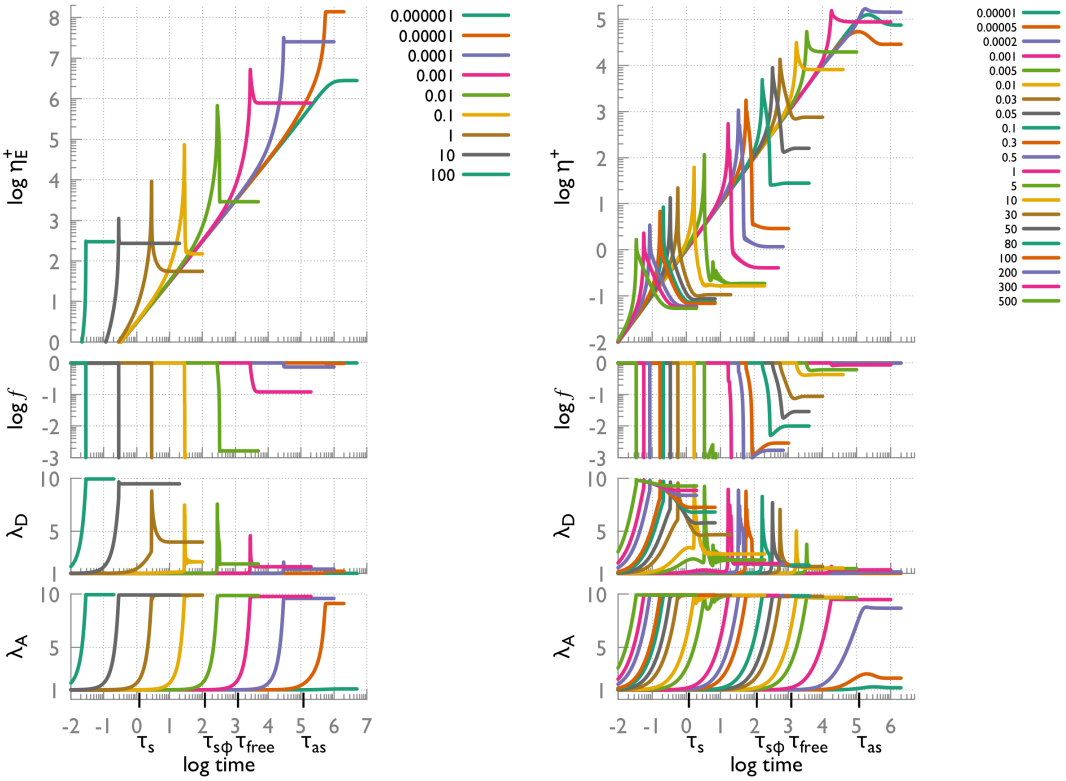

(a) Elongation (b) Shear

Figure 5.9: Preaveraged model predictions for region C_2 in the nonlinear regime, to be compared with Figure 4.11. We present the values, as a function of time, of the fraction of attached chains, f, the stretch of the attached chains λ_A and stretch of the detached chains λ_D, and stress growth coefficients, η_E^+ and η^+, for uniaxial extension (left), and step rate (right) respectively. Parameters are $\tau_{free} = 10^3$, $\tau_{as} = 10^5$, $\tau_s = 1$, $\tau_d = 10^6$, $\lambda_{max} = 10$.

This page is intentionally left blank

Chapter 6

Shear banding study of entangled telechelic star polymers

6.1 Introduction

6.1.1 Flow instabilities

The flow of viscoelastic liquids is often accompanied by interesting effects usually not seen in (simple) Newtonian liquids [Bird *et al.* (1987); Brochard & de Gennes (1992); Brochard-Wyart *et al.* (1996); Larson (1992); Maxwell & Galt (1962); Migler *et al.* (1993); Vinogradov *et al.* (1984)]. Non-Newtonian effects are frequently present during the extrusion of molten polymers at high stresses – one of the most common industrial shaping process. The surface or shape of the resulting material is altered by the presence of flow defects such as extrudate swelling, crystallization effects, sharkskin or melt flow instabilities, depending on the type of polymer as well as on the construction of the capillary device [Benbow & Lamb (1963); Leonov (1984); Paskhin (1978); Vinogradov *et al.* (1984)]. In some constant rate experiments on capillaries [den Otter (1971); Lupton & Regester (1965)]

or cone-plate [Bandyopadhyay *et al.* (2000); Soltero *et al.* (1999)] geometry, periodic oscillations of the shear stress or pressure is observed and attributed to either a structural breakdown (chain disentanglement), or to a stick-slip transition at the walls or between macrodomains [Bandyopadhyay *et al.* (2000)].

Wall-slip, a non-zero relative velocity at a solid-liquid interface, is called "true slip"; it must be distinguished from "apparent slip". For example, when we impose an external shear rate, higher than the complex-fluid characteristic time, the internal mesoscopic structure is reorganized and the shear rate may localize so that two (or more) bands experiencing different shear rates coexist. In the resulting "shear banded" state, a narrow shear band close to a wall can appear as an apparent wall slip. Since the first theoretical models for worm-like micelles [Cates (1987; 1990); Spenley *et al.* (1996; 1993)], numerous techniques and experiments were developed to understand the shear banding phenomena; cf. [Cates & Fielding (2006); Fielding (2007); Lerouge & Berret (2010); Olmsted (2008)] for reviews of experiments (mainly on worm-like micelles) and theoretical considerations.

Polymeric systems with reversible junctions, such as entanglements or associative stickers, are known to undergo flow instabilities, e.g. spurt [McLeish & Ball (1986)], shear banding [Divoux *et al.* (2015); Fielding (2007; 2016); Manneville (2008); Moorcroft & Fielding (2014)] or melt fracture [Berret & Séréro (2001); Ligoure & Mora (2013); Sprakel *et al.* (2009)]. These instabilities can alter the flow and final properties of the material and therefore controlling these phenomena is of critical industrial importance in the processing of polymers. Experimental understanding of the flow and instabilities in complex fluids generally rely on rotational rheometers [Dealy & Larson (2006)], e.g. Taylor-Couette, cone-plate, or parallel plate geometries.

In concentrated solutions of telechelic polymers, i.e. linear chains with stickers at both extremities that enable the formation of transient network, experiments

[Berret & Séréro (2001); Michel *et al.* (2001); Sprakel *et al.* (2008)] and MD simulations [Castillo-Tejas *et al.* (2017)] showed that flow instabilities can occur. Note that above a critical concentration, telechelic polymers self-assemble into overlapping flowerlike micelles whose local structure resembles star polymers because, in the limit of very sticky system ($\tau_{as} \gg \tau_d, \tau_s$ and $\phi_{as} \approx 1$), linear entangled telechelic polymers have both ends attached most of the time and, upon (rare) detachment of a sticker, the linear polymer is in a configuration akin to star polymers with one anchored end (branch point) and one free end.

In this Chapter, we investigate shear banding using the preaveraged constitutive model for entangled telechelic star polymers, that is based on the Rolie-Poly model [Likhtman & Graham (2003)] and developed in Chapter 5, and compare with experimental findings on concentrated solution of linear telechelic chains. The advantage of the Rolie-Poly model [Likhtman & Graham (2003)] over the Johnson-Segalman model (a widely used phenomenological constitutive model [Fardin *et al.* (2012); Johnson & Segalman (1977)]) is that it is derived from a full molecular model based on tube dynamics, and it includes chain stretch, contour length fluctuation, and thermal and convective constraint release (CCR) [Marrucci (1996)].

We show that our molecular constitutive model for entangled telechelic polymers of Chapter 5, predicts (i) steady state shear banding and (ii) periodic oscillatory stress response. These oscillations are generated by an "apparent slip" i.e. a narrow shear band usually close to the wall, giving the impression of a "stick-slip" behavior (though our simulations use non-slip boundary conditions). In contrast with phenomenological models of, e.g., Refs. [Head *et al.* (2002); Picard *et al.* (2002)], our molecular model reveals a novel mechanism for a stick-slip transition, arising from interaction between the structural relaxation within the material, and diffusion of the constituent species across a narrow band. In

what follows, we present our model and the mechanism of this apparent stick-slip process, and discuss how this may relate to the non trivial physical phenomena occurring in experiments. This work is also a demonstration of the utility of the constitutive model developed in Chapter 5 in addressing complex, time-dependent flows.

6.1.2 Flow curve

We briefly summarise the phenomenology of shear banding. Figure 6.1 presents a sketch of the steady state shear stress as a function of the applied shear rate, typically for $\underline{\underline{\boldsymbol{\sigma}}}$ following the Rolie-Poly model [Graham *et al.* (2003)] with $\beta \approx 0$, i.e. no CCR [Agimelen & Olmsted (2013)]. Other models that exhibit shear banding, e.g. the Johnson-Segalman [Johnson & Segalman (1977)] model, often have a similar steady state stress curve [Olmsted (2008)]. The (non-monotonic) homogeneous constitutive curve is "ABCDEF". The system is unstable in the portion "CD", and metastable in the "BC" and "DE" portions. The (shear banded) flow curve is "ABEF", i.e. when the applied shear rate is between $\dot{\gamma}_{\text{low}}$ and $\dot{\gamma}_{\text{high}}$, the system spontaneously forms two macroscopic bands of fluid, one at a shear rate $\dot{\gamma}_{\text{low}}$ and the other at $\dot{\gamma}_{\text{high}}$ [Fielding (2016)]. In the banded regime, i.e. $\dot{\gamma}_{\text{low}} < \dot{\gamma}_{\text{av}} < \dot{\gamma}_{\text{high}}$, the stress stays constant, or slightly increases due to curvature effects (not considered here) in geometries such as cylindrical Couette [Fielding & Olmsted (2003); Lerouge *et al.* (2000); Olmsted *et al.* (2000)].

For an applied shear rate such that $\dot{\gamma}_{\text{low}} < \dot{\gamma}_{\text{av}} < \dot{\gamma}_{\text{high}}$, the fraction, α_{high}, of fluid "experiencing" the high shear rate is given by the lever rule:

$$\dot{\gamma}_{\text{av}} \approx \alpha_{\text{high}}\dot{\gamma}_{\text{high}} + (1 - \alpha_{\text{high}})\dot{\gamma}_{\text{low}}. \tag{6.1}$$

This rule has been confirmed by many experiments [Lerouge & Berret (2010)].

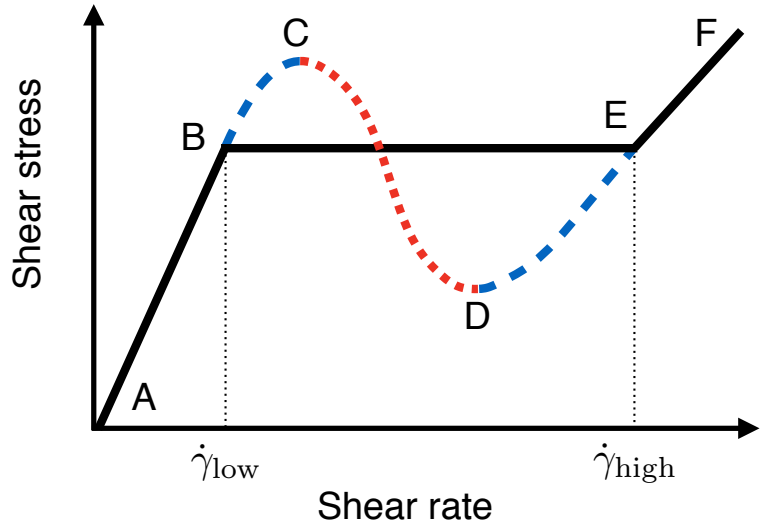

Figure 6.1: Steady state shear stress function of the applied shear rate. The "ABCDEF" line is the (non-monotonic) homogeneous constitutive curve, while the "ABEF" path is the shear-banded flow curve. The selected stress is the "BE" level and the selected shear rates are $\dot{\gamma}_{\text{low}}$ and $\dot{\gamma}_{\text{high}}$.

The stress selection that is made by the system when it bands, which corresponds to the stress plateau, is unique if we include a diffusion term in our model [Lu *et al.* (2000)].

We detail, in the following, the method we used to derive the diffusion terms (that allow a single stress selection) as well as the simulation set-up, followed by our results and discussion.

6.2 Shear banding simulations

6.2.1 Parallel plates

We consider a parallel plate configuration: the top plate at $y = L$ moves with velocity u in the x-direction with respect to the bottom plate at $y = 0$, giving fixed average shear rate $\dot{\gamma}_{\text{av}} = u/L$, cf. Figure 6.2. This may describe a cone-plate

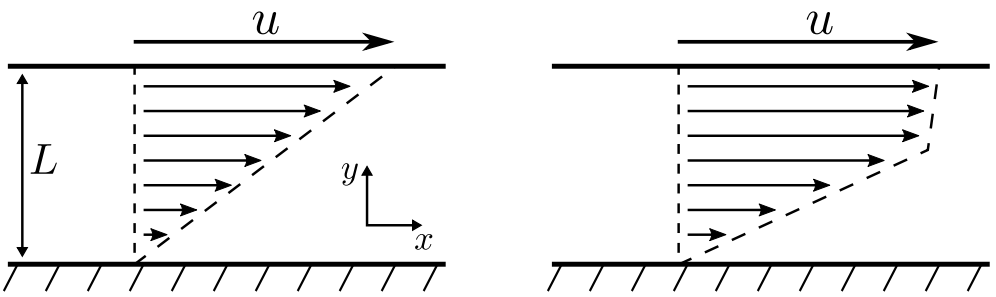

Figure 6.2: Simulation set-up. The top plate at $y = L$ moves with a velocity u in the x-direction with respect to the bottom plate at $y = 0$. Left: homogeneous flow. Right: a banded flow.

or Taylor-Couette flow, if we neglect the curvature effects.

6.2.2 Derivation of the diffusive terms

In order to study the shear banding effects associated with the set of equations presented in Table 5.1, we detail the effect of diffusion of the chains across a unidimensional channel.

We split the domain between $y = 0$ and $y = L$ into a set of "boxes" of size Δy, and we consider the effect of chains jumping between these boxes. We suppose that there are n chains in total in each box, a fraction f of which are attached and a fraction $(1 - f)$ detached. We then assume that at each time step Δt, each box exchanges δn chains with each of the adjacent boxes. These chains are selected in proportion to the number of attached or detached chains in the box from which they leave.

We can summarize by saying that at each time step, the box at "height" y loses stress related to the attached and detached population in proportion to

$$2\delta n f(y) \underline{\underline{\boldsymbol{Q}}}_{\mathrm{A}}(y), \tag{6.2}$$

$$2\delta n \big(1 - f(y)\big) \underline{\underline{\boldsymbol{Q}}}_{\mathrm{D}}(y), \tag{6.3}$$

where the factor 2 comes from the fact that, except at the boundaries, the quantities exit through the top *and* bottom. Moreover, at each time step, the box at "height" y gains some stress coming from the top and bottom boxes:

$$\delta n(f\underline{\underline{\boldsymbol{Q}}}_{\mathrm{A}})(y+\Delta y)+\delta n(f\underline{\underline{\boldsymbol{Q}}}_{\mathrm{A}})(y-\Delta y) \quad \text{from A-chains,} \tag{6.4}$$

$$\delta n\big((1-f)\underline{\underline{\boldsymbol{Q}}}_{\mathrm{D}}\big)(y+\Delta y)+\delta n\big((1-f)\underline{\underline{\boldsymbol{Q}}}_{\mathrm{D}}\big)(y-\Delta y) \quad \text{from D-chains,} \tag{6.5}$$

where we used the shorthand $(f\underline{\underline{\boldsymbol{Q}}})(y) \equiv f(y)\underline{\underline{\boldsymbol{Q}}}(y)$, and all the quantities are at time t.

Now, we can express the fraction of attached chains, f, at $t+\Delta t$. Considering that the total number of chains in the box at "height" y is n, the number of attached chains at time $t+\Delta t$ is

$$\begin{aligned} nf(y,t+\Delta t) &= (n-2\delta n)f(y)+\delta nf(y+\Delta y)+\delta nf(y-\Delta y) \\ &= nf(y)+\delta n\big(f(y+\Delta y)+f(y-\Delta y)-2f(y)\big), \end{aligned} \tag{6.6}$$

where all quantities are evaluated at time t if not specified otherwise. Dividing by $n\Delta t$ and rearranging the terms, we recognise the finite difference approximation of the time derivative and second order spatial derivative derivative, so that in the limit $\Delta t \to 0$ and $\Delta y \to 0$, taken such that $(\Delta y)^2/\Delta t$ remains constant, we find:

$$\frac{\partial f}{\partial t} = D\frac{\partial^2 f}{\partial y^2}, \tag{6.7}$$

where $D = \dfrac{\delta n}{n}\dfrac{(\Delta y)^2}{\Delta t}$. Hence, the fraction of attached chains, f, diffuses across the boxes with a diffusion coefficient D.

Now, we will derive the value of the tensor $\underline{\underline{\boldsymbol{Q}}}_{\mathrm{A}}$ at time $t+\Delta t$. According to the balance equations previously written we have that the total stress in the box

at "height" y from the attached population is

$$\begin{aligned} nf(y,t+\Delta t)\underline{\underline{\boldsymbol{Q}}}_{\mathrm{A}}(y,t+\Delta t) &= (\text{stress from A-chains at time } t \text{ in box } y) \\ &\quad - (\text{stress from A-chains leaving box } y) \\ &\quad + (\text{stress from A-chains arriving box } y) \\ &= n(f\underline{\underline{\boldsymbol{Q}}}_{\mathrm{A}})(y,t) \\ &\quad -2\delta n(f\underline{\underline{\boldsymbol{Q}}}_{\mathrm{A}})(y,t) \\ &\quad +\delta n\big((f\underline{\underline{\boldsymbol{Q}}}_{\mathrm{A}})(y+\Delta y,t)+(f\underline{\underline{\boldsymbol{Q}}}_{\mathrm{A}})(y-\Delta y,t)\big). \end{aligned}$$

Rearranging the terms and approximating the finite differences for the derivatives, we obtain the partial differential equation

$$\frac{\partial f\underline{\underline{\boldsymbol{Q}}}_{\mathrm{A}}}{\partial t} = D\frac{\partial^2 f\underline{\underline{\boldsymbol{Q}}}_{\mathrm{A}}}{\partial y^2}. \tag{6.8}$$

From Equation (6.7), we know the value of $f(y,t+\Delta t)$, hence we can deduce the value of $\underline{\underline{\boldsymbol{Q}}}_{\mathrm{A}}(y,t+\Delta t)$ from Equation (6.8) by a simple division.

Similarly, the time evolution of the tensor $\underline{\underline{\boldsymbol{Q}}}_{\mathrm{D}}$ representing the detached chains can be obtained via

$$\frac{\partial(1-f)\underline{\underline{\boldsymbol{Q}}}_{\mathrm{D}}}{\partial t} = D\frac{\partial^2(1-f)\underline{\underline{\boldsymbol{Q}}}_{\mathrm{D}}}{\partial y^2}. \tag{6.9}$$

6.2.3 Simulation parameters

The diffusion coefficient, D, is dimensionless in the simulations, as are the gap size L and timescales (e.g. τ_{as}, the longest relaxation time), corresponding to physical (dimensional) quantities $\tilde{D}$, $\tilde{L}$ and $\tilde{\tau}_{\mathrm{as}}$ respectively. D may therefore be obtained from $D = \tilde{D}L^2\tilde{\tau}_{\mathrm{as}}/\tilde{L}^2\tau_{\mathrm{as}}$, so a decrease in physical gap size $\tilde{L}$ increases the dimensionless D. For the rest of this Chapter, the (dimensionless) gap size is

set as $L = 1$, without loss of generality.

Although experimental methods can provide values of $\tilde{D}$ for "simple" polymers, which range from 10^{-15} to 10^{-10} m^2/s [Appel & Fleischer (1993); Lodge (1999); Tao *et al.* (2000); Wheeler & Lodge (1989)], data for telechelic polymers are not available. Taking $\tilde{D} \sim 10^{-14}\,m^2/s$, $\tilde{L} \sim 1\,mm$, $\tilde{\tau}_{as} \sim 10^6\,s$ [van Ruymbeke *et al.* (2010)], and $\tau_{as} = 10^3$ (as used in Section 6.3), gives a reference $D_0 = 10^{-5}$. In the following, we vary D around D_0.

We use the fourth order Runge-Kutta (RK4) method to increment Equations (5.1), (5.16), and (5.17), and the Crank-Nicolson (CN) finite difference method to increment the diffusive terms, Equations (6.7) to (6.9), over a uniform spatial grid of $N_{grid} \geq 1\,000$ points with a zero-gradient boundary condition.

The boundary condition is a zero gradient imposed on the top and bottom plates, i.e. no quantity can exit the system:

$$\left.\frac{\partial X}{\partial y}\right|_{y=0} = 0 \quad \text{and} \quad \left.\frac{\partial X}{\partial y}\right|_{y=L} = 0, \tag{6.10}$$

where X is each of $\underline{\underline{\boldsymbol{Q}}}_A$, $\underline{\underline{\boldsymbol{Q}}}_D$, and f.

We use a (common) time step for the RK4 and CN methods that is smaller than the characteristic times of the system ($\tau_{as}, \tau_{free}, \dot{\gamma}^{-1}$) and smaller than the characteristic diffusion time across a box $\Delta t_{diff} = (\Delta y)^2/D$, where $\Delta y = L/N_{grid}$ is the box size. Therefore, a finer grid (increase of N_{grid}) not only implies more computation points but could also imply a smaller simulation time step (as Δy decreases), which would highly increase the simulation time. Nevertheless, we must ensure that the transition between the high and low share rate bands (if any) is "numerically smooth", see inserts of Figure 6.8. The width of that interface, ℓ_{int}, is determined by the diffusion coefficient and a relaxation time as $\ell_{int} \approx (D\tau)^{1/2}$ [Fardin *et al.* (2015)], and we must ensure that $\Delta y \ll \ell_{int}$, so we take $\tau \equiv \tau_s$ (the smallest relaxation time). Hence, a high number of grid points are

needed for small-D simulations. In Section 6.3, we explore the effects of three values for the (dimensionless) diffusion coefficient: $D = \{10^{-7},\ 10^{-5},\ 10^{-3}\}$, with respectively $N_{\text{grid}} = \{10\,000,\ 4\,000,\ 1\,000\}$, ensuring that $\Delta y \ll \ell_{\text{int}}$.

6.2.4 Momentum equation in parallel plate geometry

The typical Reynolds number, R_{e}, is given by the balance between the inertia and viscosity as $R_{\text{e}} = \rho u L/\mu$, where $\rho \approx 1$ g/cm^3 is the density of the polymer, $u \approx 1$ mm/s is the typical velocity, $L \approx 1$ mm is the typical gap size, and μ the polymer viscosity that we take of order 10^5 Pa·s [Fetters *et al.* (1993)]. Hence, $R_{\text{e}} \approx 10^{-8} \ll 1$, so we can neglect the inertia contribution.

The momentum equation reads

$$\rho \mathrm{D}_t \boldsymbol{u} = \boldsymbol{\nabla} \cdot \underline{\underline{\boldsymbol{T}}}, \tag{6.11}$$

where $\mathrm{D}_t \equiv \partial_t + \boldsymbol{u} \cdot \boldsymbol{\nabla}$, and $\underline{\underline{\boldsymbol{T}}} = \underline{\underline{\boldsymbol{\sigma}}} + \eta(\underline{\underline{\boldsymbol{\kappa}}} + \underline{\underline{\boldsymbol{\kappa}}}^T) - p\underline{\underline{\boldsymbol{I}}}$ is the total stress (polymeric stress $\underline{\underline{\boldsymbol{\sigma}}}$, plus Newtonian solvent with viscosity η, plus isotropic pressure ensuring incompressibility), where $\underline{\underline{\boldsymbol{\kappa}}} = (\boldsymbol{\nabla}\boldsymbol{u})^T$ is the velocity gradient tensor. A direct consequence of a small Reynolds number is

$$\boldsymbol{\nabla} \cdot \underline{\underline{\boldsymbol{T}}} = \boldsymbol{0}. \tag{6.12}$$

Thus, $\partial T_{xy}/\partial y = 0$, so T_{xy} is constant across the gap. It follows that $T_{xy}(y,t) = \big\langle T_{xy}(y,t)\big\rangle$, where $\langle\ \cdot\ \rangle = \frac{1}{L}\int_0^L \cdot\, \mathrm{d}y$ is an average across the gap, with

$$T_{xy}(x,t) = \sigma_{xy}(y,t) + \eta\dot{\gamma}(y,t) \tag{6.13}$$

$$\big\langle T_{xy}(y,t)\big\rangle = \big\langle \sigma_{xy}(y,t)\big\rangle + \eta\big\langle\dot{\gamma}(y,t)\big\rangle. \tag{6.14}$$

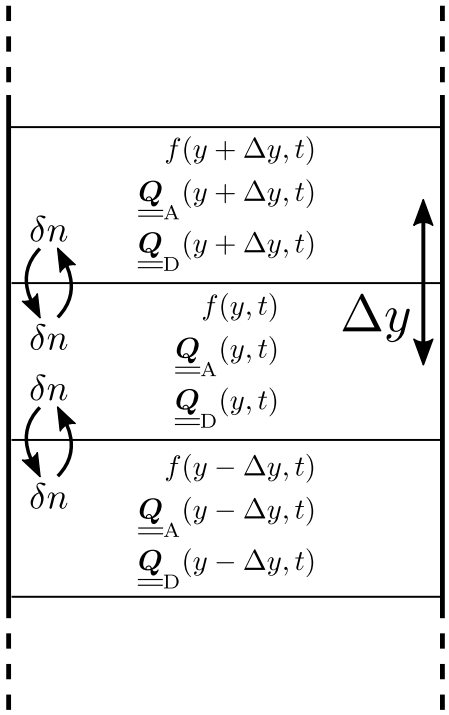

Figure 6.3: Diffusion across the simulation boxes.

Combining the two above equations gives

$$\dot{\gamma}(y,t) = \langle \dot{\gamma}(y,t) \rangle + \frac{1}{\eta}\Big(\langle \sigma_{xy}(y,t) \rangle - \sigma_{xy}(y,t) \Big), \tag{6.15}$$

where $\langle \dot{\gamma}(y,t) \rangle \equiv \dot{\gamma}_{\mathrm{av}}$ is the constant (externally) applied shear rate, or average shear rate across the gap, during step rate experiments or simulations.

At each time step, we compute the local value of the polymeric stress $\sigma_{xy}(y,t)$ using the set of equations Table 5.1 and Equations (6.7) to (6.9). Then, the average stress across the gap, $\langle \sigma_{xy}(y,t) \rangle$, is computed which, in turn, allows us to evaluate the local shear rate via Equation (6.15). This local shear rate is then used in the next step to update the polymeric stress. We increment the dynamical equations for the system by repeating this cycle for each timestep.

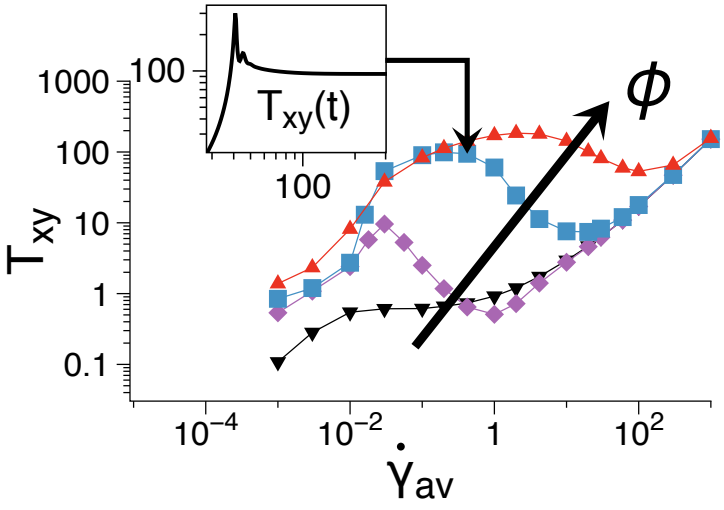

Figure 6.4: Homogeneous flow curves of the preaveraged model with $\phi_{as} = \{0.01, 0.5, 0.99, 0.9999\}$. In insert is $T_{xy}(t)$ for $\dot{\gamma}_{av} = 0.42$ and $\phi_{as} = 0.99$.

6.3 Predictions of the "diffusive" preaveraged model

6.3.1 Homogeneous flow curves

In the preaveraged model, Chapter 5, the polymeric stress tensor (in units of plateau modulus) is written as a linear combination of stress from arms with attached and detached stickers, $\underline{\underline{\boldsymbol{\sigma}}} = f\underline{\underline{\boldsymbol{Q}}}_{A} + (1-f)\underline{\underline{\boldsymbol{Q}}}_{D}$. The dynamical variables are: f, the instantaneous fraction of attached stickers ($f = \phi_{as}$ at equilibrium with no flow), and $\underline{\underline{\boldsymbol{Q}}}_{A}$ and $\underline{\underline{\boldsymbol{Q}}}_{D}$, the averaged stress (including maximum stretch) from Attached and Detached chains, respectively. The full dynamical equations are presented Table 5.1. Typical entangled telechelic star polymers have $\tau_s \ll \tau_d \ll \tau_{as}$, and, at equilibrium, most of the stickers are attached: $\phi_{as} \approx 1$ [van Ruymbeke *et al.* (2010)]. For the rest of this Chapter, we choose $\tau_s = 1$, $\tau_d = 10^2$, $\tau_{as} = 10^3$, $\lambda_{max} = 10$, and $\eta = 0.1$.

In Figure 6.4, we present the (steady state, homogeneous) constitutive curves

for the preaveraged model where we vary the equilibrium fractions, ϕ_{as}, of attached stickers, i.e. we change the "stickiness" of the system from $\phi_{as} = 0.01$ (not sticky) to $\phi_{as} = 0.9999$ (sticky). It is clear that, as ϕ_{as} increases, a non-monotonicity in the constitutive curve appears, and so shear banding phenomena may be anticipated. Additionally, as indicated in the insert in Figure 6.4, the transient stress during start-up of steady homogeneous flow exhibits a sharp stress maximum, which is a result of attached chains being stretched close to their maximum λ_{max} before the stickers are forced to detach. This detachment event, and subsequent relaxation of the detached chains, produces a rapid reduction of stress. We may anticipate that this produces interesting dynamical phenomena during the establishment of shear bands.

6.3.2 Banded flow curves

In the following, we explore the complex flow dynamics arising from the preaveraged model for $\phi_{as} = 0.99$ (sticky system) by means of 1-dimensional parallel plate simulations, as described Section 6.2.1. Therefore, the set of parameters $(\tau_s, \tau_{free}, \tau_d, \tau_{as}) = (1, 10, 10^2, 10^3)$ places the system in the region A of Figure 4.3, and in the region C_2 of Figure 4.6.

At $t = 0$, the stress tensors $\underline{\underline{\boldsymbol{Q}}}_A$ and $\underline{\underline{\boldsymbol{Q}}}_D$ are set equal to the isotropic tensor, and the fraction of attached chains, f, is set as the fraction of attached chains at equilibrium, ϕ_{as}, plus a small perturbation,

$$f(y, t = 0) = \phi_{as} + A\cos(\pi y), \tag{6.16}$$

where $A \ll \phi_{as}$ is the overall amplitude of the perturbation, which ensures f to be slightly lower than ϕ_{as} at high y and vice versa. A small value of A leads to delayed effects, i.e. longer simulation time needed to access a banded state, while large

values of A are unphysical. If banding occurs, Equation (6.16) guarantees a high shear rate band at high y values, because f drops when the flow rate increases. Other initial conditions may result in bands (either oscillatory or steady) forming away from the wall, which typically migrate towards one wall or the other, see Section 6.4.

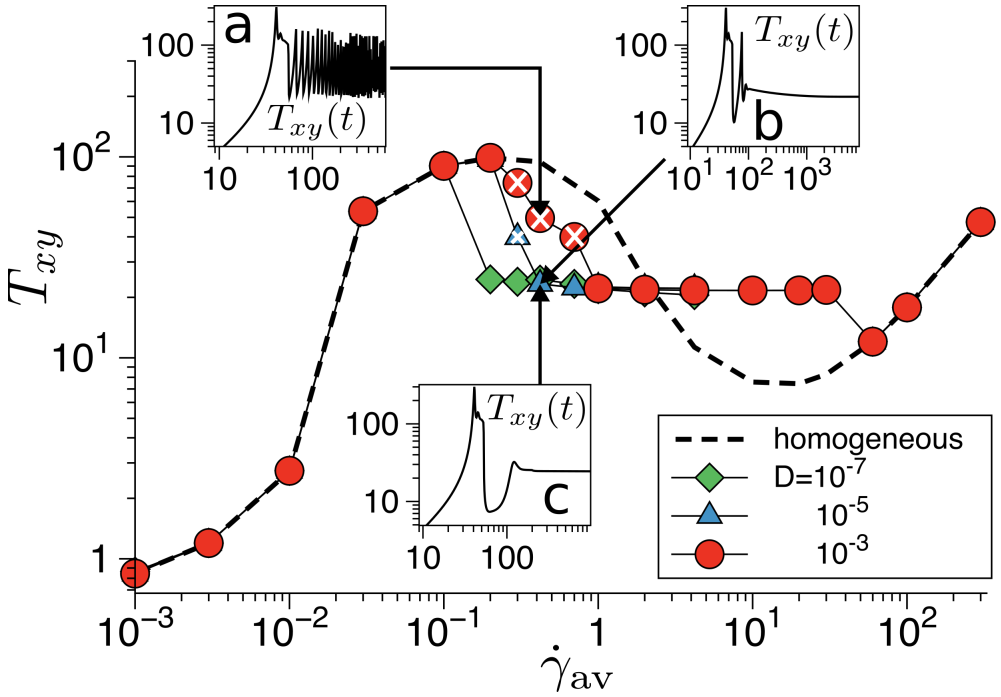

Figure 6.5: Steady state stress versus shear rate for homogeneous non-banded flow (dashed line), and for shear banding simulations (symbols), time averaged in the case of oscillatory response (white crossed symbols). Inserts (a, b, c) show the transient stress versus time, $T_{xy}(t)$, at $\dot{\gamma}_{\rm av} = 0.42$, for $D = 10^{-3}$, $D = 10^{-5}$, and $D = 10^{-7}$ respectively. Parameters are $\phi_{\rm as} = 0.99$, $A = 10^{-3}$.

In Figure 6.5 we plot the steady state stress as a function of applied $\dot{\gamma}_{\rm av}$, for various diffusion coefficients. We also show transient plots of stress versus time for different diffusion coefficient at the same $\dot{\gamma}_{\rm av} = 0.42$. We found that for large values of the diffusion coefficient and in a narrow range of applied shear rate, e.g. $D = 10^{-3}$ (equivalently, for small gap size) and $0.2 < \dot{\gamma}_{\rm av} < 1$, the total stress does not reach steady state but keeps oscillating between, roughly, the stress values

for homogeneous flow (dashed line) and for the shear banded state (white crossed symbols). Each "oscillation" appears to be, in detail, a sharp stress overshoot similar to the early event where initially attached chains reach their maximal stretch and detach. However, at smaller values of D, e.g. $D = 10^{-5}$ (equivalently, as the gap size increases), the stress oscillates for a short time, but a steady state is eventually reached. After a further decrease of D, e.g. $D = 10^{-7}$, no oscillation is seen.

6.3.3 Stick-slip and diffusion

In order to investigate the transient behavior and especially the interesting oscillatory response further, we present, in Figure 6.6, color maps (corresponding to the three inserts in Figure 6.5) of $\dot{\gamma}(y,t)$ and $f(y,t)$, and the trajectory of the simulation projected onto the plane $(T_{xy}, \Delta f)$, where Δf is the difference between the maximum and minimum value of f observed across the gap.

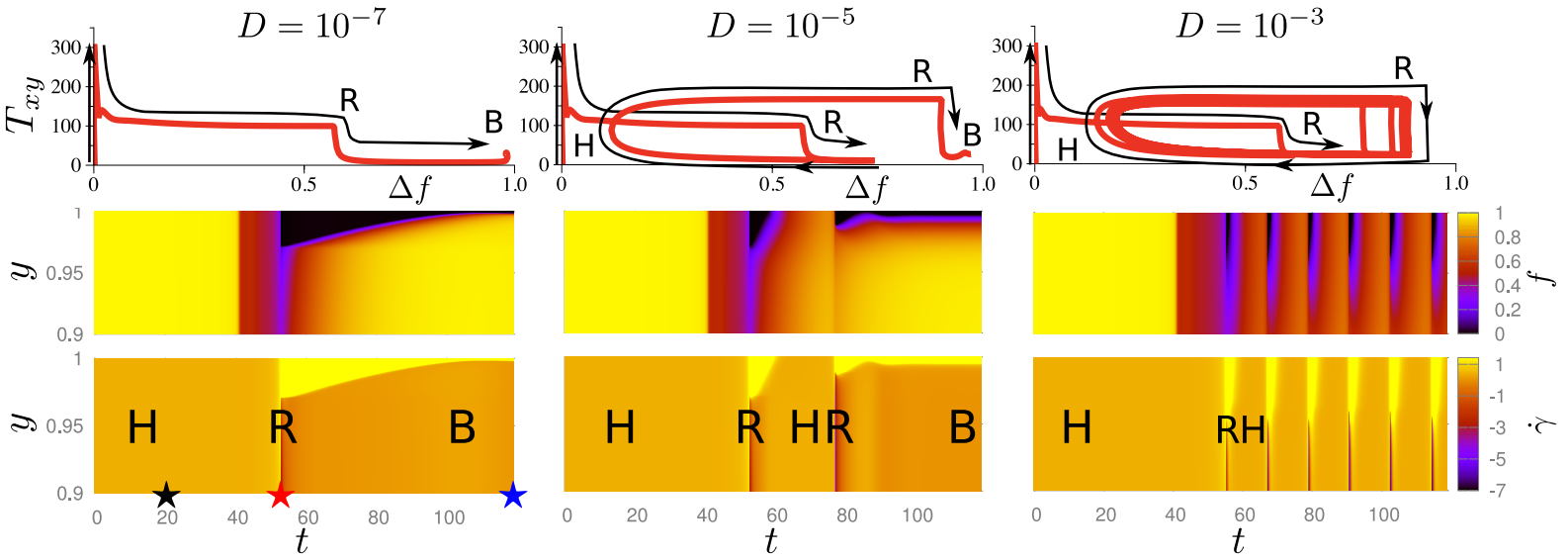

Figure 6.6: Bottom to top: Time evolution of the spatially resolved local shear rate and fraction of attached chains, and of the stress versus Δf, for various diffusion coefficient and $\dot{\gamma}_{\mathrm{av}} = 0.42$. "H", "B", and "R" stand for homogeneous flow, (steady state) banded flow, and recoil, respectively. The highest values of $\dot{\gamma}$ have been truncated for clarity, and only $y > 0.9$ is shown. Parameters are $\phi_{\mathrm{as}} = 0.99$, $A = 10^{-3}$.

Focusing first on $D = 10^{-7}$ in Figure 6.6 left, we observe that the fraction of attached arms drops across the whole width of the simulation at the time ($t \approx 40$) of the initial sharp stress maximum, and at this point no significant banding is observed. The flow remains homogeneous (H) for a time, but the $(T_{xy}, \Delta f)$ plane reveals the growth of an instability in which Δf increases. Eventually, at $t \approx 54$, a thin band of material near the upper wall reaches a state with almost all chains detached, which gives rise to a sharp recoil (R), i.e. where coexistence of negative and positive shear rates is seen, cf. Figure 6.8. This permits a release of the elastic energy stored in the remaining bulk of the material, driving the sharp recoil and a rapid drop in stress. Subsequently, the flow stabilizes to a banded state (B), with a narrow band at high shear rate close to the upper wall, effectively an apparent wall slip. Figure 6.8 displays the velocity profile during the homogeneous (H), recoil (R) and banded (B) states, at times indicated by stars in Figure 6.6 left. We see in the $(T_{xy}, \Delta f)$ plot that the system is driven away from the instability and reaches a permanent banded state, where $\Delta f \approx 1$; two shear bands are formed, one with a high number of attached stickers, and the other with most of the stickers detached.

In contrast, for larger $D = 10^{-5}$, shown in Figure 6.6 middle, after the initial recoil the simulation returns towards a homogeneous state (H) before recoiling (R) once more and eventually stabilizing into a banded state (B) where, as before, $\Delta f \approx 1$. The $(T_{xy}, \Delta f)$ plot shows the extra oscillatory cycle made before the system eventually reaches a steady state.

For large values of the diffusion coefficient, e.g. $D = 10^{-3}$, oscillation between homogeneous (H) and recoil (R) states repeats indefinitely, i.e. no steady banded state is reached. The $(T_{xy}, \Delta f)$ plot, of Figure 6.6 right, reveals the limit cycle that underpins the oscillations.

The critical process driving the oscillation is the return towards a homoge-

neous flow profile following the banding and elastic recoil. The dependence of this process on the diffusion constant indicates the following mechanism is at work: After the recoil, a narrow high shear rate band is formed, in which most chains are in the detached state. However, if diffusion is sufficiently rapid (depending upon the width of the band as well as the magnitude of the diffusion constant) diffusive exchange of chains between the narrow band and bulk of the material (which contains many attached chains) leads to an increase in the number of attached chains in the "fast" band (seen as a reduction of Δf in the $(T_{xy}, \Delta f)$ trajectory). This slows down shear in the fast band, re-establishing a nearly homogeneous flow. This then sets up a state in which the initial banding and recoil instability can reoccur, so that the cycle potentially repeats indefinitely. The oscillation is therefore a result of interaction between the diffusion and the dynamics of the internal variables of the constitutive model.

Confirmation of this oscillatory mechanism is found by examining the effect of increasing shear rate. The oscillation is first seen for $\dot{\gamma}_{\text{av}}$ on the onset of the unstable region (negative slope of the constitutive curve, Figure 6.4 right). The frequency of the oscillations increases almost linearly with increasing shear rate (circles Figure 6.7), because the time needed for a chain to reach its maximum strain (followed by detachment and recoil) decreases as shear rate increases. Indeed, by analysing the stress, T_{xy}, as a function of strain $\gamma = \dot{\gamma}_{\text{av}} t$, we see that the frequency of these oscillations is quasi-constant with increasing shear rate (squares Figure 6.7). However, according to Equation (6.1), the width of the high shear-rate band $\alpha_{\text{high}} L$, also increases with increasing shear rate until, eventually, the band becomes sufficiently wide that diffusion can no longer re-establish a homogeneous flow profile. Beyond this point, oscillations are no longer seen.

Hence, we might suggest that there is a competition between two phenomena: (i) the homogenization of f across the gap via diffusion on a timescale $\tau_{\text{dif}} =$

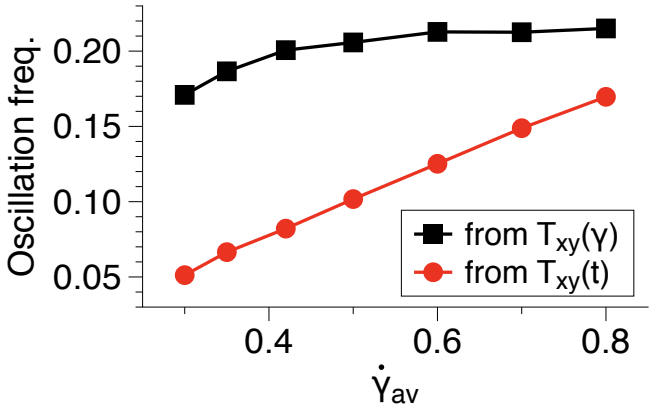

Figure 6.7: Frequency of the oscillations as a function of the applied shear rate, corresponding to $D = 10^{-3}$ in Figure 6.6. Red circles: for the stress vs time curve. Black squares: for the stress vs strain curve.

$(\alpha_{\rm high}L)^2/D$, with $\alpha_{\rm high} = (\dot{\gamma}_{\rm av} - \dot{\gamma}_{\rm low})/(\dot{\gamma}_{\rm high} - \dot{\gamma}_{\rm low})$ the fraction of gap occupied by the high shear rate band, cf. Equation (6.1); and (ii) the breaking of the associated chains in the high shear rate band that occurs at a fixed strain $\gamma_{\rm c}$, on a timescale $\tau_{\rm b} = \gamma_{\rm c}/\dot{\gamma}_{\rm high}$. Thus, oscillations on the unstable branch of the flow are expected if $\tau_{\rm dif} < \tau_{\rm b}$, i.e. if

$$\dot{\gamma}_{\rm av} < \dot{\gamma}_{\rm low} + (\dot{\gamma}_{\rm high} - \dot{\gamma}_{\rm low})(D\gamma_{\rm c}/L^2\dot{\gamma}_{\rm high})^{1/2}. \tag{6.17}$$

According to Figure 6.5, $\dot{\gamma}_{\rm high} \approx 130$, $\dot{\gamma}_{\rm low} \approx 0.02$. Therefore, Equation (6.17) gives $\dot{\gamma}_{\rm av} < 1.5$ for $D = 10^{-3}$, and $\dot{\gamma}_{\rm av} < 0.03$ for $D = 10^{-7}$ (which is before the unstable region), in qualitative agreement with Figure 6.5. Note that the critical strain, $\gamma_{\rm c}$, depends on the value of the maximum stretch ratio, $\lambda_{\rm max}$, as $\gamma_{\rm c} \approx \sqrt{3}\lambda_{\rm max}$.

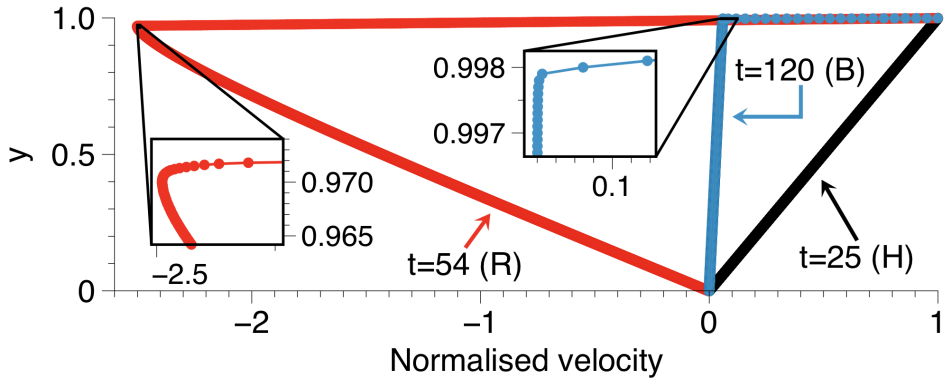

Figure 6.8: Velocity profile (normalized by $\dot{\gamma}_{\text{av}}$) for $D = 10^{-7}$ at times indicated by stars in Figure 6.6.

6.4 Influence of the initial perturbation

In the previous Section 6.3, the initial perturbation on the fraction of attached chains, f, was set using Equation (6.16), ensuring that f was slightly higher than ϕ_{as} near the upper wall ($y = 1$) and slightly lower than ϕ_{as} near the lower wall ($y = 0$) which guaranteed that, when banding occurs, the high shear rate band is located near the upper wall.

A symmetric initial perturbation such as

$$f(y) = \phi_{\text{as}} + A\cos(2\pi y) \tag{6.18}$$

ensures that, initially, the minimum of f is located at the centre of the gap. Using Equation (6.18) as initial condition, we observe that

(i) When steady banding occurs, the high shear rate band remains in the centre of the gap;

(ii) When oscillations occur (in a range of shear rates), the high shear rate band appears in the centre of the gap;

(iii) The range of shear rates at which ("permanent") oscillations are produced is slightly larger, e.g. for $D = 10^{-3}$, we see permanent oscillations for $\dot{\gamma}_{\text{av}} = 1$, see Figure 6.9 left, whereas at that shear rate the system stabilises into a steady banded state when f is initialised using Equation (6.16).

These results support the idea that diffusion destabilises the bands, especially observation (iii), since when the high shear rate band is in the centre of the simulation "box", diffusion from above and below the band rehomogenises the flow. Hence the effect of diffusion is stronger when the band is in the centre of the domain as compared to the edge, and we therefore expect oscillations when $\tau_{\text{dif}}/2 < \tau_{\text{b}}$.

Focusing on $\dot{\gamma}_{\text{av}} = 1$, we can alternatively set the initial perturbation such that f has its lowest value at $y = 1/3$,

$$f(y) = \begin{cases} \phi_{\text{as}} + A\cos(3\pi y), & 0 \leq y \leq 2/3 \\ \phi_{\text{as}} + A, & 2/3 < y \leq 1 \end{cases} \tag{6.19}$$

the high shear rate band is initially formed at around $y = 1/3$, then it is slowly pushed to the bottom, cf. Figure 6.9 right. When the high shear rate band reaches the bottom wall, oscillations cease for that particular shear rate ($\dot{\gamma}_{\text{av}} = 1$), which is consistent with our initial results, Section 6.3.

6.5 Conclusions

We have investigated shear instabilities using the novel constitutive law designed for describing the rheology of entangled telechelic star polymers of Chapter 5. The model displays shear banding, often accompanied by a strong elastic recoil in the transient response. This may appear as an "apparent" wall slip, i.e. a very

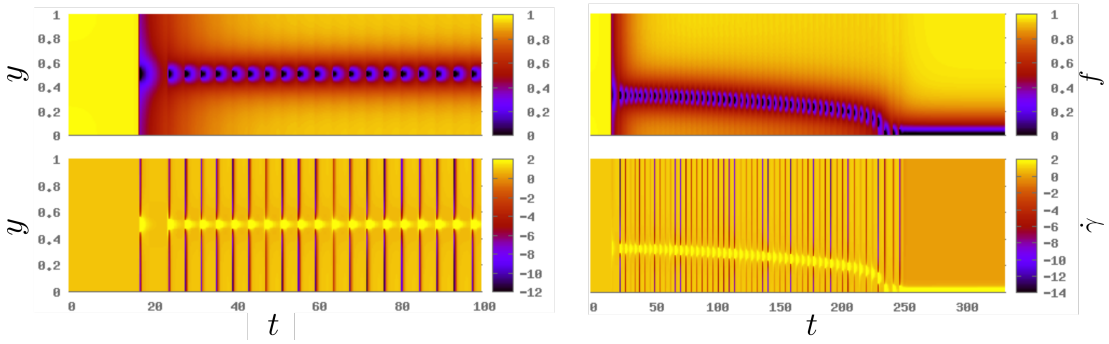

Figure 6.9: Time evolution spatially resolved of f and $\dot{\gamma}$ for an initial perturbation set as Equation (6.18) (left), and Equation (6.19) (right).

narrow band of high shear rate close to the wall. In the same sense, the model also displays an oscillatory "apparent" stick-slip behavior, driven by a cycle of elastic recoil followed by diffusive re-homogenization of the flow.

Since our modelling is entirely at the continuum level, with an imposed no-slip boundary condition, it is wholly impossible for these observed phenomena to be anything but "apparent" wall slip or stick-slip. Within this continuum approach, reducing the diffusion constant, or (correspondingly) increasing the gap size, removes the oscillations. Nevertheless, we may speculate that an identical mechanism drives stick-slip oscillations in the case of "true" wall slip, which occurs as a result of the microscopic local environment close to a wall. It seems very plausible that molecular diffusion from the material bulk into the local wall region might temporarily arrest wall slip (i.e. re-homogenize the flow) before wall slip occurs once more, driving a similar cyclic phenomenon to the one we observe. In the case of true wall slip, the local environment sets a new physical lengthscale, so that increasing the (macroscopic) gap size no longer removes the oscillations. Finally, this Chapter has demonstrated the use of the constitutive equation derived in Chapters 4 and 5 in a complex flow simulation.

Part III

General Conclusions

This page is intentionally left blank

Since brief but detailed summaries have been included at the end of each Chapter, we provide here an overview of the key achievements and outcomes of this thesis.

In Chapter 2, we presented a model aiming at predicting the linear rheology of unentangled linear polymer chains with stickers along the backbone. We proposed a new model (stochastic sticky-Rouse model) based on a similar assumption to the sticky-Rouse model [Baxandall (1989); Chen *et al.* (2013); Leibler *et al.* (1991)] that the sticker timescale and the characteristic relaxation time of Rouse segments are well separated. Firstly, we explained how we generated a population of chains such that (i) the number of stickers per chain follows a certain probability distribution characterised by an average number, N_s, of stickers, (ii) the stickers are placed randomly along the chain. We constructed a dynamical model for these chains such that the sticker, when finding a new partner, undergoes a finite sized hop in space. Subsequently, we proposed a way to compute the stress relaxation function, and thus the elastic and loss moduli, of a system composed by a polydisperse mixture of such chains, and finally we compared our model with frequency-sweep experimental data, provided by G. Cui, on PEHA-UPy polymer melts with various sticker concentration, i.e. samples with different N_s. It is clear that our stochastic model improves the intermediate frequency predictions as compared to the "standard" sticky-Rouse model while matching it at low frequencies. However, a discrepancy still exists. One way to improve the intermediate frequency predictions of the model would to define a distribution of sticker timescales, which would broaden the loss moduli low-frequency shoulder.

In Chapter 3, we proposed a simplified tube model, based on the Rolie-Poly model [Likhtman & Graham (2003)], for a polydisperse melt of entangled polymers that aims at predicting nonlinear rheology, whilst being consistent with the

"double reptation" theory [des Cloizeaux (1988)] in linear rheology. For the case of bidisperse blends (blends of long and short chains), we compared the predictions of the model with experimental data from Ref. [Read *et al.* (2012)]. The model presented has only one fitting parameter that is adjusted using linear rheology data. Then, there are no extra fitting parameter to produce the prediction of nonlinear rheology (shear and extension). The model quantitatively matches the experimental data in elongation at all elongation rates. This means that we are capturing the enhanced stretch relaxation time predicted by Auhl et al. [Auhl *et al.* (2008)] correctly. However, in shear, the model fails at predicting the moderate to high shear rates, which the more detailed model of Read *et al.* achieved. The failure at high rates indicates that a simple 2-mode model is not enough, and probably the long-chain coupling in the "full chain" model [Read *et al.* (2012)] is needed.

We generalised the model to polydisperse melts and compared our model predictions to experimental data of Münstedt [Münstedt (1980)]. Given that the nonlinear rheology is strongly influenced by the high-molar-weight components (i.e. it depends on the molecular weight distribution of the melt rather than just its weight-average molar mass, M_w), we investigated the nonlinear rheological properties of two PS melts having different molar mass distribution. The model slightly over predicted the experimental LVE. This indicates that more work needs to be done on the linear rheology. Nevertheless, the elongation hardening that was seen experimentally in Ref. [Münstedt (1980)] for the sample with high molar weight component could be qualitatively reproduced using our polydisperse model. It is a step forward to the possibility of predicting the mechanical properties of polymer melts accurately and robustly, which would be a major advance for industries manufacturing textiles, automobiles, aircraft, paints and coatings, cosmetics and consumer products, oil-field fluids, and others.

Part I of the thesis considered the rheological effects of "sticky groups" and "entanglements" in isolation. In Part II, our goal was to combine the effects of these and to produce a "toy" (i.e. "single mode") constitutive model that captures elements of the nonlinear rheology of entangled telechelic polymers (forming a transient network), and to explore the interaction between timescales set by the stickers, timescales set by the entangled polymer, and the flow rate.

In Chapter 4, we proposed a simplified stochastic tube model for telechelic star polymers able to account for both the associating dynamics of telechelic groups and the entanglement constraints. However simple, our resulting model exhibits interesting constitutive behavior. We found that the nature of the response to flow depends very much on the interaction between timescales set by the entanglements, and timescales set by the stickers. In principle, these timescales vary with temperature (and other factors) in different ways. In order to illustrate these effects, we presented "maps" of the parameter space, showing how the response may be expected to change as parameters are varied. In the nonlinear regime, we saw dramatic changes in the stress growth coefficient transients as we navigated around the parameter map, i.e. our constitutive model exhibits a rich variety of responses. We observed that particular parameter sets produce shear hardening, extension hardening, sharp stress drops, smoother stress drops, monotonic and non-monotonic flow curves. The parameter map that was produced can be of use when thinking about polymer processing. We anticipate that, in practice, it is possible to navigate around the regions of the map by tuning the external environment of the sticker (temperature, pH, counter-ion) and so modifying its association time and its stickiness.

Whilst the stochastic model gives interesting results, for flow computations it is preferable to have a simplified model which exhibits broadly the same behavior.

In Chapter 5, we therefore got rid of the stochastic nature of our model by preaveraging our set of equations. The outcome is a scalar differential equation for the time-dependent fraction of attached chains, $f(t)$, and two tensorial equations for the conformational average of the associated and dissociated chains, $\underline{\underline{\boldsymbol{Q}}}_{\mathrm{A}}(t)$ and $\underline{\underline{\boldsymbol{Q}}}_{\mathrm{D}}(t)$, similar to Refs. [Tripathi *et al.* (2006); Vaccaro & Marrucci (2000)]. The resulting model, quantitatively very close to that of the stochastic model, was computationally far less expensive and allows for flow simulations.

As an example of flow simulations, in Chapter 6, we investigated shear banding using the preaveraged constitutive model for entangled telechelic polymers, developed in Chapter 5. For particular parameter choices, we found that the continuum model displays shear banding, often accompanied by a strong elastic recoil in the transient response, which appeared as an "apparent" wall slip. For certain parameters, the model also displayed a novel "apparent" stick-slip behavior, giving rise to strong nonlinear oscillations in the stress response driven by a repeating cycle of elastic recoil followed by diffusive re-homogenization of the flow. We discussed the relation between the apparent stick-slip in our continuum model with similar behavior in "true" wall slip. We elucidated a novel mechanism leading to a "periodic apparent wall-slip" (stick slip) phenomena, driven by diffusion. It would be interesting to investigate this phenomenon further, for example by flow computations in more complex flow situations such as pipe flow, extrusion or exit from a die, where "wall slip" is thought to produce instabilities and surface defects in polymer products. Our developed constitutive model may provide a useful continuum model for examining these types of polymer processing problems.

Bibliography

Adams, J.M., Fielding, S.M. & Olmsted, P.D. (2011). "Transient shear banding in entangled polymers: A study using the Rolie-Poly model," *J. Rheol.* **55**, 1007–1032. 153

Agimelen, O.S. & Olmsted, P.D. (2013). "Apparent Fracture in Polymeric Fluids Under Step Shear," *Phys. Rev. Lett.* **110**, 204503. 164

Amin, D., Likhtman, A.E. & Wang, Z. (2016). "Dynamics in Supramolecular Polymer Networks Formed by Associating Telechelic Chains," *Macromolecules* **49**, 7510–7524. 34

Appel, M. & Fleischer, G. (1993). "Investigation of the chain length dependence of self-diffusion of poly(dimethylsiloxane) and poly(ethylene oxide) in the melt with pulsed field gradient NMR," *Macromolecules* **26**, 5520–5525. 169

Auhl, D., Ramirez, J., Likhtman, A.E., Chambon, P. & Fernyhough, C. (2008). "Linear and nonlinear shear flow behavior of monodisperse polyisoprene melts with a large range of molecular weights," *J. Rheol.* **52**, 801. 79, 93, 186

Auhl, D., Chambon, P., McLeish, T.C.B. & Read, D.J. (2009). "Elongational Flow of Blends of Long and Short Polymers: Effective Stretch Relaxation Time," *Phys. Rev. Lett.* **103**, 136001. 76

Ball, R.C. & McLeish, T.C.B. (1989). "Dynamic dilution and the viscosity of star-polymer melts," *Macromolecules* **22**, 1911–1913. 99, 104, 121

Bandyopadhyay, R., Basappa, G. & Sood, A.K. (2000). "Observation of Chaotic Dynamics in Dilute Sheared Aqueous Solutions of CTAT," *Phys. Rev. Lett.* **84**, 2022–2025. 162

Barlow, A.J., Harrison, G. & Lamb, J. (1964). "Viscoelastic Relaxation of Polydimethylsiloxane Liquids," *Proc. R. Soc. A Math. Phys. Eng. Sci.* **282**, 228–251.

25

Baumgaertel, M. & Winter, H. (1992). "Interrelation between continuous and discrete relaxation time spectra," *J. Nonnewton. Fluid Mech.* **44**, 15–36. 12

Baxandall, L.G. (1989). "Dynamics of reversibly crosslinked chains," *Macromolecules* **22**, 1982–1988. 38, 39, 65, 97, 185

Benbow, J.J. & Lamb, P. (1963). "New aspects of melt fracture," *Polym. Eng. Sci.* **3**, 7–17. 161

Bergman, S.D. & Wudl, F. (2008). "Mendable polymers," *J. Mater. Chem.* **18**, 41–62. 5

Berret, J.F. & Séréro, Y. (2001). "Evidence of Shear-Induced Fluid Fracture in Telechelic Polymer Networks," *Phys. Rev. Lett.* **87**, 048303. 162, 163

Bick, D.K. & McLeish, T.C.B. (1996). "Topological Contributions to Nonlinear Elasticity in Branched Polymers," *Phys. Rev. Lett.* **76**, 2587–2590. 98

Binder, W.H. (2013). *Self-Healing Polymers. From Principles to Applications*. Wiley-VCH, Weinheim. 5

Bird, R.B., Armstrong, R.C. & Hassager, O. (1987). "Fluid mechanics," In *Dyn. Polym. Liq.*, vol. 1, Wiley Inteterscience, New York. 161

Bisbee, W., Qin, J. & Milner, S.T. (2011). "Finding the Tube with Isoconfigurational Averaging," *Macromolecules* **44**, 8972–8980. 27

Brassinne, J., Fustin, C.A. & Gohy, J.F. (2013). "Polymer Gels Constructed Through Metal-Ligand Coordination," *J. Inorg. Organomet. Polym. Mater.* **23**, 24–40. 110

Brienne, M.J., Gabard, J., Lehn, J.M. & Stibor, I. (1989). "Macroscopic expression of molecular recognition. Supramolecular liquid crystalline phases induced by association of complementary heterocyclic components," *J. Chem. Soc. Chem. Commun.* **2**, 1868–1970. 32

Brochard, F. & de Gennes, P.G. (1992). "Shear-dependent slippage at a polymer/solid interface," *Langmuir* **8**, 3033–3037. 161

Brochard-Wyart, F., Gay, C. & de Gennes, P.G. (1996). "Slippage of Polymer Melts on Grafted Surfaces," *Macromolecules* **29**, 377–382. 161

Brunsveld, L., Folmer, B.J.B., Meijer, E.W. & Sijbesma, R.P. (2001).

"Supramolecular Polymers," *Chem. Rev.* **101**, 4071–4098. 32, 38

Cao, J., Zhu, J., Wang, Z. & Likhtman, A.E. (2015). "Large deviations of Rouse polymer chain: First passage problem," *The Journal of Chemical Physics* **143**, 204105. 112

Carothers, W.H. & Hill, J.W. (1932). "Studies of polymerization and ring formation. XV. Artificial fibers from synthetic linear condensation superpolymers," *J. Am. Chem. Soc.* **54**, 1579–1587. 5

Castillo-Tejas, J., Carro, S. & Manero, O. (2017). "Shear Banding in Telechelic Associative Polymers by Molecular Dynamics," *ACS Macro Lett.* **6**, 190–193. 163

Cates, M.E. (1987). "Reptation of Living Polymers: Dynamics of Entangled Polymers in the Presence of Reversible Chain-Scission Reactions," *Macromolecules* **20**, 2289–2296. 162

Cates, M.E. (1990). "Nonlinear viscoelasticity of wormlike micelles (and other reversibly breakable polymers)," *J. Phys. Chem.* **94**, 371–375. 98, 162

Cates, M.E. & Fielding, S.M. (2006). "Rheology of giant micelles," *Adv. Phys.* **55**, 799–879. 162

Chen, Q., Tudryn, G.J. & Colby, R.H. (2013). "Ionomer dynamics and the sticky Rouse model," *J. Rheol.* **57**, 1441–1462. 33, 39, 65, 185

Colby, R., Zheng, X., Rafailovich, M., Sokolov, J., Peiffer, D., Schwarz, S., Strzhemechny, Y. & Nguyen, D. (1998). "Dynamics of Lightly Sulfonated Polystyrene Ionomers," *Phys. Rev. Lett.* **81**, 3876–3879. 33

Cordier, P., Tournilhac, F., Soulié-Ziakovic, C. & Leibler, L. (2008). "Self-healing and thermoreversible rubber from supramolecular assembly," *Nature* **451**, 977–80. 5

Cram, D.J. (1988). "The Design of Molecular Hosts, Guests, and Their Complexes (Nobel Lecture)," *Angew. Chemie Int. Ed. English* **27**, 1009–1020. 31

Cromer, M., Fredrickson, G.H. & Leal, L.G. (2014). "A study of shear banding in polymer solutions," *Phys. Fluids* **26**, 063101. 153

de Gennes, P.G. (1971). "Reptation of a Polymer Chain in the Presence of Fixed Obstacles," *J. Chem. Phys.* **55**, 572–579. 22, 27, 29

de Gennes, P.G. (1979). *Scaling Concepts in Polymer Physics*. Cornell University

Press., Ithaca and London. 13

de Gennes, P.G. & Badoz, J. (1994). *Les objets fragiles*. Plon, Paris. 3

de Gennes, P.G. & Badoz, J. (1996). *Fragile objects*. Copernicus, New York. 3

de Greef, T.F.A. & Meijer, E.W. (2008). "Materials science: Supramolecular polymers," *Nature* **453**, 171–173. 5, 38

Dealy, J.M. & Larson, R.G. (2006). *Structure and Rheology of Molten Polymers*. Carl Hanser Verlag GmbH & Co. KG, München, 2nd edn. 27, 55, 70, 71, 162

den Otter, J.L. (1971). "Some investigations of melt fracture," *Rheol. Acta* **10**, 200–207. 161

des Cloizeaux, J. (1988). "Double Reptation vs. Simple Reptation in Polymer Melts," *Europhys. Lett.* **5**, 437–442. 31, 69, 70, 74, 93, 186

Divoux, T., Fardin, M.A., Manneville, S. & Lerouge, S. (2015). "Shear Banding of Complex Fluids," *Annu. Rev. Fluid Mech.* **48**, 150724171740009. 162

Doi, M. (1983). "Explanation for the 3.4-power law for viscosity of polymeric liquids on the basis of the tube model," *J. Polym. Sci. Part B Polym. Phys.* **21**, 667–684. 81

Doi, M. & Edwards, S.F. (1988). *The Theory of Polymer Dynamics*. Oxford University Press Inc., New York. 22, 24, 26, 27, 29, 50, 69, 111

Doi, M. & Takimoto, J.i. (2003). "Molecular modelling of entanglement," *Philos. Trans. R. Soc. A Math. Phys. Eng. Sci.* **361**, 641–652. 30

Everaers, R. (2012). "Topological versus rheological entanglement length in primitive-path analysis protocols, tube models, and slip-link models," *Phys. Rev. E* **86**, 022801. 108

Everaers, R., Sukumaran, S.K., Grest, G.S., Svaneborg, C., Sivasubramanian, A. & Kremer, K. (2004). "Rheology and Microscopic Topology of Entangled Polymeric Liquids," *Science* **303**, 823–826. 27

Fardin, M.A., Ober, T.J., Gay, C., Grégoire, G., McKinley, G.H. & Lerouge, S. (2012). "Potential ways of thinking about the shear-banding phenomenon," *Soft Matter* **8**, 910–922. 163

Fardin, M.A., Radulescu, O., Morozov, A., Cardoso, O., Browaeys, J. & Lerouge, S. (2015). "Stress diffusion in shear banding wormlike micelles," *J. Rheol.*

59, 1335–1362. 169

Feldman, K.E., Kade, M.J., Meijer, E.W., Hawker, C.J. & Kramer, E.J. (2009). "Model Transient Networks from Strongly Hydrogen-Bonded Polymers," *Macromolecules* **42**, 9072–9081. 32, 38

Ferry, J.D. (1980). *Viscoelastic Properties of Polymers*. John Wiley & Sons, Inc., New York. 25

Fetters, L.J., Graessley, W.W., Hadjichristidis, N., Kiss, A.D., Pearson, D.S. & Younghouse, L.B. (1988). "Association behavior of end-functionalized polymers. 2. Melt rheology of polyisoprenes with carboxylate, amine, and zwitterion end groups," *Macromolecules* **21**, 1644–1653. 98

Fetters, L.J., Kiss, A.D., Pearson, D.S., Quack, G.F. & Vitus, F.J. (1993). "Rheological behavior of star-shaped polymers," *Macromolecules* **26**, 647–654. 170

Fetters, L.J., Lohse, D.J., Richter, D., Witten, T.A. & Zirkel, A. (1994). "Connection between Polymer Molecular Weight, Density, Chain Dimensions, and Melt Viscoelastic Properties," *Macromolecules* **27**, 4639–4647. xxi

Fetters, L.J., Lohse, D.J., Milner, S.T. & Graessley, W.W. (1999). "Packing Length Influence in Linear Polymer Melts on the Entanglement, Critical, and Reptation Molecular Weights," *Macromolecules* **32**, 6847–6851. 82

Fielding, S.M. (2007). "Complex dynamics of shear banded flows," *Soft Matter* **3**, 1262–1279. 162

Fielding, S.M. (2016). "Triggers and signatures of shear banding in steady and time-dependent flows," *J. Rheol.* **60**, 821–834. 153, 162, 164

Fielding, S.M. & Olmsted, P.D. (2003). "Flow phase diagrams for concentration-coupled shear banding," *Eur. Phys. J. E* **11**, 65–83. 164

Flory, P.J. (1953). *Principles of Polymer Chemistry*. Cornell University Press., Ithaca. 41

Flory, P.J. (1969). *Statistical mechanics of chain molecules*. Interscience Publishers, New York. 13

Friedrich, C., Honerkamp, J. & Weese, J. (1996). "New ill-posed problems in rheology," *Rheol. Acta* **35**, 186–193. 12

Friese, V.A. & Kurth, D.G. (2009). "From coordination complexes to coordination

polymers through self-assembly," *Curr. Opin. Colloid Interface Sci.* **14**, 81–93. 31, 32

Gay, C. (1997). *Nanorhéologie et autres problèmes de polymères aux interfaces*. Ph.D. thesis, Pierre et Marie Curie - Paris VI. 26

Graessley, W.W. (1980). "Some phenomenological consequences of the Doi-Edwards theory of viscoelasticity," *J. Polym. Sci. Part B Polym. Phys.* **18**, 27–34. xxi, 82

Graham, R.S., Likhtman, A.E., McLeish, T.C.B. & Milner, S.T. (2003). "Microscopic theory of linear, entangled polymer chains under rapid deformation including chain stretch and convective constraint release," *J. Rheol.* **47**, 1171–1200. 30, 105, 164

Green, M.S. & Tobolsky, A.V. (1946). "A New Approach to the Theory of Relaxing Polymeric Media," *J. Chem. Phys.* **14**, 80–92. 33, 38, 103

Grzybowski, B.a., Wilmer, C.E., Kim, J., Browne, K.P. & Bishop, K.J.M. (2009). "Self-assembly: from crystals to cells," *Soft Matter* **5**, 1110. 32

Hadjichristidis, N., Pitsikalis, M., Iatrou, H., Driva, P., Sakellariou, G. & Chatzichristidi, M. (2012). "Polymers with Star-Related Structures," In *Polym. Sci. A Compr. Ref.*, 29–111, Elsevier, Amsterdam. 99

Hawke, L.G.D., Huang, Q., Hassager, O. & Read, D.J. (2015). "Modifying the pom-pom model for extensional viscosity overshoots," *J. Rheol.* **59**, 995–1017. 98, 99

Head, D.A., Ajdari, A. & Cates, M.E. (2002). "Rheological instability in a simple shear-thickening model," *Europhys. Lett.* **57**, 120–126. 163

Heinrich, G. & Kaliske, M. (1997). "Theoretical and numerical formulation of a molecular based constitutive tube-model of rubber elasticity," *Comput. Theor. Polym. Sci.* **7**, 227–241. 108

Hernández Cifre, J.G., Barenbrug, T.M.A.O.M., Schieber, J.D. & van den Brule, B.H.A.A. (2003). "Brownian dynamics simulation of reversible polymer networks under shear using a non-interacting dumbbell model," *J. Nonnewton. Fluid Mech.* **113**, 73–96. 111

Honerkamp, J. (1989). "Ill-posed problems in rheology," *Rheol. Acta* **28**, 363–371. 12

Iannirubertо, G. & Marrucci, G. (2002a). "A multi-mode CCR model for entangled polymers with chain stretch," *J. Nonnewton. Fluid Mech.* **102**, 383–395. 30

Iannirubertо, G. & Marrucci, G. (2002b). "A multi-mode CCR model for entangled polymers with chain stretch," *J. Nonnewton. Fluid Mech.* **102**, 383–395. 105

Johnson, B.R. & Lam, S.K. (2010). "Self-organization, Natural Selection, and Evolution: Cellular Hardware and Genetic Software," *Bioscience* **60**, 879–885. 32

Johnson, M. & Segalman, D. (1977). "A model for viscoelastic fluid behavior which allows non-affine deformation," *J. Nonnewton. Fluid Mech.* **2**, 255–270. 163, 164

Kramers, H. (1940). "Brownian motion in a field of force and the diffusion model of chemical reactions," *Physica* **7**, 284–304. 112

Kremer, K. & Grest, G.S. (1990). "Dynamics of entangled linear polymer melts: A moleculardynamics simulation," *J. Chem. Phys.* **92**, 5057–5086. 27

Kröger, M. (2005). "Shortest multiple disconnected path for the analysis of entanglements in two- and three-dimensional polymeric systems," *Comput. Phys. Commun.* **168**, 209–232. 27

Langevin, P. (1908). "Sur la théorie du mouvement brownien," *Comptes rendus Hebd. des séances l'Académie des Sci. Série B* 530–533. 22

Larson, R.G. (1992). "Instabilities in viscoelastic flows," *Rheol. Acta* **31**, 213–263. 161

Larson, R.G., Sridhar, T., Leal, L.G., McKinley, G.H., Likhtman, A.E. & McLeish, T.C.B. (2003). "Definitions of entanglement spacing and time constants in the tube model," *J. Rheol.* **47**, 809–818. 16

Lehn, J.m. (1988). "Supramolecular chemistry Scope and perspectives: Molecules Supermolecules Molecular devices," *J. Incl. Phenom.* **6**, 351–396. 31

Lehn, J.M. (1995). *Supramolecular Chemistry*. Wiley-VCH, Weinheim. 31

Leibler, L., Rubinstein, M. & Colby, R.H. (1991). "Dynamics of reversible networks," *Macromolecules* **24**, 4701–4707. 33, 34, 38, 39, 65, 97, 185

Leonov, A.I. (1984). "A linear model of the stick-slip phenomena in polymer flow in rheometers," *Rheol. Acta* **23**, 591–600. 161

Lerouge, S. & Berret, J.F. (2010). "Shear-induced transitions and instabilities in surfactant wormlike micelles," *Adv. Polym. Sci.* **230**, 1–71. 162, 164

Lerouge, S., Decruppe, J.P. & Berret, J.F. (2000). "Correlations between rheological and optical properties of a micellar solution under shear banding flow," *Langmuir* **16**, 6464–6474. 164

Ligoure, C. & Mora, S. (2013). "Fractures in complex fluids: The case of transient networks," *Rheol. Acta* **52**, 91–114. 162

Likhtman, A. (2012). "Viscoelasticity and Molecular Rheology," In *Polym. Sci. A Compr. Ref.*, vol. 1, chap. 1.06, 133–179, Elsevier, Amsterdam, 2nd edn. 51, 52

Likhtman, A.E. (2005). "Single-Chain Slip-Link Model of Entangled Polymers: Simultaneous Description of Neutron SpinEcho, Rheology, and Diffusion," *Macromolecules* **38**, 6128–6139. 30

Likhtman, A.E. (2014). "The tube axis and entanglements in polymer melts," *Soft Matter* **10**, 1895. 27

Likhtman, A.E. & Graham, R.S. (2003). "Simple constitutive equation for linear polymer melts derived from molecular theory: Rolie-Poly equation," *J. Nonnewton. Fluid Mech.* **114**, 1–12. xxi, 30, 34, 69, 72, 73, 91, 105, 107, 163, 185

Likhtman, A.E. & Marques, C.M. (2006). "First-passage problem for the Rouse polymer chain: An exact solution," *Europhys. Lett.* **75**, 971–977. 112

Likhtman, A.E. & McLeish, T.C.B. (2002). "Quantitative Theory for Linear Dynamics of Linear Entangled Polymers," *Macromolecules* **35**, 6332–6343. 30, 72, 80, 81, 88

Lodge, T.P. (1999). "Reconciliation of the Molecular Weight Dependence of Diffusion and Viscosity in Entangled Polymers," *Phys. Rev. Lett.* **83**, 3218–3221. 169

Lu, C.Y.D., Olmsted, P.D. & Ball, R.C. (2000). "Effects of Non-local Stress on the Determination of Shear Banding Flow," *Phys. Rev. Lett.* **84**, 642–645. 165

Lupton, J.M. & Regester, H.W. (1965). "Melt flow of polyethylene at high rates," *Polym. Eng. Sci.* **5**, 235–245. 161

Macosko, C.W. (1994). *Rheology: Principles, Measurements, and Applications*. Wiley-VCH, New York. 9

Manneville, S. (2008). "Recent experimental probes of shear banding," *Rheol. Acta*

47, 301–318. 162

Marrucci, G. (1996). "Dynamics of entanglements: A nonlinear model consistent with the Cox-Merz rule," *J. Nonnewton. Fluid Mech.* **62**, 279–289. 30, 98, 105, 106, 163

Masubuchi, Y., Ianniruberto, G., Greco, F. & Marrucci, G. (2008). "Quantitative comparison of primitive chain network simulations with literature data of linear viscoelasticity for polymer melts," *J. Nonnewton. Fluid Mech.* **149**, 87–92. 27

Maxwell, B. & Galt, J.C. (1962). "Velocity profiles for polyethylene melt in tubes," *J. Polym. Sci.* **62**, S50–S53. 161

McLeish, T.C.B. (2002). "Tube theory of entangled polymer dynamics," *Adv. Phys.* **51**, 1379–1527. xiii, 14, 15

McLeish, T.C.B. & Ball, R.C. (1986). "A molecular approach to the spurt effect in polymer melt flow," *J. Polym. Sci. Part B Polym. Phys.* **24**, 1735–1745. 162

McLeish, T.C.B. & Larson, R.G. (1998). "Molecular constitutive equations for a class of branched polymers: The pom-pom polymer," *J. Rheol.* **42**, 81–110. 98, 99, 138

McLeish, T.C.B. & Milner, S.T. (1999). "Entangled Dynamics and Melt Flow of Branched Polymers," In *Adv. Polym. Sci.*, vol. 143, 195–256, Springer Berlin Heidelberg, Berlin, Heidelberg. 99, 104, 121

Mead, D.W., Larson, R.G. & Doi, M. (1998). "A Molecular Theory for Fast Flows of Entangled Polymers," *Macromolecules* **31**, 7895–7914. 30, 105

Michel, E., Appell, J., Molino, F., Kieffer, J. & Porte, G. (2001). "Unstable flow and nonmonotonic flow curves of transient networks," *J. Rheol.* **45**, 1465–1477. 163

Migler, K.B., Hervet, H. & Leger, L. (1993). "Slip transition of a polymer melt under shear stress," *Phys. Rev. Lett.* **70**, 287–290. 161

Milner, S.T. & McLeish, T.C.B. (1997). "Parameter-Free Theory for Stress Relaxation in Star Polymer Melts," *Macromolecules* **30**, 2159–2166. 99, 104, 121

Milner, S.T. & McLeish, T.C.B. (1998). "Reptation and Contour-Length Fluctuations in Melts of Linear Polymers," *Phys. Rev. Lett.* **81**, 725–728. 30

Milner, S.T., McLeish, T.C.B., Young, R., Hakiki, A. & Johnson, J. (1998).

"Dynamic Dilution , Constraint-Release , and Star - Linear Blends," *Macromolecules* **31**, 9345–9353. 90

Moorcroft, R.L. & Fielding, S.M. (2013). "Criteria for Shear Banding in Time-Dependent Flows of Complex Fluids," *Phys. Rev. Lett.* **110**, 086001. 153

Moorcroft, R.L. & Fielding, S.M. (2014). "Shear banding in time-dependent flows of polymers and wormlike micelles," *J. Rheol.* **58**, 103. 162

Morton, M., Helminiak, T.E., Gadkary, S.D. & Bueche, F. (1962). "Preparation and properties of monodisperse branched polystyrene," *J. Polym. Sci.* **57**, 471–482. 99

Münstedt, H. (1980). "Dependence of the Elongational Behavior of Polystyrene Melts on Molecular Weight and Molecular Weight Distribution," *J. Rheol.* **24**, 847–867. xv, xvi, 86, 91, 92, 93, 186

Northolt, M., Sikkema, D., Zegers, H. & Klop, E. (2002). "PIPD, a new high-modulus and high-strength polymer fibre with exceptional fire protection properties," *Fire Mater.* **26**, 169–172. 4

Olmsted, P.D. (2008). "Perspectives on shear banding in complex fluids," *Rheol. Acta* **47**, 283–300. 162, 164

Olmsted, P.D., Radulescu, O. & Lu, C.Y.D. (2000). "JohnsonSegalman model with a diffusion term in cylindrical Couette flow," *J. Rheol.* **44**, 257–275. 164

Paskhin, E.D. (1978). "Motion of polymer liquids under unstable conditions and in channel terminals," *Rheol. Acta* **17**, 663–675. 161

Pattamaprom, C., Larson, R.G. & Van Dyke, T.J. (2000). "Quantitative predictions of linear viscoelastic rheological properties of entangled polymers," *Rheol. Acta* **39**, 517–531. 88

Pedersen, C.J. (1967). "Cyclic polyethers and their complexes with metal salts," *J. Am. Chem. Soc.* **89**, 2495–2496. 31

Picard, G., Ajdari, A., Bocquet, L. & Lequeux, F. (2002). "Simple model for heterogeneous flows of yield stress fluids," *Phys. Rev. E* **66**, 051501. 163

Ramirez, J., Sukumaran, S.K., Vorselaars, B. & Likhtman, A.E. (2010). "Efficient on the fly calculation of time correlation functions in computer simulations," *J. Chem. Phys.* **133**, 154103. 51, 52

Read, D.J., Jagannathan, K. & Likhtman, A.E. (2008). "Entangled polymers: Constraint release, mean paths, and tube bending energy," *Macromolecules* **41**, 6843–6853. 30

Read, D.J., Jagannathan, K., Sukumaran, S.K. & Auhl, D. (2012). "A full-chain constitutive model for bidisperse blends of linear polymers," *J. Rheol.* **56**, 823–873. 30, 69, 72, 76, 79, 80, 81, 82, 83, 88, 89, 93, 186

Ren, J.M., McKenzie, T.G., Fu, Q., Wong, E.H.H., Xu, J., An, Z., Shanmugam, S., Davis, T.P., Boyer, C. & Qiao, G.G. (2016). "Star Polymers," *Chem. Rev.* **116**, 6743–6836. 99

Rouse, P.E. (1953). "A Theory of the Linear Viscoelastic Properties of Dilute Solutions of Coiling Polymers," *J. Chem. Phys.* **21**, 1272–1280. 22, 38

Rubinstein, M. & Colby, R.H. (1988). "Selfconsistent theory of polydisperse entangled polymers: Linear viscoelasticity of binary blends," *J. Chem. Phys.* **89**, 5291–5306. 70

Rubinstein, M. & Dobrynin, A.V. (1999). "Associations leading to formation of reversible networks and gels," *Curr. Opin. Colloid Interface Sci.* **4**, 83–87. 5

Rubinstein, M. & Panyukov, S. (1997). "Nonaffine Deformation and Elasticity of Polymer Networks," *Macromolecules* **30**, 8036–8044. 108

Rubinstein, M. & Semenov, A.N. (1998). "Thermoreversible Gelation in Solutions of Associating Polymers. 2. Linear Dynamics," *Macromolecules* **31**, 1386–1397. 5, 38, 59, 97, 100

Rubinstein, M. & Semenov, A.N. (2001). "Dynamics of Entangled Solutions of Associating Polymers," *Macromolecules* **34**, 1058–1068. 34, 38, 97

Schaefgen, J.R. & Flory, P.J. (1948). "Synthesis of Multichain Polymers and Investigation of their Viscosities," *J. Am. Chem. Soc.* **70**, 2709–2718. 99

Schieber, J.D., Nair, D.M. & Kitkrailard, T. (2007). "Comprehensive comparisons with nonlinear flow data of a consistently unconstrained Brownian slip-link model," *J. Rheol.* **51**, 1111–1141. 30

Schwarzl, F.R. (1971). "Numerical calculation of storage and loss modulus from stress relaxation data for linear viscoelastic materials," *Rheol. Acta* **10**, 165–173. 117

Semenov, A.N. & Rubinstein, M. (1998). "Thermoreversible Gelation in Solutions of Associative Polymers. 1. Statics," *Macromolecules* **31**, 1373–1385. 97

Semenov, A.N., Joanny, J.F. & Khokhlov, A.R. (1995a). "Associating polymers: Equilibrium and linear viscoelasticity," *Macromolecules* **28**, 1066–1075. 97

Semenov, A.N., Nyrkova, I.A. & Khokhlov, A.R. (1995b). "Polymers with Strongly Interacting Groups: Theory for Nonspherical Multiplets," *Macromolecules* **28**, 7491–7500. 97

Sijbesma, R.P. & Meijer, E. (1999). "Self-assembly of well-defined structures by hydrogen bonding," *Curr. Opin. Colloid Interface Sci.* **4**, 24–32. 32

Snijkers, F., Ratkanthwar, K., Vlassopoulos, D. & Hadjichristidis, N. (2013). "Viscoelasticity, nonlinear shear start-up, and relaxation of entangled star polymers," *Macromolecules* **46**, 5702–5713. 129, 135

Soltero, J.F.A., Bautista, F., Puig, J.E. & Manero, O. (1999). "Rheology of Cetyltrimethylammonium p -ToluenesulfonateWater System. 3. Nonlinear Viscoelasticity," *Langmuir* **15**, 1604–1612. 162

Spenley, N., Yuan, X.F. & Cates, M.E. (1996). "Nonmonotonic Constitutive Laws and the Formation of Shear-Banded Flows," *J. Phys. II* **6**, 551–571. 162

Spenley, N.A., Cates, M.E. & McLeish, T.C.B. (1993). "Nonlinear rheology of wormlike micelles," *Phys. Rev. Lett.* **71**, 939–942. 162

Sprakel, J., Spruijt, E., Cohen Stuart, M.A., Besseling, N.A.M., Lettinga, M.P. & van der Gucht, J. (2008). "Shear banding and rheochaos in associative polymer networks," *Soft Matter* **4**, 1696–1705. 163

Sprakel, J., Spruijt, E., van der Gucht, J., Padding, J.T. & Briels, W.J. (2009). "Failure-mode transition in transient polymer networks with particle-based simulations," *Soft Matter* **5**, 4748. 162

Staudinger, H. (1920). "Über Polymerisation," *Berichte der Dtsch. Chem. Gesellschaft* **53**, 1073–1085. 3

Tam, K.C., Jenkins, R.D., Winnik, M.A. & Bassett, D.R. (1998). "A Structural Model of Hydrophobically Modified Urethane-Ethoxylate (HEUR) Associative Polymers in Shear Flows," *Macromolecules* **31**, 4149–4159. 98

Tanaka, F. & Edwards, S. (1992a). "Viscoelastic properties of physically crosslinked

networks. Part 1. Non-linear stationary viscoelasticity," *J. Nonnewton. Fluid Mech.* **43**, 247–271. 33

Tanaka, F. & Edwards, S. (1992b). "Viscoelastic properties of physically crosslinked networks. Part 2. Dynamic mechanical moduli," *J. Nonnewton. Fluid Mech.* **43**, 273–288. 33

Tanaka, F. & Edwards, S.F. (1992c). "Viscoelastic properties of physically crosslinked networks. 1. Transient network theory," *Macromolecules* **25**, 1516–1523. 33

Tanaka, F. & Edwards, S.F. (1992d). "Viscoelastic properties of physically crosslinked networks. Part 3. Time-dependent phenomena," *J. Nonnewton. Fluid Mech.* **43**, 289–309. 33

Tao, H., Lodge, T.P. & von Meerwall, E.D. (2000). "Diffusivity and Viscosity of Concentrated Hydrogenated Polybutadiene Solutions," *Macromolecules* **33**, 1747–1758. 169

Tripathi, A., Tam, K.C. & McKinley, G.H. (2006). "Rheology and Dynamics of Associative Polymers in Shear and Extension: Theory and Experiments," *Macromolecules* **39**, 1981–1999. 33, 97, 103, 109, 111, 113, 139, 188

Trouton, F.T. (1906). "On the Coefficient of Viscous Traction and Its Relation to that of Viscosity," *Proc. R. Soc. A Math. Phys. Eng. Sci.* **77**, 426–440. 22

Tzoumanekas, C. & Theodorou, D.N. (2006). "Topological Analysis of Linear Polymer Melts: A Statistical Approach," *Macromolecules* **39**, 4592–4604. 27

Uraneck, C.A., Hsieh, H.L. & Buck, O.G. (1960). "Telechelic polymers," *J. Polym. Sci.* **46**, 535–539. 97

Vaccaro, A. & Marrucci, G. (2000). "A model for the nonlinear rheology of associating polymers," *J. Nonnewton. Fluid Mech.* **92**, 261–273. 33, 139, 188

van den Brule, B.H.A.A. & Hoogerbrugge, P.J. (1995). "Brownian Dynamics simulation of reversible polymeric networks," *J. Nonnewton. Fluid Mech.* **60**, 303–334. 33

van Ruymbeke, E., Keunings, R. & Bailly, C. (2005). "Prediction of linear viscoelastic properties for polydisperse mixtures of entangled star and linear polymers: Modified tube-based model and comparison with experimental results," *J. Nonnewton. Fluid Mech.* **128**, 7–22. 34

van Ruymbeke, E., Vlassopoulos, D., Mierzwa, M., Pakula, T., Charalabidis, D., Pitsikalis, M. & Hadjichristidis, N. (2010). "Rheology and Structure of Entangled Telechelic Linear and Star Polyisoprene Melts," *Macromolecules* **43**, 4401–4411. xvi, 34, 98, 99, 110, 121, 122, 123, 154, 169, 172

Vinogradov, G.V., Protasov, V.P. & Dreval, V.E. (1984). "The rheological behavior of flexible-chain polymers in the region of high shear rates and stresses, the critical process of spurting, and supercritical conditions of their movement at T>Tg," *Rheol. Acta* **23**, 46–61. 161

Viovy, J.L., Rubinstein, M. & Colby, R.H. (1991). "Constraint release in polymer melts: tube reorganization versus tube dilation," *Macromolecules* **24**, 3587–3596. 81, 88, 90

Vlassopoulos, D., Pakula, T., Fytas, G., Pitsikalis, M. & Hadjichristidis, N. (1999). "Controlling the self-assembly and dynamic response of star polymers by selective telechelic functionalization," *J. Chem. Phys.* **111**, 1760–1764. 98

Vlassopoulos, D., Pitsikalis, M. & Hadjichristidis, N. (2000). "Linear Dynamics of End-Functionalized Polymer Melts: Linear Chains, Stars, and Blends," *Macromolecules* **33**, 9740–9746. 98

Wagner, M.H. & Rolon-Garrido, V.H. (2008). "Verification of branch point withdrawal in elongational flow of pom-pom polystyrene melt," *J. Rheol.* **52**, 1049–1068. 98

Warner, H.R. (1972). "Kinetic Theory and Rheology of Dilute Suspensions of Finitely Extendible Dumbbells," *Ind. Eng. Chem. Fundam.* **11**, 379–387. 73, 107

Wesslau, V.H. (1956). "Die molekulargewichtsverteilung einiger niederdruckpolyäthylene," *Die Makromol. Chemie* **20**, 111–142. 56

Wheeler, L.M. & Lodge, T.P. (1989). "Tracer diffusion of linear polystyrenes in dilute, semidilute, and concentrated poly(vinyl methyl ether) solutions," *Macromolecules* **22**, 3399–3408. 169

Williams, K.A., Dreyer, D.R. & Bielawski, C.W. (2008). "The Underlying Chemistry of Self-Healing Materials," *MRS Bull.* **33**, 759–765. 5

Zhou, Q. & Larson, R.G. (2005). "Primitive Path Identification and Statistics in Molecular Dynamics Simulations of Entangled Polymer Melts," *Macromolecules* **38**, 5761–5765. 27